



**Demulsification of Water/Crude Oil  
Emulsions Using Functionalised  
PolyHIPEs in an Electrostatic Field**

A Thesis Submitted to Newcastle University for the  
Degree of Doctor of Philosophy

by

**Abbas Khaleel Ibrahim Al-Gburi**

School of Chemical Engineering and Advanced  
Materials

Newcastle University

**February-2020**

---

## **DISCLAIMER**

---

This thesis is submitted in accordance with the PhD requirements at Newcastle University. I hereby declare that according to best of my knowledge and belief, all the content presented here is my own work.

I confirm that the material presented in this thesis has not been previously presented for a degree or any another qualification in Newcastle University or any another institute or university.

All of the work done reflects my view only and not obligatory the opinion of the Newcastle University or any other side.

---

## ABSTRACT

---

In petroleum manufacturing, during the crude oil extraction process, water-in-crude oil emulsions with high stability are obtained which are stabilised due to the presence of indigenous surface-active materials within crude oil. The removal of water from crude oil is critical in producing saleable product. It should be conducted at source with the aim to overcome the cost of pumping and the problems associated with the corrosion in pipes during transportation. Many separation technologies exist, e.g. gravity separators, coalescence separators, centrifugal separators, stripping columns and vacuum distillation systems, but most of these cannot remove tightly emulsified or dissolved water in addition to their high cost. Thus, chemical treatments are often required to separate water from these emulsions.

Recently, sulphonated hydrophilic micro-porous polymers (named PolyHIPE Polymers) were used as an active membrane layer in a cross-flow microfiltration process to separate water from water-in-crude oil emulsions. However, this did not sufficiently separate water from w/o emulsions under steady state conditions. Therefore, an alternative method for using polyHIPE to achieve the same results has been developed in this project.

This thesis focuses on the removal of water and surface-active components from high stability water-in-crude oil emulsions by using a novel combination of a highly porous polymeric material sorbent with an electrostatic separation field to further enhance the efficiency of the separation process. The results are compared to a conventional separation processes. Several micro-porous polyHIPEs (PHPs) with varying functionality have been produced and characterised. These PHP polymers were then utilised in water separation trials from emulsions of water-in-crude oil with high stability. A continuous demulsification process has been developed and tested on a model seawater-in-crude oil emulsion by utilising different PHPs in presence of an electric field.

In order to use the optimum samples of the PHPs in the demulsification process, the PHP samples were characterized in terms of morphology, surface area, water uptake, pore size distribution, EDX, and FTIR analyses. Different flow rates of emulsions and various electric field strengths (applied voltages) were employed in this separation process to evaluate their effect on the separation efficiency. Furthermore, the spent PHP samples were reused in the

demulsification process to evaluate the potential for sorbent recovery and the change in separation efficiency after reuse.

This study succeeded in achieving its main objective namely the production of environmentally sustainable demulsifiers on a laboratory scale. A silane PHP ecofriendly demulsifier was synthesized with a relatively high surface area of 98 m<sup>2</sup>/g, high water adsorption as well as its ability to remove surface-active species from crude oil that cause emulsification of crude oil such as Mg, Na, Cl and Ca. Another goal was to study the demulsification mechanism by utilising various types of sorbents including standard sulphonated PHP, in situ sulphonated PHP, bindzil PHP and silane PHP to identify the best performance. This required the development of a continuous demulsification process to work at a high electric field strength without breakdown (ranging from 1-5 kV over a few centimetres) and different emulsion inlet flow rates (from 100 to 1500 ml/min). It was found that the best separation efficiency was 89% by using the silane PHP demulsifier at a flow rate of 100 ml/min and an applied voltage of 5 kV. This is comparable to the best results achieved by other methods including chemical demulsification. When reusing the spent silane PHP in the demulsification process under similar parameters, the separation efficiency was reduced to 71%. The final aim, to eliminate the need for larger demulsification equipment by developing a novel approach for the separation of emulsions under the combined impacts of demulsifier and electric technique, was therefore successfully achieved.

---

## ACKNOWLEDGMENT

---

First, my humble thanks are expressed to Allah almighty for the inspiration, strength, guidance and encouragement throughout this difficult journey. In fact, many experiences and knowledge have been gained.

I would like to express immense gratitude to my supervisor Prof. Steve Bull for giving me the opportunity to work under his supervision and providing me the constant intellectual motivation and continuous guidance. Prof. Bull's commitment and endless support, both academically and personally, have been invaluable and I have been fortunate to work with him.

I wish to acknowledge and express my sincere appreciation and heartiest gratitude to my wife for being patient, enduring, making sacrifices. Most of all, I would like to thank her for guiding my children in my absence from home for the purpose of studying, Mustafa, Mehdi, Fatima, Jannat and Mojtaba. To my wife, children, brothers and sisters, I would like to say thank you for your unconditional love, care, tolerance, encouragement and continuous prayer for the success of my PhD program.

My deepest sincere thanks are also extended to the Oil Ministry, Midland Refineries Company and ministry of Higher Education and Science Research for providing this chance for me to acquire knowledge and expertise. I am also grateful to them and thank them for their financial support while pursuing my PhD study.

Newcastle University is also appreciated for providing an enabling environment as office place, various laboratory equipment and providing the opportunity to 'exploit' its talented technicians team. My acknowledgement goes to all my friends and colleagues, especially at the technologists workshops in the School of Chemical Engineering and Advanced Material (CEAM) for technical assistance including, Neville Dickman, Rob Dixon, Roy Proud, Stephen Mitchell, Rachael Dack (for FTIR analysis) and Dr. Isabel Arce Garcia (for SEM and EDX analyses) who without their support this thesis would not have been complete.

Alhamdulillah, thank you Allah for giving me the strength, patient and determination to continue.

## TABLE OF CONTENTS

DISCLAIMER .....	I
ABSTRACT.....	II
ACKNOWLEDGMENT.....	IV
TABLE OF CONTENTS.....	V
LIST OF TABLES .....	XII
LIST OF FIGURES .....	XIV
NOMENCLATURE .....	XXI
CHAPTER ONE .....	1
1. INTRODUCTION .....	1
1.1 Overview .....	1
1.2 The Aims of Thesis .....	5
1.3 Thesis Overview.....	8
CHAPTER TWO .....	10
2. LITERATURE REVIEW: THE EMULSION AND DEMULSIFICATION OF WATER- IN-CRUDE OIL.....	10
2.1 Overview .....	10
2.2 Crude Oil.....	10
2.3 Physical Properties of Crude Oil.....	11
2.4 Chemical Properties of Crude Oil .....	13
2.4.1 Saturates of Crude Oil.....	14
2.4.2 Aromatics of Crude Oil.....	15
2.4.3 Resins of Crude Oil.....	16
2.4.4 Asphaltenes of Crude Oil.....	17
2.5 Water-Oil Emulsions.....	18
2.5.1 Water-in-Oil Emulsion Formation .....	21
2.5.2 Emulsion Properties .....	23

2.5.3	<i>Stability of Emulsions</i> .....	25
2.5.4	<i>Emulsion Rheology</i> .....	29
2.5.4.1	Effect of the Volume of Dispersed Phase on the Viscosity of an Emulsion.....	30
2.5.4.2	Effect of Droplet size on the Viscosity of Emulsion .....	33
2.5.4.3	Interfacial Rheology.....	34
2.6	Emulsions of Water-in-Crude Oil .....	36
2.6.1	<i>Crude Oil Emulsions Problems</i> .....	37
2.6.2	<i>Rheology and Interfacial Behaviour</i> .....	37
2.6.3	<i>Water-in-Crude-Oil Emulsions Stability Problems</i> .....	39
2.7	Demulsification of Water-in-Crude Oil Emulsions .....	42
2.7.1	<i>Current Techniques Used in Demulsification</i> .....	44
2.7.1.1	Utilizing Demulsifiers.....	44
2.7.1.2	Electrical Treatments .....	47
2.7.1.3	Combining Different Techniques .....	50
2.7.2	<i>Pressure Effect</i> .....	54
2.7.3	<i>The Effect of the Oil Phase and Aqueous Characteristics</i> .....	54
2.7.4	<i>Electric Field Effect</i> .....	55
CHAPTER THREE .....		58
3. IMPROVEMENT OF ELECTROSTATIC SEPARATION OF WATER-IN-CRUDE- OIL EMULSIONS USING POLYHIPE DEMULSIFIERS .....		58
3.1	Overview .....	58
3.2	Mechanics Involving Electrically- Optimized Demulsification.....	58
3.2.1	<i>Charging of Droplets</i> .....	60
3.2.2	<i>Electrostatic Interactions</i> .....	63
3.2.3	<i>Interactions between Droplets</i> .....	64
3.2.3.1	Three-Stage Process.....	65
3.2.3.2	Dipole Forces .....	65

3.2.3.3 Thinning and Breaking .....	66
3.2.3.4 Chain-Formation .....	67
3.2.3.5 Electrophoresis and Dielectrophoresis.....	67
3.2.3.6 Random Collision .....	68
3.2.4 Interactions at the Droplet-Interface.....	69
3.3 Factors Affecting Electrically-Optimized Demulsification .....	70
3.3.1 AC and DC Electric Field .....	70
3.3.2 Effect of Frequency.....	71
3.3.3 Effect of Field Strength.....	72
3.3.4 Electrode Dimensions and Insulation.....	72
3.3.5 Droplets Size and Contact .....	73
3.4 PolyHIPE Polymer .....	75
3.4.1 Overview of PolyHIPE Polymer (PHP) .....	75
3.4.2 Preparation of PolyHIPE .....	78
3.4.3 Morphology of PolyHIPEs .....	82
3.4.4 Factors Affecting PHP Polymers Morphology.....	83
3.4.4.1 Volume Ratio of Internal Phase .....	83
3.4.4.2 Surfactant Parameter .....	83
3.4.4.3 Composition of HIPE Continuous Phase .....	84
3.4.4.4 Electrolyte Content .....	85
3.4.4.5 Mixing Time/Dosing Time .....	85
3.4.4.6 Temperature of Emulsification .....	86
3.4.4.7 Moulding Type.....	87
3.4.5 Properties of PolyHIPE.....	88
3.4.5.1 Mechanical Properties.....	88
3.4.5.2 Surface Area.....	89
3.4.6 Sulphonation of PolyHIPE Polymer.....	90

3.5 Summary .....	93
CHAPTER FOUR.....	94
4. APPARATUS, EXPERIMENTAL PROCEDURE FOR PREPARING POLYHIPE POLYMER & ANALYTICAL METHODS .....	94
4.1 Overview .....	94
4.2 Preparation of PolyHIPE Polymer .....	94
4.2.1 Preparation Basic PHP (B-PHP).....	95
4.2.1.1 HIPE Components .....	95
4.2.1.3 Polymerisation of PolyHIPE.....	99
4.2.1.4 Washing of PolyHIPE Polymer .....	101
4.2.1.5 Functionalisation of PHP .....	102
4.2.2 Preparation of In-Situ PolyHIPE (IS-PHP) .....	103
4.2.3 Preparation of Bindzil PolyHIPE (BZ-PHP) .....	104
4.2.4 Preparation of Silane PolyHIPE (SL-PHP) .....	105
4.3 PHP Sulphonation.....	106
4.4 Analytical Methods .....	107
4.4.1 Analytical Techniques for PolyHIPE .....	107
4.4.1.1 Surface Area and Pore Size Analysis.....	107
4.4.1.1.1 Desorption and adsorption isotherm.....	108
4.4.1.1.2 Freespace .....	109
4.4.1.1.3 Surface Area Analysis .....	111
4.4.1.1.4 Analysis of Pore Size .....	112
4.4.1.2 Environmental Scanning Electron Microscope (ESEM) .....	114
4.4.1.3 EDX (Element Analysis) .....	117
4.4.1.4 Fourier Transform Infrared spectroscopy (FTIR).....	118
4.4.1.5 Water Uptake Tests.....	118
4.4.2 Analytical Techniques of Water-in-Crude Oil Emulsions .....	120

4.4.2.1	Viscometer Measurement .....	120
4.4.2.2	Conductivity Measurements .....	121
CHAPTER FIVE .....		123
5.	POLYHIPE POLYMER (PHP) DEVELOPMENT: RESULTS AND DISCUSSIONS	123
5.1	Overview.....	123
5.2	Basic PolyHIPE (B-PHP).....	123
5.2.1	<i>Morphology</i> .....	123
5.2.2	<i>Pore Size Distribution of B-PHP</i> .....	128
5.2.3	<i>Surface Area</i> .....	129
5.2.3.1	Measurement of Surface Area of B-PHP .....	130
5.2.4	<i>Water Uptake of B-PHP</i> .....	131
5.2.5	<i>FTIR Analysis of B-PHP</i> .....	133
5.2.6	<i>Summary</i> .....	140
5.3	In-Situ Sulphonated PolyHIPE (IS-PHP).....	140
5.3.1	<i>Morphology</i> .....	140
5.3.2	<i>Pore Size Distribution of IS-PHP</i> .....	144
5.3.3	<i>Surface Area Measurement of IS-PHP</i> .....	145
5.3.4	<i>Water Uptake of IS-PHP</i> .....	146
5.3.5	<i>FTIR Analysis of IS-PHP</i> .....	148
5.3.6	<i>Summary</i> .....	150
5.4	Bindzil PolyHIPE (BZ-PHP) .....	150
5.4.1	<i>Morphology</i> .....	150
5.4.2	<i>Pore Size Distribution of BZ-PHP</i> .....	156
5.4.3	<i>Surface Area measuring of BZ-PHP</i> .....	159
5.4.4	<i>Water Uptake of BZ-PHP</i> .....	161
5.4.5	<i>FTIR Analysis of BZ-PHP</i> .....	163
5.4.6	<i>Summary</i> .....	165

5.5 Silane (vinyl trimethoxy silane) PolyHIPE (SL-PHP).....	166
5.5.1 Morphology .....	166
5.5.2 Pore Size Distribution of SL-PHP .....	172
5.5.3 Measurement of Surface Area of SL-PHP .....	175
5.5.4 Water Uptake of SL-PHP .....	176
5.5.5 FTIR Analysis of Silane PHP .....	178
5.5.6 Summary .....	183
5.6 Optimum Samples .....	183
CHAPTER SIX.....	184
6. PROCEDURES OF FORMING WATER-IN-CRUDE OIL EMULSION AND DEMULSIFICATION OF WATER-IN-CRUDE OIL EMULSION USING COMBINED PHP DEMULSIFIER AND ELECTROSTATIC FIELD .....	184
6.1 Overview .....	184
6.2 Formation of Water-in-Crude Oil Emulsion .....	184
6.3 Separation of Crude Oil and Water .....	187
6.3.1 Separator Design .....	187
6.4 Effect Emulsification Variables .....	191
6.4.1 Impact of Emulsification Variables on Stability and Viscosity of the Emulsions..	191
6.4.2 The Crude Oil Emulsion Stability.....	193
6.5 Conductivity Measurement of Crude Oil Emulsions .....	195
CHAPTER SEVEN .....	197
7. RESULTS AND DISCUSSIONS OF DEMULSIFICATION EXPERIMENTS OF WATER-IN-CRUDE OIL EMULSION USING COMBINED PHP DEMULSIFIER AND ELECTROSTATIC FIELD AND REUSE OF SPENT PHP IN THE DEMULSIFICATION PROCESS .....	197
7.1 Outlet.....	197
7.2 Separation Studies .....	197
7.2.1 Effect of Inlet Flow Rate Variation.....	197

7.2.2 <i>Effect of Electric Field Strength Variation</i> .....	203
7.3 SEM analysis, EDX analysis and water uptake of PHP-I.....	207
7.4 Reuse of Spent PHP-I in Separation Experiments Using Electrostatic Field .....	210
7.5 Mechanism of Demulsification .....	212
CHAPTER EIGHT .....	213
8. CONCLUSIONS AND FUTURE WORKS RECOMMENDATIONS .....	213
8.1 Outline.....	213
8.2 Introduction .....	213
8.3 Findings Summary .....	214
8.3.1 <i>PolyHIPE Polymers</i> .....	214
8.3.2 <i>PolyHIPEs Sulphonation</i> .....	215
8.3.3 <i>Water-in-crude oil emulsions</i> .....	215
8.3.4 <i>Demulsification of water-in-crude oil emulsions</i> .....	216
8.3.5 <i>Reuse Spent PHP-I Demulsifier in Demulsification Experiments</i> .....	217
8.4 Final Remarks .....	218
8.5 Future Work Recommendations.....	219
REFERENCES .....	220
APPENDIX.....	252

## LIST OF TABLES

Table 1: The weight percentages (wt. %) of the main classes of the crude oils compounds (Fingas, 2014). .....	14
Table 2: Models of emulsions in the industrial extraction and refining of petroleum (Roodbari et al., 2016). .....	20
Table 3: Different applications of electrical coalescence .....	50
Table 4: Electrostatic coalescence of droplets of water in oil (Eow et al., 2001).....	53
Table 5: Various applications of PHP in different fields. ....	78
Table 6: Composition of the oil phase and the aqueous phase of basic HIPE.....	96
Table 7: Molecular formulae and chemical structure for the components of PHP.....	96
Table 8: Recipe of the composition of the oil phase and the aqueous phase of in-situ HIPE. ....	103
Table 9: Composition of the oil phase and the aqueous phase of Bindzil HIPE and the molecular formula and chemical structure of Lauroyl peroxide.....	104
Table 10: Composition of the oil phase and the aqueous phase of Silane HIPE. ....	105
Table 11: Summary of the results of PHP sulphonation.....	106
Table 12: Constants values utilised by the BET machine in the distribution analysis of pore size. ....	113
Table 13: Summary of the EDX results for the points, 1 and 2 for PS50.....	127
Table 14: The results of ImageJ analysis of average pore and interconnect sizes, which were determined from the B-PHP where 30 pores from each sample were measured.....	129
Table 15: Surface area of sulphonated and unsulphonated B-PHP for different mixing times. ....	130
Table 16: Water uptake for various sulphonated and unsulphonated B-PHP samples for different mixing times.....	132
Table 17: Absorption peaks and peak assignments of unsulphonated B-PHP samples for different mixing times.....	138
Table 18: Absorption peaks and peak assignments of sulphonated B-PHP samples for different mixing times.....	139
Table 19: Summary of the EDX results for the points, 1 and 2 for IS40.....	143
Table 20: The results of ImageJ analysis of average pore and interconnect sizes, which were determined from the IS-PHP where 30 pores from each sample were measured.....	144
Table 21: Surface area of IS-PHP for different mixing times. ....	146

Table 22: Water uptake of IS-PHP samples for different mixing times. ....	147
Table 23: Absorption peaks and peaks names of IS-PHP samples for different mixing times. .....	149
Table 24: EDX composition for the all area of the image for BZ25. ....	155
Table 25: Summary of the EDX results for the points, 1, 2 and 3 for BZ25. ....	156
Table 26: The results of ImageJ analysis of average pore and interconnect sizes, which were determined from the BZ-PHP where 30 pores from each sample were measured. ....	157
Table 27: Surface area of unsulphonated and sulphonated BZ-PHP for different mixing times. .....	160
Table 28: Water uptake for various BZ-PHP samples (before and after sulphonation) for different mixing times. ....	162
Table 29: Absorption peaks and peak assignments of sulphonated BZ-PHP samples for different percentages of bindzil with mixing time, 50 minutes. ....	163
Table 30: EDX elemental composition for the all area of the image for SL20. ....	170
Table 31: Summary of the EDX compositions for the points, 1, 2 and 3 for SL20. ....	171
Table 32: The results of ImageJ analysis of average pore and interconnect sizes, which were determined the silane PHP where 30 pores from each sample were measured. ....	174
Table 33: Surface area of silane polyHIPE. ....	175
Table 34: Surface area for different discs of SL20 PHP (unwashed) from a single container. .....	176
Table 35: Water uptake for various SL-PHP samples (before and after sulphonation) for different mixing times. ....	177
Table 36: Position of two peaks of the SL-PHP samples in the stretching band between 1050 and 1230 $\text{cm}^{-1}$ . ....	182
Table 37: Specifics of the prepared water-in-crude oil emulsions. ....	191
Table 38: Conductivity of inlet (fresh) and outlet emulsions samples for various flow rates with applied voltage of 1.0 and 5.0 kV. ....	196
Table 39: EDX analysis result of PHP-I after demulsification, including the main elements adsorbed by PHP-I namely: Mg, Na, Cl and Ca. ....	208
Table 40: EDX analysis result of reused spent PHP-I after demulsification, including the main elements adsorbed by PHP-I namely: Mg, Na, Cl and Ca. ....	211

## LIST OF FIGURES

Figure 1: Measured dynamic viscosity (mPa.s) as a function of the composition of asphaltene (weight %) in a tripartite diagram based on measurement thirteen of artificial crude oils at 100°C and 35 mPa.s (Werner et al., 1998; Cameron, 2005). .....	12
Figure 2: Diagram representing API gravity versus specific gravity for the main types of crude oil (light and heavy) and others hydrocarbons ('The eniginerring toolBox,' 2019). .....	12
Figure 3: Block diagram of the typical SARA-separation (Demirbas and Taylan, 2016).....	13
Figure 4: Hypothetical structure of a crude oil saturate (Yasar et al., 2009). .....	15
Figure 5: Hypothetical structure of a crude oil aromatic (Akmaz et al., 2011). .....	16
Figure 6: Hypothetical structure of a crude oil resin (Akmaz et al., 2011) .....	17
Figure 7: Hypothetical structure of a crude oil asphaltene (Andersen and Speight, 2001) .....	18
Figure 8: Schematic diagram of emulsion types (Kilpatrick and Spiecker, 2001) .....	19
Figure 9: Schematic representation of the production of petroleum and the processes of refining in which emulsions are encountered (Sullivan and Kilpatrick, 2002). .....	22
Figure 10: Schematic representation of the potential associated with colloids (Wiącek and Chibowski, 2002).....	24
Figure 11: Pictorial representation of emulsions instability methods (Fribereg, 2001) .....	26
Figure 12: Schematic diagram of common flow behaviors (Akay et al., 2005a) .....	30
Figure 13: Schematic drawing of the contact angle between a liquid and solid (Schulman, 1954). .....	34
Figure 14: Schematic diagram of the Gibbs-Marangoni effect at an oil-water interface (Schuster, 1985) .....	35
Figure 15: A schematic diagram of droplet of a w/o emulsion with a petroleum fraction. The interfacial layer forms a skin around the droplet at an early stage (Angle, 2001).....	40
Figure 16: Schematic drawing of the crude oil components and bitumen to be considered in an emulsion droplet and the interfacial layer (Angle, 2001) .....	41
Figure 17: Schematic diagram of a conventional AC coalescer (Noor, 2006). .....	48
Figure 18: Schematic diagram of a combined AC/DC coalescer (Noor, 2006). .....	49
Figure 19: Different combination of the technology of electrical separation (Eow and Ghadiri, 2002) .....	52
Figure 20: Schematic diagram of demulsification in a coalescing apparatus illustrating the effect of the electric field (Waterman, 1965).....	60

Figure 21: Schematic illustration of; (a) and (b) Polarization of a single droplet of water in an electric field; (c) Migration of droplets and interaction as a result of contact charging upon impinging on an isolated electrode (Taylor, 1996).	61
Figure 22: Schematic illustration of coalescence forces (Draxler and Marr, 1993).	64
Figure 23: Schematic representation of polyHIPE formation (Byron, 2000).	76
Figure 24: SEM images of basic structure of the styrene/divinylbenzene polyHIPE polymer: (a) Primary pores with great interconnecting holes; (b) Primary pores with nano-sized interconnecting holes; (c) Large coalescence pores dispersed into the primary pores in the coalescence process; (d) Coalescence pores detail (Akay, 2006).	76
Figure 25: The polymerisation reaction of styrene and divinylbenzene to get polyHIPE polymer (Barby and Haq, 1982).	79
Figure 26: Styrene and divinylbenzene polymerisation to form a Polymer with an Infinite Network (Sherrington, 1998).	81
Figure 27: Graphical diagram showing the pore formation in PolyHIPE (Akay, 1995).	84
Figure 28: Difference of average pore size (D) with total mixing time (t) as a function of volume fraction of the dispersed phase ( $\epsilon$ ): speed of the Impeller=300 rpm, temperature of emulsification=25 °C, dosing time=10 min (Bokhari, 2003).	86
Figure 29: Difference of average pore size with temperature of the emulsification stage when total mixing time=100 s, dosing time=40 s, phase volume=90 %, impeller speed=300 rpm (Akay et al., 2005a).	87
Figure 30: Schematic diagram showing the chemical structure of (100%) sulphonated PolyHIPE (Calkan, 2007).	91
Figure 31: SEM micrograph of sulphonated PHP (using microwave irradiation sulphonation method) at low magnification (Mohamed, 2011).	92
Figure 32: Schematic diagram showing the stage of Functionalization of polyHIPE polymer.	93
Figure 33: Schematic diagram and picture of the mixing reactor used for HIPE preparation.	97
Figure 34: Picture of the Impellers used to mix the HIPE.	98
Figure 35: Schematic diagram of the polymerisation of PHP.	99
Figure 36: PHP samples, cut into discs with 4 mm thickness and 26 mm diameter.	100
Figure 37: Schematic diagram and picture of the soxhlet system-apparatus used for PHP washing.	101
Figure 38: The thermal (conventional) method of polyHIPE sulphonation (Burke et al., 2006).	102

Figure 39: Surface area analyzer, BET Surfer. ....	108
Figure 40: Environmental Scanning Electron Microscopy (SEM) used in the research. ....	114
Figure 41: Schematic representation of SEM with formation of secondary electrons the images on the TV screen. ....	116
Figure 42: Plot of number of measurements versus pore size using ImageJ software. ....	117
Figure 43: Fourier Transform Infrared spectroscopy (FTIR) equipment. ....	118
Figure 44: Schematic diagram showing the water uptake analysis. ....	119
Figure 45: A simplified schematic drawing of the Co-axial Cylinder HAAKE VT 550 Viscometer. ....	120
Figure 46: Mettler Toledo SevenExcellent S470 Conductivity Meter. ....	122
Figure 47: Sulphonated basic PHP (B-PHP). (a) $t_{mix}=10$ min (b) $t_{mix}=20$ min (c) $t_{mix}=30$ min (d) $t_{mix}=40$ min (e) $t_{mix}=50$ min. Oil phase: 76% styrene, 10% DVB and 14% Span 80. Aqueous phase: 99% distilled water, 1% potassium presulphate. Phase volume = 90%, Dosing time = 10 minutes. Polymerisation temperature = 60 °C, Polymerisation time = 24 hours. ....	124
Figure 48: Basic PHP (B-PHP). (a) $t_{mix}=10$ min (b) $t_{mix}=20$ min (c) $t_{mix}=30$ min (d) $t_{mix}=40$ min (e and f) $t_{mix}=50$ min. Oil phase: 76% styrene, 10% DVB and 14% Span 80. Aqueous phase: 99% distilled water, 1% potassium presulphate. Phase volume = 90%, Dosing time = 10 minutes. Polymerisation temperature = 60 °C, Polymerisation time = 24 hours. ....	125
Figure 49: Two points, 1 and 2 for EDX analysis of PS50. ....	126
Figure 50: PS50 point 1 EDX spectrum. ....	127
Figure 51: PS50 point 2 EDX spectrum. ....	127
Figure 52: SEM micrograph of B50 PHP showing the pore and interconnect size at x5000 (red arrows). ....	128
Figure 53: Plot of pore and interconnecting sizes of B-PHP for different mixing times. ....	129
Figure 54: Surface area versus mixing time for sulphonated and unsulphonated B-PHP. ....	131
Figure 55: Plot of water uptake of sulphonated and unsulphonated B-PHP for different mixing times. ....	132
Figure 56: FTIR spectra for all unsulphonated B-PHP samples. ....	133
Figure 57: FTIR spectrum for unsulphonated B10 PHP. ....	134
Figure 58: FTIR spectrum for sulphonated B10 PHP. ....	134
Figure 59: FTIR spectrum for sulphonated B20 PHP. ....	135
Figure 60: FTIR spectrum for sulphonated B30 PHP. ....	135
Figure 61: FTIR spectrum for sulphonated B40 PHP. ....	136

Figure 62: FTIR spectrum for sulphonated B50 PHP.....	136
Figure 63: FTIR spectra for sulphonated and unsulphonated B50 PHP.....	137
Figure 64: In-situ sulphonated PHP (IS-PHP). (a) $t_{mix}=10$ min (b) $t_{mix}=20$ min (c) $t_{mix}=30$ min (d) $t_{mix}=40$ min (e) $t_{mix}=50$ min. Oil phase: 74% styrene, 12% DVB and 14% span 80. Aqueous phase: 94% distilled water, 1% potassium presulphate and 5% sulphuric acid. Phase volume = 90%, Dosing time = 10 minutes. Polymerisation temperature = 60 °C, Polymerisation time = 24 hours. ....	141
Figure 65: Two points, 1 and 2 for EDX analysis for IS40. ....	142
Figure 66: IS40 point 1 EDX spectrum. ....	143
Figure 67: IS40 point 2 EDX spectrum. ....	143
Figure 68: Plot of pore and interconnect sizes of IS-PHP for different mixing times.....	145
Figure 69: Plot of surface area for various mixing times of IS-PHP.....	146
Figure 70: Plot of water uptake of IS-PHP for different mixing times.....	147
Figure 71: FTIR spectrum for IS10 PHP. ....	148
Figure 72: FTIR spectra for all IS-PHP samples. ....	150
Figure 73: Bindzil PHP (BZ-PHP). (a) 5% bindzil (b) 10% bindzil (c) 15% bindzil (d) 20% bindzil (e) 25% bindzil. Oil phase: 75% styrene, 10% DVB, 14% span 80 and 1% potassium presulphate. Aqueous phase: X% bindzil, (100-X)% distilled water, (e.g. for 15% bindzil. Distilled water was decreased to 85%). Phase volume = 90%, Dosing time = 10 minutes, Mixing time = 50 minutes. Polymerisation temperature = 60 °C, Polymerisation time = 24 hours.....	152
Figure 74: Different magnification images of 5000, 10000 and 15000x of BZ25 PHP for mixing time of 50 minutes. ....	153
Figure 75: Three points, 1, 2 and 3 for EDX analysis of BZ25.....	154
Figure 76: The complete area EDX analysis of image in Figure 89.....	154
Figure 77: BZ25 point 1 EDX spectrum.....	155
Figure 78: BZ25 point 2 EDX spectrum.....	155
Figure 79: BZ25 point 3 EDX spectrum.....	156
Figure 80: Plot of pore and interconnect sizes of BZ-PHP samples for different mixing times. .....	158
Figure 81: Plot of pore and interconnect sizes of BZ25 PHP samples for different mixing times.....	158
Figure 82: Plot of the surface area of unsulphonated and sulphonated BZ50 PHP for various mixing times.....	159

Figure 83: Plot of water uptake of sulphonated BZ-PHP for different percentage of bindzil with various mixing times.....	161
Figure 84: FTIR spectrum for all sulphonated BZ-PHP.....	164
Figure 85: FTIR spectra for sulphonated BZ25 PHP.....	164
Figure 86: SL-PHP, SL10 with 10% vinyl trimethoxy silane. ....	166
Figure 87: Vinyl trimethoxy silane PHP (SL-PHP). (a) 5% silane (b) 10% silane (c) 15% silane (d) 20% silane (e) 25% silane. Oil phase: X% silane, (76-X)% styrene, 10% DVB, 14% span 80, (e.g. for 10% silane. Styrene was decreased to 66%). Aqueous phase: 99% distilled water, 1% potassium persulphate. Phase volume = 90%, Dosing time = 10 minutes, Mixing time = 50 minutes. Polymerisation temperature = 60 °C, Polymerisation time = 24 hours.....	167
Figure 88: Vinyl trimethoxy silane PHP (SL-PHP). (a) 10% silane (b) 15% silane (c) 20% silane (d, e and f) 25% silane. Oil phase: X% silane, (76-X) styrene, 10% DVB, 14% span 80, (e.g. for 15% silane. Styrene was decreased to 61%). Aqueous phase: 99% distilled water, 1% potassium persulphate. Phase volume = 90%, Dosing time = 10 minutes, Mixing time = 50 minutes. Polymerisation temperature = 60 °C, Polymerisation time = 24 hours.....	168
Figure 89: Three points, 1, 2 and 3 for EDX analysis of SL20. ....	169
Figure 90: EDX spectrum from the complete area of image in Figure 48. ....	170
Figure 91: SL20 point 1 EDX spectrum. ....	170
Figure 92: SL20 point 2 EDX spectrum. ....	171
Figure 93: SL20 point 3 EDX spectrum. ....	171
Figure 94: Plot of pore and interconnect sizes of SL-PHP samples for different mixing times. ....	173
Figure 95: Plot of pore and interconnect sizes of BZ20 PHP samples for different mixing times.....	173
Figure 96: Plot of surface area for various percentages of silane PHP with standard errors for mixing time of 40 minutes. ....	176
Figure 97: Plot of water uptake of silane PHP for different percentage of silane with various mixing times.....	178
Figure 98: FTIR spectrum for SL5 PHP .....	179
Figure 99: FTIR spectrum for SL10 PHP. ....	180
Figure 100: FTIR spectrum for SL15 PHP.....	180
Figure 101: FTIR spectrum for SL20 PHP .....	181
Figure 102: FTIR spectrum for SL25 PHP .....	181

Figure 103: FTIR spectrum for all SL-PHPs for comparison.....	182
Figure 104: Schematic diagram of the mixer/homogeniser utilised in the emulsion preparation. ....	185
Figure 105: Schematic representation of water in crude oil emulsion preparation .....	186
Figure 106: Photographic image of the Perspex (electrostatic) electric field separation cell after use. ....	188
Figure 107: (a) Schematic diagram of the demulsification setup. (b) Photographic image of the demulsification setup. ....	190
Figure 108: Crude oil viscosity of seven samples (Emulsion I-VII) of various levels of stability versus shear rate drawn on a logarithmic scale.....	193
Figure 109: Photographic representation of the bottle test performed on crude oil emulsions. ....	194
Figure 110: The progress of natural phase separation (demulsification) of the crude oil emulsion prepared at 2000 rpm mixing and 25 minutes agitation time.....	195
Figure 111: Difference of percent water separated with emulsion flow rate through the electrostatic separator at 5.0 kV ( $69 \text{ kV.m}^{-1}$ ) applied voltage immediately after emerging from separator in the presence and absence of PHP-I. ....	198
Figure 112: Difference of percent water separated with emulsion flow rate through the electrostatic separator at 5.0 kV ( $69 \text{ kV.m}^{-1}$ ) applied voltage, 1-hour after emerging from separator in the presence and absence of PHP-I. ....	199
Figure 113: Difference of percent water separated with emulsion flow rate through the electrostatic separator at 5.0 kV ( $69 \text{ kV.m}^{-1}$ ) applied voltage, 24-hour after emerging from separator in the presence and absence of PHP-I. ....	200
Figure 114: Difference of percent water separated with emulsion flow rate through the electrostatic separator at 5.0 kV ( $69 \text{ kV.m}^{-1}$ ) applied voltage immediately after emerging from separator in the presence of PHP-I, PHP-II, PHP-III, PHP-IV and absence of PHP (standard). ....	201
Figure 115: Difference of percent water separated with emulsion flow rate through the electrostatic separator at 5.0 kV ( $69 \text{ kV.m}^{-1}$ ) applied voltage, 1 hour after emerging from separator in the presence of PHP-I, PHP-II, PHP-III, PHP-IV and absence of PHP (standard). ....	202
Figure 116: Difference of percent water separated with emulsion flow rate through the electrostatic separator at 5.0 kV ( $69 \text{ kV.m}^{-1}$ ) applied voltage, 24 hours after emerging from	

separator in the presence of PHP-I, PHP-II, PHP-III, PHP-IV and absence of PHP (standard). .....	202
Figure 117: Difference of percent water separated with electric field strength at constant flow rate of 100 ml/min, immediately after passing through the separator in the presence and absence of PHP-I.....	203
Figure 118: Difference of percent water separated with electric field strength at constant flow rate of 100 ml/min, 1-hours after passing through the separator in the presence and absence of PHP-I.....	204
Figure 119: Difference of percent water separated with electric field strength at constant flow rate of 100 ml/min, 24-hour after passing through the separator in the presence and absence of PHP-I. ....	204
Figure 120: Difference of percent water separated with electric field strength at constant flow rate of 100 ml/min immediately after passing through the separator in the presence of PHP-I, PHP-II, PHP-III, PHP-IV and absence of PHP (Standard).....	205
Figure 121: Deference of percent water separated with electric field strength at constant flow rate of 100 mi/min, 1-hour after passing through the separator in the presence of PHP-I, PHP-II, PHP-III and PHP-IV and absence of PHP (standard). ....	206
Figure 122: Deference of percent water separated with electric field strength at constant flow rate of 100 mi/min, 24-hour after passing through the separator in the presence of PHP-I, PHP-II, PHP-III and PHP-IV and absence of PHP (standard).....	206
Figure 123: SEM micrograph of the PHP-I (a) before the separation experiment (at 500x magnification) and (b) after the separation experiment (at 500x magnification). ....	207
Figure 124: EDX spectrum of spent PHP-I adsorber/demulsifier. ....	208
Figure 125: Plot of water uptake of the original and spent PHP-I.....	209
Figure 126: Difference of percent water separated with electric field strength at constant flow rate of 100 ml/min, 24 hours after passing through the separator in the presence of original PHP-I, spent PHP-I and absence of PHP (standard).....	210
Figure 127: EDX spectrum of reused spent PHP-I adsorber/demulsifier.....	211

## NOMENCLATURE

<b>1- Roman Symbols</b>	
$a$	radius of cylinder
AC	alternating current
$A_M$	cross-sectional area occupied by each adsorbate molecule, $A_M = 0.162 \text{ m}^2$ for Nitrogen
API	American Petroleum Institute
$b$	half-length of cylinder
$B$	batch demulsification
BET	Brunauer, Emmet and Teller
BJH	Barret, Joyner and Halenda
$B_o$	static magnetic field
BP	bare plate
C	continuous demulsification or constant related to the enthalpy of adsorption
COD	Chemical Oxygen Demand
Col	column (vertical direction)
CT	coated tube
CV	circular vessel (with radial flow)
$d$	distance between the near surfaces of the two droplets
DC	direct current
$D_I$	impellers diameter
$D_s$	size of droplet
$D_o$	batch mixer diameter
$d_1$	density of liquid in the internal phase
$d_2$	density of liquid in the external phase
DVB	Divinyl benzene
DVLO	Derjaguin, Verway, Landau and Overbeek
$E$	Applied electric field
$E_{\text{crit}}$	Critical electrical field
EDX	Energy Dispersive Analysis with X-ray

FTIR	Fourier Transfer Infar Red
$G$	acceleration of gravity
GT	glass tube
HIPE	High Internal Phase Emulsion
HLB	hydrophilic-lipophilic balance
HPLC	High Performance Liquid Chromatography
$K_F$	flocculation factor
$K_o$	hydration factor
$M_v$	gram molecular volume (22414 mL)
MCPs	micro-cellular polymers
$N_A$	Avogadro's number
O/W	oil-in-water emulsion
$P_{eff}$	excess polarization per unit volume
PHP	PolyHIPE Polymer
$PI$	Process Intensification
$PIM$	Process Intensification and Miniaturization
$PM$	Process Miniaturization
$P_M$	Pressure of the dose manifold
$P_{M1}$	Initial manifold pressure
$P_{M2}$	Final manifold pressure
$P_o$	Saturation pressure
$P_s$	Sample pressure
$r$	particle radius
$R$	gas constant
$RD$	rectangular duct or relaxation delay
$RK$	Kelvin radius
SARA	Saturates, Aromatics, Resins and Asphaltenes
SEM	Scanning Electron Microscopy
$S_g$	specific gravity
$S_{th}$	surfactant thickness
$t_D$	dosing time
$t_H$	total mixing time

$T_M$	temperature of the dose manifold
$TV$	tubular vessel (horizontal direction)
$u$	sedimentation rate of the spherical particle
$V_A$	volume of aqueous phase
$V_{ads_n}$	volume adsorbed
$V_{d_n}$	volume dosed
$V_M$	volume of the dose manifold
$V_m$	volume of monolayer
$V_o$	oil phase volume placed in the batch mixer
$w$	oscillation frequency
W/O	water-in-oil emulsion

<b>2- Greek Symbols</b>	
$\varepsilon$	dielectric constant
$\varepsilon'$	infinite dielectric constant
$\varepsilon_o$	permittivity of vacuum
$\varepsilon_d$	interfacial dilatational elasticity
$\varepsilon_l$	dielectric constant of the continuous phase
$\varepsilon_m$	dielectric constant of the medium
$\gamma$	shear rate
$O$	a complex function of the electrical properties of the droplet and medium
$\psi$	interfacial tension
$\eta$	viscosity of the solution
$\eta_c$	viscosity of continuous phase
$\eta_d$	interfacial dilatational viscosity
$\eta_r$	viscosity of the continuous phase
$\eta_{rel}$	relative velocity
$\zeta$	zeta potential
$\Omega$	rotational speed of the impellers
$\phi$	volume fraction of internal phase
$\Phi$	dispersed phase volume (or simply phase volume)
$\Phi_m$	maximum volume of dispersed phase
$\Phi_o$	phase volume due to oil
$\Phi_s$	dispersed phase volume due to surfactant in the vesicles
$\Phi_{EW}$	water phase volume entrapped within the bilayers
$\mu$	viscosity of the emulsion
$\mu_o$	viscosity of the crude oil
$v_t$	terminal velocity
$v_v$	velocity of the vertical oil
$\rho_o$	density of the crude oil
$\rho_w$	density of the water

---

## CHAPTER ONE

---

### 1. INTRODUCTION

#### 1.1 Overview

Presently, the oil famously known as ‘black gold’ is a subject of extreme attention by most of the world because of its wide use as a major source of fossil fuel energy. According to the Organization of Petroleum Exporting Countries (OPEC), in 2017 alone, the oil consumption of the world was 96.3 million barrels per day. The prediction was for a rise in consumption to nearly 99.2 million barrels per day by 2020 and to 109.4 million barrels per day by 2040. At the end of 2016, the reserves of the world crude oil stood at 1,492.16 billion barrels (approximately 201 billion tones). Due to the huge demand for oil and the presence of great oil reserves, crude oil production has become economically significant for many countries in the world.

During the conventional production of crude oil, two phases (oil and water) are produced together; emulsions form when the fluid in the reservoir well bore or surface facilities is exposed to considerable mixing energy. As-produced oil and water phases form two different distributions of water and oil, namely the dispersion of oil droplets in water (oil in water) and water droplets in oil (water in oil). Oil in water (O/W) and water in oil (W/O) are known as the two fundamental types of suspensions in the field of oil extraction with the later one (W/O) being most common (95 % of cases). Owing to the natural presence of the colloidal dispersed active components, such as asphaltenes and resins, these emulsions are very stable. These components are accumulated at the water-oil interface and make the interface very rigid, which hinders the droplets from reforming. Contamination of crude oil with water content above 0.5% constitutes a quality problem and consequently results in the reduction of the oil price (Sjöblom *et al.*, 2003; Hemmingsen *et al.*, 2005). Except for micro-emulsions, all W/O emulsions are stable physically but unstable thermodynamically. Nevertheless, substantial time maybe required for the destabilization, and without some kind of mechanical or chemical treatment, a stable emulsion is incapable to resolve itself in an economically viable time period (Sjöblom *et al.*, 2003; Sztukowski and Yarranton, 2005).

In the down-stream processing of crude oil, in refineries for example, the W/O emulsions are created deliberately and then demulsified in order to “wash out” the contaminants which are present in water-crude oil emulsions (Yarranton *et al.*, 2000; Rane *et al.*, 2013). However, the stable emulsions cause catalyst fouling, and thus, are undesirable in most cases. Moreover, stable emulsions have higher volume and viscosity than their parent crude oil, which constitutes severe problems in downstream separation. In the petroleum industry, for example, stable water emulsions are formed during the oil drilling process, causing a critical problem for the water recycling equipment. This makes it hard for the facilities to comply with legislation on permeable discharge limits (Spiecker and Kilpatrick, 2004). In addition, the routine maintenance challenges are no less formidable. Hence, there is high need to remove these emulsions, among which are fats, oils and greases (FOGs) in order to avoid their deposition on pipes and fouling of the filtration media. These issues demand an efficient yet inexpensive equipment for emulsion separation (Yan *et al.*, 1999; Spiecker and Kilpatrick, 2004). The prerequisite for buying and maintaining expensive equipment results in a considerable rise in the operating and capital costs. Regrettably, the elimination of this highly stable emulsified water from crude oil has become a serious challenge for the petroleum industry worldwide.

For many years, regulation of the discharge levels of oil and other organic matter into the environment has become increasingly severe. With the reduction in the discharge limits, facilities find it increasingly difficult to comply. If the oil content of an aqueous fluid is only 30 ppm it may establish a safe discharge range when 50 ppm of organic waste in the discharge is allowed. However, a facility may face a severe strain on its discharge limit for total chemical oxygen demand (COD) that may comprise any compounds prone to oxidation. Every so often it is harder to remove certain compounds which are found in the process stream. FOGs simply cannot be ignored for the facilities endeavoring to recycle water in a closed loop process. Thus, it is highly desirable to efficiently remove dispersed water phase from the continuous oil phase for both environmental and chemical purposes and, being one of the major activities of the oil and petroleum industry, this accounts for millions of dollars in costs every year (Spiecker and Kilpatrick, 2004).

Due to the complicated interaction among the various factors, the fundamental mechanisms relating to the behavior of the water in-crude-oil emulsion are still not very clear. These influencing factors can be categorized into two major groups. First, the physical factors such as temperature, pressure, and interaction force, e.g. van der Waals force and Brownian motion. Second, the chemical effects induced by the naturally present impurities in the oil, e.g. resins,

surface-active agents, asphaltenes. It is quite hard to predict the chemical effects on the different emulsion systems due to the wide variety of crude oils extracted from different geographic resources and varying methods of extraction. Therefore, an efficient and a successful method for the processing of a particular type of crude oil emulsion may not be successful for another type of emulsion. In the worst case scenario, a particular extraction method may itself further stabilize a certain crude oil emulsion (Jang and Lee, 2000; Pekdemir *et al.*, 2003b; Zhang *et al.*, 2016). As most of the oil drilling practices take place in offshore places, it is necessary for the process to be effective, intensive, compact and robust. For achieving an effective separation system, it is essential to better understand the behavior of oil-water systems, including surface-active materials in real life conditions.

A number of chemical and mechanical methods have been reported for the breakdown of petroleum emulsions. Most common among them are the hydrocyclone, pH adjustment, centrifuges, steam/air stripping, chemical additives, filters, and electrical treatments. Although most of these are proven to be reliable separation approaches, the conventional techniques may take days, weeks or even months for the treatment of these emulsions owing to the large hydraulic residence time with increase in production. The conventional mechanical systems with water flows produced need considerable settling volumes and have therefore resulted in large and costly facilities. Thus, these processes are not ideal if the space is a limiting and determining factor, especially on oil grid platforms. Moreover, the bulk size of the equipment and enlarged hydraulic residence time will lead to a dramatic increase in the amount of energy consumed during operation, consequently increasing the operational cost (Zhang *et al.*, 2016). Therefore, limiting the size and number of installations would offer significant economic benefits. In comparison with other techniques, the electrostatic separation approach has numerous advantages, such as low power consumption, no need of chemical addition, and virtually breakdown-free operation owing to the absence of moving parts (Lee *et al.*, 2001). However, due to the lack of a fundamental understanding of the electrostatic process and its working mechanisms, currently existing electro-coalesces are still quite large and unsuitable for offshore facilities (Theron *et al.*, 2001).

One of the possible solutions to this issue is to make fundamental changes in the existing method, which can result in the reduction of the processing volume without facing any compromise on the output magnitude and quality. This design philosophy is known as process intensification (PI). PI represents a novel design strategy, which can lead to energy, capital, safety and environmental benefits through a reduction in the processing volume by at least one

order of magnitude, which may go up to 3 or 4 orders. Historically, the growth of PI was majorly based on cost reduction, given that a considerable part of the design cost is associated with the structure, support structure, piping and other mechanical or civil engineering objects (Stankiewicz and Moulijn, 2002; Van Gerven and Stankiewicz, 2009). The scope of original PI can be broadened by integrating it with another design strategy known as Process Miniaturization (PM), which is commonly implemented in biological and chemical areas, meanwhile the significance of the miniaturization in intensification can be highlighted.

The integration of Process Intensification and Miniaturization (PIM) generates a synergy in acquiring the main design aim, and objectives as well as other advantages given below (Mills *et al.*, 2007; Pohar and Plazl, 2009; Akay, 2014):

- A renewable operation.
- Supply a novel intensification operation by utilizing novel products.
- Reduce the size of a process device by ten times.
- Removal of the undesirable by-products.
- A platform for other technologies.
- Plant re-activity, safety and mobility.

The philosophy of PIM design has been applied as a base of designing a specific process for water-in-crude oil separation in this project. The conventional electrostatic demulsification technique used in previous studies (Akay *et al.*, 2004; Hayman *et al.*, 2005) was used along with micro-porous polymers to achieve an integrated and simultaneous separation. In this study, additional modifications and an optimization process based on the principle of PIM were used to create appropriate forms of the polymers for the water-in-crude oil separation process. Whereas this study was only bench-scale utilizing existing facilities, with more optimizations and accurate scale up, the feasibility of this technology for the future utilized in application at the industrial-scale can be envisaged. This study provides a baseline for developing intensive and cost effective technologies for the demulsification of crude oil that can be used in actual plant in the coming years.

The separation process and methodologies that are used to typify the reaction of crude oil-water-demulsifier can likewise be used with other W/O emulsions like those used in industry e.g. nuclear reprocessing where the emulsions are stabilized by nanoparticles and surface

active factors corresponding to the water-in-crude oil emulsions considered here (Vickers, 2001; Noor, 2006).

## **1.2 The Aims of Thesis**

This study aims to develop a continuous, non-chemical demulsification method to increase the efficiency of the water separation process and remove the surface-active species from high stability water-in-crude oil emulsions based on the use of PolyHIPE Polymer (PHP) combined with an electrostatic technique. PolyHIPEs have many good features to play this role such as a high efficiency for the elimination of metal ions via a mechanism of ion exchange as well as the ability to adsorb organic toxins because of the hydrophobic and hydrophilic domains on the porous structure walls (Akay *et al.*, 2005a). Moreover, these are highly efficient as demulsifiers to remove the water and surface-active species from the water-in-crude oil emulsions (Akay, 1995). In addition, the electrostatic technique used has the appropriate features to achieve the objective of this study such as low power consumption owing to the low electrical current through dispersion (Lee *et al.*, 2001). In addition, this technique is free from mechanical breakdown because it is independent of moving parts. Moreover, it has the ability to be combined with different techniques such as, chemical emulsification, centrifugal separation, hydrocyclones, etc. in order to promote positive synergy for water removal (Eow and Ghadiri, 2002). This can be achieved by creating the coalescence of the dispersed (water) phase droplets, which are stabilised by the indigenous surface-active species present in the emulsion such as organic carboxylates, phosphate, oxides, asphaltenes and the like (Pekdemir *et al.*, 2003a), and collecting them in the PHP absorber.

- **The Oil and Aqueous Phases Characterisation:**

In this study, preparation and characterisation of model oil phases for the emulsions is done in regards to:

- 1) Distribution of the hydrocarbon chain.
- 2) Type and concentration of surfactant.
- 3) Dependence of viscosity, utilising a viscometer.

Artificial brines and other aqueous phases have been synthesized to mimic the aqueous phases that are representative of seawater.

- **Preparation and Characterisation of the Model Oil Emulsions:**

Water-in-crude oil and crude oil-in-water emulsions have been prepared utilising well-characterised crude oils and aqueous phases/industrial brines.

- **Determination of the Demulsification Mechanism:**

This is executed by utilising different PHPs, which were prepared in this study as demulsifiers. The concentration of surfactants (resins, phenols, carboxylic acid, metals ions, asphaltenes and multifunctional compounds), in the crude oil, in the emulsion and in the PHP demulsifier will be determined utilising Energy Dispersive Analysis with X-rays (EDX) and Scanning Electron Microscopy (SEM). The behaviour of indigenous surfactants in the PHP demulsifier and the mechanism of proposed demulsification is evaluated.

- **Preparation of PolyHIPE Polymer Demulsifiers with Controlling of Microstructure.**

Demulsifiers of PHP were prepared by utilising the present facilities at Newcastle University after some modification. The method reported (Akay, 1995; Akay and Vickers, 2003; Akay *et al.*, 2004; Akay *et al.*, 2005a) is utilized to get micro-cellular polymers MCPs with ranging of pore size ( $D$ ) ranging from 0.5  $\mu\text{m}$  to 250  $\mu\text{m}$  and the interconnecting hole size ( $d$ ) ranging from  $0 < d/D < 0.5$ . These PHP polymers are chemically functionalised to get sulphonated PHP demulsifiers.

The base PHP material is a styrene-based poly-HIPH that is made hydrophilic by sulphonation after manufacture. This generates a lot of acid waste so an alternative material was made with sulphuric acid in the aqueous phase during production (in-situ sulphonation). Only certain

chemical sites on the PHP surface can be sulphonated and are attractive for water adsorption. Thus, other surface functionalisation was investigated. SiO<sub>2</sub> is known to be a good desiccant so this was incorporated at the PHP surface by addition to the aqueous phase. To achieve a similar silicon addition a silane was added to the oil phase. These were tested with and without sulphonation.

### 1.3 Thesis Overview

This thesis contains the works conducted during the research period. The thesis consists of eight chapters.

- 1) The first chapter gives an idea of the production capacity and consumption of crude oil over the past few decades, as well as providing a summary regarding crude oil and its emulsions and the aims of this thesis. Moreover, PI processing, oil and aqueous phase characterisation, preparing and characterisation of the model oil emulsion and determination of the demulsification mechanism are also discussed in this chapter.
- 2) The second chapter contains a summary of the physical and chemical properties of crude oil and its hydrocarbon fractions, principles of emulsion formation and the issues of emulsion stability as clarified in the literature. Also, the problems of crude oil emulsions, methods for demulsification of water-in-crude oil emulsions and the current techniques used in demulsification (especially electrical techniques) and factors affecting their performance are reviewed.
- 3) The third chapter is divided into two parts:
  - The first part of this chapter explains the theory of destabilization of water-in-crude oil emulsions with regards to high voltage electric fields. Further, this part also discusses the related work done by other researchers in support of the enhancement process of destabilization of a highly stabilized water-in-crude oil emulsion on applying an electric field (with a high voltage) which, is the focus of the current study.
  - The second part of this chapter provides a brief description of the PolyHIPE material according to the literature in terms of preparation, characteristics, applications, properties, morphology and the factors affecting it as well as the sulphonation process to control hydrophobicity/hydrophilicity.
- 4) The fourth chapter is again in two parts:
  - The first part of this chapter describes the apparatus and experimental procedure used for the preparation of the four kinds of polyHIPEs namely

Silane polyHIPE, Bindzil polyHIPE, standard sulphonated polyHIPE and in-situ sulphonated polyHIPE. Moreover, the potential operating conditions of each type, as well as the effect of PHPs sulphonation are also explained.

- The second part of this chapter describes the various analytical instruments utilised to analyse the properties of the PHPs, crude oil and the crude oil emulsions.
- 5) The fifth chapter discusses the characterization results of the prepared PHPs such as morphology, pore size distribution, surface area, water uptake, FTIR analysis and scanning electron microscopy (SEM). The aim is to select the best materials for the demulsification tests.
  - 6) The sixth chapter presents the apparatus and experimental procedure that were used to prepare a highly stable water-in-crude oil emulsion and describes the demulsification process of these emulsions (using the electrostatic technique). The effect of emulsification variables on the stability and viscosity of the emulsions as well as the conductivity measurement of crude oil emulsions are also presented.
  - 7) The seventh chapter presents and discusses the results of the effect of inlet flow rate variation of water-in-crude oil emulsion and the variation of electric field strength on demulsification. The results of the reuse of spent PHP (which is collected after demulsification process) in a following demulsification process are also discussed in this chapter.
  - 8) The eighth chapter summarises the contributions, problems and achievements of this project. In addition, it offers conclusions on the utility of the enhanced crude oil/water separation process as well as discusses the significant findings and future work requirements.

---

## CHAPTER TWO

---

### 2. LITERATURE REVIEW: THE EMULSION AND DEMULSIFICATION OF WATER-IN-CRUDE OIL

#### 2.1 Overview

This chapter of the thesis includes two major parts.

- The first part gives a summary and pertinent literature about crude oils and their emulsions in terms of the nature, the physical and chemical properties of crude oils as well as their hydrocarbon fractions, primarily resins and asphaltenes because of their responsibility for the formation of high stability crude oil emulsions. In addition, the essential principles and the problems related to the formation of water-in-crude oil emulsions and their stability are briefly described, highlighting the requirement for demulsification of water-in-oil emulsions and reliable separation processes.
- The second part surveys the available methods of the destabilisation of water-in-crude oil emulsion including the process of electrically-enhanced demulsification, which is the method of interest in this research.

#### 2.2 Crude Oil

Crude oil is a naturally occurring liquid created by the remains of animals and plants that died millions of years ago. These remains were deposited in layers over time, compressed and mineralised and they are termed “fossil fuels”. It comes in four types; specifically, light oils, very light oils, medium oils and heavy fuel oils. It can be processed to produce various products, such as diesel, gasoline and petrochemicals. When pumped out of the land or subsea wells, crude oil consists of a complex mixture of many chemical components, primarily organic compounds (hydrocarbons) that typically comprise in the region of 95% of the crude oil, though a hydrocarbon content as low as roughly 50% has been observed in the past. It should be mentioned that these hydrocarbons differ in relation to toxicity and degradability. They include highly volatile, light materials, for instance benzene and propane, besides heavy compounds like asphaltenes, bitumen, waxes and resins. The rest consists of water and minute amounts of

nitrogen and sulphur, along with traces of a number of other elements, predominantly metals like iron, copper, nickel and vanadium (Speight, 1999; Speight, 2004b). As a result of their complex chemical composition, it is hard to determine the exact amount and structure of each molecule found in crude oils. Scientists and chemists choose crude oils in relation to their chemical composition and functional groups, though the petroleum industry tends to categorise them according to their geographical location.

The crude oil composition is reliant on the ‘raw material’ which originally formed the crude, in addition to the conditions that existed both when it was being created and afterwards. Both the chemical composition and physical properties differ from one another and even with regard to different depths in the same well. Even with these variations in the properties, every crude oil is distinctive. The physical and chemical properties such as chemical compositions, surface tension, density, viscosity and specific gravity of the parent crude oil have a vital effect on the behaviour of the water-in-crude oil emulsion (Andersen and Speight, 2001). Nevertheless, it is crucial to point out that it is impossible to predict the properties of the emulsion, because its creation and stability are dependent on the complex interaction between the various elements and compounds found in the crude oils.

### 2.3 Physical Properties of Crude Oil

Crude oil is extracted from the earth in various forms, commonly black in colour, but sometimes its colour is red or brown (Sjöblom *et al.*, 2003). There are two types of crude oil "light" and "heavy" which are classified based on the American Petroleum Institute (API) gravity. The API gravity of light (thin and volatile) crude oil ranges from 30-40 degrees, suggesting that the density is much lower than 1.0 gm/cm<sup>3</sup>, thus they float easily above the water. While, the API gravity of some heavy crude oils is lower than 12 degree so, they sink and cannot float on the water (Ghannam *et al.*, 2012). Eq.1 shows how the API gravity accounts for all petroleum liquids.

$$APIgravity = \frac{141}{Sg} - 131.5 \quad Eq. 1$$

where

Sg: represents the specific gravity (at 15° C (60°F)) of the petroleum liquid required to measure. Figure 1 shows API gravity versus specific gravity for the main types of crude oil (light and heavy) and others processed variants.

Clark and Pilehvari (1993) indicated that the range of crude oil viscosities is between 2000 and 500.000 centipoise or between 2.0 and 500 Pa.s. According to the outcomes of the experimental study by Werner *et al.* (1998) the viscosity of crude oil is directly proportional to its composition. Figure 2 displays that the crude oils viscosity is dramatically increasing with the concentration of asphaltenes within it.

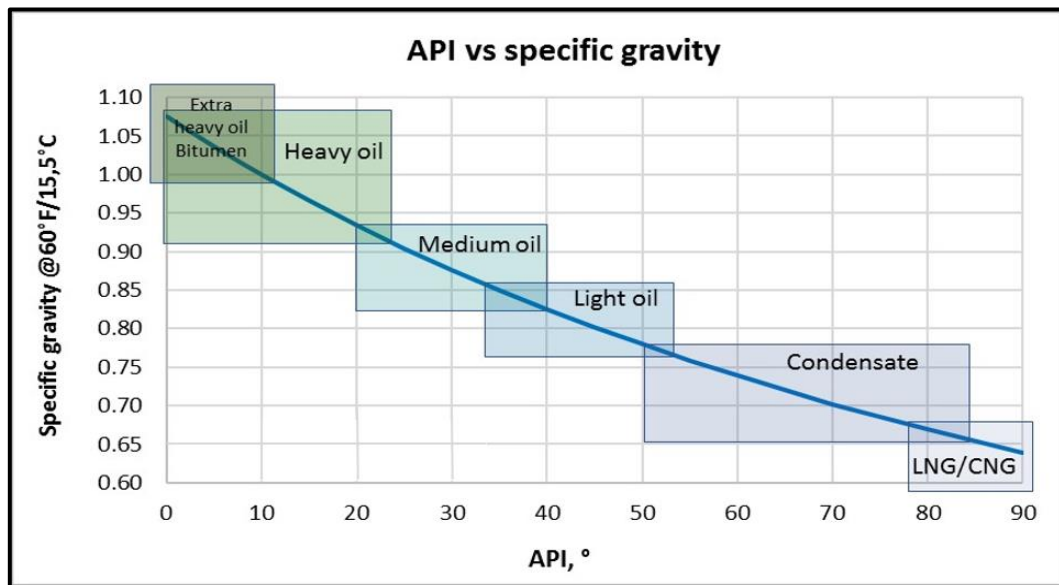


Figure 2: Diagram representing API gravity versus specific gravity for the main types of crude oil (light and heavy) and others hydrocarbons ('The enignnering toolBox,' 2019).

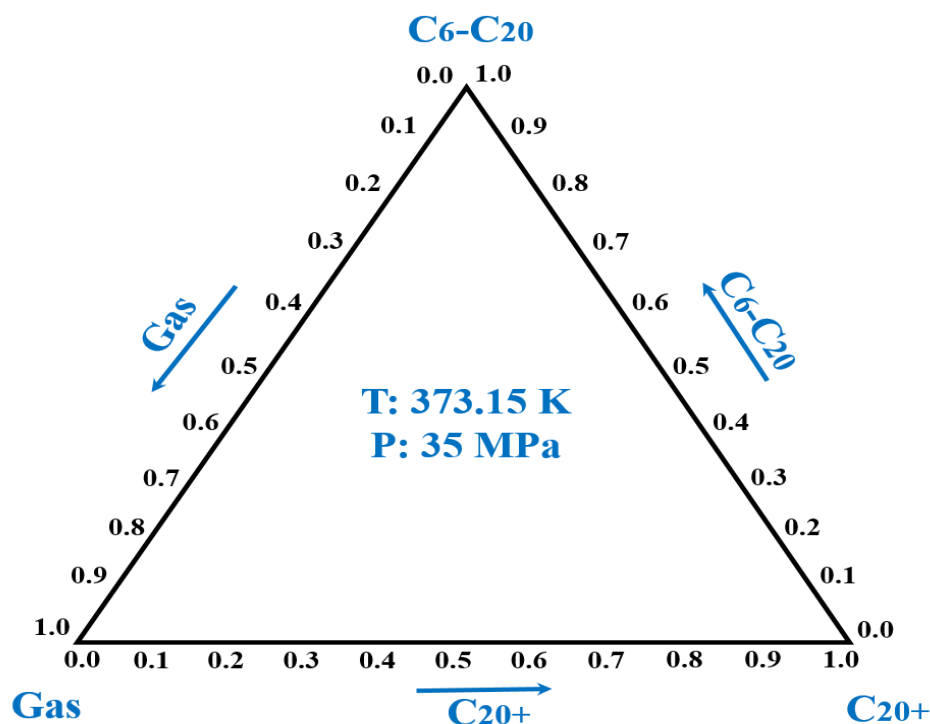


Figure 1: Measured dynamic viscosity (mPa.s) as a function of the composition of asphaltene (weight %) in a tripartite diagram based on measurement thirteen of artificial crude oils at 100°C and 35 mPa.s (Werner *et al.*, 1998; Cameron, 2005).

## 2.4 Chemical Properties of Crude Oil

Crude oils contain asphaltenes and resins, which are the main constituents of the crude oils polar fraction. The asphaltenes and resins, combine easily with other solids (inorganic and organic), reduce the interfacial tension between water and oil and lead to the formation of stabilized interfaces. These factors are responsible for the development of high stability emulsions (Lee, 1999; Ali and Alqam, 2000; Aske *et al.*, 2001; Demirbas and Taylan, 2016). There are many characterisation techniques like the SARA method used to characterize such emulsions composed of highly stable organic components together with other ingredients of crude oil (Speight, 2004a). The method of SARA-separation is a chemical-based group technique based on variations of polarity and solubility of the organic components of the emulsion that fractionate crude oil into four prime fractions; i- saturates (S) ii- aromatics (A) iii- resins (R) iv- asphaltenes (A) as displayed in Figure 3.

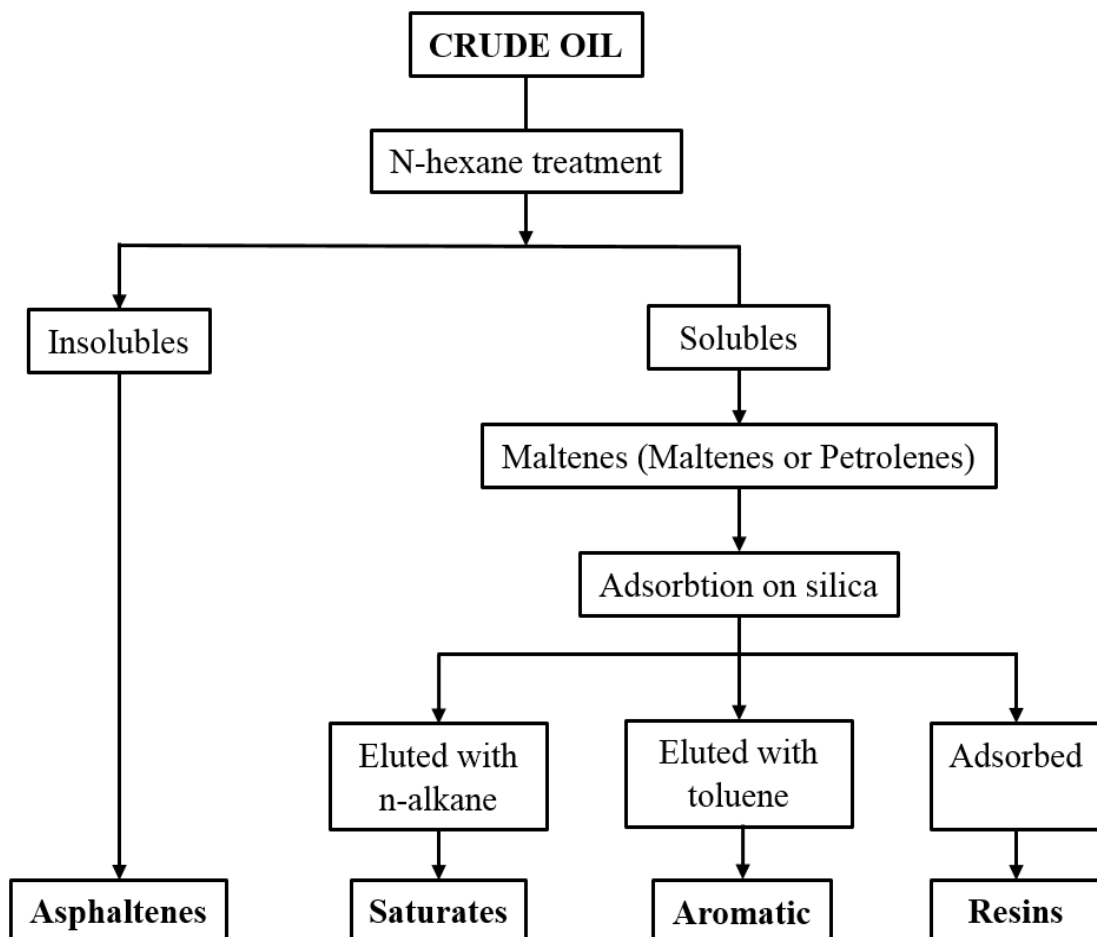


Figure 3: Block diagram of the typical SARA-separation (Demirbas and Taylan, 2016)

Treatment of crude oil with alkenes such as n-heptane, n-hexane or n-pentane is the first step (the precipitation) in the characterisation method (SARA) to eliminate the asphaltenes (Aske, 2002). Further High Performance Liquid Chromatography (HPLC) separates out the remaining ingredients of deasphalted oil into saturates, aromatics and resin fractions (Aske *et al.*, 2001). Nevertheless, due to the difficulty of distinguishing resins and aromatics compounds, other technique of separation are commonly utilised in addition.

The four fractions (groups) resulting from the method of SARA-separation are divided into two portions (soluble and insoluble). The insoluble portion called the residue includes asphaltenes which have the highest molecular weight (heaviest) and is the most polar fraction existing in the crude oil. These show insolubility in aliphatic hydrocarbons, which have comparably low-molecular weight. The soluble portion which is composed of the other three groups (saturates, aromatics and resins hydrocarbons) is called maltenes and is separated by means of HPLC (Andersen and Speight, 2001; Speight, 2004a). Table 1 illustrates the weight percentages (wt. %) of the main classes of the crude oil compounds which, are usually categorized under the SARA method. In the next sections, the chemical composition of these four groups in crude oils will be discussed.

Table 1: The weight percentages (wt. %) of the main classes of the crude oils compounds (Fingas, 2014).

Type of crude oil	Saturates	Aromatics	Resins	Asphaltenes
Light Crude <sup>a</sup>	91	8	1	0
Medium Crude <sup>b</sup>	78	15	6	1
Heavy Crude <sup>c</sup>	38	29	20	13
Diluted Bitumen <sup>d</sup>	25	22	33	20

a: Scotia Light, b: West Texas Intermediate, c: Sockeye Sour, d: Cold Lake Blend.

#### **2.4.1 Saturates of Crude Oil**

The saturates are the largest fraction in most crude oils. Generally, saturate appears in the form of a pale-yellow oily liquid but can appear as a bright green liquid when it has low viscosity. It consists of nonpolar, single-bond (without double bonds) hydrocarbons containing simple straight-chain paraffins and branch alkenes or isoprenoids, as well as cycloalkanes (naphthenic) which consist of one or more rings along with some alkyl side chains (Demirbas, 2016). In

addition, the saturates include wax which has some effect on the crude oil emulsion stability. According to the elemental analysis results reported by Ali *et al.* (1989) the hydrogen content of saturates is the highest, followed by resins, aromatic and asphaltenes. Rudzinski *et al.* (2000) showed that the saturate has a higher hydrogen/carbon ratio than resins, aromatics and asphaltenes. Figure 4 illustrates a schematic structure of the saturate in crude oil.

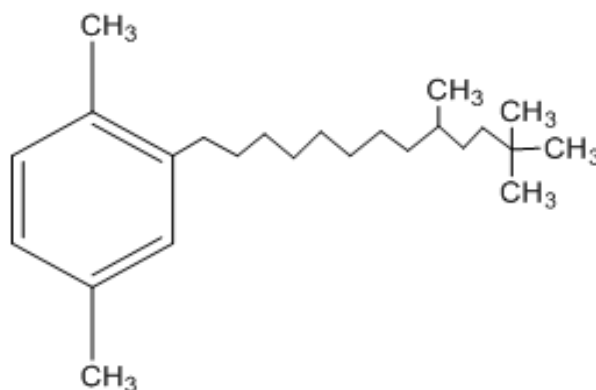


Figure 4: Hypothetical structure of a crude oil saturate (Yasar *et al.*, 2009).

#### 2.4.2 Aromatics of Crude Oil

Aromatics, so named because of having a unique and special smell, as well as the aromatic ring structure which is demonstrated by the existence of one or more of six-carbon rings, where, the carbon atoms connected to their carbon molecules by single and double bonds alternately (Ali *et al.*, 1989). This may be considered as a delocalised  $\pi$ -bonded structure where all the carbons in the ring are equivalent. Generally, they are nonpolar and immiscible with water. Because of their non-reactive nature, they are often used as a good solvent for another non-polar compounds. Recently, many different aromatic compounds were found in crude oil. One-ring aromatics are often referred to as BTEX, and are widely abundant; the most common are benzene and its derivatives that have similar structure, for example ethyl benzene, xylenes and toluene (Akmaz *et al.*, 2011). The naphthalenes are the more common aromatic compounds with two aromatic rings. In addition, they are distinguished by a sooty yellow flame due to their high carbon-to-hydrogen ratio (Armit and Robinson, 1925). They are classified based upon the number of aromatic rings existing in the molecules such as mono-, di- and tri-aromatics. Figure 5 displays the schematic structure of the aromatics in crude oil.

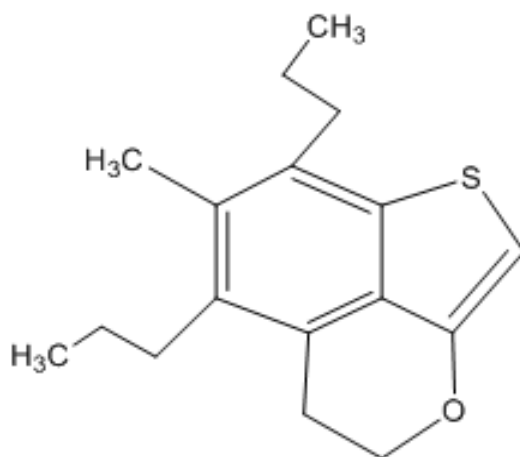


Figure 5: Hypothetical structure of a crude oil aromatic (Akmaz *et al.*, 2011).

### 2.4.3 Resins of Crude Oil

The resins fraction of hydrocarbon components in the crude oil is in the form of wax, involving polar molecules, which often contain heteroatoms such as oxygen, sulphur or nitrogen (Demirbas, 2015). The resin has a solubility in light alkanes like heptane and pentane, while, it is insoluble in liquid propane. A few studies have been mentioned in the literature with respect to resin properties (Aske *et al.*, 2001). The hydrogen/carbon ratio of resins is around 1.2 to 1.7 times higher than that found in asphaltenes; the hydrogen/carbon ratio of asphaltenes is around 0.9 to 1.2. The molecular structure of the resins is similar to that in asphaltenes, but with a lower molecular weight (lower than 1000 g/mol). The resin is a significant component with respect to the properties of crude oil, as naphthenic acids are usually considered as a partition of the resins (Ficken *et al.*, 2002). Figure 6 illustrates the schematic structure of a resin in crude oil.

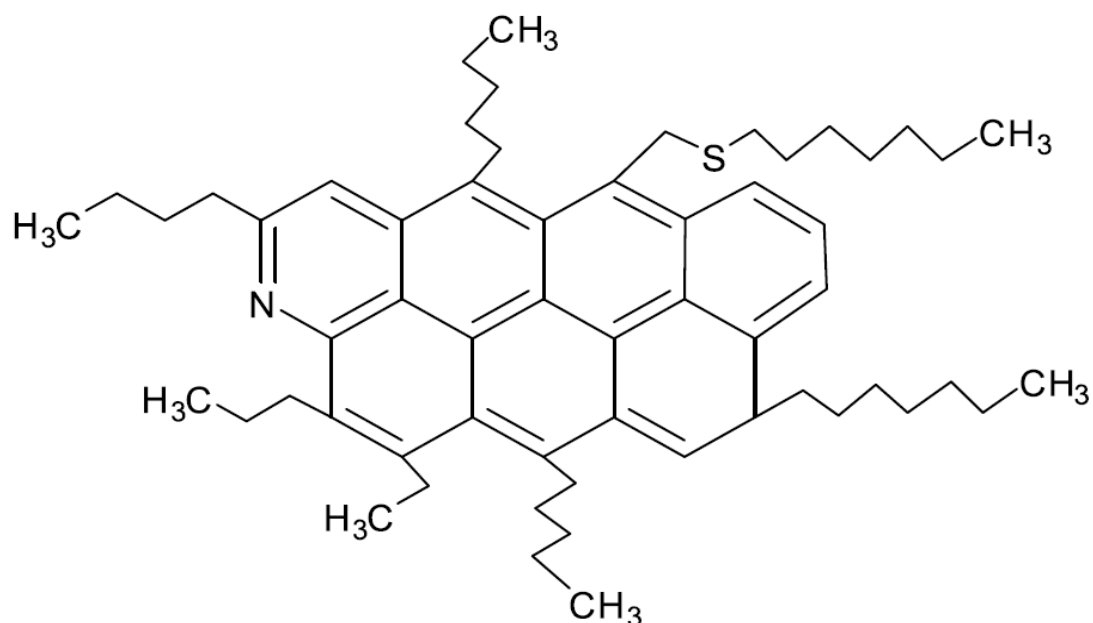


Figure 6: Hypothetical structure of a crude oil resin (Akmaz *et al.*, 2011)

#### 2.4.4 Asphaltenes of Crude Oil

The asphaltenes are usually defined depending upon their solubility due to their molecular complexity. In general, asphaltenes are the solid fraction of the crude oil with a high molecular weight that are precipitating in low-boiling alkanes like the heptane, pentane or hexane, but are soluble in aromatics such as ethyl benzene, benzene and toluene (Demirbas, 2016). The asphaltenes include the highest percentage of heteroatoms including nitrogen 0.6-3%, sulphur 0.3-10% and oxygen 0.3-5%, as well as metals like nickel, vanadium and iron (Suzuki *et al.*, 1982). Asphaltenes are characterized with a deep red color when dissolved at a low concentration in toluene or in benzene. The presence of asphaltenes is the cause of the black color of some crude oils and residues (Demirbaş, 2002). The structure of asphaltenes are condensed systems of polynuclear aromatic rings which have alkyl side chains. The measurement of the exact molecular weight of the asphaltenes is difficult because of the inclination of molecules to self-assemble, but researchers believe it is between 500-2000 g/mol (Aske, 2002). Moreover, the number of the asphaltene rings can differ between the 6 and 15 (Suzuki *et al.*, 1982). Experimentally, Yen (1974) proved that the hypothetical formula of asphaltenes is  $(C_{74}H_{87}NS_2O)$ . Figure 7 shows a schematic structure of the asphaltenes in crude oil.

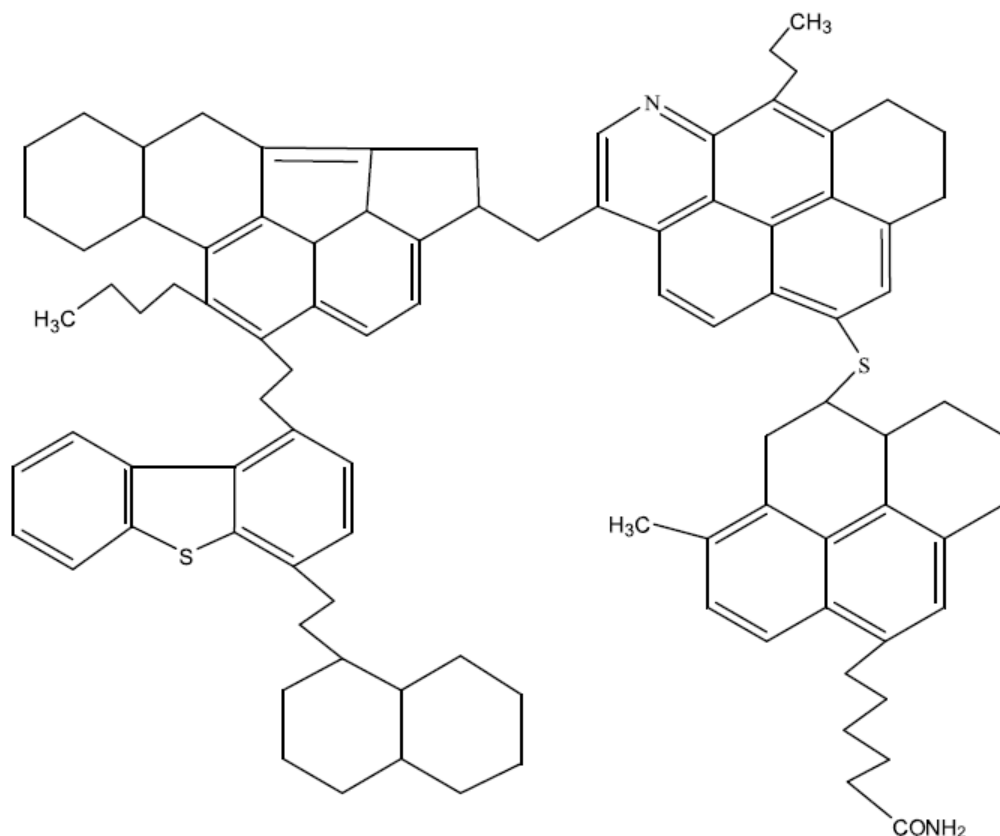


Figure 7: Hypothetical structure of a crude oil asphaltene (Andersen and Speight, 2001)

## 2.5 Water-Oil Emulsions

A system consisting of two or more immiscible liquids (such as water and oil) where one of them is mono/poly dispersed in the other is called an emulsion system. For example, when water is dispersed in oil with the droplet size in the range of 10-100 microns, the resulting system is called a water-in-oil emulsion (w/o) (Johansen *et al.*, 1988; Hajivand and Vaziri, 2015). Similarly, when oil is dispersed in water, the oil-in-water emulsion (o/w) is produced. In this study the dispersed phase is sometimes denoted as internal phase and the other continuous phase is referred as external phase. Emulsions are classified into three categories based on their droplet size: 1) micro-emulsions (10-100 nm), 2) mini-emulsions (100-1000 nm), 3) macro-emulsions (0.5-100  $\mu\text{m}$ ) (Jafari *et al.*, 2008; Subramaniyan *et al.*, 2014). According to the rule of thumb the emulsion is more stable if the average size of the droplets of the dispersed phase is smaller. The droplet size distribution of the resultant emulsion is influenced by the nature of emulsifying agents, interfacial tension, presence of solids and shear and bulk properties of both water and oil (Dudášová *et al.*, 2009; Giraldo *et al.*, 2013). Generally, all the emulsions other than micro-emulsions are thermodynamically unstable,

however, due to the presence surface active compounds these emulsions are kinetically stable for months or even years (Angle, 2001; Drelich *et al.*, 2010; Ekott and Akpabio, 2010; Pradilla *et al.*, 2015). An emulsion is stable if its structure does not alter with time regardless of how it was prepared and consists of small water droplets with low conductivity (Fingas, 1995; Márquez *et al.*, 1996; Robins *et al.*, 2002; Roodbari *et al.*, 2016). The emulsion stability is influenced by the difference between the density of phases, oil phase viscosity, interfacial viscosity, interfacial tension, water droplet size, film compressibility, surfactant concentration, electrolyte concentration and by operating conditions (Menon and Wasan, 1984; Isaacs *et al.*, 1990). For example, high emulsion stability is required for long duration in the food industries, while in crude oil processing the main focus is to destabilize these undesirable stable emulsions, which is a complex, difficult and costly task (Boode and Walstra, 1993; Fredrick *et al.*, 2010). Figure 8 shows both emulsions.

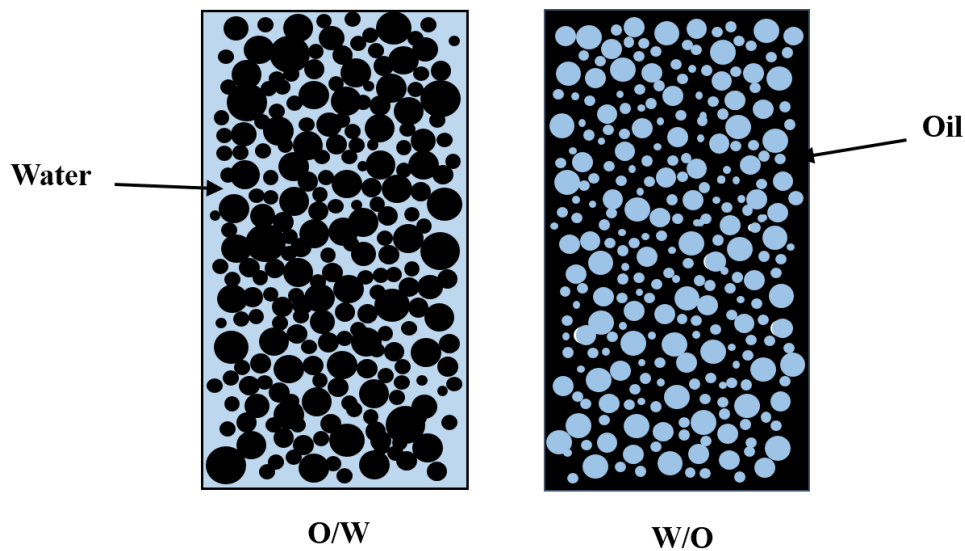


Figure 8: Schematic diagram of emulsion types (Kilpatrick and Spiecker, 2001)

Generally in the oil industry, emulsions are either regular emulsions i.e. w/o referring to oil fields or reverse emulsions i.e. o/w which account for the 5% of the resultant emulsions (Fingas, 1995; Fingas *et al.*, 2001; Abdurahman *et al.*, 2007; Fingas and Fieldhouse, 2009; Ekott and Akpabio, 2010; Feng *et al.*, 2011; Hou *et al.*, 2012). Bancroft's rule, which was formulated in the second decade of the twentieth century, is used to determine the type of emulsion. This rule states that an emulsion's continuous phase is the one in which the surfactant is favourably soluble. Therefore, a surfactant with high solubility in water will prefer the formation of o/w emulsion; similarly, a surfactant with better solubility in oil phase will favour the forming of w/o emulsions (Akay *et al.*, 1998; Kronberg and Lindman, 2003; Langevin *et*

*al.*, 2004; Martínez-Palou *et al.*, 2011; Hoshyargar and Ashrafizadeh, 2013). This rule was used until Griffin presented the Hydrophile-Lipophile balance (HLB) number concept in 1949. HLB gives a quantitative measurement of Bancroft's rule. It is an important variable in finding the emulsion type depending on the molecular composition and structure of the surfactant. The HLB number has a maximum value of 20. Low values of HLB number refer to the hydrophobic surfactants with better solubility in oil; on the other hand higher values of HLB number indicate the hydrophilic nature of the surfactants which help in the formation of o/w emulsions (Davis, 1994; Binks, 2002; Vander Kloet *et al.*, 2002; Li *et al.*, 2016b). The HLB number has been widely used to determine the emulsion type, however, it does not consider other factors involved such as oil phase nature, additives in the aqueous phase, temperature effects, interactions between the oil phase and water phase and other lipophilic groups present in the emulsions. Moreover, the volume ratio of both phases can also define the resultant emulsion type because the phase with smallest volume will be the dispersed phase (Abdurahman *et al.*, 2007; Ekott and Akpabio, 2010; Roodbari *et al.*, 2016), Table 2 gives various models of petroleum emulsions (Roodbari *et al.*, 2016).

Table 2: Models of emulsions in the industrial extraction and refining of petroleum (Roodbari *et al.*, 2016).

Occurrence		Usual type
Desirable Emulsion	Emulsion drilling fluid, oil-emulsion mud.	O/W
	Heavy oil pipeline emulsion.	O/W
	Oil sand flotation process slurry.	O/W
	Enhanced oil recovery in situ emulsion.	O/W
	Emulsion drilling fluid, oil-base mud.	W/O
	Asphalt emulsion.	O/W
Undesirable Emulsion	Fuel oil emulsion (marine).	W/O
	Oil sand flotation process, dilute forth.	W/O or O/W
	Well-head emulsion.	W/O
	Tinker bilge emulsion.	O/W
	Oil spill mousse emulsion.	W/O

In real world applications in the petroleum industry, these emulsions are formed by different routes. For example, for transportation purposes it is necessary to reduce the viscosity of a heavy crude oil and o/w emulsions are formed with a viscosity between 1000 cP to 100000 cP at 25 °C (Zaki, 1997; Ahmed *et al.*, 1999; Abdurahman *et al.*, 2012; Azodi and Nazar, 2013). Though it could be achieved by heating or by adding low viscosity hydrocarbon diluents, these approaches are either expensive, inconvenient or impossible in many situations. As an

alternate, a heavy crude oil viscosity is reduced to 200 cp by addition of water to make it suitable for pipeline flow (Zaki, 1997). As a consequence, the o/w emulsion is deliberately prepared. This practice is also common in the metal finishing industries, most of the chemical industries and refineries (Simões *et al.*, 2010). Further details about these emulsions and the methods to break them are beyond the scope of this study and therefore are not presented here; however, these are studied in a series of publications (Lipp *et al.*, 1988; Faibish and Cohen, 2001; Lobo *et al.*, 2006; Gutiérrez *et al.*, 2008; Qiu *et al.*, 2009). Similar emulsion systems are encountered throughout the exploration, processing and transportation of crude oil. Emulsion based systems have become an important subject of investigation due to the widespread use of w/o emulsions.

### **2.5.1 Water-in-Oil Emulsion Formation**

Water-free-crude oil seldom exists (Quintero *et al.*, 2009; Maia Filho *et al.*, 2012). About 10-60% of the produced crude oil is water depending on the conditions of the oil reservoir (Aveyard *et al.*, 1990; Zaki *et al.*, 2000). Actually, in the oil industry there have been numerous processes which enhance the formation of emulsions. In a virgin reservoir crude oil naturally exists together with gas and water and this is a reservoir-wide property (Mohebbali *et al.*, 2012; Zhang *et al.*, 2013; Oliveira *et al.*, 2017). A large quantity of divalent cations are present in this water such as Magnesium, Calcium, Strontium and Barium (Marlow *et al.*, 1987; Dudášová *et al.*, 2009). The quantity of this water is expected to increase from both offshore and onshore fields where the environment of production is more risky, challenging and expensive. In order to help the crude oil come out of a depleted reservoir, water is injected into it in order to enhance the oil recovery (Sullivan *et al.*, 2007; Fakhru'l-Razi *et al.*, 2009). As a consequence, some amount of this water is coproduced with oil as free water and some of the water in emulsion form because of dropping pressure in valves and turbulence at the wellhead (Dudášová *et al.*, 2008; Maia Filho *et al.*, 2012). This artificial water consists of dissolved organic compounds, minerals, suspended solids, heavy metals and chemical additives from the production line. It is quite easy and quick for the free water to settle out but other treatment techniques are required to extract the water in emulsion form (Schoeggl *et al.*, 2002; Zehetner *et al.*, 2009).

In order to prevent refinery catalyst fouling and equipment corrosion the crude oil requires desalting by washing with water. Therefore, in the preliminary refinery treatments the crude oil is brought into contact with water where interactions take place and the water becomes

emulsified in the oil. Moreover, stable emulsions are also generated in heavy oil production fields where hot water is utilized for the extraction of bitumen (Bhardwaj and Hartland, 1998; Sams and Zaouk, 2000; Chiesa *et al.*, 2005; Sullivan *et al.*, 2007). When the crude oil along with its water is passed through choke valves and pumps, emulsions are also produced. A schematic drawing of the production of petroleum and the processes of refining in which emulsions are faced is given in Figure 9. Also, w/o emulsion is also formed as a result of large amount of crude oil spills into seas and oceans during crude tanker accidents followed by agitation facilitated by the wind. One real world example of these emulsions was the recent catastrophic oil rig explosion in the Gulf of Mexico which resulted in oil leakage for several months into the Atlantic Ocean. It is important to mention that these emulsions will one day separate into oil and water phases, unless there are some surface active compounds that can stabilise them (Mansurov *et al.*, 1987; Elsharkawy *et al.*, 2008; Zhang, 2017).

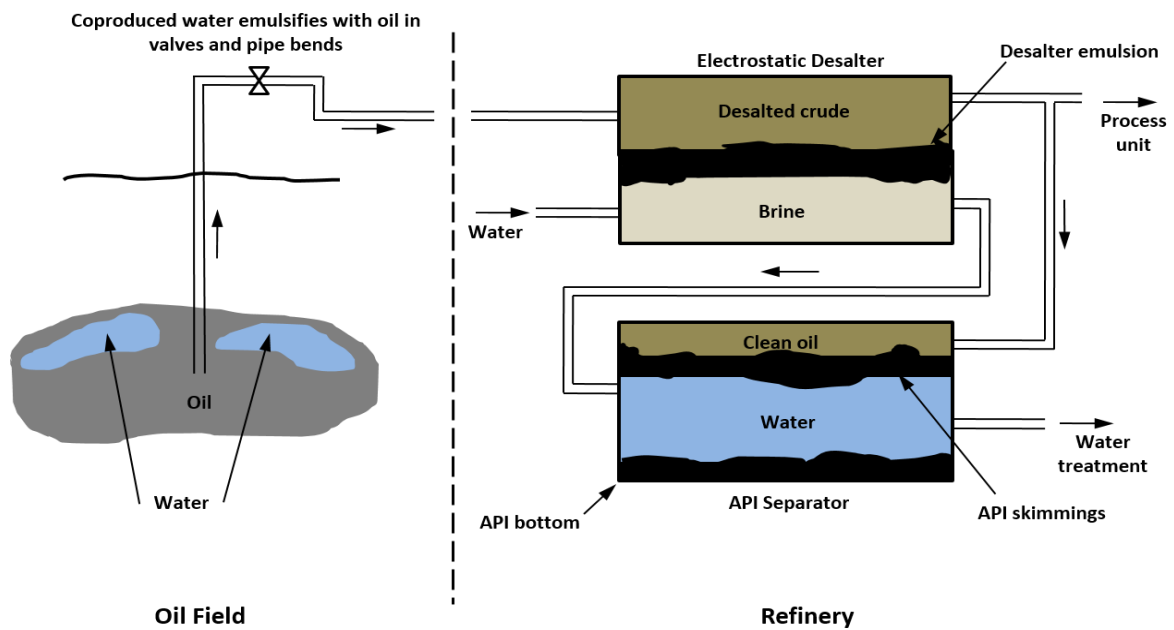


Figure 9: Schematic representation of the production of petroleum and the processes of refining in which emulsions are encountered (Sullivan and Kilpatrick, 2002).

The properties of crude oil change to some extent upon the emulsion formation (McLean *et al.*, 1998; Fingas and Fieldhouse, 2004; Yahaya Khan *et al.*, 2014). It has also been stated that the viscosity of emulsions with high asphaltene content can increase by 500 to 1000 times, resulting in a heavy semi-solid material but the density only increases by about 25% which increases the kinematic viscosity (Sjöblom *et al.*, 2007; Fingas and Fieldhouse, 2009). The viscosity of an emulsion is a function of the viscosities of both water and oil, the volume fraction of water, the temperature, the droplet size distribution, the amount of solids present

and the shear rate (Schoeggl *et al.*, 2002; Zehetner *et al.*, 2009). Moreover, the acidity of the emulsions is directly related to the amount of asphaltenes in the emulsion. Clays have been reported to increase the density and kinematic viscosity of the emulsions (Schoeggl *et al.*, 2002).

### **2.5.2 Emulsion Properties**

An emulsion is composed of three phases: The internal (discontinuous) phase is made of finely divided droplets. The external (continuous) phase is the matrix that maintains the droplets in suspension. Thirdly, the interphase includes an emulsifier or stabilizer that holds the stability of emulsion, grouping the internal and external phases together, and maintaining droplets away from reaching each other and coalescing.

Generally, emulsifiers are surfactants and soaps that exist either by themselves or as elements of the makeup of the formula of a detergent. An emulsifier comprises of a molecule containing hydrophobic and hydrophilic ends. If an immiscible liquid is present, the emulsifier moves towards the interface between internal and external phases, creating a protection sheath around droplets of the dispersed phase; the hydrophobic end from the molecule moves into the droplets, whilst the hydrophilic side remains in water.

The emulsion properties will depend to a large degree on the physical and chemical aspects of the emulsification. There a large number of factors in emulsification namely viscosity, stability, concentration and particle size that need to be monitored to acquire an emulsion with qualities that are desirable (Wong *et al.*, 2015). For example, smaller particles imply that higher stability and viscosity are introduced into the system. Typically, a highly concentrated emulsion is more viscous but there is often a constraint between high stability and high concentration (Subramanian *et al.*, 2017).

In the equilibrium state, the size of droplets an emulsion from the internal phase relies on the quantity of available emulsifier to keep that equilibrium. Consequently, the emulsifier concentration must be in balance with its droplet size to prevent particles from coalescing. If the droplets are smaller, more emulsifier will be needed to compensate for the large surface area. This mean that the emulsifier concentration quantifies the amount of stabiliser contained at the interface (Becher, 1966; Lissant, 1976).

Apart from oil, emulsifier and water, the creation of an emulsion spends energy and takes place away from the equilibrium state. Droplets suffer disruption caused by shear forces or due to differences in local pressure as caused by inertial forces. This can provide energy to make new surface and reduce droplet size. In addition, there can be lowering of the surface tension by the action of the emulsion with a small dispersed phase stabilising the fine scale emulsion. The kinetics from absorbing these emulsifiers at the O/W interface influences the size distribution of the droplets. Nevertheless, emulsions having low interfacial tension are not easy to separate.

The physical properties of the emulsion depend strongly on the nature and the dimensions of the particle-liquid interface and the dynamics of the sensitivity of aqueous dispersion to ionic and electrical structure of the interface (Olijve *et al.*, 2001). The stability and formation of the emulsions are both strictly related to the commonly known electrical double layer that defines the interface. Moreover, an electro-kinetic gradient called the Zeta potential is located across the interface of all liquids and solids (Hong *et al.*, 2018). In fact, the Zeta potential is the electrical potential that exists between the shear plane and the bulk solution, which is considered as imaginary sphere surrounding the particle as illustrated in Figure 10.

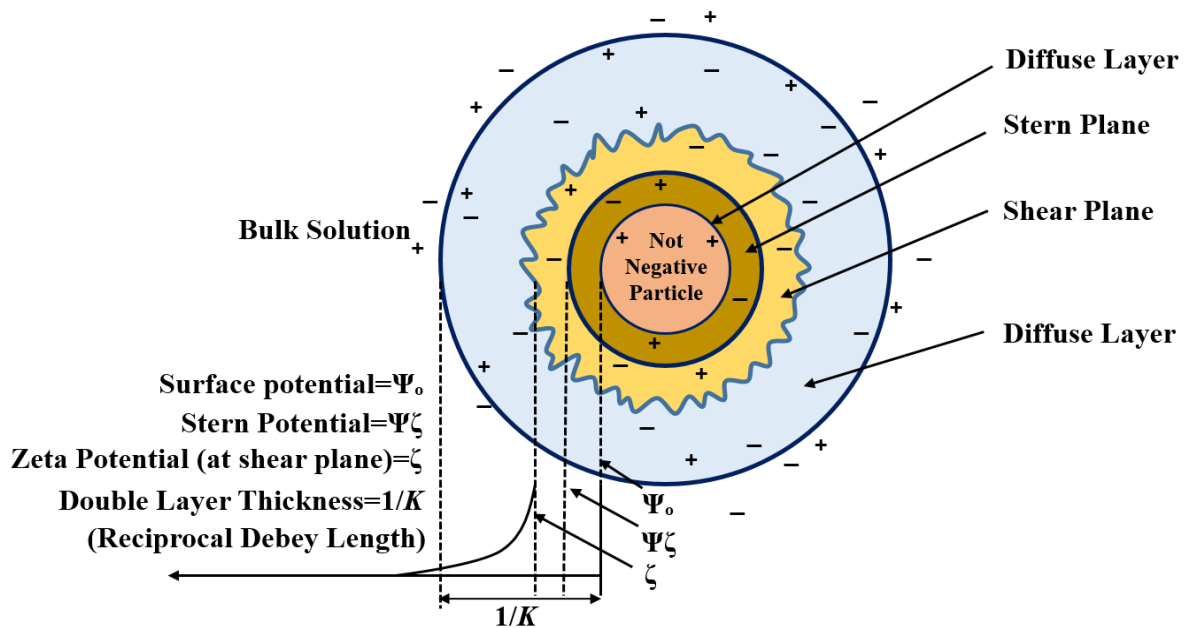


Figure 10: Schematic representation of the potential associated with colloids (Wiącek and Chibowski, 2002)

In principle, it is a hypothetical parameter that is computed from the electrophoresis velocity based on a sophisticated formulation of the phenomenon, obtained by using the Helmholtz-Smoluchowski equation (Eq.2) (Sherman, 1968; Clarkson and Smedley, 1988)

$$\zeta = \frac{4\pi v_t \eta}{\varepsilon E} \quad \text{Eq. 2}$$

where

$v_t$ : is the terminal velocity ( $\mu\text{m/s}$ );

$\varepsilon$ : is the dielectric constant;

$E$ ; is the applied electric field ( $\text{V/cm}$ ), and

$\eta$ ; is the solution viscosity (poise).

The measured Zeta potential is directly related to structure and behaviour of the electrical double layer at the interface between the particle and the liquid. Stable dispersions have relatively constant zeta potential values. It should be clear that the terminology, stability as applied to colloidal dispersions has, in general, the same meaning, i.e. to express resistance to modification of the dispersion with time. Hence, its magnitude is correlated to stability in colloidal dispersion as mentioned in many similar studies (Olijve *et al.*, 2001; Wiącek and Chibowski, 2002). The discharge of the Zeta potential followed with the colloid precipitation, takes place when polyvalent ions with opposite signs to the colloidal particle are added.

### 2.5.3 Stability of Emulsions

The diameter of the dispersed droplets is a paramount factor for achieving stability of an emulsion, which is related to the interfacial area and the volume of the dispersed phase. For instance, in oil purification partly a filled-water container, the oil tends to float and coalesce on the surface of the water as a thin layer. The oil creates a second phase or layer due to its lower gravity compared to the water. If water is added into the container with stirring, the physical effect of this on oil will enable emulsification of some droplets or dispersion in the water. At the ceasing of stirring, the coalescence of oil will take place very rapidly.

Emulsifier particles poured into the container will cause the easier dispersion of oil into the water. The system can be viewed as a group of small spheres being dispersed in the continuous phase of the water. To be held in suspension the droplets must be relatively small due to thermal forces, otherwise they will migrate to the surface and create a layer of droplets known as creaming. If left idle, collision and coalescence of oil droplets will happen, if there is not sufficient emulsifier present to envelope the whole interfacial area. During a period of time,

droplets with larger size will emerge at the surface and coalesce into one layer (Becher, 1966; Lissant, 1976).

There are three distinct methods to reduce the stability of an emulsion such as creaming, coagulation (flocculation) and breaking, any or all which may manifest after the preparation of the emulsion as portrayed in Figure 11. The emulsion creaming speed at which the oil will emerge at the surface of water is given by Stoke's Law, as follows (Fribereg, 2001):

$$u = \frac{2 g r^2 (\rho_1 - \rho_2)}{9 \mu} \quad \text{Eq. 3}$$

where

$u$ : is the sedimentation rate of a spherical particle;

$g$ : is the acceleration due to gravity;

$\rho_1$ : is the liquid density in the internal phase;

$\rho_2$ : is the liquid density in the external phase;

$r$ : is the particle radius, and

$\mu$ : is the emulsion viscosity.

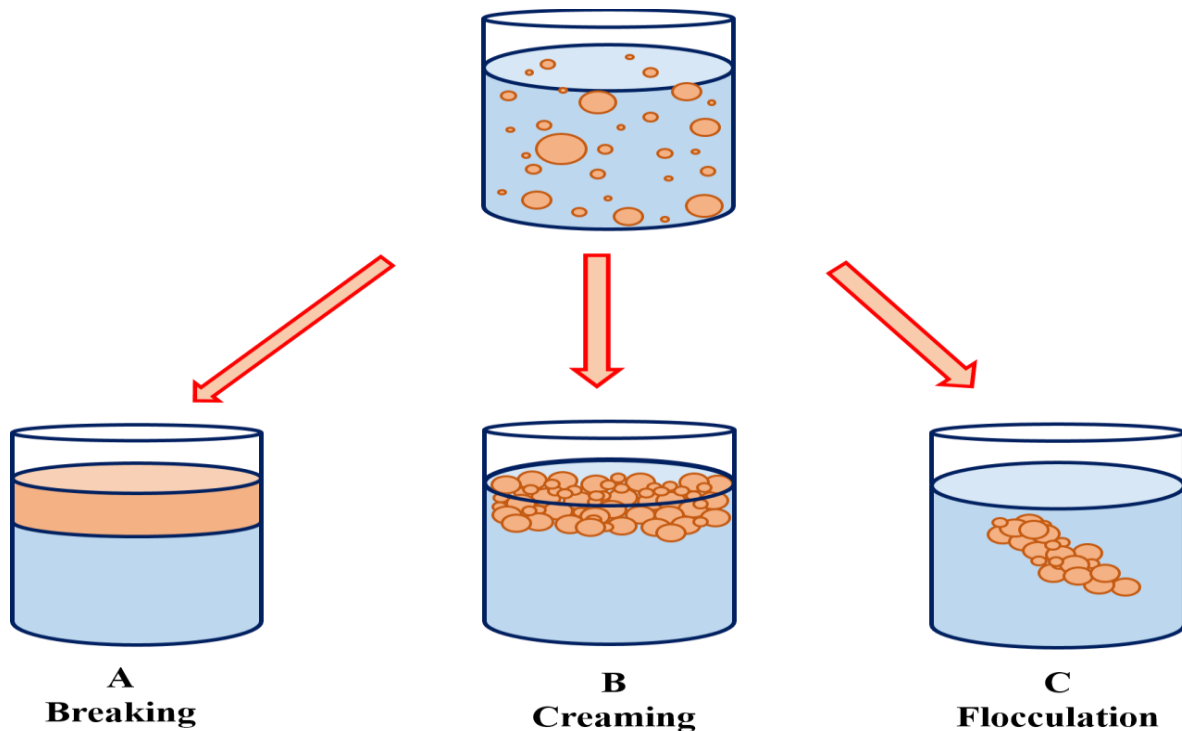


Figure 11: Pictorial representation of emulsions instability methods (Fribereg, 2001)

Small droplets rise or fall very slowly compared to larger droplets. In addition, droplets move faster in a liquid with low viscosity. Hence, provided  $\rho_1 < \rho_2$ , the droplet rises, but it will fall if  $\rho_1 > \rho_2$ . The setting velocity is a function of the square of the droplet diameter. Since the water density is usually larger than that of oil, creaming or upward sedimentation will take place (Khadim and Sarbar, 1999).

The emulsion stability relies on the size of droplet and the distribution of droplet sizes. Narrow size distribution emulsions termed as monodispersed emulsions are more stable compared to wide size distribution termed as poly-disperse systems (Khadim and Sarbar, 1999; Al-Roomi *et al.*, 2004). This is because the poly-dispersed emulsion has a layer droplets which can grow at the expense of the smaller droplets to minimise total surface energy that promotes droplet coalescence and rupture. On the other side, monodispersed system are a group of droplets with almost no distinction in the thermodynamic stability, thus having fewer break ups. A study conducted by Borwankar and Case (1997) suggested that polydispersity is a less relevant factor in influencing emulsion rheology. Nevertheless, Mason (1999) in his insightful review on emulsions argued that polydispersity has the same level of importance as monodispersed emulsion in promoting emulsion rheology.

Flocculation, sometimes-called aggregation, is another method that occurs in emulsions with low amounts of internal phase, as in the typical case of wastewater. Sliding of droplets happens as group which do not coalesce create clumps or chains of clumps with greater effective size (Hoshyargar and Ashrafizadeh, 2013). In other words, in low-viscosity emulsions, the surface forces like adhesion and repulsion forces are essential for flocculation to occur, where, high adhesion and low repulsion forces result in droplet flocculation. Flocculation occurs as soon as the droplets approach each other, then the thin film which is prepared from the continuous phase surrounding the dispersed droplets undergoes thinning and ultimately breakage (coalescence). Nonetheless, this process becomes more complicated with rising asphaltene concentration (along with solid particles) in the form of a thick, and aggregate-containing film surrounding a water droplet. This in turn enhances the stability of the emulsion (Zaki, 1997; Al-Roomi *et al.*, 2004; Langevin *et al.*, 2004; Hoshyargar and Ashrafizadeh, 2013).

The time scale and treatment conditions are also factors affecting the stability of emulsions. There is evidence that the degradation rate for different kinds of emulsion varies considerably. For example, unstable water-in-oil emulsions may separate in a fraction of a second if standing because of the Brownian dynamics and particle sedimentation which may be sped up through

slight agitation. This is the so called “orthokinetic flocculation” and is influenced by small shear stresses and the different movement rates for larger particles causing continuous collisions.

On the contrary, a potentially stable emulsion, for example a water in crude oil emulsion can suffer no variations although standing for a long time (as in months). This is because there is no effective closeness between the touching droplets as the emulsifier creates a blockage layer between the water droplets. Because of the robustness of the surfactant layer, there is no deformation of the interface so as to provide touching between two droplets (Sherman, 1968). Moreover, when oil is wastewater-emulsified, normally up to 5% ppm, it requires only a low quantity of detergent in for the oil to be emulsified into a stable emulsion. For stabilised emulsion like this several factors apart from long-term aging exist such as the disappearance of the smallest droplets caused by transference and dissolution into larger droplets through diffusion, freezing and bacterial action (Sherman, 1968; Sjöblom, 2006).

The external phase viscosity is an additional contributor to the stability. Increasing the viscosity of the external phase will diminish the collision rate between the droplets that consequently improves stability. Regarding artificial preparation of emulsions, agitating or mixing velocity as well as the mixing period also influences, the stability of the emulsions. Emulsions with longer mixing time and higher mixing velocity are, in theory, more stable compared to those with shorter time and lower velocity. In fact, this happens because the agitation facilitates the formation of the mono-dispersed emulsion with small droplet size distribution. As mentioned earlier, monodispersed systems tend to be more stable than their counterpart, poly-dispersed systems. This is due to the fact that the emulsion droplets have more thermodynamic stability which reduces breaking up (Sjöblom, 2006).

Altering the thermodynamic parameters (specifically pressure and temperature) including those affecting the hydrodynamic forces (such as surface viscosity, surface elasticity, bulk viscosity, etc.) will have also impact on emulsion stability. Ivanov and Kralchevsky (1997), suggested that the effect of pressure is accounted for by the DVLO (Derjaguin, Verwey, Landau and Overbeek) and non-DVLO surface forces namely steric polymer adsorption forces, hydrophobic attraction, hydration repulsion and many others. It was suggested that incrementing the temperature in the emulsification process will inversely impact the size of the droplet. In more stable emulsions, smaller droplet sizes were found to increase with temperature controllable within a range. The phase viscosity is largely different, but rising

temperature cause the convergence of viscosities when breaking up occurs more easily. On the other hand, in W/O HIPE, increments in temperature caused droplet size to increase (Akay, 1995; Akay, 2002a).

#### **2.5.4 Emulsion Rheology**

Rheology is defined as the study of the deformation or the mechanism of flow produced from the applied force on a system. A rheology test technique is usually used to study the properties and uniformity of emulsion structure ranging from fluids to solids. The response of the emulsion system to a given force can show various behaviors such Newtonian flow or a complex non-Newtonian flow based on their volume fraction of dispersed (internal) phase,  $\Phi$  (Akay *et al.*, 2005a) as defined by:

- Emulsions with a low-internal phase: The volume of the dispersed phase is lower than 30%;
- Emulsions with a medium-internal phase: The volume of the dispersed phase is between (30% to 55%); and
- Emulsions with a high-internal phase: The volume of the dispersed phase is more than 55%.

Emulsions with a low-internal phase volume or very dilute emulsions normally demonstrate Newtonian flow and behave like simple liquids while emulsions with a high-internal phase volume like emulsions of water-in-crude oil normally exhibit the characteristics of non-Newtonian flow.

As shown in Figure 12, for the shear stress versus shear rate, a Newtonian liquid demonstrates a linear relationship and consequently viscosity does not rely on the shear conditions. In contrast, a non-Newtonian fluid does not demonstrate such a relationship. The more common behavioral form of non-Newtonian flow is the pseudo-plasticity or shear thinning, giving an increase in shear rate with decreasing viscosity; this is found in more complex fluids such as gels, concentrate solutions, and colloids as well as in emulsions. The reverse and less common behavioral form of non-Newtonian flow is dilatancy or shear thickening, it is the phenomenon where the viscosity increases with shear. An example of a material that shows this is cornstarch in water and is the reason that cornstarch is used as a thickening agent in cooking.

The behavior of non-Newtonian fluid is as a result of the interactions between the flow field and the microstructure of the fluid. To date, no fully accepted theory has been reached to clarify the characteristics of non-Newtonian flow because of the microstructure physical-chemical features, which show an extensive difference from one fluid to an other. The descriptions of these behaviors in most theories depend on the deflocculation and flocculation reactions that dominate the development of particle collections at low shear rate. Hydrodynamic forces and Brownian motion influence this reaction. The former is important at low to moderate shear rate and become less significant as the size of a droplet/particle rises and/or shear rate increases. Nonetheless, the exact value of the factor of proportionality of these factors is not known.

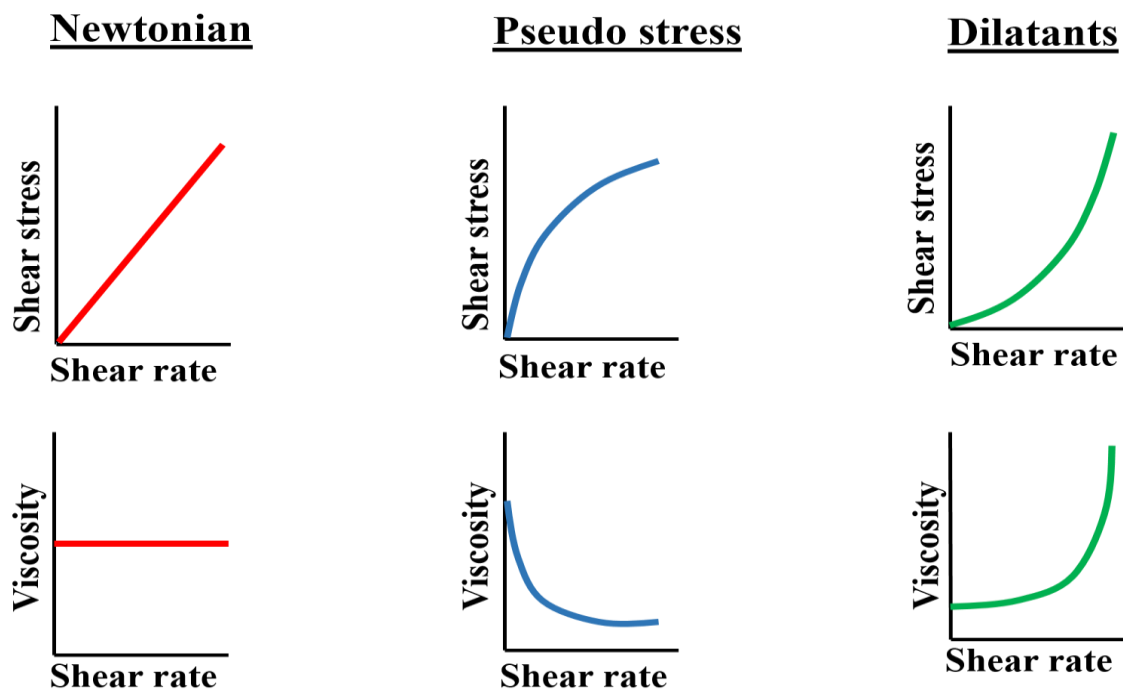


Figure 12: Schematic diagram of common flow behaviors (Akay *et al.*, 2005a)

#### 2.5.4.1 Effect of the Volume of Dispersed Phase on the Viscosity of an Emulsion

Generally, W/O emulsions exist in the form of concentrated emulsions with the volume of dispersed phase ranging from medium to high. The interaction among particles increases with an increase in the volume of the dispersed phase owing to the closer approach of the particles in the flow configuration in the continuous (external) phase, when particles are sufficiently close. The hydrodynamic interaction begins to dominate and Brownian motion of particles is

less important. This interaction can be demonstrated quantitatively in the general relative viscosity equation as follows:

$$\eta_{rel} = 1 + K_1\Phi + K_2\Phi^2 + K_2\Phi^3 + K_2\Phi^3 + \dots \quad \text{Eq. 4}$$

where

$\Phi$ : is the dispersed phase fraction.

In emulsions with a high concentration, the relative viscosity ( $\eta_{rel}$ ) rises by a significant amount with increasing the volume of the internal (dispersed) phase (Sherman, 1968). At this condition, the flow turns out to be pseudo-plastic and the relative viscosity increases greatly by a small increment in the volume of the internal phase. As a result, the aggregation of particles is enhanced due to the increase in the number of particles of the internal phase. Mooney (1964) described that each aggregate acts like a sphere at low shear rates, which has a volume more than the sum of constituent particles owing to the existence of the continuous phase inside the structure.

The particles are bound together by Van der Waals forces inside the aggregates. Thus, the structure of an aggregate is affected a lot due to a small rise in shear stress. That is why, an increase in the shear rate causes the aggregates to breakup, resulting in a decrease in the viscosity and the discharge of the continuous phase fluid.

A more suitable expression for the monodispersed system viscosity is the one presented by Krieger (1972)

$$\eta = \eta_c \Phi_m \left(1 - \frac{\Phi}{\Phi_m}\right)^{-n} \quad \text{Eq. 5}$$

where

$\Phi_m$ : is the maximum packing fraction of the dispersed phase;

$\eta_c$ : is the viscosity of the continuous phase.

According to the arguments of Pal and Rhodes (Pal and Rhodes, 1989), the above equation and any equations which involve  $\Phi_m$  are solely suitable for hard-sphere dispersions and are not suitable for an emulsion. Later on, Pal (1998) presented an effective dispersed phase equation as follows:

$$\Phi_{eff} = \Phi \left( 1 + \frac{S_{th}}{D_s} \right) \quad \text{Eq. 6}$$

where

$D_s$ : is the size of droplet;

$S_{th}$ : is the thickness of surfactant.

To apply equation 6 to a dispersion of soft-spheres in which multi-particle interactions are involved, Pal (Pal, 1998) and replacing  $\Phi$  by  $\Phi_{eff}$ , it becomes

$$\frac{\Phi}{\ln[\eta_{rel}]} = \frac{1}{K_o[\eta]} - \frac{\Phi}{\Phi_m[\eta]} \quad \text{Eq. 7}$$

where

$K_o$ : is the hydration factor.

The above equation can be condensed to the following simplified formula

$$\eta_{rel} = [1 - K_f K_o(\gamma)\Phi]^{-2.5} \quad \text{Eq. 8}$$

where

$\gamma$ : is the share rate;

$K_f$ : is the flocculation factor.

Akay (Akay, 1998) reported that emulsion contain two kinds of particles: 1) very small particles (50 nm) which are multi charged and multi lamellar vesicles; 2) comparatively large particles (1000 nm) which have low charge density. It is known that true phase volume can be considerably smaller than the expected phase volume because the vesicles entrap water inside their bilayer. The true volume of the dispersed phase is thus represented by the next equation.

$$\Phi = \Phi_s + \Phi_{Ew} + \Phi_o \quad \text{Eq. 9}$$

where

$\Phi_s$ : is the volume of dispersed phase because of surfactant in the vesicles;

$\Phi_{Ew}$ : is the water phase volume entrapped inside the bilayers;

$\Phi_o$ : is the phase volume because of oil.

Therefore, if the highest packing fraction of a dispersed phase is assumed to be close to 0.7, increasing  $\Phi_{Ew}$  and  $\Phi_s$  during emulsion formation will result in a very fast increase of viscosity.

#### **2.5.4.2 Effect of Droplet size on the Viscosity of Emulsion**

Several studies on emulsions assessed the relationship between droplet size and the mono-dispersity of emulsions, which is never the same as droplet size distribution for polydispersity. This is essential to provide a correct understanding of rheological data. Moreover, the effect on stability of an emulsion was also assessed in these study.

The viscosity of an emulsion is directly related to its average droplet diameter. In theory, as the dispersed droplet size diminishes, the total droplet surface area increases. Consequently, the viscosity of the emulsion and its relative viscosity increases. It can be generically assumed that the stability of an emulsions is somehow proportionally related to its viscosity. However, the relationship is complex with factors as the diverse as type of emulsion (O/W or W/O), the number of available emulsifiers and the dispersed phase volume (Maa and Hsu, 1996; Pal, 1996) having an effect.

Studies conducted by Richardson (1953) and Becher (1966) found that, in concentrated W/O emulsions, with  $\Phi \geq 0.75$ , which were highly viscous and showed non-Newtonian behaviour, the  $\eta_{rel}$  at high shear rate rises as the droplet size reduces. This is true because emulsions having smaller droplets size take more work to shear than those with large size due to the structure of these emulsions.

Sherman (1968) proved that the viscosity of O/W and W/O emulsions exhibited non-Newtonian pseudo plastic behaviour and stabilising with non-ionic emulsifiers was caused by the size of the droplets within a large range of  $\Phi$ . Nonetheless, the width of the distribution of the mean diameter of the droplets was reduced and had less impact on O/W emulsions than W/O emulsions.

Another study conducted by Johansen and co-workers (Johansen *et al.*, 1988) concerning the emulsions of water-in-crude oil yielded from crude oil extracted from the Norwegian Continental Shelf, showed that the higher the mixing rates used the more the droplet size is reduced, whilst increasing the duration of mixing of the emulsion gave a narrower distribution of droplet size, thus, highly viscous emulsions with greater stability were yielded. Galvin and

co-workers (Galvin *et al.*, 2001) noted that a concomitant rise in the viscosity was observed when concentrated W/O emulsions were refined with air bubbles.

### 2.5.4.3 Interfacial Rheology

The interfacial data is an essential requirement on the emulsification process to deliver the account concerning the efficiency that disperse the discontinuous phase over emulsification relative to the approach used for the preparation of emulsions (Sherman, 1968). This can also be a tool to estimate the contact angles, spreading coefficients and the interfacial interaction between liquid-liquid and solid-liquid. These concepts are useful to describe the type of emulsions that can be created.

The interaction between two droplets within a liquid setting as they get closer one to another is defined by two major forces: surface force and hydrodynamic force. It is understood that the formation of stable emulsion requires the interfacial film to be stable as well. This can be done with small interfacial tension in W/O. Surfactants exert this kind of function in emulsion. The film, created by surfactant particles at O/W interface, was treated as containing distinct surface tensions on either end of the film by Bancroft and utilized this knowledge to describe the production W/O or O/W emulsions (Galvin *et al.*, 2001). In theory, higher tension film would be bent concavely to encapsulate on liquid on the concave region. Thus, the internal phase becomes the encapsulated liquid.

Schulman (1954) has demonstrated that the existence of powder surfactants, O/W emulsions are produced when the angle of contact,  $\Theta$ , is less than  $90^\circ$  in the water phase as shown in figure 13. Nonetheless, when the contact angle exceeds  $90^\circ$  W/O emulsion are generated.

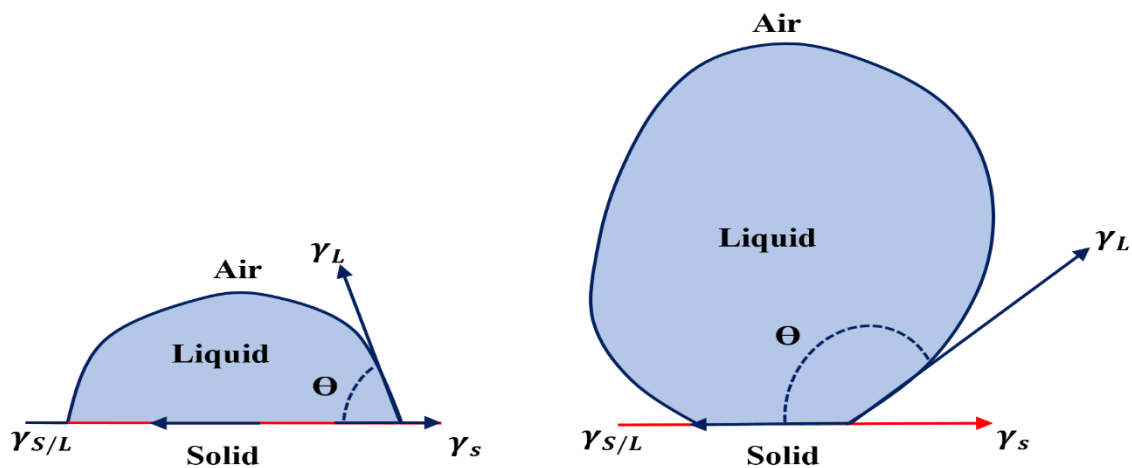


Figure 13: Schematic drawing of the contact angle between a liquid and solid (Schulman, 1954).

The Interfacial rheology of solutions containing surfactants is also of great importance when considering several systems including emulsions, froths and foams as it contributes significantly to their stability. In theory, stretching of a foam or a thin liquid film, with high concentration of surfactant, causes interfacial tension to increase; thus, interfacial tension gradients are formed. This may cause liquid flow towards the stretched area, which delivers both a resisting force versus further thinning (elastic behaviour of the interface) and a healing force (Schuster, 1985). This is illustrated in Figure 14 and is termed as Gibbs-Marangoni effect. The emulsion droplets suffer stretching but resist coalescence because of elastic films, hence they are more stable.

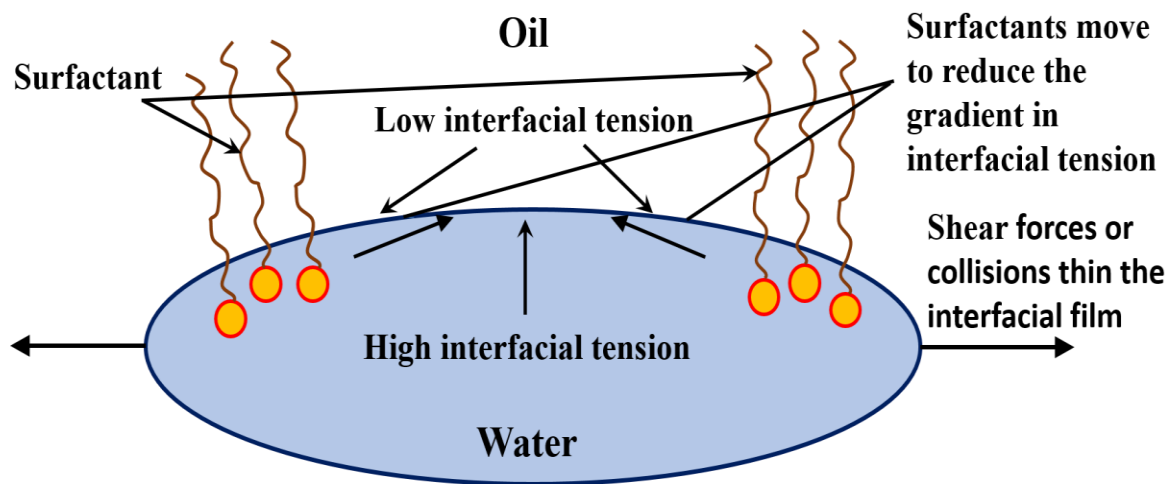


Figure 14: Schematic diagram of the Gibbs-Marangoni effect at an oil-water interface (Schuster, 1985)

The Dilatational modulus ( $\epsilon$ ) is a measure of the resistance to the formation of new interfacial area and is usually used as an estimate for Interfacial rheology. It is described as the increment in interfacial tension over the relative increases in the surface area (Akay, 2002b).

$$\epsilon = \frac{d\gamma}{d \ln A} \quad \text{Eq. 10}$$

where  $A$  is the interfacial area and  $\gamma$  is the interfacial tension. The changes in the interfacial tension due to deformation in the area is given by:

$$\Delta\gamma = \text{viscous} + \text{elastic} = \eta_d \left( \frac{d \ln A}{dt} \right) + \epsilon_d \Delta \ln A \quad \text{Eq. 11}$$

where  $\eta_d$  and  $\epsilon_d$  are interfacial dilatational viscosity and interfacial dilatational elasticity, respectively. Both parameters can be calculated separately by giving small periodic oscillations to the interface based on

$$\Delta \ln A \propto e^{i\omega t} \quad \text{Eq. 12}$$

where  $\omega$  is the oscillation frequency. Based on above expression, the interfacial dilatational modulus  $c$ , can be calculated by:

$$c = i\omega\eta_d + \varepsilon_d \quad \text{Eq. 13}$$

where the imaginary,  $\eta_d$ , and the real,  $\varepsilon_d$ , parts of the equation stands for different contribution to the dilatational modulus and elasticity.

## 2.6 Emulsions of Water-in-Crude Oil

Highly stable water-in-crude oil emulsions consist of fine water droplets within crude oils. This kind of emulsion normally forms with existing surface-active species (indigenous surfactants) that are physically present in crude oil. Also, commonly termed as chocolate mousse for their resemblance to the frothy dessert, these emulsions inject challenges into the yield of crude oil as it not desirable from the process quantity and product perspective (Clause, 1983).

The creation of these emulsions that are highly stable is a major issue that is often seen in different stages of crude oil production such as extraction, processing and transporting. In the crude oil extraction from a well, oil and water are simultaneously produced and mixed at high energy when these phases squeeze together in the narrow pores of reservoirs. As a consequence, water-in-crude oil emulsions with high stability are formed when asphaltenes are stuck to the external side of a considerable number of small droplets of water in the crude oil and decrease surface tension (Clause, 1983). This can occur at high pressures and temperatures. During the processing stage, water and oil may potentially be mixed in separation processes; thus, the possibility of emulsion formation. These potentially stable emulsions have much higher viscosity relative to the parent crude. They pose issues in the process of refining and cause the induction of corrosion of tanks and pipelines. Because of high power consumption and wearing of the equipment due to increased viscosity and volume, dehydration of oil to 1% of water concentration with initial values from 10 to 60%, at the site of the well must occur, before the downstream processing of oil (Sherman, 1968; Clause, 1983).

Apart from the petroleum industry, emulsions of water-in-crude oil can also be formed based on oceanic oil spills as in the case of a tanker incident. Stable emulsions with high viscosity, are very difficult to remove and hence their cleaning up is challenging. They will not

immediately only generate environmental harm only but also financial problems. Long-term impact will also be possible as their stability lasts for years with tendencies to bio-accumulate and bio-magnify in the aquatic marine environment.

### **2.6.1 Crude Oil Emulsions Problems**

Crude oil emulsions are undesirable and cause numerous operational and commercial problems, which require attention and necessitates thorough studies in order to find suitable solutions. Amongst these problems, corrosion of pumps, pipes, tanks and equipment are made worse by the existence of contaminants like chloride. Moreover, the production of off-specification crude oil, failure of separation equipment in the units of the gas-oil separation, poisoning of catalysts, increase in the use of demulsifier(s), losses of production, increase in viscosity of crude oil in the transportation pipeline, also necessitate further funds and cost of operations. The deposition of organics in processing equipment, inadvertently requires accommodating an increased volume from the presence of water in order to produce crude oil to conform with specifications. (Thompson *et al.*, 1985; Isaacs *et al.*, 1990; Sjöblom *et al.*, 1992; Kokal *et al.*, 1995; Førdeedal *et al.*, 1996; Khadim and Sarbar, 1999; Angle, 2001; Eow and Ghadiri, 2002; Kim *et al.*, 2002; Pekdemir *et al.*, 2003a; El Gamal *et al.*, 2005; Elektorowicz *et al.*, 2006; Moran and Czarnecki, 2007; Less *et al.*, 2008a; Verruto *et al.*, 2009; Ekott and Akpabio, 2010; Chen *et al.*, 2014; Roodbari *et al.*, 2016). Thus, due to these challenges, the breaking of crude oil emulsions is of great importance and feasibility for crude oil producers.

### **2.6.2 Rheology and Interfacial Behaviour**

The relevance of both rheology interfacial behaviour in defining the stability of emulsions of water-in-crude oil has been illustrated in several studies (Thompson *et al.*, 1985; Eley *et al.*, 1988; Sjöblom *et al.*, 1992; Mohammed *et al.*, 1993; Mohammed *et al.*, 1994; Kim *et al.*, 1995; Aomari *et al.*, 1998; Dicharry *et al.*, 2006). The rheology characteristics of emulsions of water-in-crude oil and their stability are inherently dependent on thermodynamic factors, the chemical structure of water and oil and the volume fraction of the dispersed phase  $\Phi$ .

The most common measured rheological parameter is the viscosity of the emulsion with respect to the viscosity of the continuous phase  $\eta_r$ . Generally, the viscosity of the emulsions of water-

in-crude oil is higher compared to that of the parent crude oil and has a close relation to the water fraction or water content. In addition, it depends also on the level of water dispersion through the oil. In the sea, the viscosity of emulsions of water-in-crude oil tends to increase with time as the oil adsorbs more water that disperses more uniformly in the oil. Research undertaken by Thompson and co-workers (Thompson *et al.*, 1985) and Eley and co-workers (Eley *et al.*, 1988) demonstrate that viscosity from crude oil emulsions grows considerably as water content increases and the droplet size reduces. Briefly, these researches suggested that viscosity and stability are directly related in emulsions of water-in-crude oil.

The dynamic viscosity is usually estimated at low shear rates due to the non-Newtonians nature of water-in-crude oil emulsions as these are shear-thinning fluids. Consequently, the viscosity declines as the shear rate is increased. According to Aomari and co-workers (Aomari *et al.*, 1998), relative viscosities measured at rates of shear below the critical value  $\gamma^*$ , caused the emulsion to behave as Newtonians fluids and the viscosity remained constant, Nonetheless, measuring beyond the critical value a pseudoplastic behaviour was observed.

The interfacial rheology of crude oil with asphaltenes was observed to have different behaviour with and without salt. The values for the dilatational modulus viscosity which promote highly stable emulsions of water-in-crude oil, was influenced by the flocculation of asphaltene-resin micelles at the interface. Because resins and asphaltenes are molecules with active interfacial properties, they induce the Gibbs-Marangoni phenomenon upon the droplets of water in the continuous phase of the oil, thus, developing their resistance to coalescence. But, in the absence of resins, asphaltenes could not be dispersed and adsorbed at the interface leading to multilayer formation and precipitation (Acevedo *et al.*, 1993).

Mohammed and co-workers (Mohammed *et al.*, 1993) in their analysis of the rheology of emulsions of water-in-crude oil calculated interfacial tensions of crude oil, as well as solutions of resins and asphaltenes in a model oil. In their analysis, the area curve for monolayers of resins, asphaltenes and their mixtures has been plotted against surface pressure. It was shown out that the pseudoplastic dilatational modulus is low for high resins to asphaltenes ratio and high for low resins to asphaltenes ratio.

### 2.6.3 Water-in-Crude-Oil Emulsions Stability Problems

It has been reported by Lee (1999) that w/o emulsions with high stability, in which the water droplets last for 5 days (or a longer period up to years) have high water content (50-90 % or 60-80 %) and high viscosity. Elsewhere, it was reported that the emulsions with small water droplets (1-10  $\mu\text{m}$ ) have low conductivity and are more dense than the original oil (Fingas and Fieldhouse, 2003; Roodbari *et al.*, 2016). The stability of the oil-water interface is the main deciding factor for the stability of the emulsion. The stability of the emulsion is also influenced to some extent by the droplet size of the emulsified phase, the density difference of the two liquids, the viscosity of the continuous phase and the volume percentage of the water fraction (Lewis, 2004; Buist *et al.*, 2005). Indeed, unstable emulsions are characterised by large droplet size, which is why they merge rapidly (Benayoune *et al.*, 1998; El Gamal *et al.*, 2005).

The mechanism of w/o emulsion stabilization has been explained by Kumar and co-workers (Kumar *et al.*, 2001; Nour *et al.*, 2007; Khajehesamedini *et al.*, 2018). They proposed that water droplets in water oil emulsions are widely dispersed in the crude oil, however, they will be surrounded by a layer of surface-active components present in the oil, such as resins and asphaltenes. Due to multiple body interactions, these droplets will still attempt to contact each other. However, some repulsive forces are induced between these water droplets due to the surrounding oily film; these forces hinder the water droplets from approaching each other and that is why they cannot flocculate or combine (Roodbari *et al.*, 2016).

A high concentration of emulsifying agents impedes the coalescence of water droplets resulting in the formation of stable emulsions (Benayoune *et al.*, 1998; El Gamal *et al.*, 2005; Umar *et al.*, 2017). Conventionally, the responsible components for the crude oil emulsions have been claimed as surfactants such as asphaltenes, resins, soluble organic acids, and other finally divided substances which form a layer around the surface of the dispersed droplets. These emulsifying agents have a great strong ability to diffuse from the bulk phase, resulting in the reduction of the interfacial tension between oil and water leading to widening of the interfacial layer and hindering droplet coalescence (i.e. emulsion stability promotion) (Maia Filho *et al.*, 2012; Oliveira *et al.*, 2017). Angle (2001) gives a similar description of the interface matrix that the water droplets are surrounded by in crude oil components with their hydrophilic heads toward water phase and hydrophobic tails leaning toward the oil phase as shown in Figure 15.

The higher the ratios of the concentration of resins to asphaltenes the more the asphaltene aggregate dissolve in the oil phase, thus, leading to reduction of the amount of asphaltene

aggregates. In addition, if there is a reduction in the pressure above the bubble point, there is a decrease in solubility of asphaltene. Moreover, further reduction in the pressure to a level below the bubble point resulted in an increase in solubility of asphaltene (Li *et al.*, 2010; Chen *et al.*, 2012; Gharbi *et al.*, 2017). Also, the asphalt contributes to building a viscous film at the interface

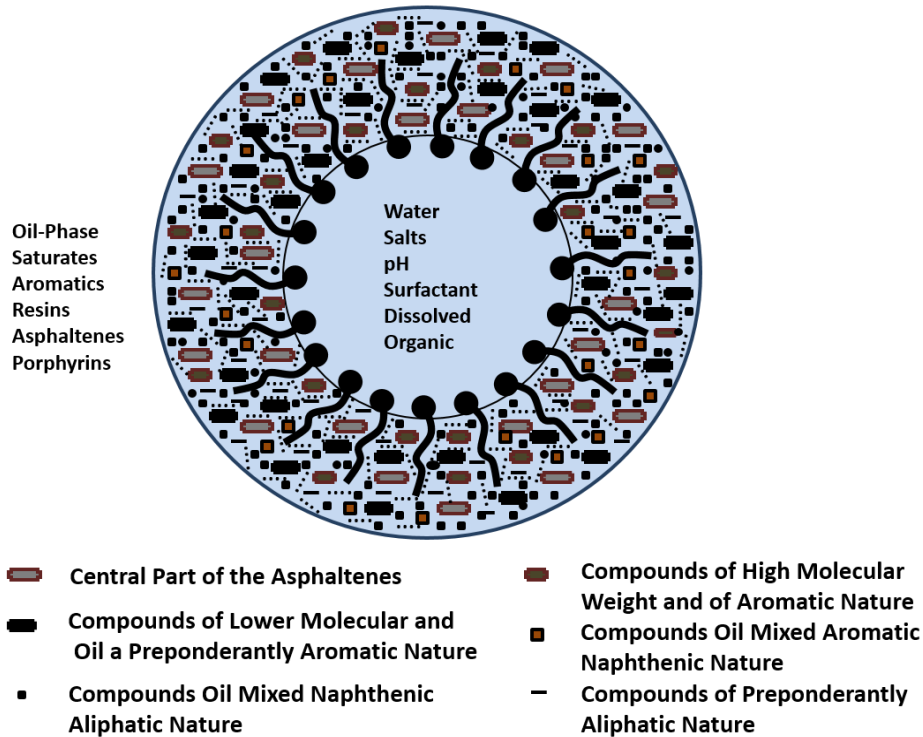


Figure 15: A schematic diagram of droplet of a w/o emulsion with a petroleum fraction. The interfacial layer forms a skin around the droplet at an early stage (Angle, 2001)

between water and oil that causes an increase in the stability of w/o emulsions. This film is formed due to the presence of solids in a crude oil such as carbonates of calcium and iron etc.; adsorption of asphaltenes on the finely divided solids occurs because of the hydrophobicity of these solids. Thus, a change in the features of these solids occurs allowing more adsorption and then, re-construction. Yet, because of the complicated of chemical nature of the crude oils and variances in the composition of the crude oil, it is difficult to create a global mechanism that characterises the behaviour of the dispersion from the physico-chemical properties at the interface of oil water (Eley *et al.*, 1988; Ali and Alqam, 2000; Harbottle *et al.*, 2014).

Moreover, organic-clay particulates, clay particles and silica particles present in the sea contain both hydrophobic and hydrophilic parts making them similar to surfactants; thus, they selectively adsorb to the oil-water interface (Buist *et al.*, 2002; Yang *et al.*, 2015). As a

consequence, some reactions take place between clay particles (hydrophobic-hydrophilic) and the asphaltene particles (hydrophobic); therefore, a matrix is produced with extremely high hydrophobic properties which increases the stability of the emulsion (Levine and Bowen, 1992; Yang *et al.*, 2014). In addition, Angele and Kilpatrick (Angle, 2001; Kilpatrick, 2012) pointed out that the indigenous surfactants of the crude like metallic salts, organometallics, organic acids, bases and water phase particles like sediments, particulates and particles like asphaltenes and waxes play a significant role in the stability of emulsion by staying at the oil-water interface as shown in Figure 16. Furthermore, when the concentration of these surfactants and particles is high; stable emulsions are produced in which the droplets of water cannot coalesce.

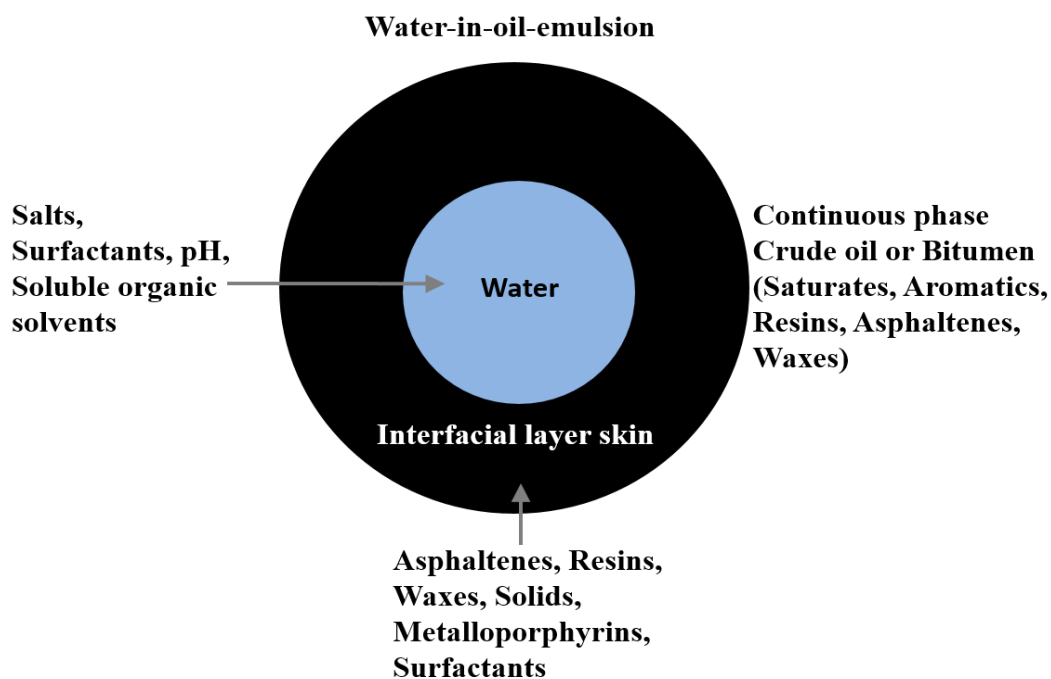


Figure 16: Schematic drawing of the crude oil components and bitumen to be considered in an emulsion droplet and the interfacial layer (Angle, 2001)

Emulsions are stabilized at two grades, which are stable emulsions (tight) and un-stable emulsions (loose) (Ali and Alqam, 2000; Harbottle *et al.*, 2014); each grade has a special chemical and physical properties. The first grade (tight) is difficult to break and may require a period ranging from a few hours up to years, while the second grade (loose), requires only a few minutes to break (Elsharkawy *et al.*, 2005; Ilyin *et al.*, 2017). This depends heavily on the quantity and characteristics of both the water and oil phases, and the indigenous emulsifying agents (concentration and nature of these agents) present in the crude. Fingas and Fieldhouse (Fingas and Fieldhouse, 2004) classified the stability of emulsions into four classes (stable, unstable, mesostable emulsions and entrained water) based on the visual appearance of the

emulsion and its lifetime, flexibility and the variations in viscosity. The emulsions of the latter class are black in colour with lower than 10 % water content entrained by viscous oil. The stable emulsions have a reddish-brown colour with water content of 80 % and viscosity more than three times of the viscosity of original crude. This increase of viscosity is due to the ability of resins and asphaltenes to reside at the interface to form dense visco-elastic films. The unstable emulsions are characterised by a colour black to red with lower than 50 % water content and viscosity up to 20 times greater than the viscosity of the original oil. In this class, the water and oil need only few hours to separate out. While, the mesostable emulsions are brown, red or black in colour and because of a high content of their aliphatic/paraffinic and aromatic content compared to asphaltenes, their emulsions have low stability with a destabilizing tendency. However, due to their high viscosity they stay stable for a period of time and they produce stable emulsions and layers of oil upon their decomposition (Wasan and Nikolov, 2001; Fingas and Fieldhouse, 2004; Sztukowski and Yarranton, 2005; Kralova *et al.*, 2011).

Furthermore, McLean and Kilpatrick (1997) have stated that the pH can have an influence on the stability of the film and hence the stability of an emulsion because of the acidity of the active components at the interface of oil and water. It was found that the increasing pH value is connected with ionization of the polar functional groups in the molecules of resins and asphaltenes. This ionization process results in developing the high surface charge densities which alter and destroy the mechanical properties of the film via several internal repulsive reactions, which finally minimizes the stability of the emulsion. In addition, it was found that the temperature has an effect on the stability of emulsion. The increasing of the emulsion temperature causes reduction in the viscosity of the oil phase and an increase in the rate of collision between the droplets of the aqueous phase, which finally leads to a reduction of the stability of the system (Thompson *et al.*, 1985; Tambe *et al.*, 1995; Schoeggl *et al.*, 2002).

## **2.7 Demulsification of Water-in-Crude Oil Emulsions**

In many cases, the separation of the components of emulsion is highly desired. In this process the emulsion is broken down in to oil and water constituents. This process is called “demulsification”. Demulsification is a very complex and difficult part of the whole oilfield production because the crude emulsions are mostly very stable. In the whole process, the emulsions are disintegrated into two main phases: an oil phase and an aqueous phase. This

disintegration process generally consists of three distinct stages (Saether *et al.*, 2004; Drelich *et al.*, 2010): (1) the movement of two single droplets toward each other, also identified as flocculation; (2) the distortion of mutually approaching droplets and the creation of a plane-parallel film; (3) the thinning of that film to critical thickness,  $s_c$ , whereby the film turns unstable and splits, which results in the coalescence process.

Whereas, in flocculation, existing droplets found in the dispersed phase form clusters or aggregates via weak to moderate agitation. Coalescence can be described as the combination of two or more droplets to build a large cluster (Sjöblom *et al.*, 2007). When two or more drops are combined by means of flocculation, the interface is separated by an oil film, which influences the stability of the emulsion. For these drops to combine, the interfacial films need to be broken. These larger clusters are evident and moreover, can be separated (Sjöblom *et al.*, 2003). Hypothetically, the coalescence process is permanent, for the reason that it needs a significant amount of energy to separate the larger clusters.

To demulsify w/o emulsions economically and effectively, it is important to know how they are stabilised. This, as illustrated in the previous sections, necessitates the knowledge about the properties and interaction of resins and asphaltenes, since they are the main stabilisers of emulsions. Other stabilisers which are mentioned in previous sections are also crucial because of their extreme inclination to react with resins and asphaltenes.

Although Nour *et al.* (2012) stated that a few works have been reported on the demulsification of emulsions, most of these were commercially undertaken; Therefore, there is patent literature with little new science in the field. Recently, some progress has been made; where, thermal, chemical and electrical demulsification experiments have been reported. Treatment of emulsions via the use of surface active agents (chemical demulsifiers) is the major method utilised to breakdown stabilised emulsions (Hajivand and Vaziri, 2015). Microfiltration demulsification (Shakorfow, 2012) and demulsification by heating/microwaves (Akbari *et al.*, 2016) have been used as well. Electro-demulsification (Mhatre *et al.*, 2018) to breakdown the w/o emulsions is also under development. The combination of these two technologies has been reported, with the aim of enhancing the efficiency of demulsification (Ekott and Akpabio, 2010). Sullivan *et al.* (2007) observed that there was no universal technique that can be utilised for different emulsions. This means, techniques that are application-specific have been developed on trial and error basis for a given emulsion because of the variety of crude oils and brines and; consequently, resultant emulsions.

This section presents a summary of the electro-demulsification technique, demonstrating the theoretical details and practical implementation highlighting the mechanism, which this technique uses of demulsification. Moreover, the mechanism of electrically-optimized demulsification will be separately discussed in detail in the next chapter.

### ***2.7.1 Current Techniques Used in Demulsification***

At present, various chemical and mechanical methods are employed to separate petroleum emulsions. The most common methods in use employ hydrocyclones, filters, pH adjustment, centrifuges, steam/air stripping, and chemical additives, in addition to electrical treatments. Moreover, a combination of two or more of these separation techniques identified previously can be utilised occasionally.

It is essential to mention that when selecting the appropriate process, in many commercial operations cost, time, current legislation, and size factors must be taken into account. Regarding commercial operations, time is extremely limited; therefore, it is advisable to apply a faster separation rate, although this can be challenging to achieve, particularly for extremely stable emulsions. Conventional methods can take a considerable time to treat these emulsions as a result of large hydraulic residence time as production intensifies. With the importance placed on settling volume, conventional mechanical systems like centrifugal separators, gravity settling tanks, hydrocyclone vessels and stripping columns have become progressively more expensive and bigger with an increase of the water flows produced. Consequently, it may not be appropriate to install them in places where space is at a premium, such as on an oil platform. Moreover, high operating costs may be accrued owing to the large hydraulic residence time, along with the huge equipment required. Furthermore, a substantial amount of energy will be expended for operating the equipment. Therefore, it will be an economic benefit regarding commercial operation to keep a minimum number and size of demulsification units.

#### ***2.7.1.1 Utilizing Demulsifiers***

It should be pointed out that the use of demulsifiers have become a popular method in destabilising emulsions as a result of the limitations pertaining to applying mechanical separation techniques. Demulsifiers which are commercially available can be explained as a chemical cocktail where synergistic effect of one or more active components dissolved in the active solvent can be found (Sjöblom *et al.*, 2003; Sjöblom *et al.*, 2007). The solvent must be

extremely hydrophobic to make sure that the active components dissolve in the crude oil, and not expensive or occupying a high volume. Ordinarily, these chemicals tend to be added to already-formed emulsions with the aim of breaking them down. Furthermore, demulsifiers can also be employed as a pre-treatment to hinder the emulsification procedure by way of adding them to the crude oils (Eow *et al.*, 2001; Clause *et al.*, 2005).

Demulsifiers are a combination of various chemical compounds with several chemical structures and a big distribution of molecular weights (Djuve *et al.*, 2001). Demulsifiers can be categorised with regards to their molecular weight; low molecular weight demulsifiers (LMW) of  $1000 >$  and high molecular weight demulsifiers (HMW) of 1000-10000, besides pure solvent demulsifiers, that are used in the destabilisation of crude oil emulsions to separate crude oil (Jones, 1978; Clause *et al.*, 2005).

The HMW molecules consist of various sorts of macromolecules and polymers in conjunction with polyelectrolytes. These molecules should pierce the interfacial film that surrounds the droplets of the water and as a result, change the rheological properties of the film material. In view of the fact that demulsifiers are exceedingly efficient as film modifiers, they tend to be used in an extremely low concentrations, e.g. 5 to 20 ppm (Mohammed *et al.*, 1994; Wu *et al.*, 2003). The principal functions of LMW demulsifiers are to change the wettability of stabilizing components and increase interfacial activity. Moreover, solvent demulsifiers have several uses as emulsions stabilisers. The commonly used method of destabilising via solvent demulsifiers is to dissolve the particles of the aromatic compounds in a swelling process which generates the monomeric and oligomeric asphaltenes (Mhatre *et al.*, 2015). Subsequently, the aromatic content will be reduced slowly, eliminating the interfacial activity of the components of the crude oil.

Demulsifiers have the ability to change interfacial activity and separate. The components of the demulsifiers combine to have different characteristics. For this to take place, the combination of these chemicals should have the following capabilities: be able to act like flocculants speeding up the sedimentation rate, change the rheology of the oil/water interface, function as wetting agents (changing the solid contact angle). In addition, they should be able to destabilise the protective film enclosing the droplet since they are strongly attracted to the oil/water interface (Zapryanov *et al.*, 1983; Kim *et al.*, 1995; May *et al.*, 1998).

Given that they exhibit these properties, demulsifiers are capable of splitting up emulsions with or without the help of a physical separation techniques. This is one of the reasons that they are

employed in researchers' experiments and are commonly utilised in the industry. They speed up the rate of interfacial film thinning, reduce the interfacial viscosity and shorten its time to rupture (Ese *et al.*, 1999; Langevin and Argillier, 2016). Moreover, it was established that a number of HMW demulsifiers are able to modify the asphaltene film on the surface of water in the same way as the resin fraction (Mason *et al.*, 1995). Consequently, the compressibility of the film is enhanced which results in decreased film rigidity (Goldszal and Bourrel, 2000; Rondón *et al.*, 2007; Zhang *et al.*, 2011).

Research conducted by Mason *et al.* (1995), showed that adding demulsifiers boosts droplet growth; a bigger droplet size indicates the conditions of the demulsification that are effective in damaging the interfacial films surrounding the droplets of the water in primary emulsions. As well as the mean droplet size, it was observed that the size distribution varies greatly if demulsifiers were present.

The interaction at the oil/water interface is mostly based on the interfacial activity and diffusivity of demulsifiers. Theoretically, this distinguishing feature is favoured by low molecular weight, given that high molecular weight demulsifiers show low diffusivity which produces low dynamic interfacial activity and results in a poor performance. In contrast, Kim *et al.* (1995), discovered that separation ability increases with increasing the molecular weight of the polymeric demulsifiers. In another study, Mohammed *et al.* (1994), stated that the ideal demulsifiers concentration regarding the destabilisation of emulsions is typically based on the type of emulsifiers as well as the molecular interaction that takes place between the crude oil emulsion and the demulsifiers. In view of the fact that there are various sorts of demulsifiers plus different compositions of crude oil emulsions, robust emulsion resolution is regulated by the interfacial properties of a combination of demulsifiers.

Research conducted by Goldszal and Bourrel (2000), ascertained that the dynamics of demulsification of water-in-crude oil emulsions is primarily dependent on the kinetics of the demulsifier adsorption at the interface. The findings obtained from their study proposed that coalescence is ideal for the rapid adsorption of demulsifier molecules. This is accomplished when the average interactions of the surface-active species are equilibrated with oil and water. It is also essential to note that Bhardwaj and Hartland (1994), reported on the necessity of the rate of adsorption of the demulsifier. The rate of demulsification improves under the following three conditions:

1. Increase in the system's temperature.

2. Increase in bulk concentration.
3. Increase in solubility of the demulsifier in water.

However, these chemical additives are extremely toxic, especially to marine organisms when demulsifiers are employed, which indicates that the aquatic environment is at risk of severe pollution. As a result, intense research is being undertaken to create environmentally friendly chemical additives. Additionally, the use of chemical demulsifiers in conjunction with other separation techniques is also being explored, with the intention of attaining a separation process that is sustainable and highly effective.

### ***2.7.1.2 Electrical Treatments***

By employing precipitators, electrical treatment has been effectively applied in crude oil refining (Cottrell and Speed, 1911). The apparatus used in producing the breakdown of emulsions under an electric field is called an electrical coalescer; Waterman (1965), described this apparatus in relation to its application in the petroleum industry. Currently, it is operated extensively for the division of water droplets in oil in various liquid-liquid dispersed systems. This is for the reason that it provides low operating and equipment costs, because it is adaptable to large throughputs and several effective and reliable designs have been produced over the years. Most conventional applications of electrocoalescence in the separation of the aqueous phase from the oil phase, apply a high voltage alternating current (AC) electric field. Numerous manufacturers employ AC fields due to their non-electrolytic nature and tolerance of high water contents.

AC dehydrators consist of an electrostatic field generator employing a transformer stimulating a single, horizontal electrode beneath a grounded electrode as illustrated in Figure 17. A weak potential gradient is produced between the energized electrode and the oil-water interface and a strong potential gradient is found between the energized electrode and the earth electrode. The lower electric field helps the rapid coalescence of wet oil that enters the vessel above the water interface and then the higher electric field causes further coalescence and dehydration. Once the oil is above the earth electrode, further electrostatic coalescence is unable to take place because an electrostatic field cannot exist above it (Noor, 2006; Aryafar and Kavehpour, 2009).

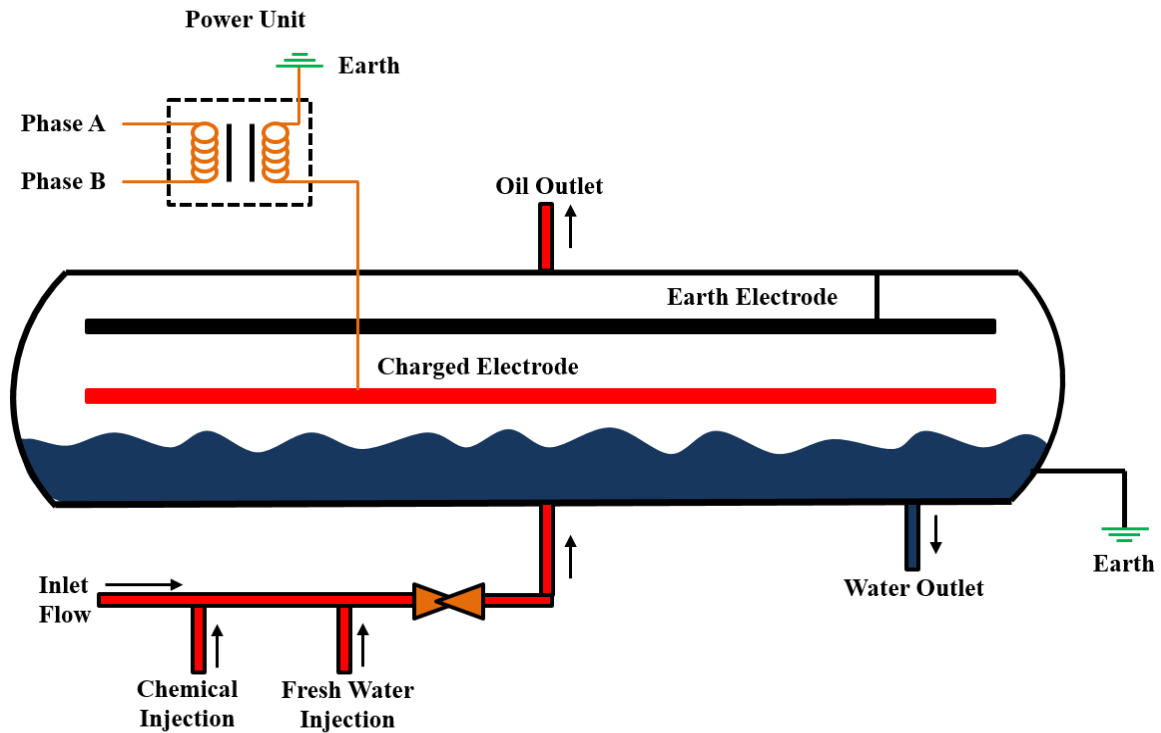


Figure 17: Schematic diagram of a conventional AC coalescer (Noor, 2006).

Typically, direct current (DC) is employed to separate the droplets of water from the emulsions of crude oil that have low water content. Even though the DC electric field has been used less in the past, in contrast to the AC field, the introduction of insulated electrodes and pulsed DC (Eow *et al.*, 2001), expanded the use of the DC electric field in this technology, for example in the treatment of emulsions with a high water content (Taylor, 1996). In another study, Eow (2002) created an electrocoalescer that applies pulsed DC which delivered good efficiency of separation of the aqueous droplets in a viscous oil flow.

The combined AC/DC field produces high water separation by combining the DC field (for low concentrations of water) with the efficacy of the AC field (for high concentrations of water). These sorts of electrocoalescers contain an array of electrodes (parallel and vertical) that are typically placed diametrically inside and along the vessel over the centreline, as illustrated in Figure 18. These separators employ around 1-3 transformers connecting two reversed diodes to create a DC field between neighbouring electrodes. To operate the AC/DC coalescer, an AC field is set up between the bottom of the electrodes and the interface of the oil/water. Moreover, similar to an AC desalter, the gradient of lower electric field encourages coalescence of the initial droplets in the high water content environment specifically over the interface (Noor, 2006; Aryafar and Kavehpour, 2009).

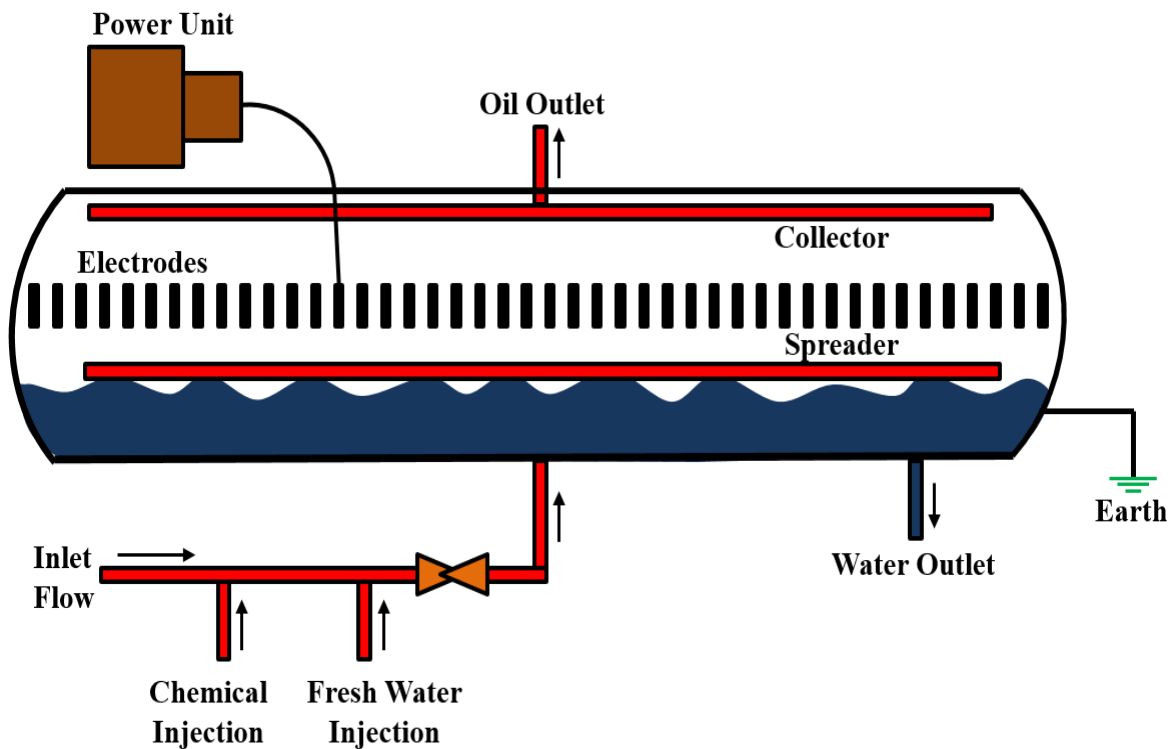


Figure 18: Schematic diagram of a combined AC/DC coalescer (Noor, 2006).

It should be mentioned here that the implementation of the electrostatic treatment to break up the emulsions of water-in-oil is possible for the reason that the system becomes non-conducting when the oil exists as a continuous phase. Moreover, this procedure is based on the coalescence and dynamic behaviours of the droplets of water within the emulsion (primarily W/O phase), while being in an electric field (Meredith, 1923; Eddy, 1937).

Electrical coalescence has various other applications as shown in Table 3 (Taylor, 1996):

Table 3: Different applications of electrical coalescence

Electrical coalescence applications	Applications summary
<b>Liquid membrane extraction</b>	In this application, stable water-in-oil emulsion is added to an aqueous phase that contains the surface-active species to be removed. This results in the improvement of the interior liquid membrane water phase. It is critical to break up the emulsion to recover the removed species.
<b>Solvent extraction</b>	This is where the low stability dispersion in mixer-settlers is improved by means of the electric field application.
<b>Dehazing of refinery distillates (electrofining)</b>	In this application, the entrained water (e.g. in gas oil or kerosene) is decreased to a tens of ppm which is below the solubility limit.
<b>Crude oil refinery desalting</b>	In this application, the corrosion of the distillation equipment is prevented by removing salt from crude oil.

The application of electrostatic separation of the water-in-oil emulsions has numerous distinctive advantages; specifically, low power consumption attributable to low electrical current flow through the dispersion. Similarly, the procedure does not rely on moving parts, which indicates that it will not experience mechanical breakdown (Lee *et al.*, 2001; Eow, 2002). Conventional electrocoalescers commonly operated in the industries of oil and petroleum are large and take up a great deal of space as a result of the large setting zones and long residence time required to isolate the droplets of water from the continuous phase (Urdahl *et al.*, 1996; Midtgård, 2009). Therefore, to develop equipment which is more compact, robust, transportable and efficient it is necessary to intensify the separation process.

### 2.7.1.3 Combining Different Techniques

As a result of improvements in modern day technology, researchers have gained a better understanding relating to crude oil and its emulsifying properties. Consequently, attempts are being made to design equipment that is more reliable with the aim of quickly separating the emulsion. Blending the technology of electrical separation with several other procedures, for

example, the application of mechanical separation methods like centrifugal force (Bailes and Watson, 1992; Edmondson, 1998), gravitational force (Eow *et al.*, 2002), heating (Woelflin, 1937; Edmondson, 1998) and the addition of chemicals (Fisher, 1931; Herbsman, 1933), was found to improve the electrocoalescence process of the water droplets in oil. Additional methods that have been identified such as membrane filtration (Cottrell and Speed, 1911; Eddy, 1936), mixing (Eddy, 1936; Bailes, 1987), and the use of high pressure and temperature (Eddy, 1932; Eddy, 1937), were also combined with technique of electrical separation in order to increase the performance efficiency. The combination of the electrical separation with other technology is summarised in Figure 19. Also, the details of previous works conducted pertaining to the emulsion of water-in-oil phase separation by way of applying an electric field are illustrated in Table 4.

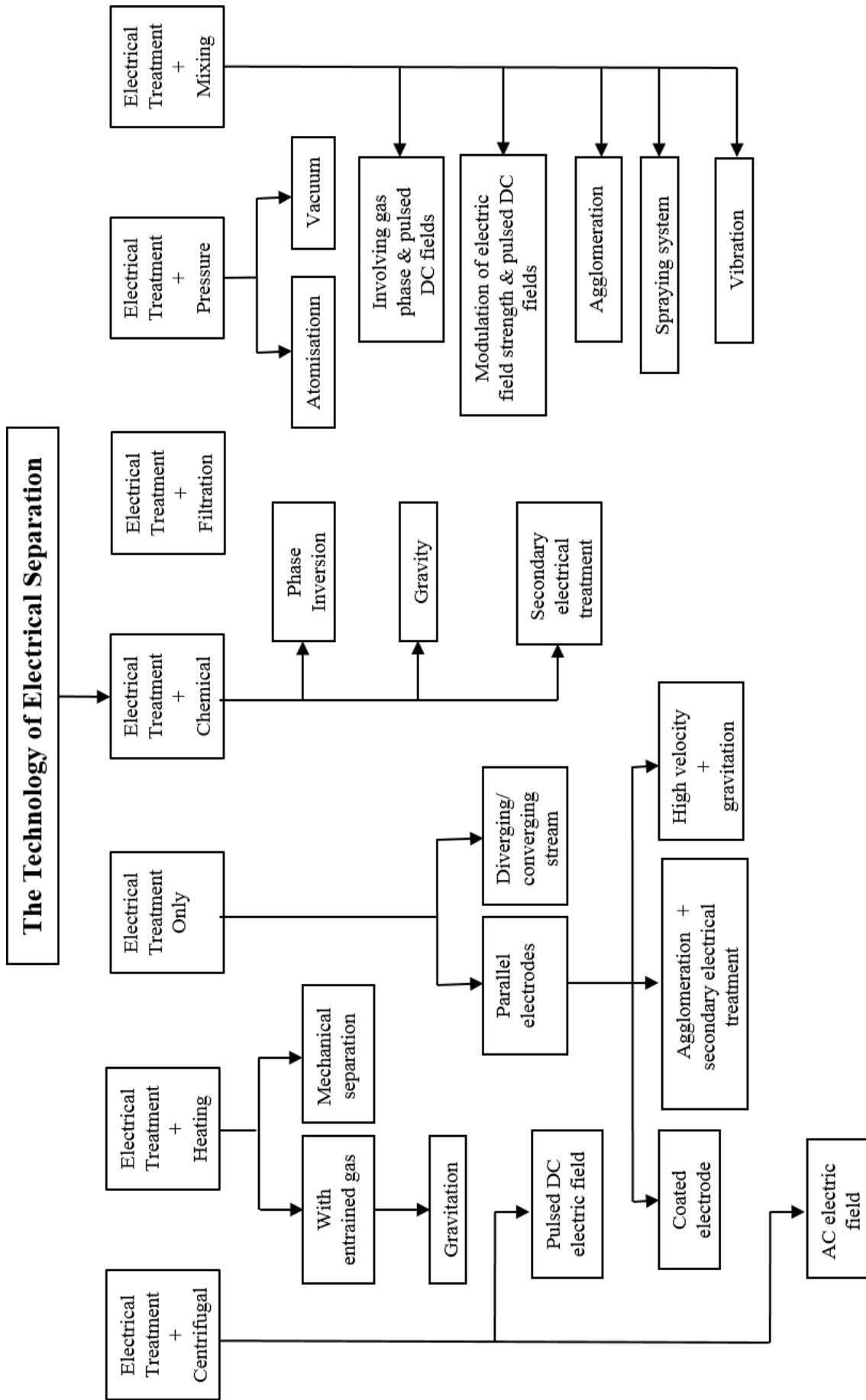


Figure 19: Different combination of the technology of electrical separation (Eow and Ghadiri, 2002)

Table 4: Electrostatic coalescence of droplets of water in oil (Eow *et al.*, 2001).

Investigator	Type <sup>I</sup>	Apparatus <sup>II</sup>	Electrode <sup>III</sup>	Dispersed phase (hold up, vol %)	Continuous phase
Charles and Mason, 1960b	B	CV	CP; d.c.	Water (single drop)	Heptane
Bailes and Larkai, 1982a, 1981	C	RD	CP; pulse d.c. (1, 1.5, 60 Hz)	H <sub>2</sub> SO <sub>4</sub> (standard)	Escaid 100-LIX64N
Ino <i>et al.</i> , 1983	B	CV	GT; a.c.	NaCl aq. sol.	Kerosene-Span 80-LIX64N
Galvin, 1986, 1982	C	RD	CP; pulse d.c. (1-10 <sup>3</sup> Hz) and d.c.	Water (50%)	Mix sol.-aluminine 336
Yamaguchi <i>et al.</i> , 1985	C	COL	BP; d.c.	NaCl aq. sol.	Kerosene-Span 80
Hsu and Li, 1985	C	CV	CT; a.c.	FeSO <sub>4</sub> aq. (33%)	Paraffin-Polyamimr-D2EHPA
Kriechbaumer and Marr, 1985	C	RD	CP; a.c.	CuSO <sub>4</sub> aq.sol. (14%)	Shellsol-ECA4360-LIX64N
Kataoka and Nishiki, 1986	C	RD	BP; pulse d.c.	NaCl aq. sol., others	Kerosene, -Span 80-TOA, LIX64N
Mori and Eguchi, 1986	B	RD	CP; a.c. (60-1800 Hz)	LiOH, HCL aq.sol.	Dodecane-SP-010, ECA4360J
Bailes and Stitt, 1987	C	Col	CT; pulse d.c. (4 Hz)	NMP + ethylene glycol (80%)	Isopar M
Yan <i>et al.</i> , 1987	B	CV	CT; pulse d.c. (0.5, 5, 50, 500 Hz)	NaOH aq.sol. (20, 70%)	Kerosene-Polyamine TOA, others
Kumar <i>et al.</i> , 1987	C	Col	CT; pulse d.c. (1-100 Hz)	Cu aq.sol. (25, 50%)	Escaid 100-LIX64N
Taylor, 1988	B	Microscopic cell	GT; a.c.	Distilled water (5%)	Crude petroleum oil
Hano <i>et al.</i> , 1988	C	CV	CT; a.c.	CuSO <sub>4</sub> aq. sol., others (50%)	Kerosene-Span 80, others
Goto <i>et al.</i> , 1989	C	TV	CP; a.c.	CuSO <sub>4</sub> aq.sol., others	Kerosene-Span 80-LIX64N, others
Hauertmann <i>et al.</i> , 1989	C	RD	CP; a.c. (0.1-2 kHz)	H <sub>2</sub> SO <sub>4</sub> aq.sol., other	Kerosene-Span 80-D2EHPA, others
Taylor, 1991	B	Cylindrical microscopic cell	GT; a.c.	Double distilled water containing 0-0.5 M (4%) AnalarR NaCl	Dry, export grade Kuwait crude oil
Hirato <i>et al.</i> , 1991	B	TV	BP; d.c.	Na <sub>2</sub> CO <sub>3</sub> aqueous (50%)	Kerosene
Chen <i>et al.</i> , 1994	B	Microscopic stage cell	BP; d.c. (1-50 Hz)	Water (20%)	Buchan crude oil
Williams <i>et al.</i> , 1995	C	RD	CP; a.c.	Water (2.5%)	Gas oil
Figuroa and Wagner, 1997	B	CV	CT; a.c (200 Hz); pulsed d.c. (600 Hz)	Distilled water (2.5-50%)	Guayule resins dissolved in xylene

<sup>I</sup>B: batch demulsification; C: continuous demulsification.

<sup>II</sup> Col: volume (Vertical direction); CV: circular vessel (with radial flow); RD: rectangular duct;

TV: tubular vessel (horizontal direction).

<sup>III</sup> BP: bare plate; CP: coated plate; CT: coated tube; GT: glass tube; a.c.: alternating current; d.c: direct current.

### **2.7.2 Pressure Effect**

Water-in-crude oil emulsions are commonly formed under high pressure (>5000 psi) in real operating conditions. Only a few studies have been performed concerning the effect of high pressure on separation. Nevertheless, Sjöblom *et al.* (2003), conducted a study approximately 17 years ago with respect to characteristics the emulsion of water-in-crude oil and the performance of separation under high pressure. The experiments they conducted revealed two major effects of pressure: (i) an increase of pressure gave an emulsions of a high stability for the separation at pressure above the internal bubble pressure, and (ii) an increase of pressure below the bubble pressure gave an increase in the separation. The bubble pressure is described as the pressure essential to expel the bubble of an air through a pore of a particular size in a certain liquid.

Sjöblom *et al.* (1992) also demonstrated in previous research that a good correlation exists between emulsions stability and the interfacial pressure. Zadymova *et al.* (2017), explored the implication of phase pressure (inner and outer), on the strength of the interfacial film on numerous emulsions. The obtained outcomes indicated that the emulsion long term stability was reliant on the osmotic pressure of droplets in the dispersed phase.

Pressure has also some effect on the properties of crude oil such as distribution of the chemical composition and solubility. However, Dale *et al.* (1997), have proved in their study that the effect of pressure on the distribution of aromatic hydrocarbons in crude oils is only marginally effected. Pekdemir *et al.* (2003b), observed in their research that an increase in pressure generated the demulsification acceleration. Nevertheless, dissolved carbon dioxide pressure did have an influence on the rate of demulsification.

Thus, high pressures are not useful for demulsification but low pressure can have some use.

### **2.7.3 The Effect of the Oil Phase and Aqueous Characteristics**

Research conducted previously reports that the stability of the emulsion of a water-in-crude oil is exceedingly dependent on the given crude oil properties. Aomari *et al.* (1998), claim that data considering the state and stability of these emulsions are crucial with respect to selecting the most appropriate method regarding time, budget and effectiveness to destabilise or treat these emulsions expediently.

Although the emulsions of water-in-crude oil are macro-emulsions unstable thermodynamically, it is worth noting that they are incredibly resistant to coalescence and demonstrate high dynamic stability through a long period. This stability is caused by means of the natural presence of surface-active substances in the crude oil. Primarily, crude oil includes numerous aliphatic molecules which vary in regard to their composition and shape. Additionally, it has been observed that the asphaltenes and resins act as the crucial surfactant at the interface of the water/oil as a result of their attraction to each of water and oil (Schorling *et al.*, 1999; Ali and Alqam, 2000). However, additional factors such as the rheological behaviour of the emulsions, for instance surface tensions, interfacial tensions and viscosity, besides the volume fraction of the dispersed phase, also have an effect on the stability of emulsions that are reliant on the chemical content to both of aqueous and oil phase. Additionally, this influence is considerably boosted by specific metal ions that are observed in the aqueous phase; especially,  $\text{Ca}^{2+}$  and  $\text{Mg}^{2+}$  (Jones, 1978).

The dissolved  $\text{Mg}^{2+}$  is liable to enhance the film relaxation, developing low-stable emulsions. Nevertheless,  $\text{Ca}^{2+}$  was detected to have the opposite effect and produce more stable emulsions. While the amount of water fraction was not discovered to affect the emulsions stability, extremely low (<30%) or extremely high (>90%) of water content will produce emulsions that are observed to be unstable (Figuroa and Wagner, 1997).

Thus, the operating conditions for any separator unit should be flexible enough to be adopted for different crude oils or variations in oil composition.

#### **2.7.4 Electric Field Effect**

The key basic features with respect to electric field formation with a high voltage in demulsification of water-in-oil emulsions can be classified based on the dominant electrical mechanisms in the system. It should be pointed out that DC, AC and pulsed DC are used commercially and have been employed in numerous studies. Each sort of field performs in a different way in stimulating phase separation by way of coalescence of droplets.

Taylor (1995), in his study, has illustrated that the AC fields operate as a consequence of the polarization of water droplets and the subsequent dipole induction, whereas DC fields work by means of producing rapid electrophoretic motion of droplets of the water that are pre-charged via an immediate contact with electrodes through more static conditions than for AC methods.

Systems of pulsed DC are known to be fairly similar to AC procedures which include an induced dipole on droplets that in turn creates gravitation (moving closer) and coalescence between neighbouring droplets. Nevertheless, more robust modern alternatives are available as regards to the efficiency of separation, particularly when combined with isolated electrodes.

The separation efficiency of the water and oil phase via the application of an electric field is regulated by different factors; specifically, the type field such as DC, AC or pulsed DC, the voltage, the frequency, and the design of the electrodes and the electrocoalescer. Gang and associates (Gang *et al.*, 1997), have operated a batch DC electric demulsifier to break-up an emulsion of water-in-oil. Despite the fact that the implementation of various electric fields will usually produce similar outcomes, the size of the diameter of the internal emulsion droplet and the demulsification rate will be vary depending on the type of field and the field intensity. Therefore, this stipulates the use of diverse fields depending on the starting material and furthermore, the desired end product.

Generally, and based on theory, the efficiency of coalescence is predicted to be directly proportional to the field strength. Mostly this is correct, although the performance of separation is also dependent on the surface and physical properties of the system, as well as the average size of inlet droplets, the hold-up fraction of dispersed phase and the surfactant (type and concentration) (Eow and Ghadiri, 2002). Consequently, intensifying the field will not always enhance the best phase separation and thus, there will be an operational limitation to the demulsification method. With regard to the application of this process, there are other drawbacks, for instance problems produced by the diffusion of entrained water. Nevertheless, modifications to the system can enable these problems to be surmounted (Taylor, 1995 ).

To date, the use of the external electric field in the research that has been conducted, is designed to explore ways to improve the efficacy of the coalescing process by means of using of various field directions and field strengths. Over the years, there have been several crucial developments pertaining to the basic knowledge relating to the electrocoalescer. Nevertheless, understanding of the droplet coalescence in an electric field has not been mastered yet, as a result of the complication of electrostatic interactions (Taylor, 1996; Zhang *et al.*, 2011).

There is a noticeable disadvantage in an electric field in relation to the separation of aqueous/oil dispersions that limits the performance of electrocoalescers. Despite improving the coalescence of water droplets in oil, the electrostatic fields which a rise from exceedingly high voltage can produce deformation and the breakup of aqueous drops into smaller droplets. For instance, a

study undertaken by Ha and Yang (1999) demonstrated that numerous small emulsion drops were created when an electric field was employed to remove bigger droplets in the emulsion. Which were not easy to remove under the same electrostatic field conditions.

The kinetics of droplet deformation and coalescence in an electric field have been the subject of numerous laboratory experiments. These phenomena can be extremely difficult to predict accurately, seeing as there are various factors to take into account. Eow and Ghadiri (2003c) demonstrated that in the presence of a high strength electric field, aqueous drop deformation in dielectric liquids was dependent upon the electrical conductivity and the characteristics of the continuous oil phase along with the viscosity and the surface tension of the aqueous drop. Hypothetically, more of polar liquids have a greater effect on the drop deformation but this is difficult to predict for a given composition. Thus, in view of the fact that the deformation and breakup of the drop under the intensification of the electric field is complicated, experimental investigation is necessary to optimise an electrocoalescence process.

Three particular aspects must be considered before any implementation of electro coalescence; specifically:

- The electrocoalescer design;
- The electric field nature: and
- The kind and properties of the emulsion that will be dealt with.

To design an electrocoalescer in respect to the electrode geometry and the direction of applied electric field, the required knowledge must be a detailed understanding of the mechanisms of coalescence that occurs in the separation of oil/water in an electric field. However, this knowledge is yet to be investigated systematically. It should be noted that the best design of an electrocoalescer should be based shorter residence time, with the aim of minimising the equipment's size and weight to save cost and time (Eow and Ghadiri, 2003b).

---

## CHAPTER THREE

---

### 3. IMPROVEMENT OF ELECTROSTATIC SEPARATION OF WATER-IN-CRUDE- OIL EMULSIONS USING POLYHIPE DEMULSIFIERS

#### 3.1 Overview

This chapter of the thesis includes two major parts.

- I. The first part summarises the available methods for optimized electrostatic demulsification along with the major factors that affect their performance.
- II. The second part presents the fundamentals of micro-porous polymers often termed as polyHIPE and highlights generic aspects regarding their physical characteristics, structure as well as morphology. Applications and additional functionalities of these polymers are also taken into consideration.

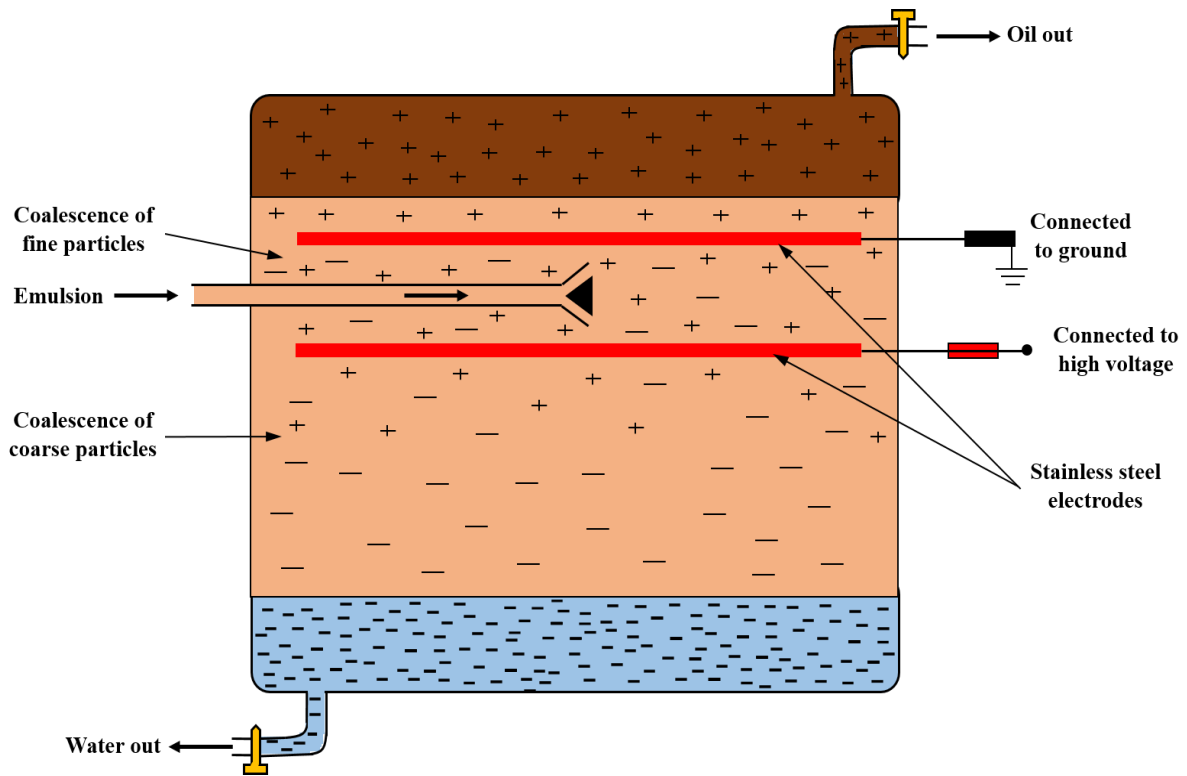
#### 3.2 Mechanics Involving Electrically- Optimized Demulsification

Laboratory work by Bailes and Larkai (1984), proved that enhancements of phase separation of water-in-oil dispersions can be achieved by the use of a high electric field of any type. Despite lack of study of the actual mechanics of such a phenomenon, it remains reasonable for the majority to believe that the externally-generated electric field has the potential to originate two coalescences and/or interactions namely droplet-droplet and droplet-interface with both having potential for phase separation. Since 1911, when the electrocoalescer was patented (Cottrell and Speed, 1911), not much progress has been made as regarding the theoretical aspects of the principles and the associated factors underlying the advantageous performance. Nevertheless, considerable attention has focussed on the way to design new and improved electrocoalescers. According to Taylor (1996), the main points featuring in the electrocoalescer design are as described below:

- Improved potential for contact between the dispersed droplets.
- Stimulation of the thinning of the interfacial film of the droplets.

- Ease of droplet-droplet coalescence by film rupture, followed by sedimentation by gravity.
- Induction of droplet-interface coalescence, thus leading to phase separation.

When two droplets of a W/O emulsion are close to one another in the presence of an electric field  $\mathbf{E}$ , the charges thus induced will cause the particles to experience mutual attraction. In the case of two liquid spheres of equal radius and dielectric constant,  $a$  and  $\varepsilon$ , respectively, and with a distance  $d$  of separation within an oil with dielectric constant  $\varepsilon'$  the attractive force can be estimated by the electrostatic formula as  $6 (\varepsilon/\varepsilon') E^2 a^2 (a/d)^4$ . The quantity  $(a/d)^4$  is proportional to the dispersed phase concentration (Bailes and Larkai, 1984; Taylor, 1996; Lesaint *et al.*, 2009; Mousavi *et al.*, 2014). Also, it is almost independently related to particle size for the purpose of maintaining the factor  $(a/d)^4$  almost unchanged until the occurrence of partial phase separation. The rate of coalescence has a linear relationship with  $E^2 a^2$ . Nonetheless, with a large particle size, the applied electric field causes deformation and disruption of the particles. Generally, separation is possible by applying either a direct or alternating voltage to the isolated electrode whilst injecting the emulsion between the electrodes where the electric field is greatest as illustrated in Figure 20. The flow pattern is designed such that in parts of the emulsion where the particles do not attain a sufficient diameter, they will be upcycled into the area between the electrodes where coalescence occurs at much faster rate (Waterman, 1965; Ino, 1983; Urdahl *et al.*, 1996; Sams and Zaouk, 2000).



Note: + signals positive charges, - signals negative charges

Figure 20: Schematic diagram of demulsification in a coalescing apparatus illustrating the effect of the electric field (Waterman, 1965)

### 3.2.1 Charging of Droplets

Theoretically, by applying an electrical field to the W/O emulsion a variation in the electrical charge characteristics of the droplets will be induced. This will further promote either a charge redistribution or an increment in the free density of charge in the actual system. Zhang *et al.* (1995), suggested that however strong, the applied electrical field is capable of inducing opposite charges on the nearby surface of two aqueous droplets. During emulsion processing with uncharged particles, dipolar coalescence becomes the dominant dynamics (Williams and Bailey, 1986; Tarantsev *et al.*, 2013). If a droplet of water is placed in an electric field of low dielectric constant and low conductivity, the droplet will experience polarisation because the dipole molecules will re-orientate regarding to the electric field shown in Figure 21 (Taylor, 1996).

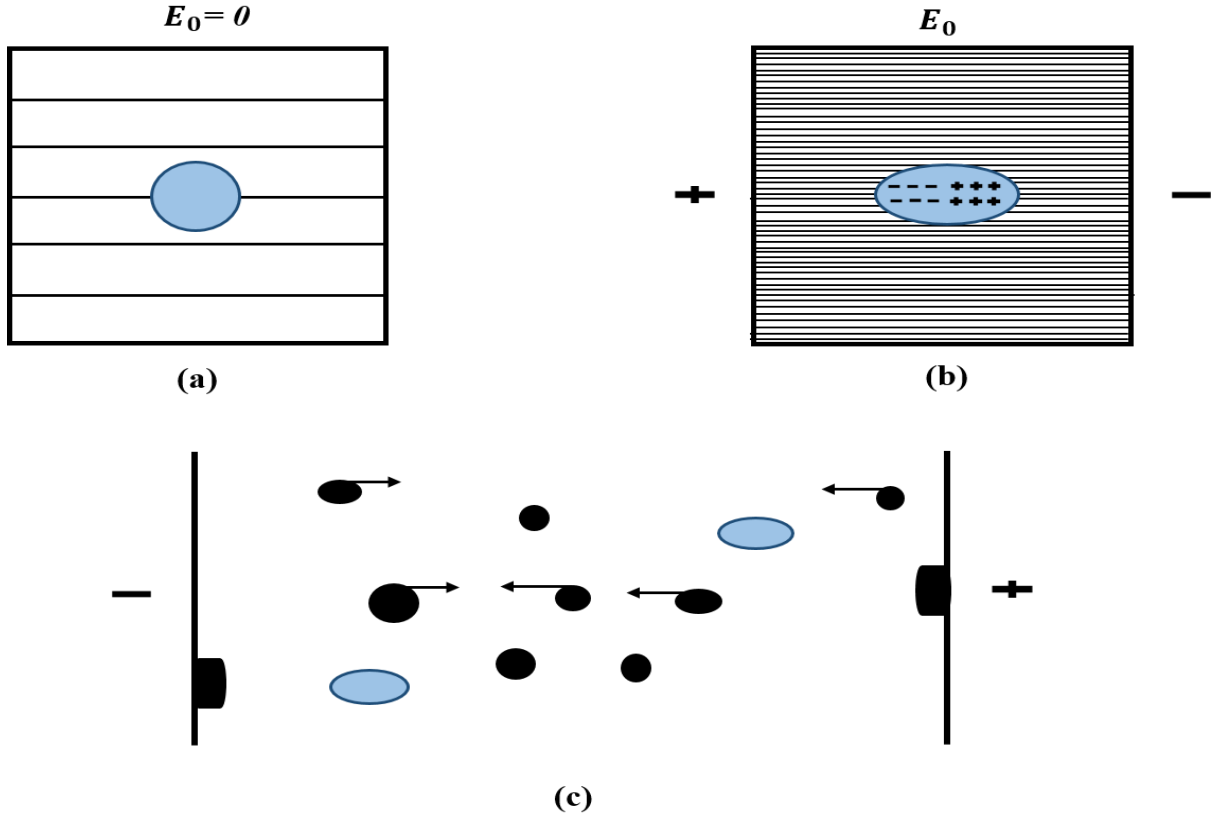


Figure 21: Schematic illustration of; (a) and (b) Polarization of a single droplet of water in an electric field; (c) Migration of droplets and interaction as a result of contact charging upon impinging on an isolated electrode (Taylor, 1996).

By exposing the droplet to an electric field of strength  $E$ , a constant sphere of dielectric constant  $\epsilon$ , within a medium of infinite dielectric constant  $\epsilon'$ , it senses a built-in electric field in the  $z$  plane direction  $E_{iz}$  estimated by the following formula (Taylor, 1996)

$$E_{iz} = \frac{3\epsilon'}{2\epsilon' + \epsilon} E \quad \text{Eq. 14}$$

With regard to emulsions of W/O with  $\epsilon > \epsilon'$  and considering that the intensity of the electric field is less in the aqueous droplets compared to the continuous phase. This reverses in the operation of the O/W systems. The momentum of the effective dipole characterising a spherical droplet ( $\mu_{eff}$ ) of radius  $r$  is estimated by

$$\mu_{eff} = \left(\frac{4}{3}\right) r^3 \pi P_{eff} \quad \text{Eq. 15}$$

where  $P_{eff}$  is the polarisation excess per unit volume given by  $(\epsilon - \epsilon')E_{iz}$ .  $\epsilon_0$  is the permittivity of vacuum.

Polarisation is compensated by elongating droplets into prolate spheroids of minor and major x-axis and y-axis and the extent of deforming of a droplet  $D$  from its premier radius  $r$  is calculated by

$$D = \frac{9rE^2\varepsilon'\varepsilon_0}{16\psi} O \quad \text{Eq. 16}$$

where

$O$ : is the complex function representing electrical properties of the droplet and medium,

$\psi$ : is the interfacial tension.

Considering a high level of applied field as described by a critical electrical field  $E_{crit}$  (which can also cause deformation of spherical droplet) it is found that

$$E_{crit} = K \left[ \frac{\psi}{r \varepsilon_0 \varepsilon'} \right]^{\frac{1}{2}} \quad \text{Eq. 17}$$

The above expression suggests that the electric field needed to cause a droplet deformation in aqueous systems is dependent on both interfacial tension and droplet radius.

As a consequence, the droplets move in the counter direction towards the other electrode resulting in droplet-droplet collision and coalescence at a specific radius from the electrode. This phenomenon is often termed as contact charging. In 1970, Panchenkov and Vinogradov (Panchenkov and Vinogradov, 1970), illustrated theoretically, for ellipsoidal droplets, that the droplet speed is the net sum of the speed due to the charge contribution and the speed that caused by gravity. On the other hand, in 1996, Taylor (Taylor, 1996) suggested that the results of the theory were very different from his experimental results for the following reasons:

- Droplet-electrode contact times are limited, causing the charge magnitude not to be optimized.
- Mis-considering of droplet distortion due to the electric field.
- Charge leakage to the continuous phase over droplet movement.
- Limitation in the applications of Stokes's law which predicts the deposition and separation of large droplets due to gravity.
- Errors in experiments.

### 3.2.2 Electrostatic Interactions

Five forces, namely, gravitational, drag, dipolar, electrophoretic and di-electrophoretic forces are applied to a water droplet suspended between pairs of electrodes as shown in Figure 22. Gravitational forces are just equal to the weight of the studied droplet and act to drive the water droplet down to the bottom of the vessel (Draxler and Marr, 1993). Drag forces are also imposed by the rising oil sliding past the water droplet and act to uplift it to the oil outlet. Provided that the water droplet becomes larger than the Stokes' droplet diameter  $d_{stoke}$  computed by the following formula,

$$d_{stoke} = \sqrt{\left(\frac{18v_v\mu_o}{g(\rho_w - \rho_o)}\right)} \quad \text{Eq. 18}$$

where

$\rho_w$ : is the density of water,

$\mu_o$ : is the viscosity of crude oil,

$\rho_o$ : is the density of crude oil,

$v_v$ : is the velocity of the vertical oil.

then the drag is less than the weight and hence the droplet of the water will separate from the oil.

To optimize the process performance of demulsification, the electrostatic forces have to provide droplet coalescence to diameters higher than the stokes' diameter. There are three electrostatic forces in the process namely dipolar, electrophoretic and dielectrophoretic (Draxler and Marr, 1993).

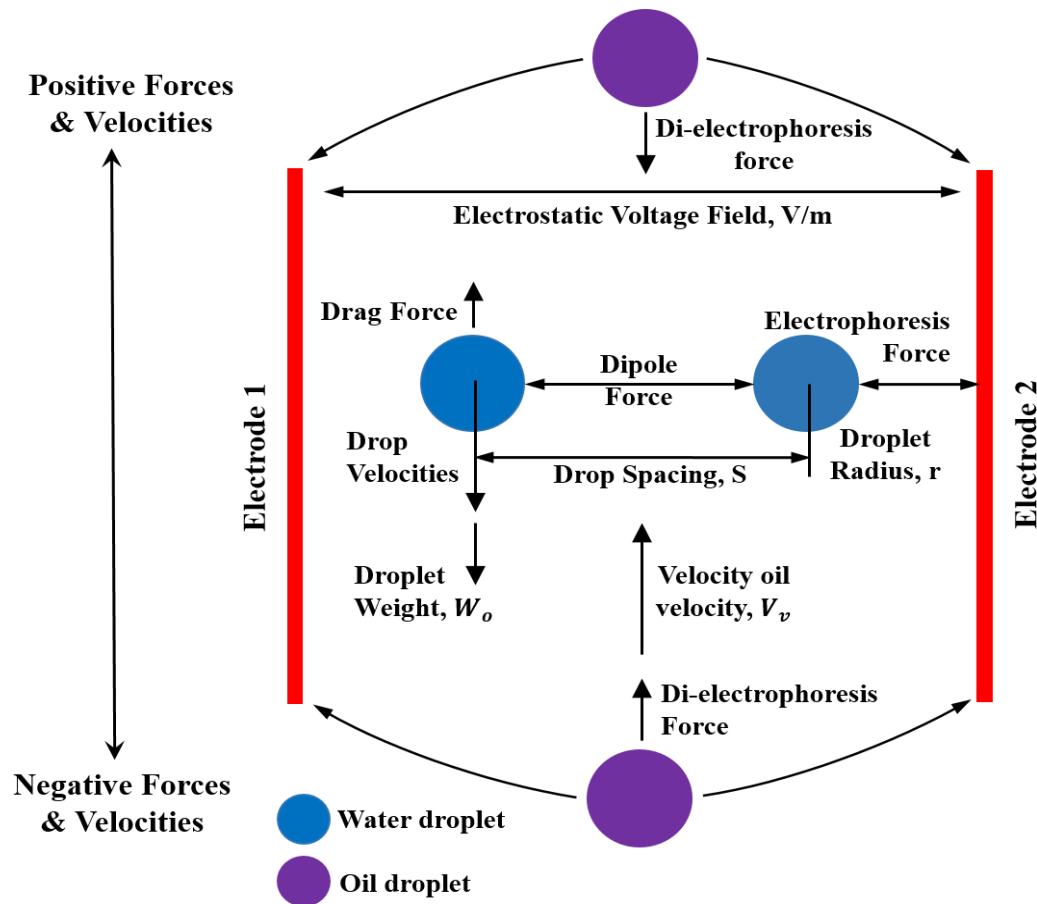


Figure 22: Schematic illustration of coalescence forces (Draxler and Marr, 1993).

### 3.2.3 Interactions between Droplets

The phenomenon of electrocoalescence has been used for some time without a fully comprehensive knowledge of its working principles. One reason of this gap of understanding is due to the complexity of interactions between the electrostatic and hydrodynamic fields. Nonetheless, many mechanisms have been put forward for the separation of emulsions within an electric field in a practical environment. The available mechanisms are as diverse can include the three stage process, electrophoresis, dielectrophoresis, chain formation, formation of intermolecular bonds, electrofining and dipole coalescence and random collisions (Ptasinski and Kerkhof, 1992; Scott *et al.*, 1994; Taylor, 1996; Eow and Ghadiri, 2002; Eow and Ghadiri, 2003a; Lesaint *et al.*, 2009). Interestingly, in the process of separation, one mechanism typically becomes the predominant and this relies on distinct factors such as volume fraction of the disperse phase, topology of the electric field and electrode geometry (Eow and Ghadiri, 2002; Lesaint *et al.*, 2009).

### 3.2.3.1 Three-Stage Process

Regarding coalescence, a mechanism called the three-stage process was proposed as described in (Sun *et al.*, 1998; Dezhi *et al.*, 1999; Less *et al.*, 2008b; Mhatre *et al.*, 2015). The occurrence of this process can be either between droplets within an immiscible liquid setting or between a droplet and its bulk phase. As the name suggests, this process consists of three stages in a sequential order. In the first stage, two or more droplets are separated by a film of continuous phase, with each approaching the other. This is followed by the second stage in which the film between the droplets begins to thin so that the interfacial area is reduced (Chen *et al.*, 1998; Less *et al.*, 2008b; Li *et al.*, 2016a). The fluid stage consists of film rupture and coalescence.

The thinning of the film is governed by many other factors such as disjoining pressure, capillary pressure as well as Marangoni effects in the presence of surfactant (Isaacs *et al.*, 1991; Isaacs and Chow, 1992; Rommel *et al.*, 1992; Ha and Yang, 1998; Teigen and Munkejord, 2010). With a high shear rate, the film thinning is characterized by a rate which is reciprocally proportional to the square root of drop size. When the film achieves a specific thickness, it becomes easier for rupture by any significant disturbance as in case of an applied electric field (Isaacs *et al.*, 1991; Isaacs and Chow, 1992; Ha and Yang, 1998; Suslick, 1998). Because the film thinning is often the rate controlling step, the faster the rate of film thinning, the smaller the droplets and consequently the quicker the coalescence process.

### 3.2.3.2 Dipole Forces

Major studies (Bailes, 1987; Xie and Yan, 1993; Williams *et al.*, 1995; Lee, 2003) have considered that dipole forces are to be the dominant drives of electrocoalescence in any electric field. This only happens when droplets are sufficiently closed to each other for the interaction of dipole forces to be significant. Brownian motion, sedimentation, mixing, flocculation and specially electrophoresis are amongst the available methods of bringing the droplets close to each other. Additionally, if two droplets are sufficiently close, Van der Waals attraction acts to pull of nearby droplets into contact. Alignments in the polar water molecules establish the dipole force  $F_d$ , and this is related to the electric field. Both the water droplet diameter and the distance between the droplets can be seen in the equation below

$$F_d = \frac{24\pi\epsilon_1\epsilon_0r^6E^2}{(2r + d)^4} \quad \text{Eq. 19}$$

where

$r$ : is the radius of the drop;

$\epsilon_1$ : is the dielectric constant of the continuous phase;

$d$ : is the distance between nearby droplet surfaces.

$\epsilon_0$ : is the permittivity of free space.

$E$ : is electric field strength.

Assuming the droplets of the water are of the same size and have a homogeneous distribution, it is clear to see that both the distance and the dispersed water volume are inversely related. Arguably, as the dispersed water is coalesced and is not mixed with the oil, the distance sees an increase and dipole forces suffer a rapid decline. As a result, the dipole forces become weak very quickly as droplets coalesce but do not separate from the oil.

### **3.2.3.3 Thinning and Breaking**

The strength and the stability of the film of oil between the water droplets is directly related to the properties of W/O emulsions. A two-stage process controls the life time of film and is termed thinning and breaking. The drainage of the liquid by the action of gravity (Taylor, 1996; Eow *et al.*, 2001; Eow and Ghadiri, 2003c) causes the film to become thin. By the time an interfacial film reaches ultra-thin levels (100-1000 Å) it becomes unstable. The instability caused by Van der Waals forces is maximum at a specific thickness,  $s_c$ , and gives rise to rupture in the layer. Following this droplet-droplet coalescence occurs. However, because of surfactants the rate of film thinning is reduced and so is the demulsification rate (Taylor, 1988; Mohammed *et al.*, 1994; Ha and Yang, 1998; Teigen and Munkejord, 2010). Earlier studies as in (Charles and Mason, 1960; Charles, 1961; Brown and Hanson, 1965) have proved that the underlying process of droplet-interface coalescence in an electric field is due to film thinning which is further optimized by electrical forces on the droplet at the region of interface. The electric field between nearby droplets results in the break down of the dielectric of the continuous phase leading to much faster droplet-droplet coalescence.

#### **3.2.3.4 Chain-Formation**

When an electric field is applied to a W/O emulsion, chains of aqueous droplet can extend between electrodes. These chains are triggered by the dynamics of single droplets and are aligned parallel to the electric field direction. After chain formation, the coalescence of adjacent droplets takes place and the size of the droplets close to the electrodes greatly increase while new droplets are driven into the chain. This phenomenon is present in AC and DC electric fields, and is subject to many influential conditions involving the viscosity of the oil phase, the volume fraction of the dispersion phase as well as the size of the applied electric field (Skodvin and Sjöblom, 1996).

In 1954, Pearce suggested that chain formation indicates the presence of induced dipoles and continuous charges on the droplets (Pearce, 1954). One reason for this is the fact that the dipole-dipole interaction of nearby droplets gives rise to force of mutual attraction. Nonetheless, this is not always the case as suggested by Bezemer and Croes (1955); their suggestion was that an additional dielectric force causing the migration of droplets towards the region of high field strength has also the potential to affect relatively dilute emulsion systems .

#### **3.2.3.5 Electrophoresis and Dielectrophoresis**

Electrophoresis refers to the motion of charged colloidal particles based on a static approach under the influence of an applied electric field. Its governing principle is that charged particles will travel towards the opposite charge electrode and will be separated from each other by repulsion depending on their physical characteristics. The speed of the charged particles is a function of the zeta potential at the particle interface. This speed when divided by the magnitude of the electric field results in a quantity known as electrophoretic mobility (Stevens *et al.*, 1990; Isaacs and Chow, 1992; Galvin, 2013).

Dielectrophoresis refers to the phenomenon that takes place when a force is applied to a dielectric particle which is experiencing a non-uniform distribution of electric field (Pohl, 1958). If the permittivity of a droplet is higher than the suspension medium, for instance droplets of water in oil, it migrates to the region of greatest electric field. However, this happens even when the particle is uncharged and relies on the force experienced by all polar materials subjected to non-uniform electric field. Because the field is not uniform, one end of the dipole will be within a weak field region compared to the other which produces a net force, driving

the dipole to the greatest field region. In case of a field-aligned cylinder, the corresponding dielectrophoretic force (Pohl, 1958; Pohl, 1978),  $F_{dep}$  is given by

$$F_{dep} = \frac{\pi b a^2}{3} R_e \epsilon_m \left( \frac{\epsilon - \epsilon_m}{\epsilon_m} \right) \nabla |E|^2 \quad \text{Eq. 20}$$

where

$\epsilon$ : is the dielectric constant of the cylinder.

$\epsilon_m$ : is the dielectric constant of the medium.

$a$ : is the cylinder radius.

$b$ : is the half -length of the cylinder.

$\nabla |E|$ : is the electric field gradient.

This is only true as long as the electric field remains strictly constant over the particle length. The above formula only considers the dipole formed and does not apply to any higher order polarisation.

Pohl (Pohl, 1958; Pohl, 1978) is credited with the development of the basic theoretical aspects and early applications of this phenomenon. One crucial distinction between dielectrophoretic effects and those from electrophoresis is the involvement of AC rather than DC electric fields (Pethig *et al.*, 1992; Ramos *et al.*, 1999; Lackowski, 2015). In fact, in practical scenarios, it is usual to rule out this strategy because the speed of suspended droplets in a dielectric medium which are subjected to dielectrophoretic forces is relatively low in a strongly divergent electric field (Pohl, 1951; Pohl, 1978; Galvin, 1986; Galvin, 2013) in comparison to the speed caused by other forces. However, in scenarios where a droplet is difficult to be substantially charged, the dielectrophoretic effects in coalescence are regarded to be significant.

### 3.2.3.6 Random Collision

Random collision is the cause of coalescence during the electrofining process and is believed to happen due to collisions of charged particles. In this process, the electrode polarises to the same sign charge as the droplets which cause the droplets to be repelled by the electrode. As a consequence, droplet coalescence takes place after a collision of recombining opposite charged droplets occurs. This also happens when there is not a direct contact between the droplets and

the electrode. In this case, enough charging can take place via charge migration in the neighbourhood of the electrode (Eow *et al.*, 2001; Wagner and Nelson, 2016).

### ***3.2.4 Interactions at the Droplet-Interface***

Likewise, droplet-interface coalescence also takes place in two circumstances. Firstly, film thinning followed by film rupture as described previously Charles (1960a). Typically, a droplet suffers deformation when subjected to a liquid-liquid interface under the action of gravity; thus, the contact area increases due to the flatness of the surface (Wang *et al.*, 1994; Eow, 2003; Mhatre *et al.*, 2015). Droplet-interface coalescence takes place when a film thinning process consisting of draining of the intervening continuous phase and any stable moieties is able to weaken the remaining film sufficiently. At the beginning, both gravitational and inertial force trigger the thinning despite the further thinning stage due to viscous forces at later stages. When the film reaches a critical thickness,  $s_c$ , the thinning process ends and any disturbance applied to the system will cause the rupturing of the film.  $s_c$  was seen to increase as DC potential increased (Charles, 1960b). Additionally, Charles and Mason, suggested that electrical coalescence has short range and the probability of film rupture increases as the thickness of the film is reduced.

AC and DC electric fields have significant impact on the interface of droplets carrying both induced and direct charge (Allan and Mason, 1961). It was noticed that AC or DC fields did not led to different droplet-interface interactions. Nevertheless, with an applied potential coalescence was seen to become a process with a single stage. Moreover, it was also found that primary droplets with direct charge responded more quickly to the applied electric field compared to the droplets with induced charges.

Major studies (Charles, 1960b; Charles, 1960a; Brown and Hanson, 1965; Taylor, 1988; Ghadiri and Eow, 2003), on an electrically-optimized demulsification process, show that the stability of a water droplet, as measured by mean coalescence time, is reciprocally proportional to the electric field strength. An applied field may generate a force of attraction between droplets that can withstand the force of gravity. Temperature, however, affects the droplet-interface process due to the decrease of the viscosity of oil that it causes. Hence, film thinning happens at a much quicker rate at higher temperature.

Another factor is the addition of a surfactant, such as sorbitan monooleate (span 80) to the continuous phase which has considerable impact on demulsification (Allan and Mason, 1961).

Arguably, despite the fact that the induced electrical strength was seen to promote coalescence, the critical electrical strength decreased as the surfactant concentration rose. It is apparent that the surfactant in the continuous around the interface phase caused a reduction of the life time of water droplets, the interfacial tension decline this causes resulting in coalescence. In the situation of water droplets in a polar organic continuous phase, salts or electrolytes were observed to decrease the coalescence time (Chen *et al.*, 1998; Eow *et al.*, 2002; Eow *et al.*, 2007). In large contrast, the impacts were the opposite for organic droplet coalescence in an aqueous phase.

### **3.3 Factors Affecting Electrically-Optimized Demulsification**

The main purpose of the applied high-voltage electric field is to optimize the rate of the coalescence of water droplets in emulsion of water-in-oil in order to grow the droplets into a specific size so as to separate them from the continuous phase by centrifugal and gravitational forces. This is done by the promotion of droplet-droplet contact in the process environment as mentioned earlier. Nonetheless, coalescence will not require the contact between droplets to occur because there are other factors which influence the performance and efficiency of the separation that need to be taken into account.

#### ***3.3.1 AC and DC Electric Field***

If coalescence of a dispersed phase in an emulsion is to happen in an electric field, the conductivity of the continuous phase must be lower than that of the dispersed phase. Any type of field such as DC, AC, DC pulsed or any combination of them, has its corresponding approach in optimizing droplet-droplet coalescence. Generally, an AC field is useful for non-insulated electrodes in an emulsion of W/O with a high volume of dispersed phase (Galvin, 1986; Midtgård, 2009; Galvin, 2013). One suggestion is that high coalescence efficiency with increasing field size and frequency is achieved with the use of insulated electrodes (Hauertmann *et al.*, 1989). A recent study from Lee and co-workers (Lee *et al.*, 2001) supports this. They discovered that AC fields increased the coalescence at a greater rate compared to DC fields. However, opinions in this regard, diverge. Taylor (Taylor, 1988), suggested that an AC field has a considerable polarising effect and is typically applied in the presence of crude oil. Nonetheless, short circuits will arise if the continuous phase is distillate and when the

dispersed phase is either caustic or acidic. In this situation, a proper combination of AC and DC electric field is employed (Winslow Jr, 1977; Schorling *et al.*, 1999; Kang *et al.*, 2006).

The application of DC electric fields is not so common as compared to other types of fields and combinations because of inefficiency when performing demulsification. Bailes and Larkai (Bailes and Larkai, 1982; Bailes and Larkai, 1984), suggested that this inefficiency is either due to the field strength leakage or current leaking through the insulating liquid because of interfacial polarisation. On the other hand, a DC field promotes fast electrophoretic dynamics of water droplets since water droplets charge by direct contact with electrodes initially (Schorling *et al.*, 1999; Kang *et al.*, 2006). As a result, the rate of droplet-droplet collision will be more relevant as the speed of droplets increases along the electrodes.

After the works of Bailes and Larkai (Bailes, 1981; Bailes and Larkai, 1982; Bailes and Larkai, 1984) the use of DC fields with insulated electrodes gained an extended applicability. They have pointed out that by employing insulated electrodes, pulsed DC fields achieved improved efficiency compared to constant DC or AC. Moreover, their analysis has proposed the theory of an enhanced frequency (Taylor, 1996). The phase separation methods are like those of AC fields in which dipole-dipole forces are introduced on the droplets of the water by means of polarisation that results in attraction and coalescence amongst adjacent droplets. During this process, insulation of the electrodes is crucial because lack of insulation short-circuits the electrodes and the emulsion with a high volume of dispersed phase.

### ***3.3.2 Effect of Frequency***

Selecting the correct frequency is as important as the other influential factors the reason being the faster occurrence of droplet coalescence at this frequency. This is specifically valid at very low applied potentials. The primary description of this concept focuses on the properties of the dielectric coating materials and the dielectric constant in the continuous phase. Nonetheless, this is still open to argument as it remains unclear if an optimum frequency is caused by a power supply limitation or electromechanical relaxation of the dispersion (Chen *et al.*, 1994; Taylor, 1996; Eow and Ghadiri, 2003b; Zhang *et al.*, 2011).

### **3.3.3 Effect of Field Strength**

Apart from the type of field being used, the direction of the applied field was seen to have a considerable effect on the efficiency of coalescence (Chen *et al.*, 1994; Eow and Ghadiri, 2003b; Zhang *et al.*, 2011). These factors have suggested that in order to electrically induce a force strong enough to allow deformation of the close surfaces of the droplets before the action of droplet-droplet coalescence, the angle between the centre line of two droplets and the electric field must be brought near to zero.

Despite in many cases the coalescence rate increases with an increase in applied electric field (Bailes and Larkai, 1984; Goto *et al.*, 1989; Dezhi *et al.*, 1999; Less *et al.*, 2008b; Mhatre *et al.*, 2015), the reverse can also take place if the field becomes high enough (Less *et al.*, 2008b). Excessively strong fields can cause droplet break-up, which results in a highly-stabilized emulsion. Moreover, depending on the physical properties of an emulsion, the electric field has varying effects on the efficiency of the demulsification which are difficult to estimate because of solvent, surfactant and ionic species (Opawale and Burgess, 1998; Drelich *et al.*, 2010; Tshilumbu *et al.*, 2014).

### **3.3.4 Electrode Dimensions and Insulation**

The features and dimensions of an electrode (plate or cylinder) may also influence the performance of an electrically optimized process of demulsification. Typically, the selection of electrode characteristics depends on the electric field type and the emulsion type. Regarding the geometry of electrodes, the application and safety are the governing parameters for selection. Also, the arrangement of the electrodes and the spaces between them are functions of the electrical circuitry, the transformer design and the type and the direction of the field (Chen *et al.*, 1994; Eow and Ghadiri, 2003b). For example, electrodes are aligned vertically when a DC field is used to facilitate droplet growth and sedimentation to happen between electrodes whereas in AC coalescers, the electrodes are aligned horizontally for water droplets to pass along their length.

The selection of either insulated or bare electrodes is influenced strongly by the dispersed phase volume. When bare electrodes are utilised with high water content emulsions because of direct conductivity between electrodes short-circuiting may take place. This phenomenon results in electric field disruption; the field will decline considerably or in very severe situations be

reduced to zero, significantly reducing the electrocoalescer efficiency (Eow *et al.*, 2001; Atta *et al.*, 2011). Nonetheless, the major downside of insulated electrodes is due to the reduction of electrical potential at the electrode-emulsion interface. This issue is solved by the integration of a pulsed DC field with the insulated electrodes. A few examples of insulating materials used are TUFNOL, PTFE and ABS.

It should be noted that coalescers are usually not operated under conditions where dielectric barrier discharges are formed.

### ***3.3.5 Droplets Size and Contact***

Fast droplet-droplet contact does not always occur at the same rate as droplet-droplet coalescence (Taylor, 1996; Zhang *et al.*, 2011). In these scenarios, chains of droplets will be aligned in the direction of the externally existing electric field. This affects the electric field so that it becomes short circuit and compromises the performance of the system. For W/O emulsion systems, the existence of this type of chains is accounted for the viscous interfacial films enveloping any droplet (Taylor, 1988; Chen *et al.*, 1994; Galvin, 2013). This also thrives to avoid coalescence when an electric field is applied but introduce a lagging for highly viscous crude oil (Chiesa *et al.*, 2006; Mohammadi *et al.*, 2014). Luckily, by means of chemical additives to cause the weakening of the film this problem can be overcome.

Apart from viscosity, the droplet size of the dispersed phase accounts for another intrinsic properties in W/O emulsion that affects the electrocoalescence efficiency. In terms of naturally generated W/O emulsions, major factor affecting the size of the droplets include the following:

- Volume of water present,
- The strength of force applied to emulsion over the production,
- Shelf-life span of the emulsion,
- Quantitative and qualitative properties of crude oil interfacial (existence of naturally produced surfactant like resins and asphaltenes).

The major aim to apply electric field to unwanted or disturbed emulsions is to electrically induce coalescence. The field has the potential of promoting droplet-droplet coalescence by reducing the interfacial strength of the film between close droplets. In comparison, very strong electric fields promote dipole, sedimentation and especially migratory coalescence. This causes

the droplets to merge to a single extended droplet. According to Williams and Bailey (Williams and Bailey, 1986), the average diameter of droplets departing from electrocoalescer was seen to rise with time. This is a real evidence that an electric field strongly promoted droplet -droplet coalescence. In addition, it was found out that the size of the droplet is proportional to the applied field strength, despite the slight decline after a while. However, as mentioned earlier, high field strength can cause droplet break-up because of hydrodynamic and electrostatic stresses (Wagner and Hsu, 1983; Williams *et al.*, 1995; Wagner and Nelson, 2016). As a result, the droplet size was diminished. In fact, it should be considered, that in some electrocoalescence scenarios, turbulences may cause increments of the size of droplets despite the absence of electric field (Urdahl *et al.*, 1996; Wagner and Nelson, 2016).

Thus it can be seen that the optimised design of an electrostatic coalescer depends on the composition and properties of the water-oil emulsion it is intended to treat. Chemical changes at the water/oil interface are critical and this will depend on both the natural composition of the oil and the addition of process chemicals. This adds cost to the process and risks in disposal (e.g. of solvents) physical absorption of some of these additives and impurities may play a role in improving the electrocoalescence process and polyHIPEs might achieve this. The production and properties of polyHIPEs are reviewed in the rest of this chapter.

## 3.4 PolyHIPE Polymer

### 3.4.1 Overview of PolyHIPE Polymer (PHP)

A macroporous material, PolyHIPE Polymer (PHP) is synthesized via polymerization of the external (continuous) phase of a High Internal Phase Emulsion (HIPE). Emulsions commonly comprised of two immiscible liquids; one of these liquids (commonly called dispersed, aqueous or internal phase) is dispersed in another (known to as the continuous, oil or external phase) in droplet form (Zhang and Cooper, 2005). The emulsion is generally made by slowly adding the dispersed phase to the continuous phase under conditions of agitation (stirring). The stirring action disperses the added phase as droplets which can be broken up and coalesce to form a stable emulsion of controlled droplet size.

Mostly, the systems of the emulsion can be categorized as water-in-oil (W/O) or oil-in-water (O/W) based on the external phase nature (Cameron, 2005). Lissant (1974) stated that emulsions with more than 74% of the internal phase volume fraction ( $\phi$ ) relative to the overall volume of emulsion are called HIPEs, between 50 to 74% called medium internal phase emulsions and lower than 50% called low internal phase emulsions. HIPE- Internal phase more than 74% as this is the theoretical packing density of hard spheres of the same diameter. To get a HIPE, the internal phase droplet needs to distort from spherical shape. Hexagonal arrangement of spherical droplets gives the maximum packing density. The value of ( $\phi$ ), may be more than 99%, which represents the ultimate ratio of volume of uniform non-deformable spheres by packing with a highly efficient technique (Cameron, 2005). Cameron *et al.* (1996) inferred from the work done by Lissant that at high volume fraction of the continuous phase, the droplets become crowded and lose their ability to maintain their spherical shape and turn into deformed polyhedral droplets that have great contact areas surrounded by thin surfactant films for stabilization. This leads to a material with highly porous structure and a pore volume fraction that may increase above 99%. Besides, it has an open-cell structure, where the adjacent cavities are connected to each other. Figure 23 shows the formation of the PolyHIPE Polymer.

Williams and Wroblewski (1989) have stated that one of the important features of PHP is the ability for tailor-made modifications with respect to their usage by adjusting the inter-connect size ( $d$ ) and pore size ( $D$ ). In addition, PHP with a highly porous interconnected monolithic structure can be prepared with a well-defined, open-cell and uniform macrostructure with low

dry density of around  $0.1 \text{ gm/cm}^3$ . Figure 24 illustrates the structure of a typical polyHIPE polymer.

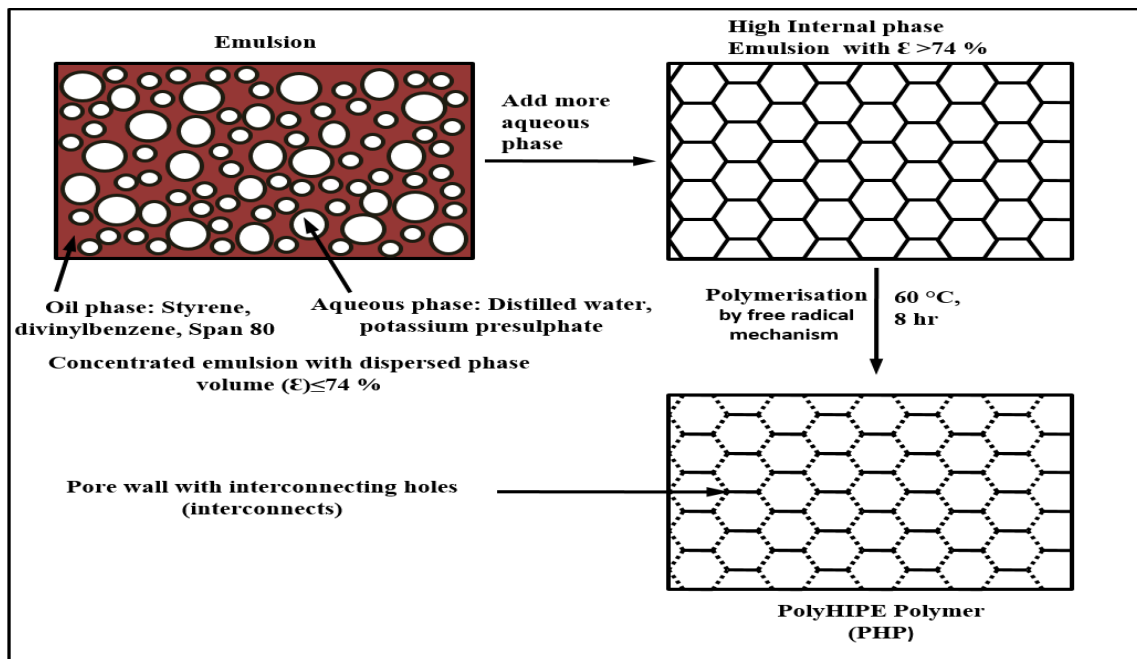


Figure 23: Schematic representation of polyHIPE formation (Byron, 2000).

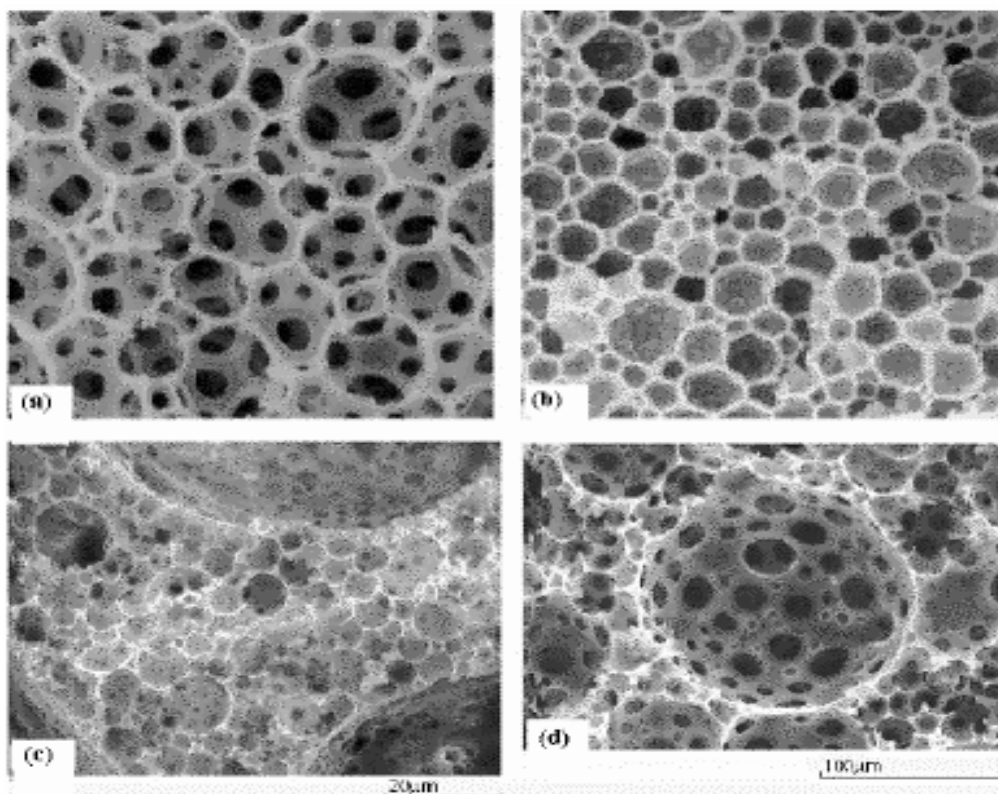


Figure 24: SEM images of basic structure of the styrene/divinylbenzene polyHIPE polymer: (a) Primary pores with great interconnecting holes; (b) Primary pores with nano-sized interconnecting holes; (c) Large coalescence pores dispersed into the primary pores in the coalescence process; (d) Coalescence pores detail (Akay, 2006).

According to the International Union of Pure and Applied Chemistry (IUPAC), the classification of pore size is categorised as follows (Thommes *et al.*, 2015)

- 1) Macroporous pores: are the pores with sizes exceeding about 50 nm (0.05  $\mu\text{m}$ ).
- 2) Mesopores pores: are the pores of size between 2 to 50 nm (0.002  $\mu\text{m}$ -0.05 $\mu\text{m}$ ).
- 3) Micropores pores: are the pores with sizes not exceeding about 2 nm (0.002  $\mu\text{m}$ ).

As identified in various papers such as Akay *et al.* (2005a) and Akay and Tong (2000), PHP materials can be produced with different pore size by controlling the initial emulsions and by using the coalescence polymerisation. The pores are categorized into four categories:

- 1) Primary pores: these are formed by the creation of droplets of the dispersed phase in the continuous phase, polymerisation of the continuous phase and removal of the dispersed phase. Their size depends on the emulsion chemistry and stirring conditions.
- 2) Coalescence pores: these are larger than the primary pores form due to coalescence of primary pores at high mixing energy or after soluble polymer addition to the aqueous phase.
- 3) Interconnect pores: The aqueous phase droplets generally do not closed cell structures but the cell walls rupture during polymerisation allowing the escape of the internal phase. This produces a hole in the cell wall called an interconnect pore.
- 4) Nano pores: these are seen in the remaining cell walls after polymerisation and are formed from fillers and porogens in the oil phase, particularly after solvent extraction during washing.

Akay and Vickers (2003) explained that the pores with more than 200  $\mu\text{m}$  size are prepared via a technique of coalescence polymerization. Furthermore, Hayman and co-workers (Hayman *et al.*, 2004) mentioned that adding a little amounts of water-miscible organic to the aqueous phase of HIPE will result in a controlled coalescence due to Ostwald ripening, where the coalescence-two droplets just contact and merge. Ostwald Ripening small droplet dissolves and material migrates to a big droplet where it is collected. Hence big droplets grow at the expense of small droplets. Moreover, Akay (2006), concluded that asymmetric materials can be prepared by controlling the PHP's surface porosity which, occurs as a result of changing the chemistry of the materials surface against which the polymerisation of HIPE initiator. Because of their unique structures, characteristics and significant properties, PolyHIPEs have been used in numerous applications as shown in table 5.

Table 5: Various applications of PHP in different fields.

PolyHIPE applications	Literature references
Demulsification of water-in-crude oil emulsions via crossflow microfiltration	(Shakorfow, 2012)
Gas-liquid separation	(Dogru <i>et al.</i> , 2019)
Water treatment	(Kahdim, 2017; Chen <i>et al.</i> , 2018)
Tissue engineering	(Nalawade <i>et al.</i> , 2016; Paterson, 2017)
Removal of tars from syngas	(Hasan, 2013)
Cartilage regeneration	(Naranda <i>et al.</i> , 2016)
Preparation of metal foams	(Akay and Calkan, 2015)
Purification of materials	(Pulko <i>et al.</i> , 2011)
Oil recovery	(Zhang and Guo, 2017; Mahadik <i>et al.</i> , 2018)

The following material properties are necessary to meet the requirements for PHP in the above-mentioned fields (Noor, 2006):

1. The PHP produced should have the required internal architecture or morphology with specific pore/interconnect sizes.
2. The PHP produced should have the ability to form monolithic structures
3. The PHP produced should be optimised for specific applications by functionalizing the surface with different species.
4. Sustainable production and modification of PHP is essential.

### 3.4.2 Preparation of PolyHIPE

In the past few decades, the preparation of HIPEs has been widely investigated, as detailed by Lissant (1974). According to the report of Barby and Haq (1985), HIPE is prepared by polymerization of monomers, which are in the form of a water-in-oil emulsion with water phase as the internal phase consisting  $\geq 90\%$  of the total weight of the emulsion. Recently, several other related procedures of PHP producing have been reported (Barbetta *et al.*, 2000; Cameron, 2005). Moreover, Mezzenga *et al.* (2003), characterize a new technology which does not require polymerization to produce similar materials.

The preparation of PolyHIPE is a relatively simple process, the emulsion consists of two phases, namely continuous phase and disperse phase. The continuous phase includes

monomers, surfactants and cross-linking agents and, in some cases, the additives/filler. Also, polymerization initiators which have solubility in oil-phase are added, while the disperse phase mostly contains distilled water or light oil (with has a low molecular weight) (Akay *et al.*, 2005b). If a polymerization initiator like lauryl peroxidecan or potassium presulphate as well as additives/filler (in certain cases) has been added, this is dispersed dropwise in a monomer, surfactant and cross-linker solution. The emulsion containing (up to 90% water) of in the monomer can then be achieved before being polymerised (Bhumgara, 1995; Cameron and Sherrington, 1997; Tai *et al.*, 2001; Cameron, 2005). Figure 25 shows the reaction of polymerisation between divinylbenzene and styrene to get polyHIPE polymer.

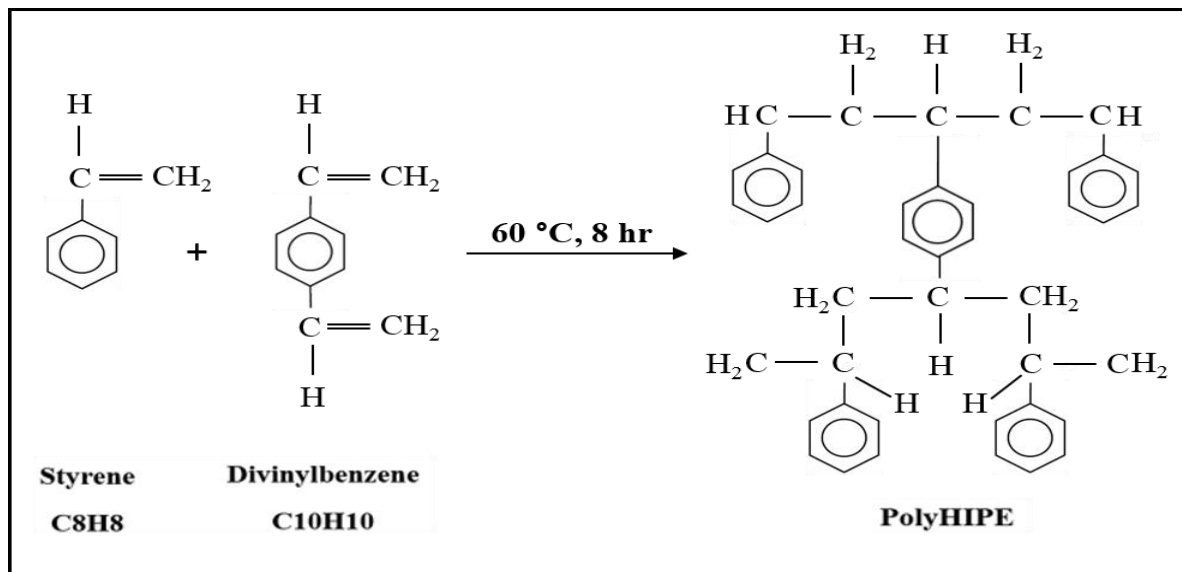


Figure 25: The polymerisation reaction of styrene and divinylbenzene to get polyHIPE polymer (Barby and Haq, 1982).

Akay *et al.* (2005b) have stated that there are two stages of PHP processing is:

1. First stage process – In this stage, mixing of dispersed (aqueous) phase and continuous (oil) phase in a mixing vessel occurs with adequate care taken to minimize the jet mixing of these two phases. The rotation of an impeller during this dosing process reduces the droplet size in the dispersed phase.
2. Second stage process – This process is carried out to reduce the droplet size of the aqueous phase obtained from the previous stage by further mixing. This helps in reducing the size of pores after the polymerization process. If the dosing rate is low, then there is no need for an additional homogenization stage.

The rate of the relative dosing which has the deformation rate dimension is utilised to describe the dosing rate of the internal (aqueous) phase.

$$R_D = \frac{V_A}{V_O t_D} \quad \text{Eq. 21}$$

where

$R_D$  relative dosing rate, ml/s.

$t_D$  = the dosing time of the aqueous phase, min.

$V_O$  = the oil phase volume which placed in the batch mixer, ml, and

$V_A$  = the aqueous phase volume, ml.

The definition of the total mixing time  $t$  is given by the following formula,

$$t = t_H + t_D \quad \text{Eq. 22}$$

where

$t_H$  = the time of the homogenization, min.

The rate of the mixing is defined by the following equation,

$$R_M = \frac{D_i}{D_O} \Omega \quad \text{Eq. 23}$$

where

$D_i$ : is the impellers diameter, m

$D_O$ : is the batch mixer diameter, m and

$\Omega$ : is the impellers rotational speed, r.p.m

Bokhari *et al.* (2003) stated that if the mixing rate is much less than the relative dosing rate, the formation of HIPE does not occur; instead a dilute internal emulsion of oil-in-water (O/W) is created. If the rate of dosing is quite low then the additional stage of mixing (homogenization) will not be needed, HIPE polymerisation can be done without phase separation (occurs only when HIPE is stable).

The most common monomers used in the process of free radical polymerisation to prepare PolyHIPE are styrene and divinylbenzene (DVB) (Cameron *et al.*, 1996; Tai *et al.*, 2001; Barbetta and Cameron, 2004). The use of styrene in the preparation of PolyHIPES has begun due to its characteristic immiscible nature with water, further various hydrophobic materials (crosslinkers and monomers) like divinylbenzene (added in differing quantities) were used to

promote the stability of the structure. Figure 26 illustrate the infinite network connectivity composed of effective linking among the PolyHIPE chains resulting from the polymerisation of styrene and divinylbenzene to produce PolyHIPE (Sherrington, 1998).

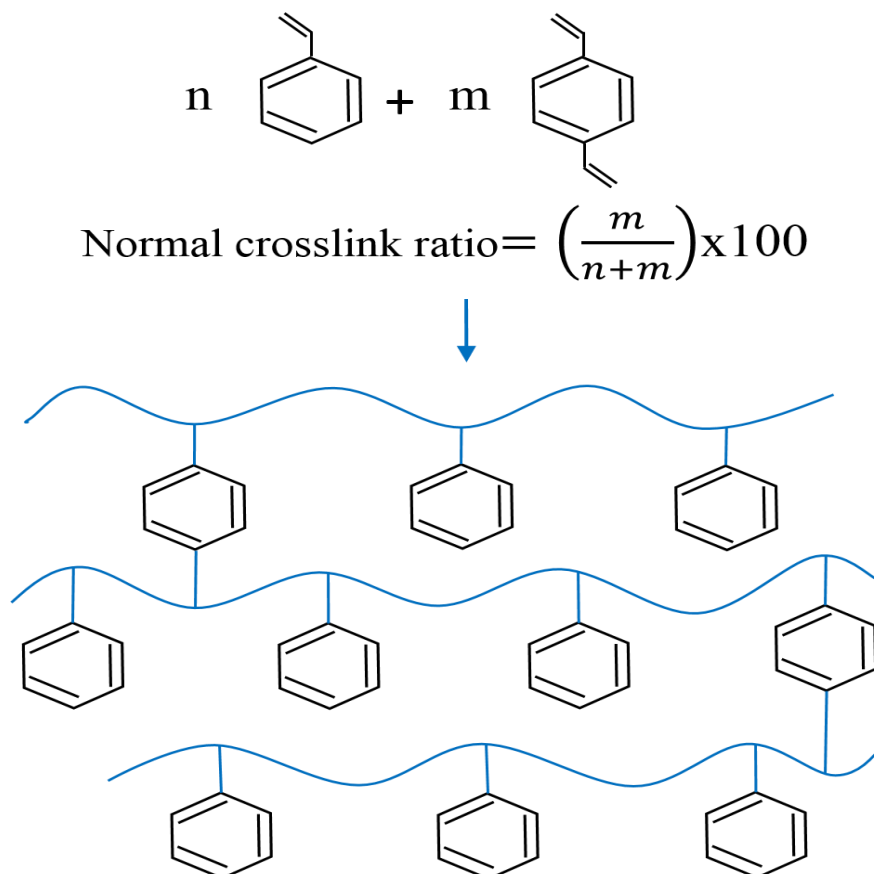


Figure 26: Styrene and divinylbenzene polymerisation to form a Polymer with an Infinite Network (Sherrington, 1998).

Generally, a homogeneous PolyHIPE production from water-in-oil HIPEs cannot be achieved unless the organic continuous phase is hydrophobic to the required extent. So, several hydrophobic monomers/crosslinkers have been used for that purpose such as butyl acrylate (BA), isoboryl acrylate (IBA) and 2-ethylhexyl acrylate (2-EHA) (Cameron, 2005). Likewise, Elmes and co-workers (1988) mentioned that different organic liquids of hydrophobic in nature are used to produce PHP likes paraffines, cyclohexane and kerosene, which are emulsified in poly-(acrylic acid) or poly-acrylamide. Formaldehyde and urea are also used to produce hydrophilic PHP. In 2006, Noor (Noor, 2006) successfully prepared various homogenous hydrophilic PHP by adding vinylpyridine, which is used as hydrogen acceptor/donor in the external phase.

### 3.4.3 Morphology of PolyHIPEs

PHP typically has an open cellular structure with spherical cavities and has pore interconnection windows, which are formed because of the polymerization process in which the aqueous phase trapped in the continuous phase also escapes. The pore size of PHP is directly proportional to the stability level of the HIPE. Because of lower interfacial tension, smaller droplets are produced in a system with high emulsion stability and thus forming a larger interfacial area. On the other hand, merging of emulsion droplets happens in the case of less stable emulsion systems which in turn leads to larger cell polymers (Akay *et al.*, 2005a). Preparation parameters like mixing speed and mixing time greatly affect the stability of HIPEs. Stability is directly proportional to the increased mixing time and speed, as this breaks the emulsions into more uniform droplets. Walsh (1996) reported the production of micro-size open structure HIPE with increased mixing time, because of the fact that the water cavity gets reduced and the windows of inter-connection increase.

Williams and Wroblewski (1988) identified that production of a closed-cellular structure is also possible. In that study, the cellular structure was determined by the concentration of the surfactant with minor effects on the internal phase volume. Usage of a low concentration of surfactant i.e. (<5% in term of w/w) relative to the monomer phase resulted in closed-structure materials. If the concentration of the same surfactant is more than 7 % then it resulted in open-cellular materials. The reason behind this is that there is a decrease in the thickness of monomer film between the adjacent droplets. The closed-cellular structure was formed because the shrinking of the windows between the adjacent droplets during polymerisation does not lead to rupture because of the less dense monomer (Pulko and Krajnc, 2012).

In general, the PHP morphology is dependent on the fact that the internal architecture (interlinked structure and pores) is controllable by processing conditions, the chemical modification of their walls and the fabrication method. They are complex structures and fundamentally possess open cellular architectures with cavities called as voids or pores. PHP are also tailored to have increased range of pore size between (0.1-5000  $\mu\text{m}$ ) (Barbetta and Cameron, 2004; Akay *et al.*, 2005a). Moreover, the component dimensions may be optimized from thin films to larger organized monolithic materials (Barbetta and Cameron, 2004). Today, PHP are used in a wide range of application, in which specified application will require specific component properties (physical, morphology, thermal, mechanical, etc.).

### **3.4.4 Factors Affecting PHP Polymers Morphology**

Some researchers and co-workers from Unilever Williams and Wroblewski (1988); Gregory (1989) investigated for the first time factors that control the cellular quality of the components. It was found that despite that fact that volume fraction of internal phase ( $\phi$ ) can be an influential factor, the concentration of surfactant remains the dominant factor to determine the cellular behaviour of PHP. In the next sections, the factors affecting PHP polymer morphology will be discussed.

#### **3.4.4.1 Volume Ratio of Internal Phase**

Studies carried out by William and co-workers (Williams *et al.*, 1990), found out that the DVB/styrene ratio employed in the producing of a HIPE of DVB/styrene (ranging between (0-100%) DVB), performs a key role in dictating the behaviour of the final HIPE. It was observed that emulsions containing DVB blended more easily and evenly than those containing only styrene. Consequently, an increased DVB/styrene ratio within a HIPE produces a more stable emulsion, which results in a reduction in the average pore diameter from 15 to 5  $\mu\text{m}$ . Moreover the researchers mentioned above also noted that small increases in the surfactant content effectively reduced the pore size. However, 50% and above surfactant concentration (wt/wt) with respect to the monomer content produced weak and crumbly polyHIPEs.

#### **3.4.4.2 Surfactant Parameter**

The amount of surfactant used is essential to dictate the kind of structure that will be produced. The three major factors affecting directly the cellular structure formed are surfactant amount, surfactant concentration and Hydrophile-Lipophile balance (HLB). Surfactants employed to create HIPEs require a low HLB value in the range of 2 to 6 and the best surfactant for styrene based polyHIPEs is believed to be Sorbitan Monooleate (Span 80), which has an HLB number of 4.3 (Barby and Haq, 1982). Further study suggested that a surfactant concentration of at least 4% by volume in relation to the overall oil phase was needed to form PHP (Cameron *et al.*, 1996). Williams and Wroblewski (1988) suggested that a level of surfactant in the range of 4% to 5% by volume is believed to promote in the structure of materials that show closed porosity, whilst from 7% to 50% promote cell structures which are open with a fully interlinked microstructure. The surfactant concentration was found to be more significant in structural

control compared to the volume of the internal phase. This may be due to the fact that with the increase in the surfactant concentration, the monomer membranes that separate the surrounding emulsion drops can be thinner. With critical thickness of this membrane, windows between the drops start to open up in the polymerisation process.

Akay (1995) proposed a scheme that describes the relationship between the pore structure of PHP and the surfactant. During the polymerisation process the molecules of the surfactant (which do not associate with the polymer chain) create an isolated phase in the region of the interface between the HIPE aqueous internal phase and the polymerisation monomer. Steric effects amongst the tails of surfactant molecules that oppose one another (Figure 27 (A)) will cause the molecules of the surfactant to agglomerate into a separate phase as shown in Figure 27 (B). Additional surfactant that does not fill a space at the interface remains as micellular droplets within oil phase, and so is a separate surfactant phase. The molecules of the surfactant that agglomerate in regions in the external phase reduce the volume of the polymerised component. Since the surfactant is removed these regions then turn into small pores within the cell walls. However, if an excess of surfactant is applied for producing the HIPE, the surfactant starts to agglomerate to larger groups, that breaks up the wall structure and collapses the polyHIPE.

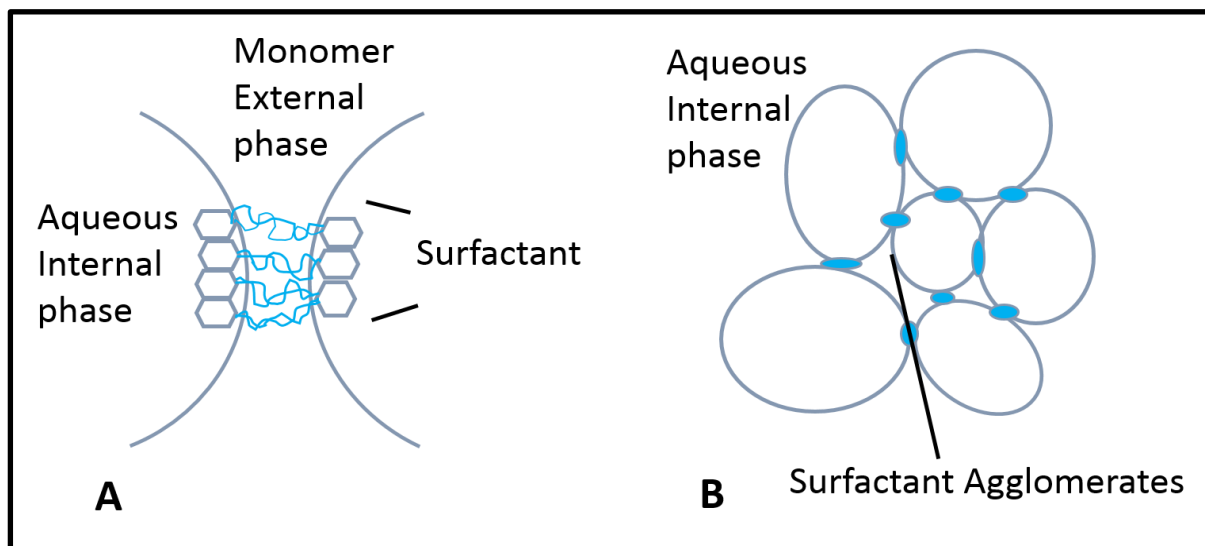


Figure 27: Graphical diagram showing the pore formation in PolyHIPE (Akay, 1995).

#### 3.4.4.3 Composition of HIPE Continuous Phase

It is widely acknowledged that the composition of the continuous phase of HIPE can have an impact on pore size (Cameron, 2005). Barbetta *et al.* (2000) illustrated that for the PHP which were prepared under 4-vinylbenzyl chloride (VBC) as well as under DVB, the average droplet

diameter was smaller compared those prepared under mixture of DVB and styrene. Moreover, incrementing the VBC content, caused the pore diameter to diminish to a minimum of 5 $\mu$ m. Cameron and Barbetta (2000) believed that 4-vinylbenzyl chloride was co-absorbing in the interface of the emulsion and surfactant, hence reducing the interfacial tension, which results in a much smaller average droplet size. A similar impact was seen when a non-polymerisable solvent was applied (Barbetta *et al.*, 2000).

#### **3.4.4.4 Electrolyte Content**

Cameron (2005) illustrated that an the electrolyte concentration present in the aqueous phase can have a significant effect on the average pore size. The diameter of the pore can be reduced a minimum of 10 fold as there is an increase from 0 to 10 gm/100 cm<sup>3</sup> in the salt concentration in the aqueous solution with AIBN (azobisisobutyronitrile) as initiator. If the electrolyte concentration is increased, it reduces the tendency for Ostwald ripening (i.e. the increased in average droplet diameter to minimise the overall interfacial energy). Consequently, limitation in the Ostwald ripening improves the stability of emulsions such that there is smaller average diameter of the drops. Many other researchers have illustrated that the inclusion of electrolyte also the causes emulsion to be more stable as interfacial tension is reduced, thus leading to a finer PHP structure (Gregory, 1989; Aronson and Petko, 1993).

#### **3.4.4.5 Mixing Time/Dosing Time**

Many factors influence the stability of HIPEs, since the stability of the HIPE relies significantly on the preparation parameters such as the duration of mixing and the mixing shear stress (i.e. the agitating speed). If an emulsion is stirred to a high agitating speed, it is capable of experiencing an easy breakdown to small droplets, hence yielding a highly stable emulsion. Slow mixing can have the same impact, as demonstrated in the study conducted by Walsh *et al.* (1996); as mixing time increases the droplet size of water reduces and the number of windows between droplets increases, creating macro-size material with an open structure. Further studies were carried out by Bokhari (2003) to estimate the total impact of dosing and mixing time. It was shown that these two parameters yield an open pore PHP with large size

of the pore. Figure 28 illustrates that the average size of the pore is reduced as there is an increase in the mixing time.

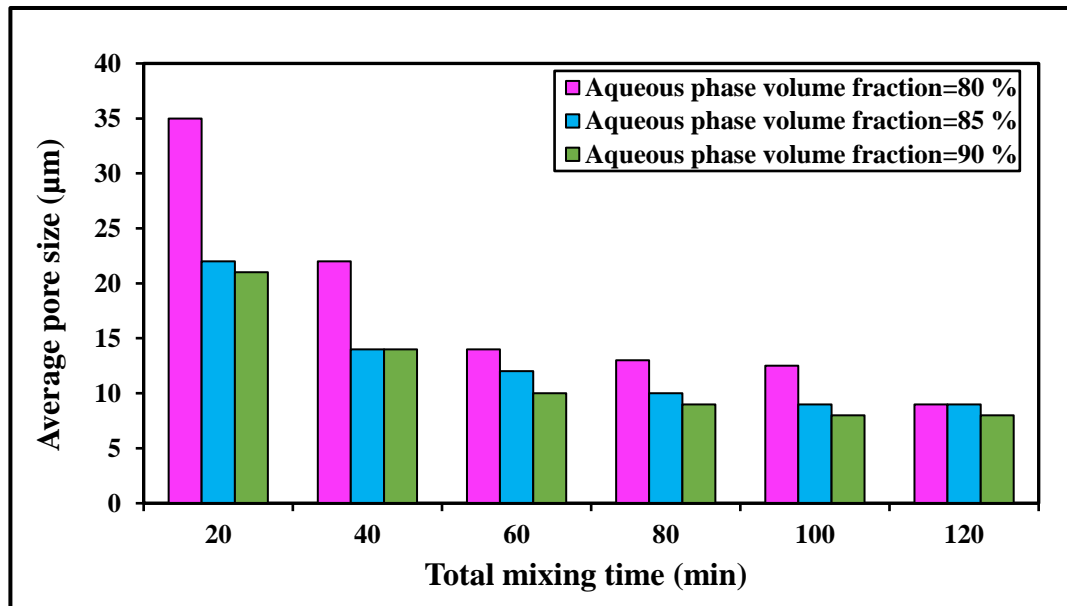


Figure 28: Difference of average pore size ( $D$ ) with total mixing time ( $t$ ) as a function of volume fraction of the dispersed phase ( $\epsilon$ ): speed of the Impeller=300 rpm, temperature of emulsification=25 °C, dosing time=10 min (Bokhari, 2003).

#### 3.4.4.6 Temperature of Emulsification

Various studies evaluated the impact of emulsification temperature on size of the pores. When the operation is carried out at high temperature, larger pores are formed (Bokhari *et al.*, 2003). As the emulsion prepared through the phase inversion method did not go through a stage of homogenization, an enormous distribution of pore size for PHP was achieved using a high temperature. The reason for this is the number of water-containing oil particles which declines in the homogenization process (Akay *et al.*, 2005a; Zhang *et al.*, 2015). HIPE is formed at 60 °C or 80 °C with larger average size of pores ( $D$ ) when the temperature in the emulsification stage rises from (30 to 80 °C), where the average pore size is directly proportional to the increase in temperature as illustrated in Figure 29. This process is potentially hazardous in the case that safety systems are not available, such as the availability of a strong air-drift system to assist in the withdrawal of chemical vapours from the material formed. It is necessary to conduct experimental in an area of good extraction even at room temperature to minimise the effect of such vapours.

In attempting to further study PHPs as biomaterials, Akay *et al.* (2004) utilised various temperatures during the emulsification process to achieve a better size of pore for a very

particular case. For instance, Akay and Vickers (2003) found that rapid cell penetration is a result of the largest pores with size of 100 $\mu\text{m}$  whilst a PHP pore size of (40 $\mu\text{m}$ ) had more cells in layer in the regions below the surface in contrast to another size of pore.

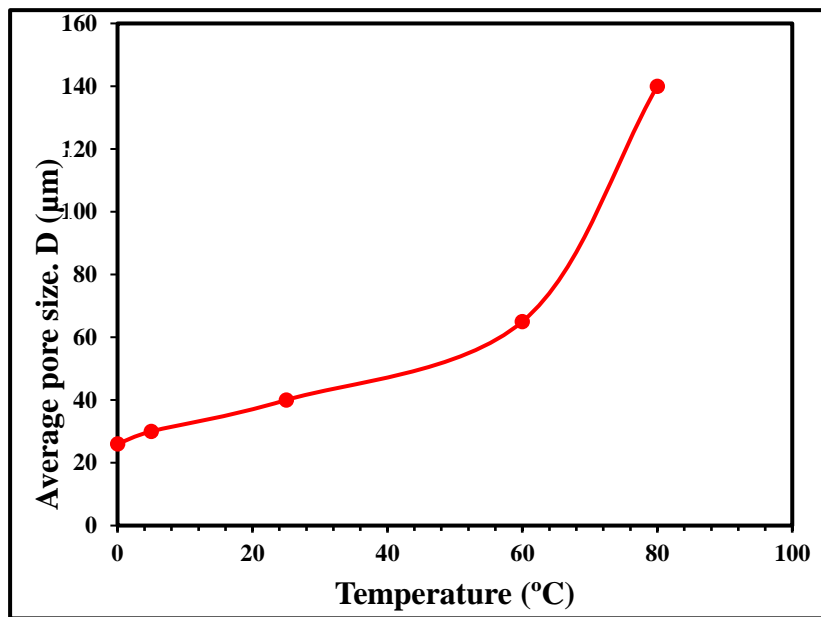


Figure 29: Difference of average pore size with temperature of the emulsification stage when total mixing time=100 s, dosing time=40 s, phase volume=90 %, impeller speed=300 rpm (Akay *et al.*, 2005a).

#### 3.4.4.7 Moulding Type

Typical, PHP components are polymerised in a specific container, acting as a mould which can have varying size and shape. Some results demonstrate that the mould material influences significantly the level of adhesion to the mould and the morphology of the polyHIPE surface (Akay, 1995). Cameron (2005) discovered that if a glass mould is used, there is bonding of the surface to the PHP which leads to a distinct layer morphology between the internal surface and the contact surface. HIPE stability is affected by using a polyvinyl chloride (PVC) mould because of leaching from the plastic mould. Despite the use of a polypropylene mould not resulting in adhesion, the contact surface morphology of the polyHIPE was observed to show a closed cell structure. Moreover, good mould surface wetting by either emulsion phase can lead to phase separation. Consequently, the monomer films changes into a surface skin during polymerisation.

Akay and co-workers (Akay *et al.*, 1995) demonstrated that a PTFE mould does not show adhesion nor exhibit a different morphology with an open cell structure at the interface between PHP and mould and in the bulk. PTFE has yielded outstanding results and hence other kinds of mould may be made by spraying PTFE spray to the mould surface of another material.

Different moulds have been applied by other researchers, namely falcon tubes and aluminium foil, however there is no report on these having a considerable impact on the PHP morphology (Menner *et al.*, 2008).

### ***3.4.5 Properties of PolyHIPE***

#### ***3.4.5.1 Mechanical Properties***

To yield a product which is commercial and attractive, sufficient strength and toughness polymers need to be developed. Several schemes can be applied to make material tougher and alter the properties of the polymers by means of combining various distinct factors. Choosing the right monomers and crosslinker is very critical on mechanical properties; for example, PHPs associated with divinylbenzene and styrene are brittle and chalky (Williams and Wroblewski, 1988; Cameron, 2005), whilst bisphenol-A-polycarbonate has remarkable mechanical properties (Cameron and Sherrington, 1997). This is a result of the hindered dynamics of the main-chain phenyls in bisphenol-A-polycarbonate, associated with a tendency to micro-segregate as opposed to the free rotation of the main-chain phenyls. Consequently, the monomer characteristics has an impact on the ultimate properties of final product.

However, PHPs products created by high internal phase emulsions are either elastomeric or rigid. If the styrene monomer is changed to 2-ethylhexyl acrylate (2-EHA), the ultimate polymer can be produced in the form of an elastomer. Alternatively, the base material may be modified to be strongly rigid by changing to methacrylate from methyl or resorcinol-formaldehyde (Cameron and Sherrington, 1997). In this case, the toughening dynamics are quite complex because of the summation of physical properties and the impact of supramolecular structure (Sherrington, 1998). In fact, a huge amount of cross-linking can result in embrittlement in the styrene-divinylbenzene system (Hainey *et al.*, 1991).

Putting in extra fillers changes the morphological characteristics as well as enhances the mechanical properties of the polyHIPE components. If polyHIPEs (DVB/styrene) are loaded with short fibre fillers, considerable enhancements in flexural strength toughness and compressive modulus can be generated. In fact, it has been shown that Kevlar fibres bond especially well to this matrix, causing improved properties (Cameron, 2005).

Recently, studies have shown that applying an adequate reinforcement in the polymerized organic phase is an outstanding way to improve the mechanical properties of polyHIPE.

Haibach *et al.* (2006) illustrated that by incorporating nano-sized silica particles in the polymer phase, the Young's modulus and the foam crush strength is increased by 218% and 280% compared to foam in absence of reinforcement. Additionally, Menner *et al.* (2008) reported that reinforcing PolyHIPEs with titania in oxidised carbon nanotubes in the water or in the organic phase, enhanced the mechanical performance with no increase in the density, allowing polyHIPE scaffolds to be applied in filters and tissue engineering.

Apart from mechanical reinforcement of PHP, silica particles were utilised to make properties of oil in water emulsions more stable (Binks and Whitby, 2004). Work carried out by Binks and Lumsdon (1999) suggested that stable emulsions can be achieved by particles of increased diameter which stabilised water droplets in the macro and micro size range. Also, further researchers have discussed the development novel polymer foams with enhanced properties in the structure and chemistry of the material as well as permeabilities compared to classical polyHIPEs based on stabilizing by silica particles (Kim *et al.*, 2006).

#### **3.4.5.2 Surface Area**

Although possessing walls in a highly permeable pore window like structure, the polyHIPE surface area prepared in the way mentioned in section 3.4.2 is not very high, with (2 m<sup>2</sup>/g) to (3 m<sup>2</sup>/g) in the normal range (Noor, 2006). This can be understood by noting the pore sizes of these components, which are comparatively large at 10s of microns maximum. It is the surface area of the walls which is important in controlling the overall surface area of the polyHIPE and these are reasonably smooth by the normal manufacturing methods. Nonetheless, some applications of polyHIPE components, like chromatographic support (Kreutzer *et al.*, 2005), need a larger surface area in the multiples of hundreds of meters square per gram. However, the surface area of these components can be enhanced in several ways.

Hainey and co-workers (Hainey *et al.*, 1991) demonstrated that a polyHIPEs surface area can be increased by placing an organic porogenic solvent, instead of some monomer, and increasing the quantity of cross linker (DVB) in the continuous phase in a styrene-based polyHIPE. With this, monoliths can be produced with a surface area of 350 m<sup>2</sup>/gm. One disadvantage of this approach is that the mechanical properties of the final polyHIPEs are seriously impaired.

The structure of the monoliths can collapse easily when exposed to low or moderate stress and to liquid flow. The natural behaviour of the porogen has a major influence on surface area, and is related to the type of solvent used. Higher surface areas are achieved when better solvents are involved in the growing network. This motivated Barbetta and Cameron (2004) to discover alternative porogenic solvents to achieve higher surface areas for polyHIPE components that share the same mechanical characteristics compared to the ones with lower surface areas. It was found that by exchanging the toluene (T) solvent with chlorobenzene (CB) or chloroethylbenzene (CEB), the BET (Brunauer, Emmett and Teller theory) surface area of the polyHIPE increased from 350 m<sup>2</sup>/g to 457 m<sup>2</sup>/g.

Despite the fact that the CEB increased the surface area, it also produced a variation in the morphology of the final material. Based on scanning electron microscopy (SEM), the final polyHIPE material was noticed as not possessing the same morphology as the structure of the original polyHIPE, and with larger windows. Moreover, despite the large surface area, it did not improve the mechanical properties. A study conducted by Barbetta and Cameron (2004) observed that a mixture of CB and CEB with a ratio of 1:1 (vol:vol) produced a material with the same surface area as mentioned before of 457 m<sup>2</sup>/g as well as preserving the original morphology of polyHIPE material. Despite claims that the material had more robustness it was brought out that this particular kind of polyHIPE was not highly durable compared to the ones prepared with the combination of DVB/styrene (Noor, 2006).

### ***3.4.6 Sulphonation of PolyHIPE Polymer***

Apart from the use of distinct monomer types in the oil phase to produce hydrophilic or hydrophobic components, the polyHIPE chemistry can also be changed in other ways. If an aromatic electrophile is substituted into the phenyl rings of styrene, sulphonic acid can be produced through the process of sulphonation. In this process the sulphonic acid functional group SO<sub>3</sub><sup>-</sup>H<sup>+</sup> is attached to a molecule of an organic compound by means of chemical bonding. Aromatic sulphonation is a replacement organic reaction by which a hydrogen atom of an arene compound is substituted by a SO<sub>3</sub><sup>-</sup>H<sup>+</sup> functional group via an electrophilic aromatic replacement as in Figure 30. However, a sulphonation level of 100% is not possible to achieve because of the existence of stress within the polymer matrix. Haq (1985) suggested that sulphonation level between 68% and 80% was possible whereas Calkan (2005) demonstrated that the level of sulphonation rose with increased sulphonation time and peaked at a plateau

value of 60%. Akay and Vickers (2003) suggested that at this level in PHP the material become hydrophilic.

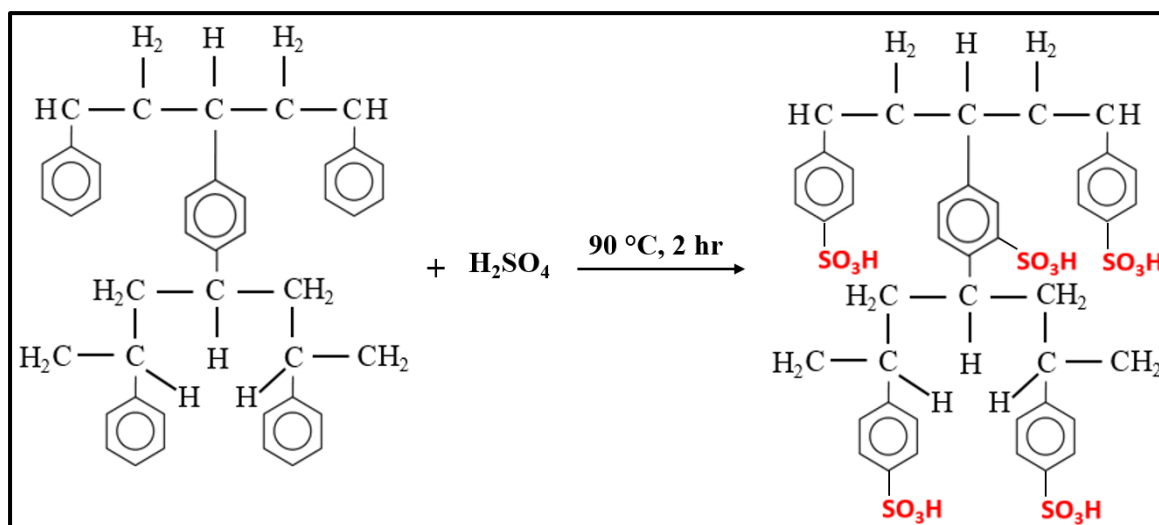


Figure 30: Schematic diagram showing the chemical structure of (100%) sulphonated PolyHIPE (Calkan, 2007).

The most commonly used functionalised polyHIPE, because of its potential for metal ion removal, is the sulphonated form. These materials absorb water effectively in acid and salt form (generally, a sodium salt). The sulphonated PHP production method consists of simply heating the polymer immersed in concentrated sulphuric acid to a temperature that depends on the concentration of the acid. Many schemes have been introduced to achieve sulphonation of PHP. Despite of the widely use of sulphonated form of coupled styrene-DVB copolymer PolyHIPE, where hydrophilic behaviour is critical, modern methods of sulphonation (Haq, 1985; Cameron *et al.*, 1996; Akay and Vickers, 2003) are non-ideal due to the large production of waste acid at the completion of the sulphonation process. The classic approach by Menner *et al.* (2008) illustrated that using concentrated sulphuric acid causes the acid to be unable to infiltrate the material; hence it is not adequate for sulphonation of large monolithic structures. Additionally, because sulphuric acid reacts very strongly, the surface becomes more sulphonated than within the bulk. Other types of sulphonation reagents that were evaluated are sulphur trioxide (Thaler, 1983) and chlorosulfonic acid within chlorinated solvents (Li *et al.*, 2001). Moreover, uniform sulphonation was achieved by the use of lauroyl sulphate in cyclohexane and acetyl sulphate in 1,2 DCE (dicloro-ethane) (Cameron and Sherrington, 1997). Polymerisation was done before sulphonation in all cases.

In last decade, researchers at Newcastle University found a novel method with high sustainability and efficiency for sulphonation (Akay *et al.*, 2005b; Calkan, 2007). In this

method, sulphonated PHP material is created by the internal phase during the emulsion process. Because sulphuric acid already exists in the pores of the polymers, an excessive amount of acid was no longer needed. This approach is applied to some PHP used in this study. The general structure of sulphonated PHP is demonstrated in Figure 31. The SEM micrographs shows that coalescence pores dominate due to the sulphuric acid in the aqueous phase which makes the emulsion unstable. Consequently, cross-link reactions and water droplet coalescence happen at the same time, causing the formation of coalescence pores spread in the primary pores. The volume and the size fraction of the coalescence pores depends on the primary pore size, and also the temperature and rate of polymerisation.

Polymers can be sulphonated by thermal approaches (with presence or absence of acid in the emulsification process, utilizing diluted or concentrated acid). After sulphonation, the surface area of the surface is significantly diminished (around  $3 \text{ m}^2\text{g}^{-1}$ ). The area is also decreased when 2-vinyl pyridine was added.

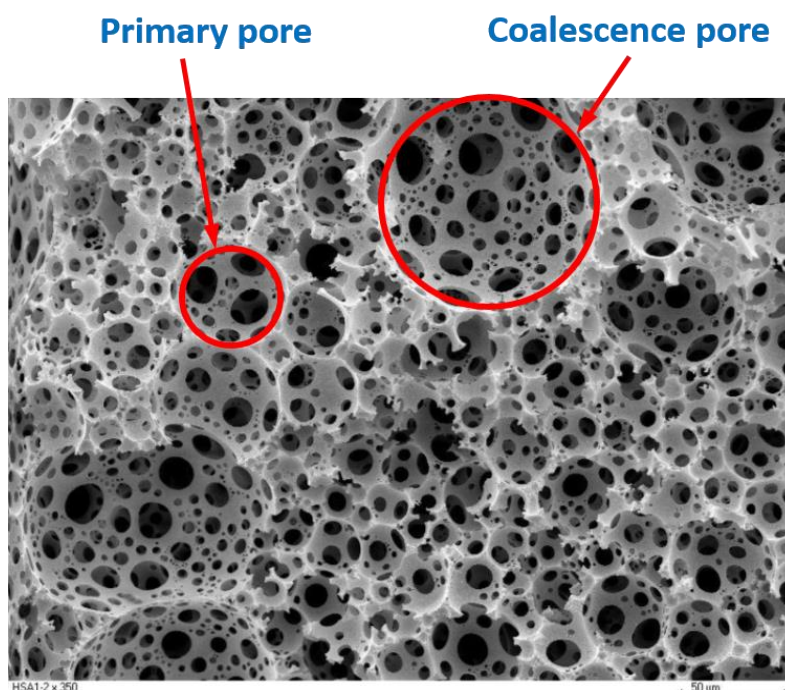


Figure 31: SEM micrograph of sulphonated PHP (using microwave irradiation sulphonation method) at low magnification (Mohamed, 2011).

Mohamed *et al.* (2006) and Akay (2006) together proposed an intensified approach where PHP experience nitration and sulphonation at the same time by utilising nitric and sulphuric acid. Simultaneous nitration and sulphonation can be achieved by mixing these acids. Similarly, on polymerisation of the HIPE emulsion (consisting of 10 w% acid when it is dispersed) in a cylindrical mold, disk shaped samples were cut and soaked, for two hours, within the

concentrated sulphuric acid. Then it was irradiated inside a microwave oven for a fixed time (~10 s) to allow sulphonation and nitration to happen. After, the process the samples were dried in vacuum at about 60 °C to increment from (10%) to (70%) the sulphuric acid concentration prior to sulphonation, hence accelerating the sulphonation rate. Because of the increments in temperature in the samples under microwave irradiation, air cooling and intermittent radiation is required to prevent material degradation. Generally the cooling time  $t_c = t_i/2$ , follows an irradiation period,  $t_i$ . This was iterated N times to make the total irradiation time  $t_T = Nt_i$ . Moreover, 40 °C was the average temperature during sulphonation. Samples were then washed, following sulphonation, in a water/iso-propanol mixture to extract residual such as monomer or crosslinker, excess acid and initiator.

After that, polymer disks were dried in vacuum and stored for estimation of the degree of sulphonation based on the approach of Akay (1995). The schematic for preparing functionalized PHP is shown in Figure 32. Mohamed and co-workers (Mohamed *et al.*, 2006) observed that PHP sulphonation by microwave irradiation caused surface area to increase from ( $3.52 \text{ m}^2\text{g}^{-1}$ ) to ( $243 \text{ m}^2\text{g}^{-1}$ ).

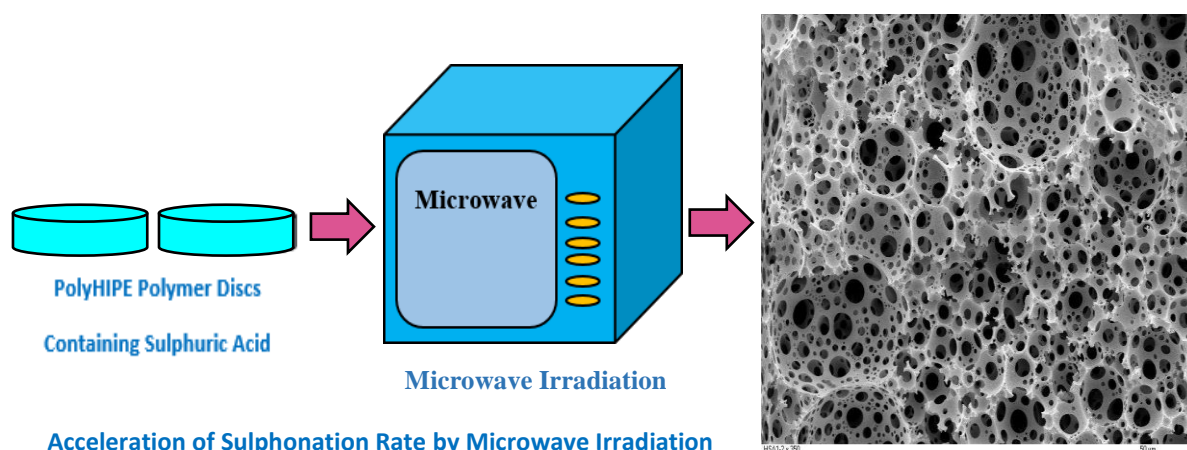


Figure 32: Schematic diagram showing the stage of Functionalization of polyHIPE polymer.

### 3.5 Summary

Thus it is possible to produced open-cell polyHIPE polymers with hydrophilic surfaces that can absorbed water and other compounds. The structure can be controlled to optimise water take-up and mechanical properties. Thus, the objective of this project is to combine such optimised polyHIPE with an electrocoalescer design to remove water from water-in-oil emulsions. The next chapter describes the preparation of stable polyHIPE materials to achieve this.

---

## CHAPTER FOUR

---

### 4. APPARATUS, EXPERIMENTAL PROCEDURE FOR PREPARING POLYHIPE POLYMER & ANALYTICAL METHODS

#### 4.1 Overview

This chapter of the thesis is presented two main parts.

- i. The first part describes the apparatus and experimental procedures employed for the preparation of four kinds of polyHIPEs namely post sulphonated polyHIPE, in-situ sulphonated polyHIPE, silane polyHIPE and Bindzil polyHIPE. The basic sulphonated and in situ sulphonated PHPs were versions a composition that had already had so success in removing water from oil emulsions. The addition of silica as particles or chemical additives was expected to improve the hydrophilicity and mechanical strength of the PHPs. Furthermore, the operating conditions of the experimental apparatus are explained.
- ii. The second part presents the analytical instruments utilised to characterise the properties of the PHPs, crude oil and the crude oil emulsions namely BET, FTIR, scanning electron microscopy (SEM), water uptake, conductivity and viscometry.

#### 4.2 Preparation of PolyHIPE Polymer

In this study, polyHIPEs (PHPs) perform a significant function as a means to achieve an intensified process of stabilised water-in-crude oil demulsification using a high voltage electric field. Due to its macro-porous structure, open-cells, interconnect pore size and hydrophilic surface, it can act as a demulsifier in the separation process of oil/water emulsions. This is not only because they are simple to synthesize, but also due to their low cost of production. Despite that PHPs were utilised throughout this research, they were continuously produced and adjusted until the last step. Akay and Vickers (Akay and Vickers, 2003) developed the PHP which was used in the experiments as the standard PHP. Subsequently, various PHPs with different improved compositions were evaluated. These were made to undergo chemical modification with particular attention to sulphonation with the aim of improving

hydrophilicity, in addition to increasing the surface area to make them appropriate for separation of water-in-oil emulsions.

#### **4.2.1 Preparation Basic PHP (B-PHP)**

PolyHIPE polymers are polymeric materials with high porosity, hierarchical and interconnected pore structure synthesized via polymerization of the continuous phase of a High Internal Phase Emulsion (HIPE). These polymers can be prepared in the form of monoliths or can be moulded into particulates with any shape and size at the stage of emulsion. Since each cell in the PHP structure is connected with all its adjacent cells, the drops of dispersed phase leave these cells easily during polymerisation process. Thus, controlling of the pore size (dispersed droplets diameter in the emulsion) by controlling the concentration of surfactants, volume of dispersed phase, cross linking agents and co-monomers is extremely important.

PolyHIPEs with a range pore sizes between 5.0 $\mu\text{m}$ -180 $\mu\text{m}$  were produced in this study mimic the range of pore sizes in previous studies (ranging between 0.5 $\mu\text{m}$ -200 $\mu\text{m}$ ) that was successful when used as demulsifier to separate water and remove the active-surface species from emulsions of water/oil (Akay and Vickers, 2003).

##### **4.2.1.1 HIPE Components**

The procedure used to prepare the HIPE is reported by a number of workers (Akay, 1995; Akay *et al.*, 1995; Akay and Vickers, 2003; Akay *et al.*, 2004) and is illustrated in Figure 28. HIPE contains two phases continuous and dispersed. The continuous phase (oil phase) which consists of styrene monomer, divinylbenzene (DVB) crosslinker, where most research on PHPs to date is based on styrene-DVB due to its emulsion stability and ease of polymerisation. This is also a relatively low cost system. Other monomers have been suggested for higher value applications (Kimmins and Cameron, 2011). The material is suitably stiff and robust for the application to be developed here. Sorbitan monooleate (Span 80) surfactant has been prepared by adding and mixing these materials in the reactor, where its volume is about of 10% (25 cm<sup>3</sup>) relative to the whole volume (250 cm<sup>3</sup>) of the HIPE emulsion. The dispersed phase (aqueous phase) consisting of potassium persulphate as polymerisation initiator and double distilled water, presents around 90 % (225 cm<sup>3</sup>) of the total HIPE emulsion volume was mixed in a separate a container. Tables 6 and 7 illustrate the weight percentage ratios for both continuous

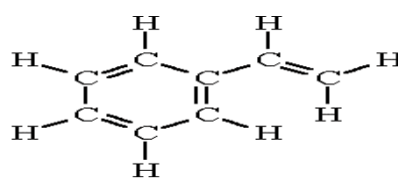
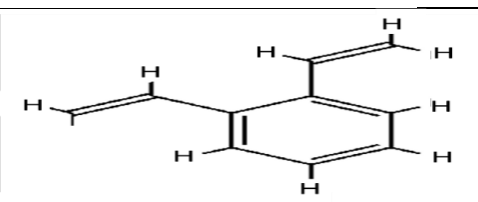
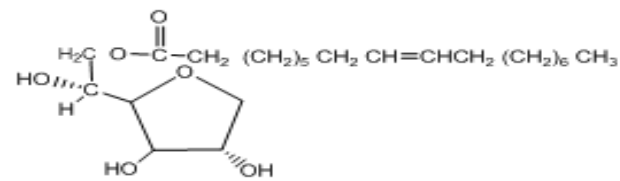
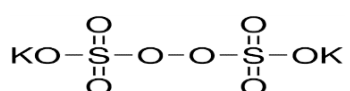
and dispersed phases as well as the molecular formula and chemical structure for the components of PHP, respectively.

Table 6: Composition of the oil phase and the aqueous phase of basic HIPE.

	Compounds	Volume (ml)	Vol%
Oil phase	Styrene*	19	76
	Sorbitan monooleate (Span80)*	3.5	14
	Divinylbenzene (DVB)*	2.5	10
Total		25	100
Aqueous phase	Potassium persulphate*	2.25	1
	Distilled water (double)	222.5	99
Total		225	100

\*These chemicals were purchased from (Aldrich Chemicals) and utilized as received.

Table 7: Molecular formulae and chemical structure for the components of PHP.

Composition	Molecular formula	Chemical structure
Styrene	$C_8H_8$	
Divinylbenzene (DVB)	$C_{10}H_{10}$	
Sorbitan monooleate (Span 80)	$C_{24}H_{44}O_6$	
Potassium persulphate	$K_2S_2O_8$	

#### 4.2.1.2 Experimental Manufacture

The HIPE utilized in this study has been synthesized in non-continuous process (batch process) in the university laboratories by employing apparatus as illustrated in the picture and schematic diagram in Figure 33.

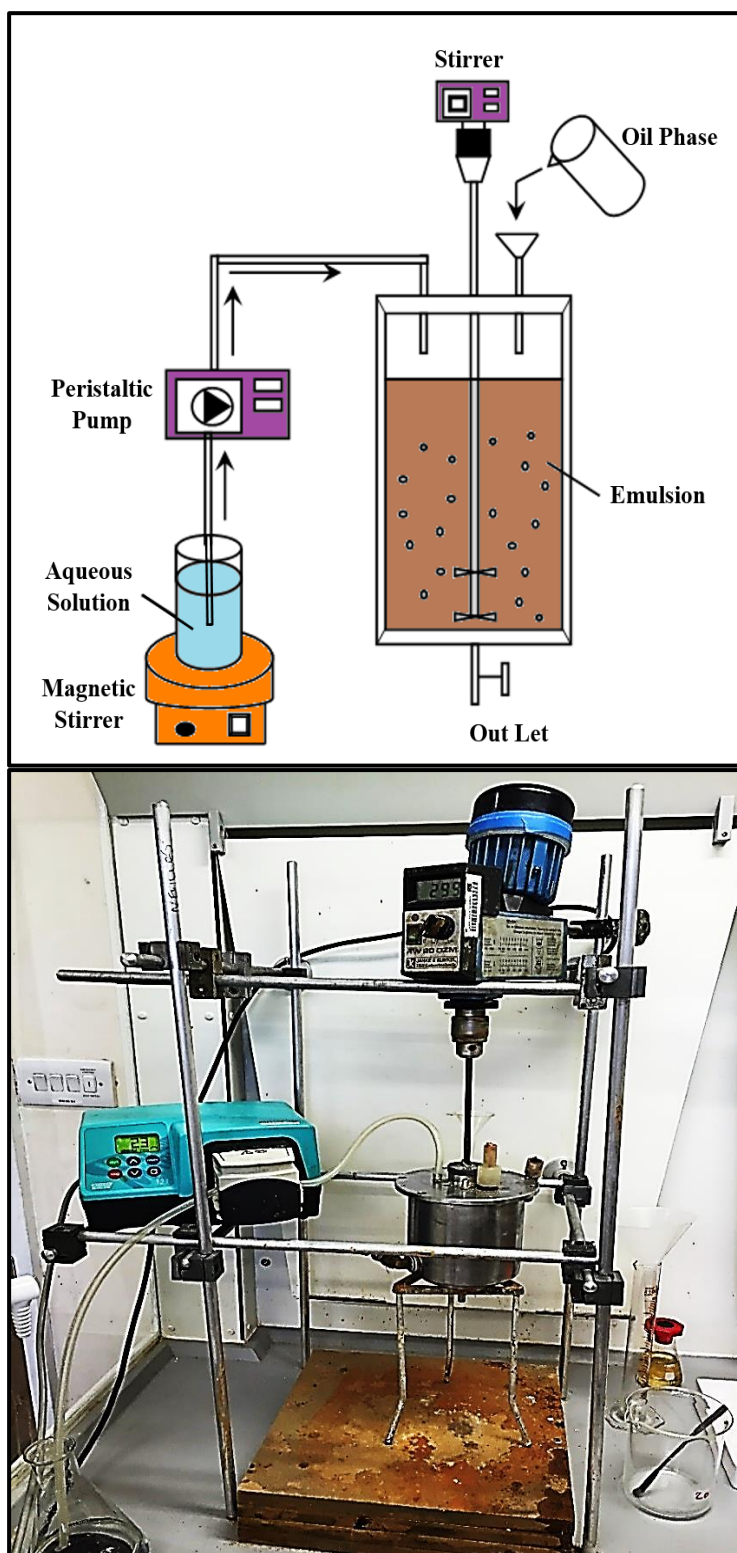


Figure 33: Schematic diagram and picture of the mixing reactor used for HIPE preparation.

Generally, the oil phase (external phase) was added manually into a mixing vessel of 12 cm internal diameter. The agitating system comprising two sets of impellers, each set consisting of 2 flat paddles of 9 cm in diameter, were used to mix the emulsion. The two sets were stacked at 90 degrees to each other (Figure 34) and the bottom impeller was placed at the closest possible distance to the bottom of the vessel (<1 mm). The impeller was rotated at 300 rpm to ensure a good mix is achieved. The agitating speed and the total mixing time were used to optimize the sizes of pores and interconnectivity of the macro-porous polymers. Further details for the optimization of these parameters are presented in the literature (Akay *et al.*, 2000; Akay *et al.*, 2005a).

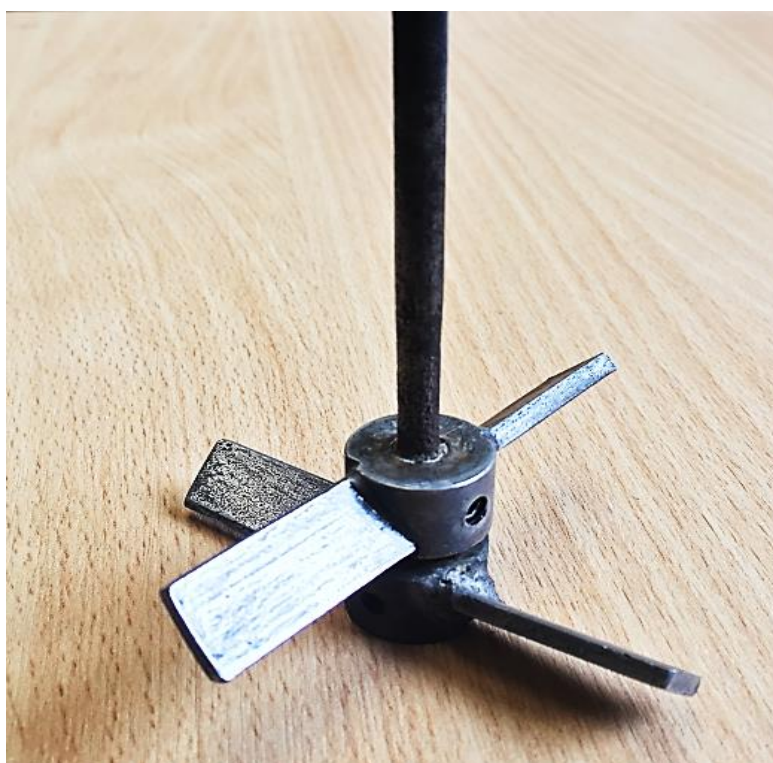


Figure 34: Picture of the Impellers used to mix the HIPE.

The pumping of the aqueous phase (internal phase) using a peristaltic pump was started within 5 minutes after transfer of the oil phase into the vessel with flow rate of 20 ml/min (dosing time=10 minutes). The impellers were started immediately the aqueous phase was pumped inside the vessel. Once all the aqueous phase was added, the emulsion mixing process continues with different times namely 10 min, 20 min, 30 min, 40 min and 50 min to evaluate the effect of the mixing time on the structure of PHP.

After emulsification, the produced HIPE was transferred into a 50 ml polypropylene containers with an internal diameter of 2.6 cm. These containers were further transferred to a polymerization oven.

#### ***4.2.1.3 Polymerisation of PolyHIPE***

The small containers containing the HIPE emulsion were then placed in an oven at 60 °C for 8 hours as shown in Figure 35. After polymerisation, the polypropylene containers were taken out of the oven, and then the PHP blocks were extracted from the containers and cut into small discs with thickness of 0.4 cm as shown in Figure 36 using a sharp knife. After that, PHP discs were transferred to the washing stage.

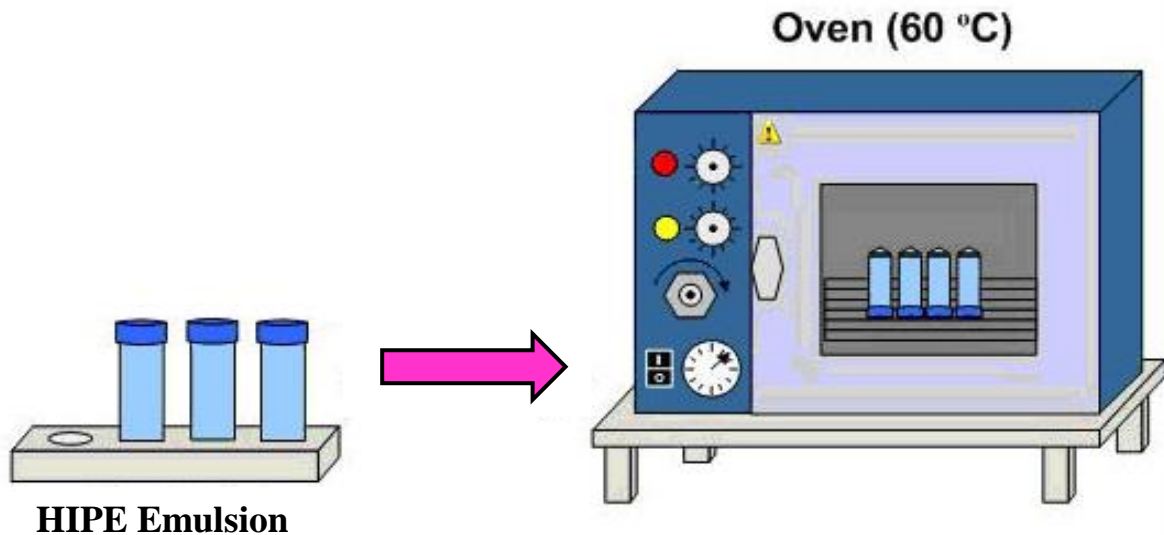


Figure 35: Schematic diagram of the polymerisation of PHP.



Figure 36: PHP samples, cut into discs with 4 mm thickness and 26 mm diameter.

#### 4.2.1.4 Washing of PolyHIPE Polymer

The samples of PHP were washed by using a soxhlet system as illustrated in Figure 37. This process was conducted with iso-propanol for 3 hours and with double distilled water for another three hours. The aim was to eliminate residual surfactant, unreacted monomer and electrolytes from the pores and interconnects of the micro-porous polymer. The PHP discs were then dried using the oven overnight (12 hr) at 60 °C to vaporise the residual water and isopropanol and make it ready for functionalisation.

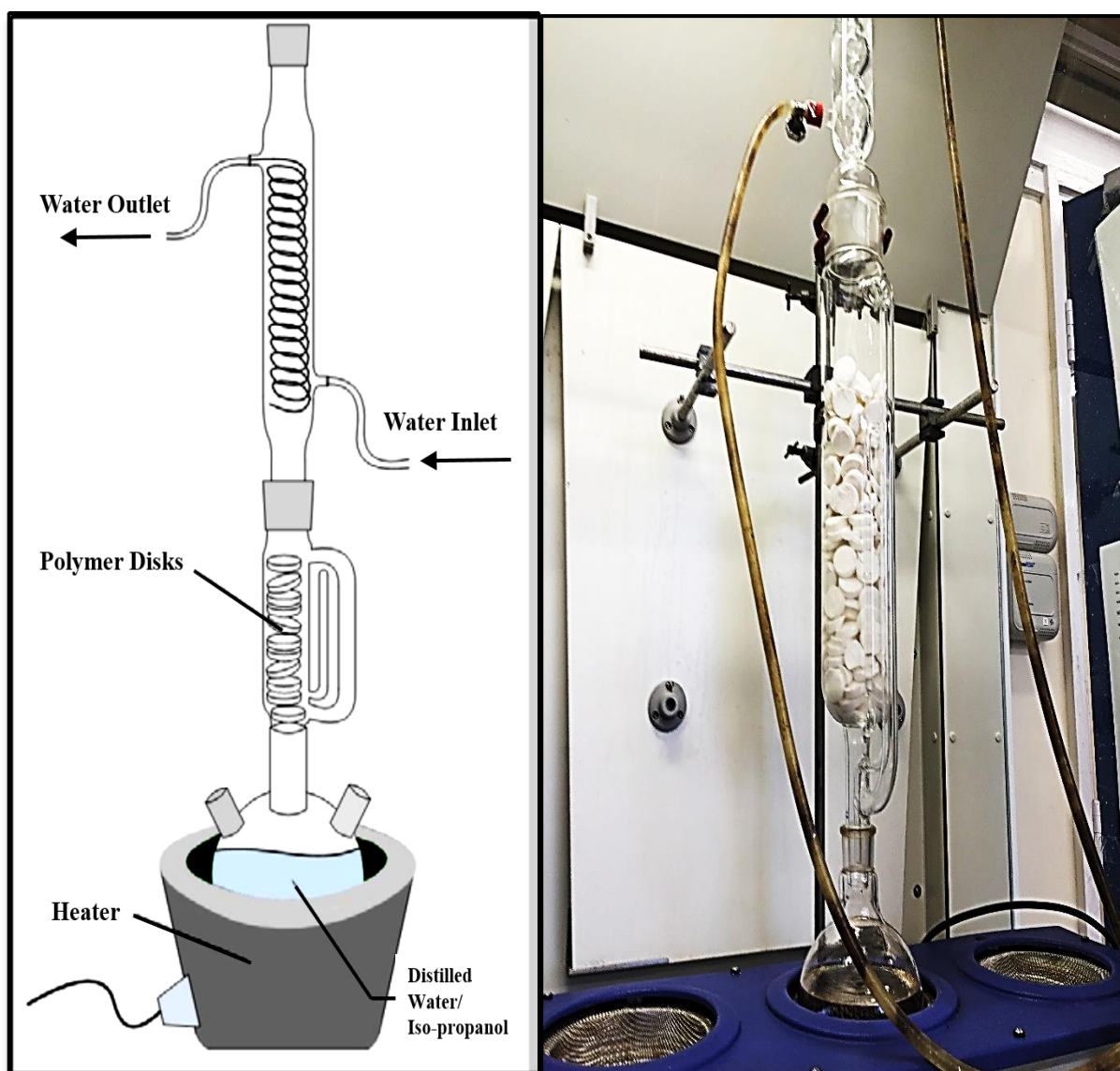


Figure 37: Schematic diagram and picture of the soxhlet system-apparatus used for PHP washing.

#### 4.2.1.5 Functionalisation of PHP

In this stage, the sulphonation process is used so that the PHP surface is altered from hydrophobic to hydrophilic. Two methods were tried for sulphonation, namely microwave irradiation and conventional (thermal) methods. Before microwave irradiation or thermal treatment, the discs of PHP were soaked in concentrated sulphuric acid for two hours. This allows the bisulphate ion group  $(\text{SO}_3^-\text{H}^+)^-$  from concentrated sulphuric acid to attach to the polyHIPE surface; an atom of hydrogen in the polymer was replaced by the  $\text{SO}_3\text{H}$  group as shown in Figure 30. In the microwave irradiation method, the discs were put in microwave for 40 seconds, the discs were flipped four times (every 10 seconds) during microwave treatment as shown in Figure 32. In the thermal method, a conventional oven was used to treat PHP thermally at  $90\text{ }^\circ\text{C}$  as shown in Figure 38. The discs were then washed with deionized water by using the soxhlet system to remove all residual unreacted sulphuric acid from inside the discs. They were dried by using the oven again at  $60\text{ }^\circ\text{C}$  to get them ready for characterization and morphological analysis via SEM, BET and FTIR.

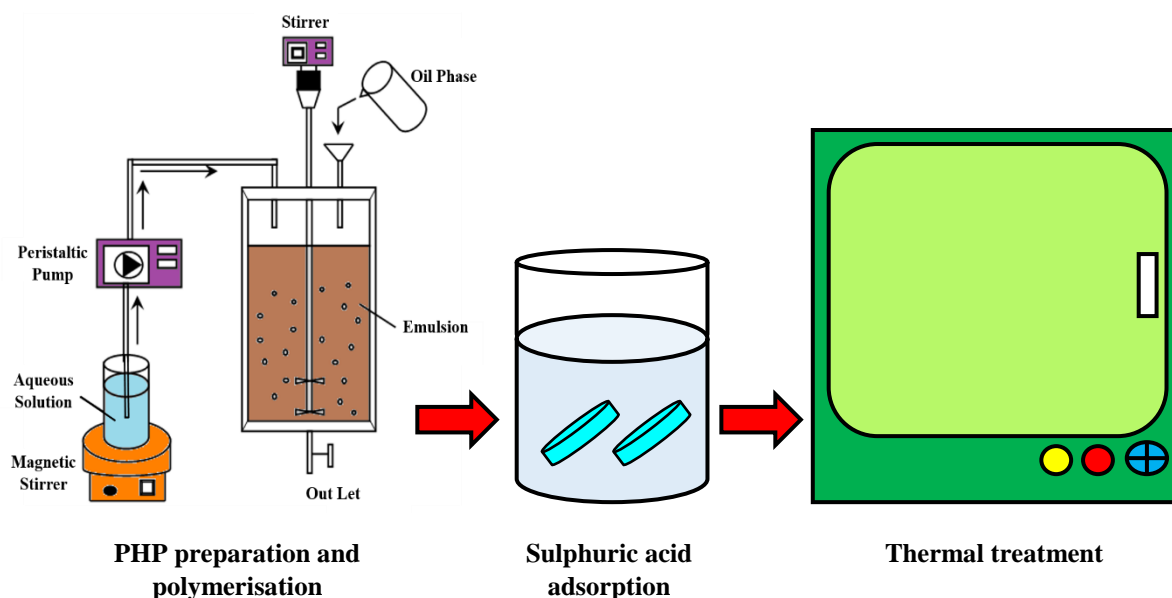


Figure 38: The thermal (conventional) method of polyHIPE sulphonation (Burke *et al.*, 2006).

#### 4.2.2 Preparation of In-Situ PolyHIPE (IS-PHP)

The process used to prepare in-situ PHP is the same as used for the preparation of post sulphonation HIPE except that sulphuric acid was used in the aqueous phase. The proportions of chemicals of both aqueous and oil phases were different as shown in Table 8. The sulphuric acid was added to obtain a hydrophilic polyHIPE (in-situ polyHIPE) instead of sulphonated polyHIPE after polymerisation process to make it hydrophilic PHP. The mixing time are (10 minutes, 20 minutes, 30 minutes, 40 minutes and 50 minutes), the stages of polymerisation, the washing procedure (the washing was repeated twice to insure the elimination of non-reacting sulphuric acid) and drying remains the same as that of the preparation of standard polyHIPE.

Table 8: Recipe of the composition of the oil phase and the aqueous phase of in-situ HIPE.

	Compounds	Volume (ml)	Vol%
Oil phase	Styrene	18.50	74
	Sorbitan monooleate (Span80)	3.50	14
	Divinylbenzene (DVB)	3.00	12
Total		25	100
Aqueous phase	Potassium persulphate	2.25	1
	Distilled water (double)	211.50	94
	H <sub>2</sub> SO <sub>4</sub> (98% conc.)*	11.25	5
Total		225	100

\*The sulphuric acid was also purchased from Aldrich Chemicals and utilized as received

### 4.2.3 Preparation of Bindzil PolyHIPE (BZ-PHP)

The Bindzil polyHIPE has been prepared via same procedure used for basic PHP. While, the proportions of chemicals of both aqueous and oil phases were different as illustrated in Table 9. Bindzil CC40 (this is a trade name for colloidal silica) was used at various ratios namely, BZ5 (5 vol. %), BZ10 (10 vol. %), BZ15 (15 vol. %), BZ20 (20 vol. %) and BZ25 (25 vol. %); the aqueous phase solutions have been diluted by double distilled water. Both lauroyl peroxide and potassium persulphate initiators have been used to prepare in-situ polyHIPE. Using lauroyl peroxide was not successful due to the separation of the HIPE emulsion into the two layers of oil phase and aqueous phase during the polymerisation process. While the potassium persulphate has achieved success. According to the supplier (KEA Chemicals), the Bindzil CC (Clear Coat products) are clear liquid and colloidal solutions. Bindzil CC40 is an aqueous colloidal solution with 40 wt% SiO<sub>2</sub> and a particle size around 12 nm. The pumping time and agitating time used were 10 minutes and 50 minutes, respectively.

Table 9: Composition of the oil phase and the aqueous phase of Bindzil HIPE and the molecular formula and chemical structure of Lauroyl peroxide.

	Compounds	Volume (ml)					Vol%					
		Vol (ml)	Vol %	Vol ml	Vol %	Vol (ml)	Vol %	Vol (ml)	Vol %	Vol (ml)	Vol %	
Oil phase	Styrene	18.75					75					
	Span 80	3.50					14					
	Divinylbenzene (DVB)	2.50					10					
	Potassium persulphate	0.25					1					
Total	25					100						
Aqueous phase	Compounds	Vol (ml)	Vol %	Vol ml	Vol %	Vol (ml)	Vol %	Vol (ml)	Vol %	Vol (ml)	Vol %	
	Distilled water	213.75	95	202.5	90	191.25	85	180	80	168.75	75	
	Bindzil CC40*	11.25	5	22.5	10	33.75	15	45	20	56.25	25	
Total	225		100	225		100	225		100	225		100

#### 4.2.4 Preparation of Silane PolyHIPE (SL-PHP)

The Silane polyHIPE has been prepared via same procedure used for basic PHP. While, the proportions of chemicals of both aqueous and oil phases were different as shown in Table 10. Silane (Vinyl trimethoxy silane) was used at various ratios namely, SL5 (5 vol %), SL10 (10 vol %), SL15 (15 vol %), SL20 (20 vol %) and SL25 (25 vol %). The dosing time and agitating time used were 10 minutes and 50 minutes, respectively.

Table 10: Composition of the oil phase and the aqueous phase of Silane HIPE.

	Compounds	Vol. (ml)	Vol %	Vol (ml)	Vol %	Vol (ml)	Vol %	Vol (ml)	Vol %	Vol (ml)	Vol %
Oil phase	Styrene	17.75	71	16.50	66	15.25	61	14.00	56	12.75	51
	divinylbenzene (DVB)	2.50	10	2.50	10	2.50	10	2.50	10	2.50	10
	Span 80	3.50	14	3.50	14	3.50	14	3.50	14	3.50	14
	Vinyl trimethoxy silane *	1.25	5	2.50	10	3.75	15	5.00	20	6.25	25
Total		25	100	25	100	25	100	25	100	25	100
	Components	Volume (ml)					Vol%				
Aqueous phase	distilled water (double)	222.75					99				
	Potassium presulphate	2.25					1				
Total		225					100				

\*The vinyl trimethoxy silane was purchased from Aldrich Chemicals and utilized as received.

### 4.3 PHP Sulphonation

PHP sulphonation was carried out by using microwave irradiation and thermal (through conventional oven) heat treatment methods. The sulphonation of SL-PHPs utilising microwave irradiation were successful, while the thermal method failed due to swelling and crumbling of the PHPs. Sulphonated B-PHPs were easily produced via the thermal method, while the microwave irradiation was failed due to a burned and crumbed structure of the PHPs. Trials on BZ-PHPs utilising the thermal method have also failed, whilst microwave irradiation was successful. Table 11 presents the ‘as produced’ sulphonated PHPs.

Table 11: Summary of the results of PHP sulphonation.

PHP sample name	Thermal method			Microwave irradiation		
	% acid	Soaking time (hr)	The result	% acid	Soaking time (hr)	The result
SL5	98	2	Failure	98	2	Success
SL10	98	2	Failure	98	2	Success
SL15	98	2	Failure	98	2	Success
SL20	98	2	Failure	98	2	Success
SL25	98	2	Failure	98	2	Success
B10	98	2	Success	98	2	Failure
B20	98	2	Success	98	2	Failure
B30	98	2	Success	98	2	Failure
B40	98	2	Success	98	2	Failure
B50	98	2	Success	98	2	Failure
BZ5	98	2	Failure	98	2	Success
BZ10	98	2	Failure	98	2	Success
BZ15	98	2	Failure	98	2	Success
BZ20	98	2	Failure	98	2	Success
BZ25	98	2	Failure	98	2	Success

## 4.4 Analytical Methods

The different analytical methods utilized in this study are the following.

- 1- Analytical techniques for PolyHIPE:
  - i- Surface area and pore size analysis.
  - ii- Environmental Scanning Electron Microscopy (ESEM).
  - iii- EDX (elemental analysis).
  - iv- Fourier Transform Infrared spectroscopy (FTIR).
  - v- Water uptake.
  
- 2- Analytical techniques of water-in-crude oil emulsions.
  - i- Viscometer Measurement.
  - ii- Conductivity Measurement.

### *4.4.1 Analytical Techniques for PolyHIPE*

#### *4.4.1.1 Surface Area and Pore Size Analysis*

The surface area of PHP is considered an important physical characteristic. Depending on its surface area important properties like capacity of solvent/water uptake (based on the polymer polarity) can be assessed; a high surface area PHP material commonly has a high capacity of solvent/water uptake. The efficiency of PHP to absorb water is significant in separation experiments of water/oil and, thus the PHP surface area needs to be assessed. In this study, The BET Surfer instrument, manufactured by Thermo Scientific Company was utilized to measure the PHPs surface area and pore size distribution. Figure 39 shows an image of the machine. This machine utilizes the technique of Gas Sorption to get the overall surface area and pore size distribution between 0.4-200 nm diameter. The gas used for absorption is nitrogen. The technique is used to assess the physical adsorption in material structures, where known size molecules of gas are adsorbed (condensed) on the specimen surface at a constant temperature. The resultant system pressure and the amount of gas adsorbed by the sample are recorded and used to create an adsorption isotherm. The isotherm is then utilized in calculation models to determine surface area and porosity. In this research, the BET (Brunauer, Emmet and Teller) and BJH (Barret, Joyner and Halenda) calculation models are utilised to calculate specific surface area and for pore size distribution, respectively.

Through the process of adsorption, attachment happens between the adsorbate molecules and the materials surface, via chemisorption or physisorption processes. The BET machine presumes that the whole adsorption detected is as a result of physically adsorbed gas and is reversible. Therefore, the models of calculation do not depend on the chemisorption process but rather depend on physisorption process.



Figure 39: Surface area analyzer, BET Surfer.

#### ***4.4.1.1 Desorption and adsorption isotherm***

BET measures both, branches of desorption and adsorption isotherm. The surface area is evaluated depending on the adsorption branch whilst the distribution of pore size is evaluated depending on the desorption or adsorption branch and on the branches together. The adsorption isotherm is defined as the amount of adsorbed gas on the materials surface at constant temperature as a function of pressure. The volume of gas is determined at a standard temperature and pressure (STP) and denoted in  $\text{cm}^3/\text{g}$ . The branch of desorption presents the process of reverse adsorption. The pressures of adsorption differ with temperature; therefore, at a specific temperature the isotherm data is unique.

Practically, the isotherm shows the relative pressure vs volume adsorbed ( $\text{cm}^3/\text{g}$ ). The relative pressure is represented as the specimen pressure divided by the saturation vapour pressure. The specimen pressure is the pressure remaining in the specimen chamber because of residual

molecules, which are un-adsorbed during the adsorption of gas on the surface of the material. In other words, the adsorption does not occur for all adsorbed gas molecules. The measurable relative pressure values range between 0-0.995 with the BET Surfer. The liquid gas boiling pressure can be used as the saturated vapour pressure. Nevertheless, because of a liquid nitrogen contamination via atmospheric gas condensation, it is necessary to measure the saturation vapour pressure during the specimen analysis period.

Practically, the desorption process can be measured volumetrically by utilizing the method of static fully equilibrated volumes. Each point of discrete data is measured after the system is fully equilibrated according to pre-defined conditions. A high resolution can be obtained through using a large number of data points. The volume of an empty (unoccupied by the sample) sample tube is measured by utilizing nitrogen gas and named (free space). For each data point, a fixed volume of nitrogen is dosed into the chamber the pressure is determined, and used thereafter to determine the adsorbed gas volume conserved inside the sample. Each dose of gas has a constant volume pre-regulated at the factory. For the adsorbed gas, the (y-axis) isotherm data is estimated by deducting the value of sample tube freespace from the whole volume that is dosed to the sample. For the relative pressure, the (x-axis) isotherm data is gained via division of the pressure of the sample by the pressure of saturation vapour.

#### **4.4.1.1.2 Freespace**

The volume of dosed gas and freespace are estimated by applying the ideal gas law. The moles of gas, which are dosed inside the manifold, can be calculated by using the following formula.

$$P_M V_M = nRT_M \quad \text{Eq. 24}$$

where n: is the moles of gas.

$V_M$ : is the dose manifold volume.

$P_M$ : is the dose manifold pressure.

$R$ : is the gas constant

$T_M$ : is the dose manifold temperature.

The freespace volume is specified from the resulting pressure change. It can be determined from the nitrogen gas dose by

$$\frac{P_{M1}V_M}{T_M} = \frac{P_{M2}V_S}{T_S} + \frac{P_{M2}V_M}{T_M} \quad \text{Eq. 25}$$

where

$T_S$ : is the sample temperature.

$V_S$ : is the sample volume.

$T_M$ : is the temperature of the manifold.

$V_M$ : is the volume of the manifold.

$P_{M1}$ : is the manifold pressure before gas dose and

$P_{M2}$ : is the manifold pressure after gas dose.

The dosed gas volume is obtained by the equation below

$$V_{dn} = \frac{V_M(P_{M1} - P_{M2})}{T_M} * \frac{273.15}{760} + V_{d_{n-1}} \quad \text{Eq. 26}$$

where

$V_{dn}$ : is the volume dosed.

$T_M$ : is the temperature of the manifold.

$P_{M1}$ : is the initial manifold pressure.

$P_{M2}$ : is the final manifold pressure.

$V_M$ : is the volume dosed from former data point, and

273.15/760: is the standard temperature and pressure conversion.

At least three points are measured in nitrogen data at increasing pressure. The nitrogen freespace correction is determined from the linear plot of volume dosed versus pressure of sample. The slope corresponds to the sample tube volume per unit of pressure in the sample tube. Hence, the specified freespace is utilised to calculate the volume adsorbed in following equation. The calculation is carried out at all the measured data points.

$$V_{ads_n} = V_{d_n} - [(P_{s_n} * slope) + intercept] \quad \text{Eq. 27}$$

where

$V_{ads_n}$ : is the volume adsorbed volume.

$P_{s_n}$ : is the pressure of sample.

$V_{d_n}$ : is the volume dosed.

Slope: freespace measurement slope, and

Intercept: is the freespace measurement intercept.

A full analysis for desorption and adsorption isotherm has been conducted to gain BET surface area and BJH desorption and adsorption distribution of pore size.

#### 4.4.1.1.3 Surface Area Analysis

The equation of BET (Brunauer, Emmet and Teller), is the most generally utilised method to calculate PHPs surface area.

$$\frac{P_s}{V_A(P_o - P_s)} = \left[ \frac{1}{CV_M} \right] + \frac{P_s}{P_o} * \left[ \frac{C - 1}{CV_M} \right] \quad \text{Eq. 28}$$

where

$V_A$ : is the adsorbed.

$V_M$ : is the Monolayer volume.

$P_s$ : is the sample pressure.

$P_o$ : is the saturation pressure.

$\left[ \frac{C-1}{CV_M} \right]$ : is the slope, and

$\left[ \frac{1}{CV_M} \right]$ : is the intercept.

The plot of  $\frac{P_s}{V_A(P_o - P_s)}$  versus relative pressure  $\frac{P_s}{P_o}$  gives a straight-line having a slope and intercept  $\left[ \frac{C-1}{CV_M} \right]$  and  $\left[ \frac{1}{CV_M} \right]$ , respectively.  $V_M$  and  $C$  can be determined from the slope and intercept values measured.

The following Equation gives the BET surface area; the unit is  $\text{m}^2/\text{g}$ .

$$S_{BET} = \frac{A_M * N_A * V_M}{M_V} \quad \text{Eq. 29}$$

where

$N_A$ : is the Avogadro's number.

$M_V$ : is the gram molecular volume,  $22414 \text{ cm}^3$ , and

$A_M$ : is the cross sectional area that, each adsorbate molecule occupies (for nitrogen,  $A_M=0.162 \text{ nm}^2$ ).

Due to the use of nitrogen as the adsorbate, the cross sectional area is supposed as  $(0.126 \text{ nm})$ .

The parameters of BET that selected before calculation of a t-plot was “10” which is equivalent to ten data points for the common settings of relative pressure, i.e. (0.05 to 0.2).

The method of t-plot is utilised to calculate the micropore area and micropore volume ((this is done by comparing the adsorption isotherm of the material to be calculated with an adsorption isotherm reference of nonporous material with a similar surface chemistry such as zeolite with MCM-1 (Galarneau *et al.*, 2014)). The output of the machine is the values of macropore and meso pore surface area and the volume of micropores. In combination with the surface area of BET, the surface area of a micropore is obtained. The film thickness ( $t$ ), can be calculated using Hasley’s method or Harkins and Jura’s method. In this study, Harkins and Jura’s calculation method is utilised, as illustrated in the next equation.

$$t = 3.54 * \sqrt[3]{\frac{5}{2.303 * \log \frac{P_0}{P_s}}} \quad \text{Eq. 30}$$

The area of meso/macropore is then determined by utilizing the t-Plot slope of the linear section. The values of the mesopore surface area and micropore volume are calculated by the following formulae.

$$VOLUME_{MICROPORE} = [(0.001547) * (t - Plot\ intercept)] \quad \text{Eq. 31}$$

$$SURFACE\ AREA_{MESOPORE} = [1547 * (t - Plot\ intercept)] \quad \text{Eq. 32}$$

The surface area of a micropore may subsequently be attained by the following equation, ( $SURF$ =Surface).

$$SURF.\ AREA_{MICROPORE} = SURF.\ AREA_{BET} - SURF.\ AREA_{MESOPORE} \quad \text{Eq. 33}$$

The resolution selection for t-Plot data points was standard which is equivalent to around 20 data points. The range of t-plot that was selected is the maximum accessible range of thickness allowed by the machine and software, i.e. 0.5-0.70 nm. This extent was selected because of the scope for the distribution of pore size from the calculation of BJH. The low range of BET setting of 0.005 – 0.05 was selected for calculation of the t-plot.

#### 4.4.1.1.4 Analysis of Pore Size

The distribution analysis of pore size can be conducted by utilizing either of the isotherm branches of adsorption or desorption. Computationally, a cylindrical pore sample with open

end, and absence of pore connection are assumed. The calculation is based on the method of BJH (Barret, Joyner and Halenda). Equation 34 (the Kelvin equation) is used to obtain the radius of a liquid core in a capillary.

$$R \ln \left[ \frac{P_S}{P_O} \right] = -2\gamma \frac{V_M}{R_K} \quad \text{Eq. 34}$$

where  $R$ : is the gas constant.

$R_K$ : is the Kelvin Radius.

$\gamma$ : is the adsorbate surface tension at T, in (mN/m).

$T$ : is the nitrogen boiling point.

$P_S$ : is the sample pressure.

$P_O$ : is the saturation pressure, and

$V_M$ : is the nitrogen molar volume

Substituting the constant values and reorganizing the terms in equation 35 yields the following equation for (Kelvin radius).

$$R_K(\text{Angstroms}) = 4.14 * \log \frac{P_O}{P_S} \quad \text{Eq. 35}$$

The film thickness of absorbed nitrogen on the walls of pore at each relative pressure is determined by utilizing the equation of Harkins and Jura (Eq. 30). The  $t$  (film thickness) is added to  $R_K$  (the Kelvin radius) with a view to obtain  $R_P$  (the actual radius of the pore). Table 12 lists the constant values that are utilised by the machine in the calculation of distribution analysis of pore size.

Table 12: Constants values utilised by the BET machine in the distribution analysis of pore size.

Constants	Values
Nitrogen surface tension	8.855 mN/m
Normal boiling point of nitrogen (T)	77.3 K
Molar volume ( $V_M$ )	34.6 cm <sup>3</sup> mole
Ideal gas constant (R)	8.314 J/mole*K
	8.31*10 <sup>7</sup> erg/mole*K
STP to liquid volume	0.00156

#### ***4.4.1.2 Environmental Scanning Electron Microscope (ESEM)***

Along with the surface area analysis, further morphological characterization of the prepared PHPs was done via Environmental Scanning Electron Microscopy (ESEM). Both the unsulphonated and sulphonated PHPs were investigated using ESEM. SEM was first discovered in the 1930's, when Max Knoll obtained the first image. Nonetheless, it was first introduced in the market by Charles Oatley and Gary Steward in 1965 via the Cambridge Instrument Company, under the name Stereoscan. It is now in widespread use, both in terms of global production and research laboratories, it has been continuously modified and upgraded in terms of image resolution and image recording time.

As a result of the multiple imaging signals created in a SEM, the wide magnification range (between 3 to 15,000 times or more), the ease of forming a simple image of the specimen morphology with high resolution and large depth of field (around 30 times higher compared with a normal light microscope) SEM has emerged as an excellent candidate for imaging procedures. The magnification is a result of the controlled scanning (rastering) of the primary electron beam on the sample surface and is determined by the ratio of area investigated upon the sample to the area of the imaging screen, instead of depending on a lens. Figure 40 shows the ESEM used in this project.



Figure 40: Environmental Scanning Electron Microscopy (SEM) used in the research.

ESEM was employed to demonstrate fresh PHP samples internal architecture before and after functionalisation; for example, the PHP wall porosity, distribution of pore size and the interconnecting structure. Oil-fouled samples could also be investigated using the differentially pumped ESEM but a sample with no volatile component (s) of oil that may evaporate and contaminate the unit should be used. In this current work, a FEI XL30 SEM field emission gun (FEG) ESEM based in the Newcastle University-Advanced Chemical and Material Analysis (ACMA), UK was used. Despite the fact that it is usual to coat non-conductive specimens with a conductive media to prevent charging, in this work, the specimens were inspected without any carbon/gold coating after being prepared, modified and dried as they are hydrophilic in nature and thus are sufficiently conductive. Every specimen was cut and fixed on an aluminum stub of 12.7 mm diameter for analysis.

The SEM functions as follows. The microscope makes use of an electron beam, produced from a gun positioned at the top of the microscope, which is focused to a highly magnified spot on the sample under examination. The electron beam is created from a negatively biased filament or emitter and is extracted from the gun by a positive anode with a small hole in it. The electron beam enters a chamber that is kept under vacuum to permit the effective travel of an electron beam in a vertical direction. Once it enters the chamber, the electron beam goes through several system namely: (1) an extraction electrode; (2) a magnetic lens (concentrate the beam of electron onto the sample surface); (3) scanning coils, respectively. Inside the vacuum chamber finally, the beam of electrons strikes the specimen/sample, which results in ejection of electrons and x-ray from the specimen. These electrons are identified as: (i) primary back-scattered electrons; (ii) secondary electrons; (iii) Auger electrons. Afterwards, one or more detector gathers these x-rays and electrons into a signal, which is subsequently transmitted to a TV screen to signify the image of specimen scan coils are used to move the electron beam in a controlled pattern on the surface. This raster pattern is synchronized with the TV raster pattern to create an image. The magnification is increased by reducing the size of the raster pattern on the sample. This procedure shows schematically in Figure (41).

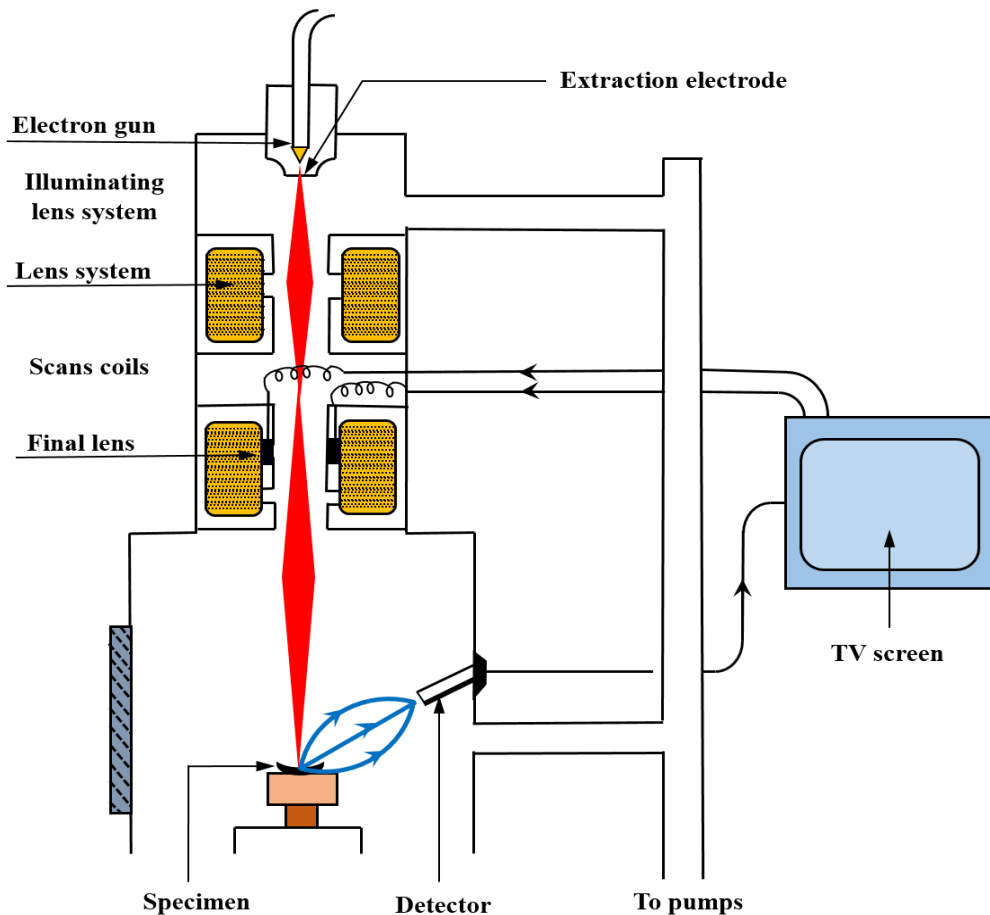


Figure 41: Schematic representation of SEM with formation of secondary electrons the images on the TV screen.

For imaging, secondary electrons were selectively attracted to a grid held at a low positive potential (~50 volts). Behind the grid, a disc is held at approximately 10 kilovolts and is positive with respect to the specimen. The disc consist of a scintillant layer coated with a thin aluminum layer. Electron impact on the disc creates light which is capture by a photodiode and converted to a voltage single. This voltage is reliant on the number of secondary electrons, which are striking the disc. Hence, there is a voltage signal that is of a specific strength produced from the secondary electrons created from a small area of the specimen. The voltage is used to modulate the brightness of pixels in a TV screen to create the image.

SEM images were used to assess the structure and morphology of the PHPs produced. Quantitative analysis of the size of the larger pores in the structure was undertaken using ImageJ software (Reinking, 2007). A range of pores were measured from SEM images (at least 30 measurements) to give the distribution shown in Figure (42).

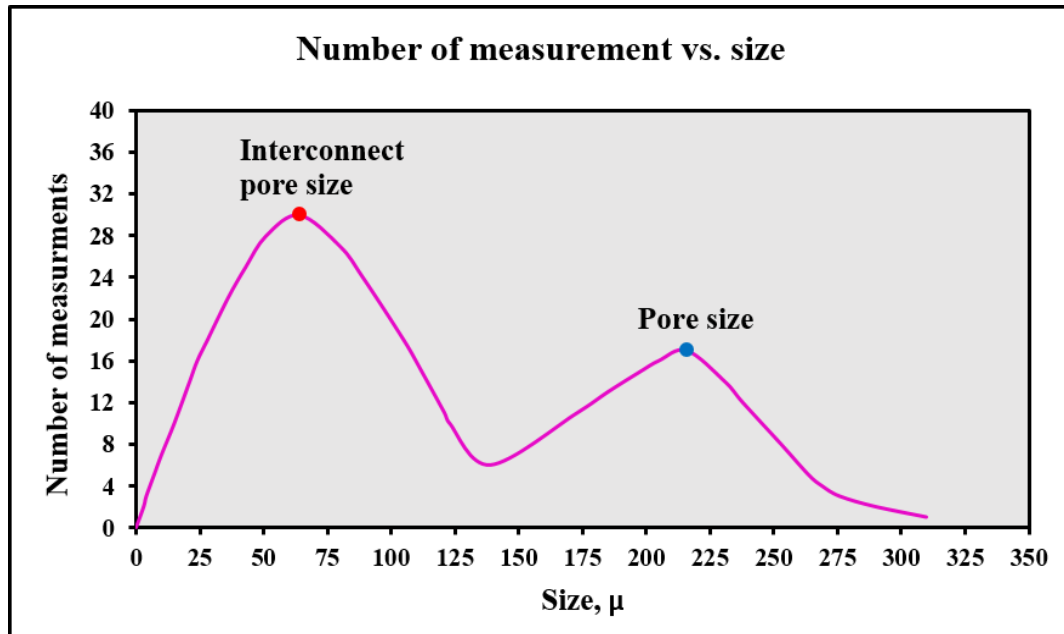


Figure 42: Plot of number of measurements versus pore size using ImageJ software.

Two peaks were observed in the distribution and the average size of the pores was determined from the peak at larger size. The other peak gives the average size of the interconnection holes between these pores.

#### 4.4.1.3 EDX (Element Analysis)

The described SEM equipment in the previous section is also fitted with a Rontec Quantax detector for identification of local element analysis (EDX). The equipment includes a light element analyser designed to detect and quantify the elemental composition of elements with atomic number higher than five. The detector is a liquid nitrogen cooled silicon-lithium device which can be measure the energy of an impacting x-ray photon. Typically, X-ray spectra consist of peaks corresponding to different electronic transitions in different elements superimposed on a background signal caused by multi scattering events (Bremsstrahlung). The energy of each peak can be used to identify the elements present by comparison with known results from pure materials. The amount of an element can be estimated from the peak intensity again by comparison to pure elemental standards. Typically, the spectra were collected for 100 seconds to enable sufficient counts for analysis.

#### ***4.4.1.4 Fourier Transform Infrared spectroscopy (FTIR)***

FTIR analysis is widely used for different functions such as to recognize unknown materials, identify the composition of a mixture, and to determine sample quality and uniformity. In this process, infrared radiation (IR) is passed through a specimen; which absorbs some of this radiation while the rest is passed out of the specimen (transmitted). The outcome a spectrum of absorption or transmission as a function of IR frequency, producing a molecular fingerprint of the specimen. Peaks of absorption relate to particular bonds in the chemical structure which vibrate at given frequencies.

The spectrometer system utilised to analyse the solid specimens was a Spectrum Two FTIR Spectrometer manufactured by the Perkin Elmer Company. Figure 43 shows a picture of the FTIR system. The machine creates a spectrum from  $4000\text{ cm}^{-1}$  to  $400\text{ cm}^{-1}$  wavenumber (i.e. cycles per meter) to analyze the liquid, oil and solid samples by utilising a Pick Technology diamond crystal plate ATR (attenuated total reflection) detection method.

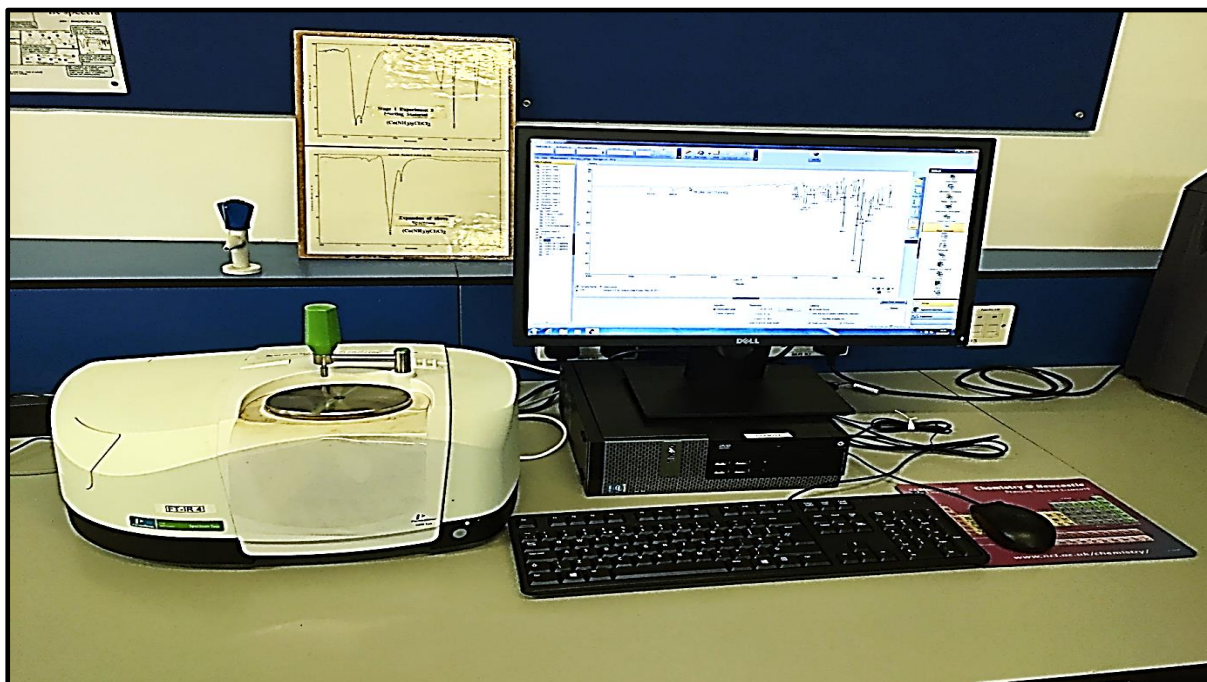


Figure 43: Fourier Transform Infrared spectroscopy (FTIR) equipment.

#### ***4.4.1.5 Water Uptake Tests***

Among the characteristics of the PHPs are their high porosity, low density and interconnectivity along with their internal pore architecture. These characteristics afford them to be useful in the separation process. During microwave irradiation, the sulphonation process

increases the surface area of PHP and the porosity. The small surface area  $16 \text{ m}^2/\text{g}$  of PHP was successfully promoted to  $81 \text{ m}^2/\text{g}$  after sulphonation process without affecting the mechanical stability. With an increase in the surface area of the PHPs, the hydrophilic behavior also increases enabling them to absorb water of 275% of their own weight (Hasan, 2013). Thumbarathy (2018) supported the result in which this hydrophilic behavior can increase to 1700 times their own weight under optimized processing conditions.

The test of water uptake was carried out on the batches of B-PHP, IS-PHP, BZ-PHP and SL-PHP that successfully polymerised with the aim of determining the performance of hydrophilic surfaces before and after the sulphonation process. The test was simple and quick. Figure 44 shows the water uptake test. Each type of these PHPs was divided into small discs as mentioned in the first part of this chapter. Initial weight and dimensions of three discs for each type of these PHPs were recorded (the size and weight are nearly the same), and then the discs were immersed into a beaker of distilled water, (different beakers for each type of polymer, with a similar amount of distilled water). During this test, the discs were removed from the water and their weight and dimensions were measured every hour for eight hours. The final readings were taken after 24 hours and then the PHP discs were totally removed from the water. In order to calculate the water uptake of these PHPs, the weight of the water absorbed by the PHP disc is divided by the dry (original) weight of the PHP disc. The water uptake results for the B-PHP, IS-PHP, BZ-PHP and SL-PHP are mentioned in sections 5.2.4, 5.3.4, 5.4.4 and 5.5.4, respectively.

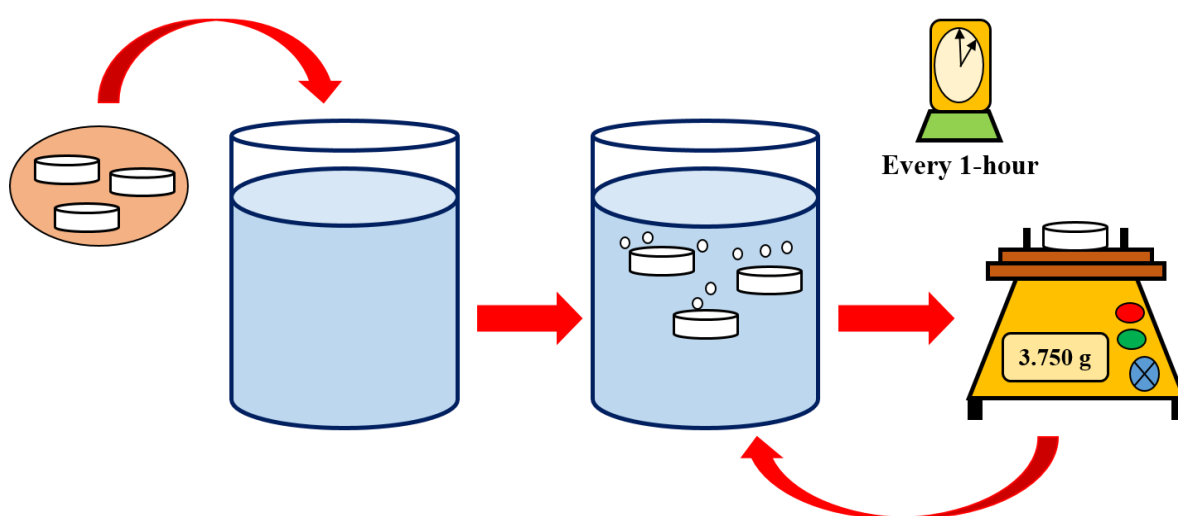


Figure 44: Schematic diagram showing the water uptake analysis.

## 4.4.2 Analytical Techniques of Water-in-Crude Oil Emulsions

### 4.4.2.1 Viscometer Measurement

In this study, the viscosity (one of the rheological properties) of the prepared water-in-oil emulsions was measured utilising a co-axial cylinder Geometry Haak VT 550 viscotester manufactured by Thermo Fisher Scientific Company. This viscometer (VT 550), is a microprocessor controlled rotation instrument with a LED- display of the shear rate ( $\text{s}^{-1}$ ), shear stress (Pa), temperature of the sample T ( $^{\circ}\text{C}$ ), rotor speed ( $\text{min}^{-1}$ ) and viscosity ( $\text{mPa s}$ ). It was not connected with a computer during the experiment but still provided digital data which can be processed off-line by a computer. As shown in Figure 45, the viscometer consists of a fixed outer cylinder and a surrounding jacket used to heat or cool the sample during testing. A water bath was used for controlling the system's temperature. A reduced diameter-inner cylinder, which was rotated by the motor was controlled at a constant or planned speed.

The sample used for testing was injected in the measuring chamber of the sensor speed system during spindle rotation. It causes an opposition to this rotational motion because of its viscosity, which becomes clear as a torque on the viscometer-measuring shaft. A torque detector is used to measured this and determine viscosity. In this test, a fixed rate of the controlled shear was employed on the sample by tuning the speed of rotor and the resultant shear stress permits the relative viscosity computation of the emulsions via the control computer.

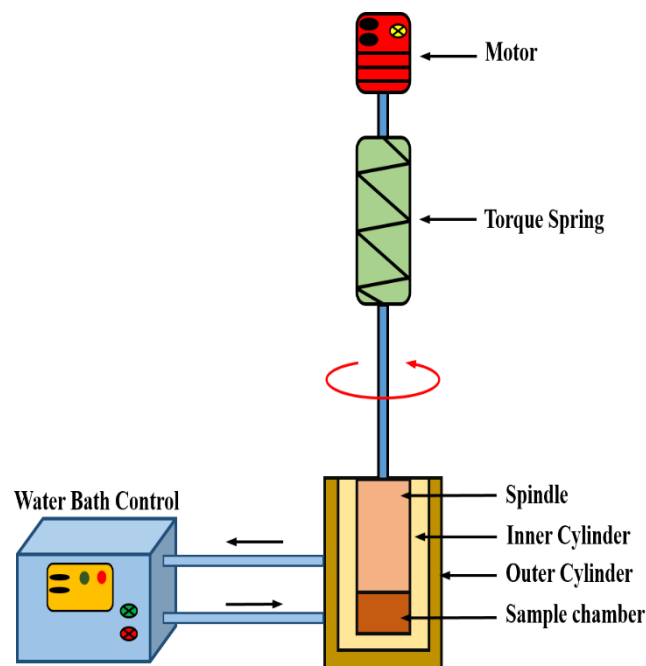


Figure 45: A simplified schematic drawing of the Co-axial Cylinder HAAKE VT 550 Viscometer.

#### 4.4.2.2 Conductivity Measurements

The conductivity (G) is one of the main important properties of solutions. Conductivity signifies the ability of the solution to conduct (namely the ability to carry the electric current or not). Mainly, this is based on the amount and type of ions in the solution. The conductivity is directly proportional to the concentration of ions. Nevertheless, there are conditions at which there is no linear relationship between conductivity and solution concentration due to ionic interactions which may amend the behavior of conductivity.

On this basis, the conductivity is the opposite of the resistance of solution. Thus, it can be expressed by a re-write the Ohm's law as follows:

$$G = \frac{1}{R} = \frac{I(A)}{E(V)} = (Ohm)^{-1} \quad \text{Eq. 36}$$

where

$G$ = the conductivity ( $Ohm^{-1}$ ).

$I$ = the current (A).

$R$ = the resistance (Ohm); and

$E$ = the electric field (V).

The above equation illustrates that the ( $Ohm^{-1}$ ) is the unit of conductivity, which can be read oppositely as mho. Recently, this unit has been rarely utilised and has been substituted with Siemens/cm or most commonly micro/milli-Siemens/cm.

The main use of the conductivity test is to measure the effect of the sum of the impurities existing in the solution. However, the measurements of conductivity does not provide a particular correspondence with any ion existing in a solution. Actually, it gives a combined measurement in one reading for all ions, which exist in the solution. In emulsion systems, it can be utilised to differentiate between w/o and o/w emulsion as in a continuous medium emulsions (emulsion of w/o), the conductivity is a lower than the water, or in a o/w emulsion where the continuous phase is water (Lee, 1999).

The conductivity of the crude oil and the emulsions of water-in-crude oil were measured before and after the separation process by using a Mettler Toledo SevenExcellent S470 Conductivity

Meter manufactured by FisherScientific (part of Thermo Fisher Scientific) Company as shown in Figure 46.

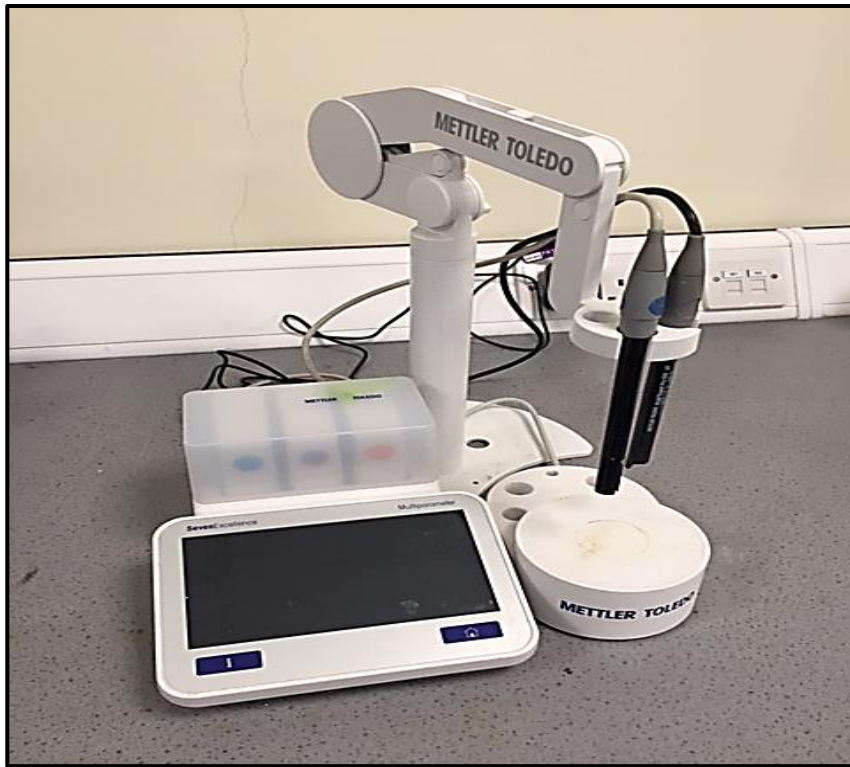


Figure 46: Mettler Toledo SevenExcellent S470 Conductivity Meter.

---

## CHAPTER FIVE

---

### 5. POLYHIPE POLYMER (PHP) DEVELOPMENT: RESULTS AND DISCUSSIONS

#### 5.1 Overview.

This chapter discusses the production of four kinds of polyHIPEs in terms of the following:

- i. Morphology.
- ii. EDX analysis to verify the elements in the structures.
- iii. Pore size distribution using ImageJ software analysis.
- iv. Surface area measurement using the BET technique.
- v. Water uptake measurement.
- vi. FTIR analysis, and
- vii. PHP sulphonation.

#### 5.2 Basic PolyHIPE (B-PHP)

##### 5.2.1 Morphology

SEM images of the B10, B20, B30, B40 and B50 PHP structures are shown in Figure 47, which were synthesized by using different mixing times of 10, 20, 30, 40 and 50 minutes, respectively (the ratios of components are mentioned in Table 6). In the SEM images, almost identical structures with coral-like pores can be observed. Moreover, as shown in Figure 48, at higher magnification of 2000x a uniform pore structure and many coalescence pores can be noticed in B10, B20, B30 and B40 PHP. In addition, the open pores and interconnects between the porous walls are apparent at higher magnification (5000x) images Figure 48 (e and f). Although these structures show the high porosity of B-PHP, the higher magnifications show their smooth wall surface, which might lead to decrease in ability of absorption.

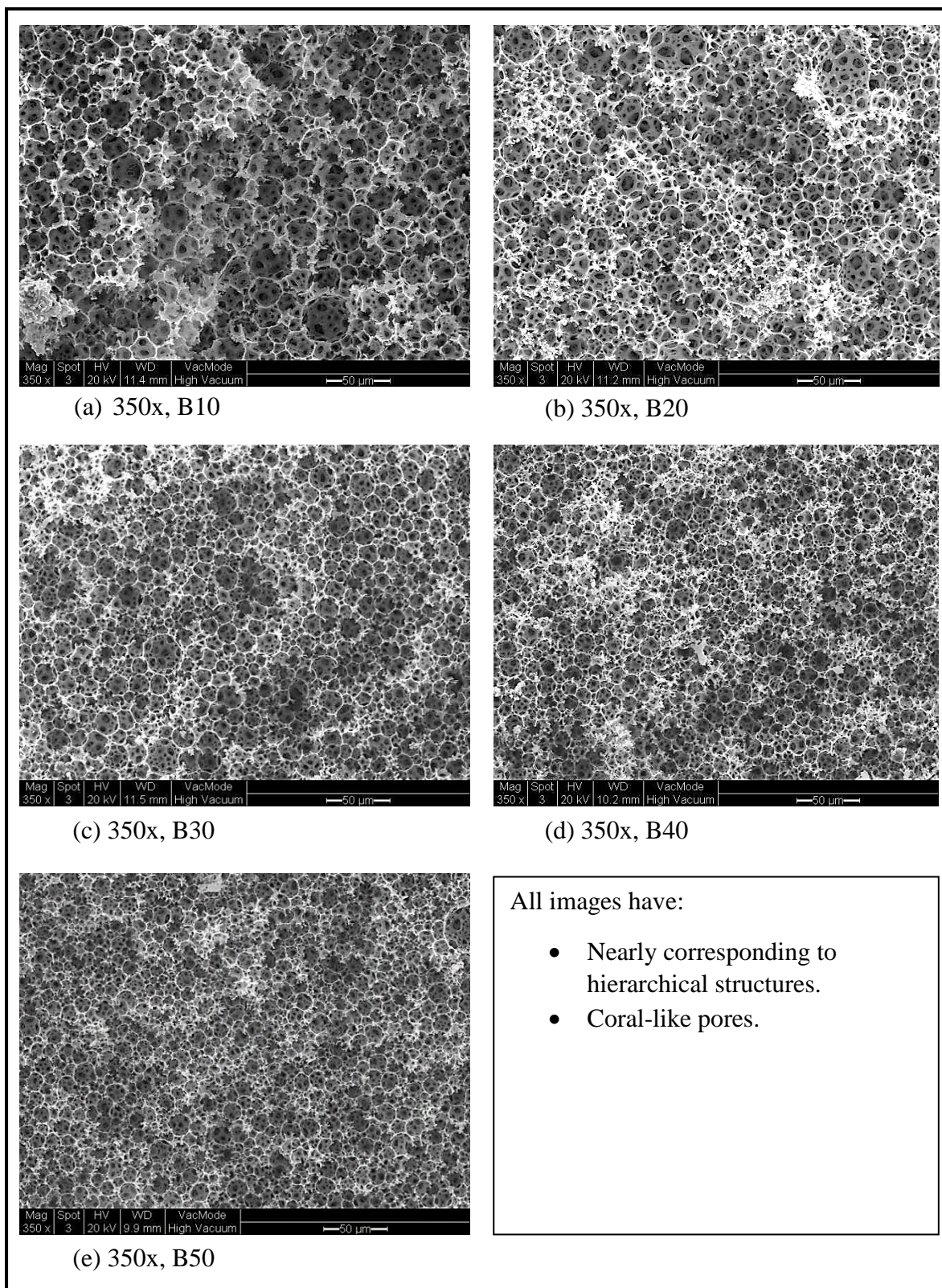


Figure 47: Sulphonated basic PHP (B-PHP). (a)  $t_{\text{mix}}=10$  min (b)  $t_{\text{mix}}=20$  min (c)  $t_{\text{mix}}=30$  min (d)  $t_{\text{mix}}=40$  min (e)  $t_{\text{mix}}=50$  min. Oil phase: 76% styrene, 10% DVB and 14% Span 80. Aqueous phase: 99% distilled water, 1% potassium persulphate. Phase volume = 90%, Dosing time = 10 minutes. Polymerisation temperature = 60 °C, Polymerisation time = 24 hours.

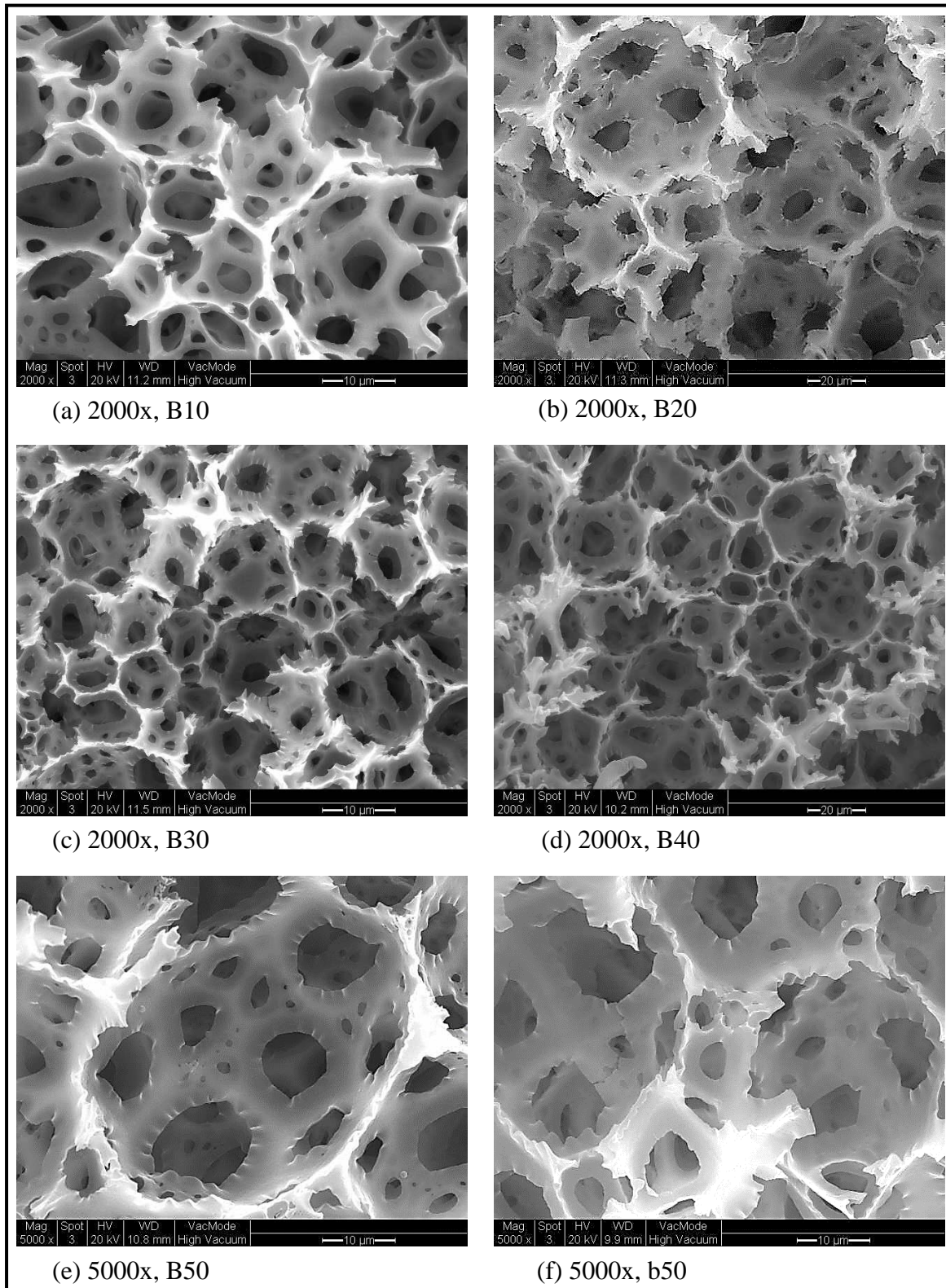


Figure 48: Basic PHP (B-PHP). (a)  $t_{mix}=10$  min (b)  $t_{mix}=20$  min (c)  $t_{mix}=30$  min (d)  $t_{mix}=40$  min (e and f)  $t_{mix}=50$  min. Oil phase: 76% styrene, 10% DVB and 14% Span 80. Aqueous phase: 99% distilled water, 1% potassium persulphate. Phase volume = 90%, Dosing time = 10 minutes. Polymerisation temperature = 60 °C, Polymerisation time = 24 hours.

With the aim of verifying the elements of B-PHP structure, Energy Dispersive X-rays (EDX) spectroscopy was conducted on B50. The spectra for two locations are illustrated in Figure 50 and Figure 51 depending on the points in Figure 49. The results are given in Table 13 are from the centre of a pore and at the edge of a pore. The two points clarify the presence of Carbon, Oxygen and Sulphur, with similar weight percentage and atomic percentage of these elements between locations. The existence of Sulphur in the sample proves the integration of sulphuric acid in the B-PHP, which indicates the success of sulphonation process.

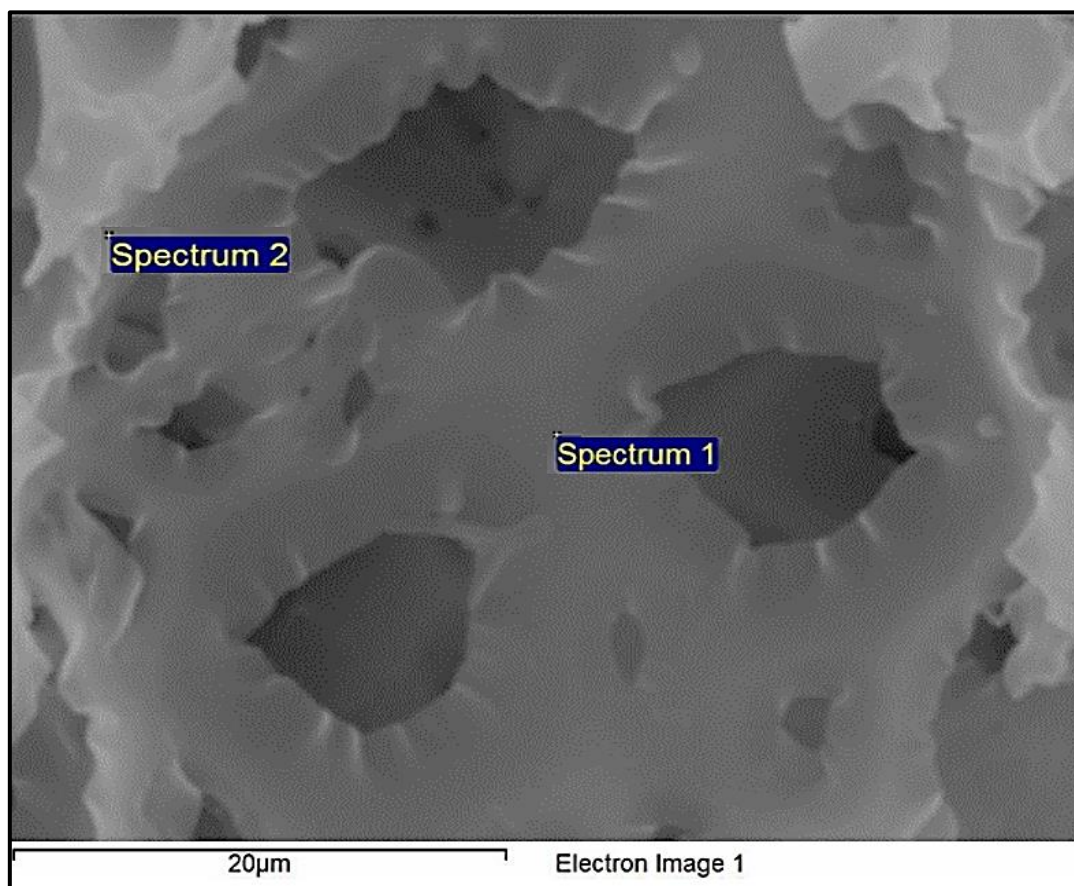


Figure 49: Two points, 1 and 2 for EDX analysis of PS50.

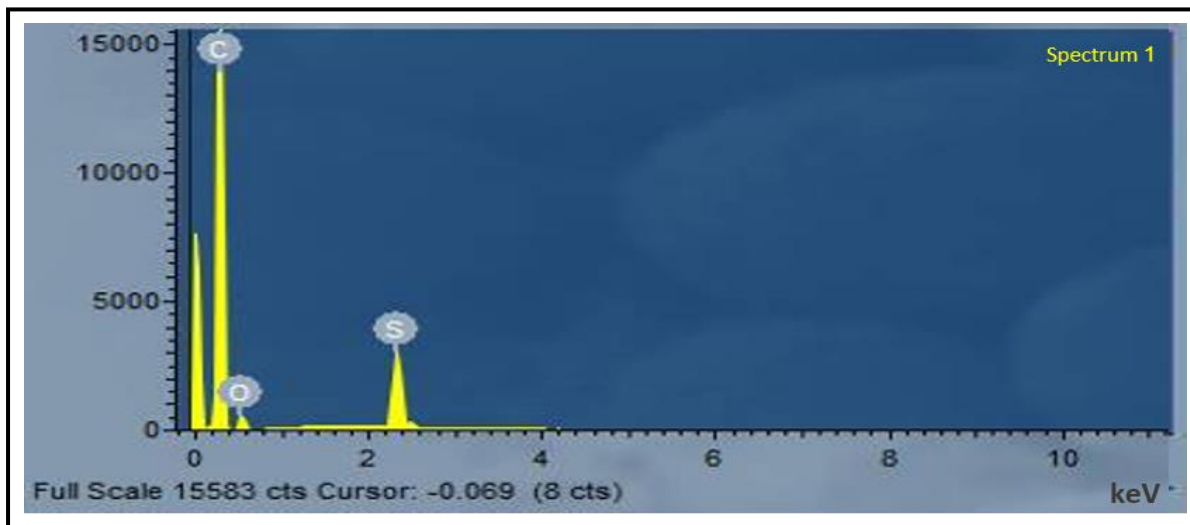


Figure 50: PS50 point 1 EDX spectrum.

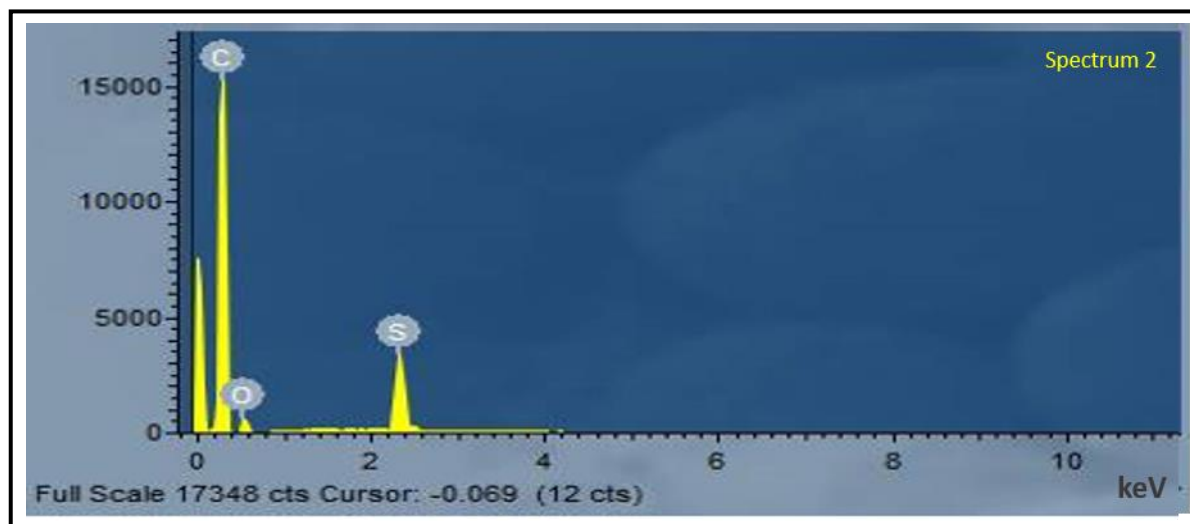


Figure 51: PS50 point 2 EDX spectrum.

Table 13: Summary of the EDX results for the points, 1 and 2 for PS50.

Element	Point 1		Point 2	
	Weight %	Atomic %	Weight %	Atomic %
Carbon	86.59	91.06	85.79	90.53
Oxygen	9.26	7.30	9.71	7.69
Sulphur	4.15	1.64	4.50	1.78
Total	100.00	100.00	100.00	100.00

### 5.2.2 Pore Size Distribution of B-PHP

ImageJ software (which depends on SEM micrograph analysis) was utilised to estimate distribution of pore size. The diameters of the pores measured by ImageJ were an underestimation of the real values because few pores are not clearly visible at the equatorial plane (Menner *et al.*, 2008). The pore and interconnect pore sizes have been determined for all the B-PHP samples with different mixing times of 10, 20, 30, 40 and 50 minutes, namely B10, B20, B30, B40 and B50 by using ImageJ software on SEM images, as shown in Figure 52. An average of pore size was measured from the coalescence pores and interconnect pores in the maximum in the distribution of pore size at higher pore diameter is due to coalescence pores and the maximum in the pore distribution at lower pore size is due to interconnect pores, the results are displayed in Table 14 and Figure 53. Increased energy input from stirring leads to smaller pores. Too much energy leads to pore coalescence (Greco, 2014). Thirty pores from each sample were measured to take the average, where the average value of pore and interconnect pore sizes was ranging between 8-302  $\mu\text{m}$ . This confirms the success of producing a macro porous material with hierarchical pore structure of B-PHP as shown in Figure 47.

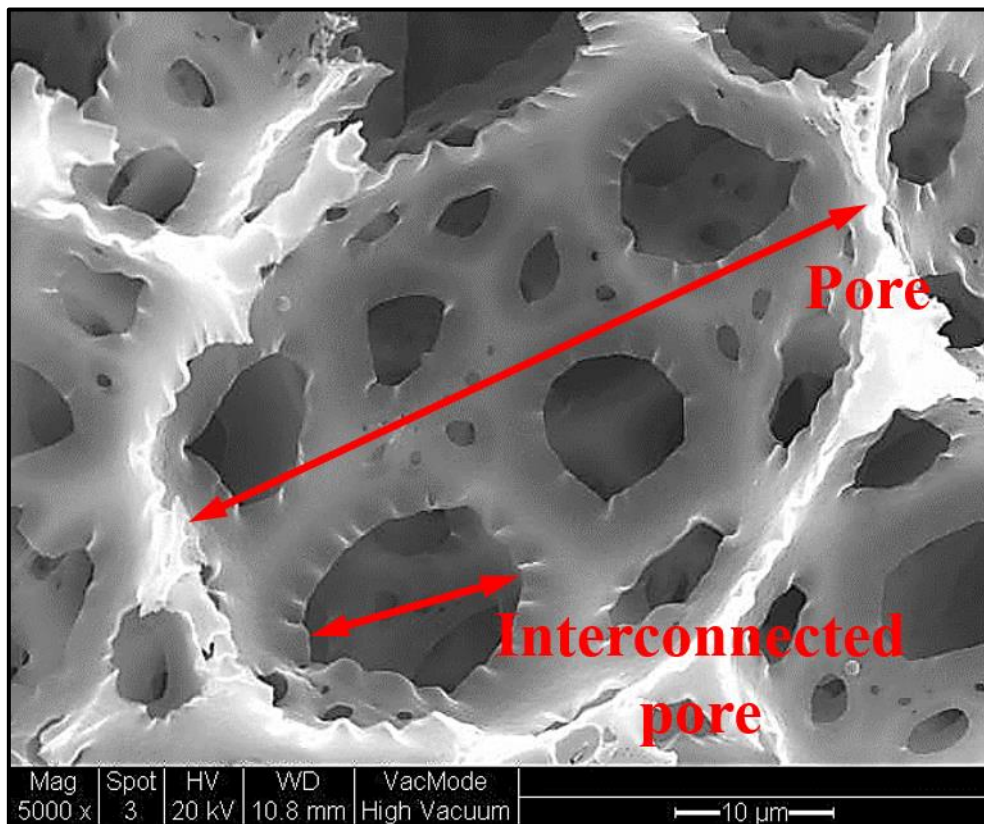


Figure 52: SEM micrograph of B50 PHP showing the pore and interconnect size at x5000 (red arrows).

Table 14: The results of ImageJ analysis of average pore and interconnect sizes, which were determined from the B-PHP where 30 pores from each sample were measured

B-PHP sample	Mixing time (min)	Average pore size ( $\mu$ m)	Average interconnect ( $\mu$ m)
B10	10	302 $\pm$ 17	20 $\pm$ 6
B20	20	235 $\pm$ 13	15 $\pm$ 5
B30	30	178 $\pm$ 12	15 $\pm$ 6
B40	40	129 $\pm$ 9	10 $\pm$ 4
B50	50	108 $\pm$ 7	8 $\pm$ 4

Both the average pore size and average interconnect size decrease with mixing time (Figure 53).

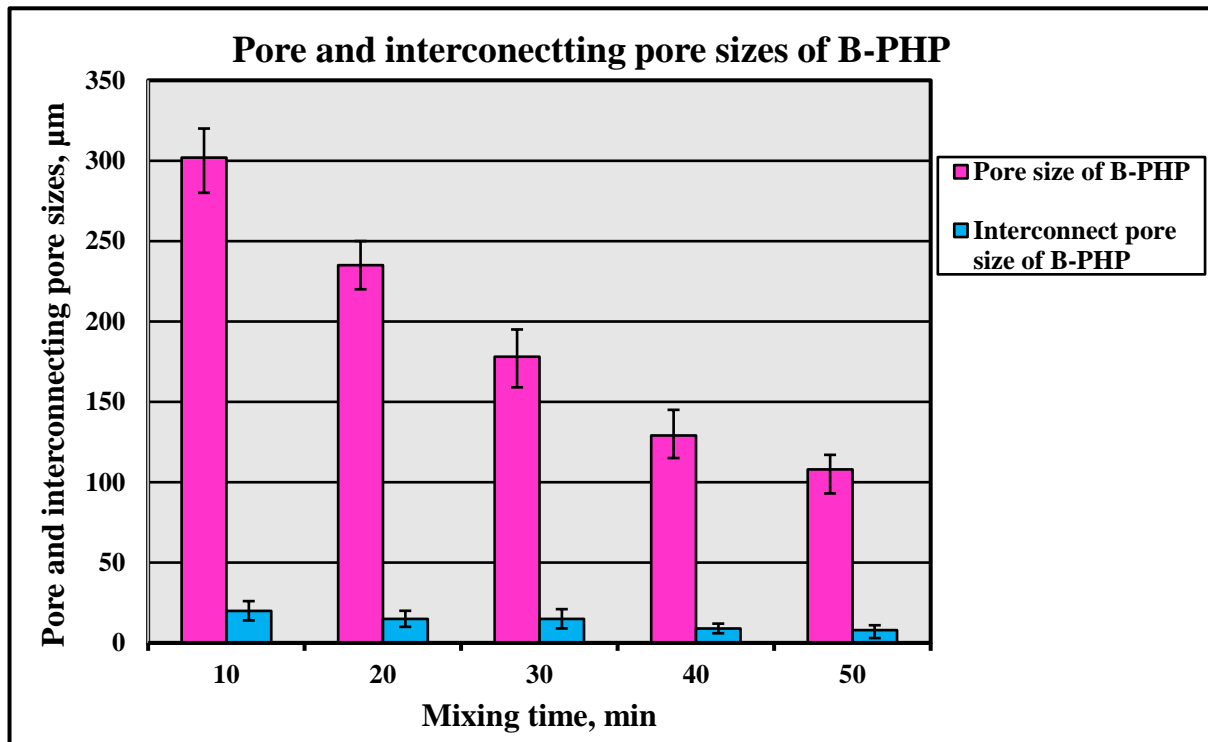


Figure 53: Plot of pore and interconnecting sizes of B-PHP for different mixing times.

### 5.2.3 Surface Area

The surface area study was performed using Brunauer-Emmett-Teller (BET) process of the nitrogen physisorption as the adsorbate at the temperature of liquid nitrogen, -196 ° C (77 ° K). Examination for the results reproducibility was carried out in up to seven runs producing

### 5.2.3.1 Measurement of Surface Area of B-PHP

The surface areas of B-PHP for different mixing times of 10, 20, 30, 40 and 50 minutes were determined by using BET technique as described in section 4.3.1.1. The outcomes of surface area for different B-PHP polymers are presented in Table 15 and Figure 54. In general, it is noticed that the surface area of the unsulphonated PHP increases clearly with the increasing of the mixing time up to 40 minutes and then increases slightly to reach of 14 m<sup>2</sup>/g at a mixing time, 50 minutes. Typical non-modified PHP surface area is 3-20 m<sup>2</sup>/g (Menner *et al.*, 2006) which is comparable to what was achieved here). This shows the effective role of increasing mixing time in reducing the size of aqueous phase droplets and spreading it inside the oil phase, leading to a decrease in the pore and interconnect of pore size and thus increasing the surface area. For the sulphonated PHP samples, the surface area increases significantly with increasing of the mixing time from 10 minutes toward 50 minutes. In addition, it can be seen that the surface area of sulphonated samples was significantly higher, 2.11 to 3.36 fold increase compared to unsulphonated samples. This demonstrates the importance of the sulphonation process, which is used to alter the B-PHP surface from hydrophobic to hydrophilic. Moreover, the surface area also increases as a result of effectiveness the sulphuric acid attack on the wall surfaces of the pores to make them rough. However, If there is too much coalescence porosity the performance is worse (usually occurs with longer period of mixing of 60 minutes).

Table 15: Surface area of sulphonated and unsulphonated B-PHP for different mixing times.

B-PHP sample	Mixing time (min)	Surface area of unsulphonated sample (m <sup>2</sup> /g)	Surface area of sulphonated sample (m <sup>2</sup> /g)
B10	10	1±0.3	4±1
B20	20	4±1	10±2
B30	30	8±2	16±2
B40	40	13±2	28±3
B50	50	14±2	35±3

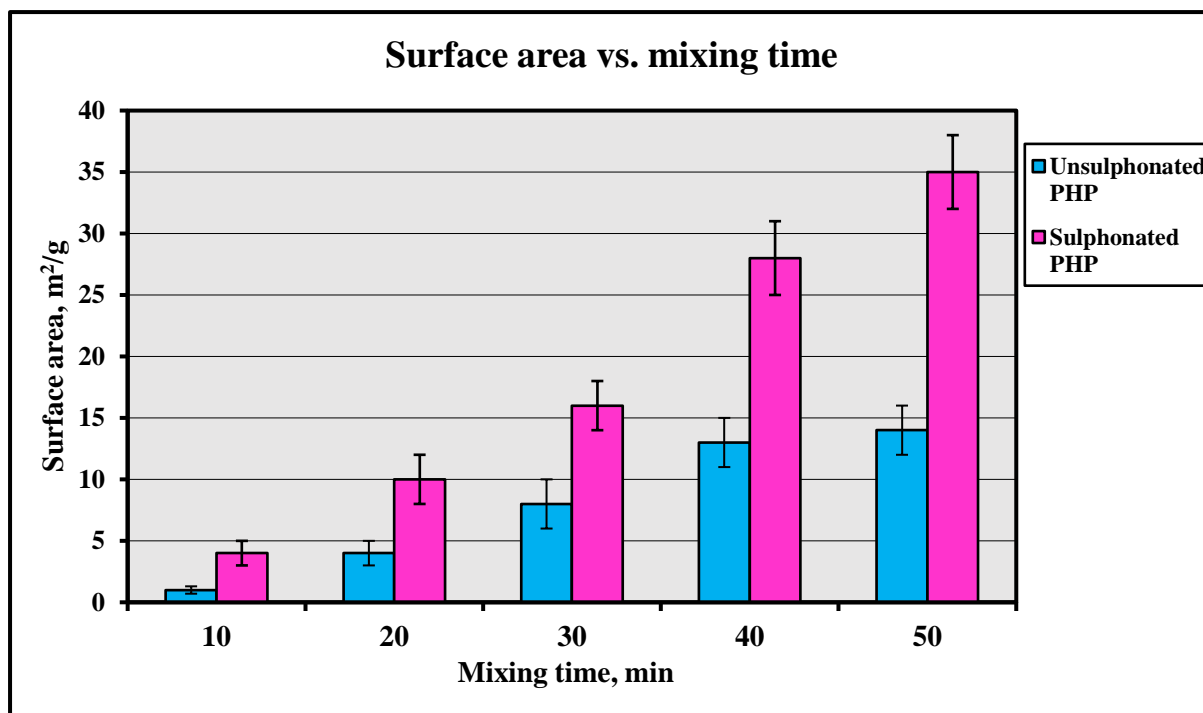


Figure 54: Surface area versus mixing time for sulphonated and unsulphonated B-PHP.

By comparing the surface area of B-PHP with the mixing time of 50 minutes for this study to previous study (Hasan, 2013). The surface area of this study was increased from 14 m<sup>2</sup>/g before sulphonation to 35 m<sup>2</sup>/g after sulphonation (using thermal sulphonation), while for the previous study was increased from 4 m<sup>2</sup>/g before sulphonation to 15 m<sup>2</sup>/g after sulphonation (using microwave sulphonation). This means this study achieved surface area after sulphonation about 20 m<sup>2</sup>/g more than the previous study.

#### 5.2.4 Water Uptake of B-PHP

The water uptake of the B-PHP for different mixing times of 10, 20, 30, 40 and 50 minutes was examined. Three discs for each sample were tested and the results are displayed in Table 16 and Figure 55. The results illustrate that the unsulphonated samples have a high water uptake capacity that is directly proportional to the increase in mixing time up to 50 minutes. Moreover, the outcomes illustrate that the process of sulphonation considerably increases the ability of water uptake of all the sulphonated samples. The water uptake of sulphonated B50 sample at mixing time of 50 minutes was significantly higher, 3.9 fold increase compared to the unsulphonated B50 sample. However, the sulphonated B10 sample at mixing time of 10 minutes obtained the lowest water uptake of 4.3 times more than unsulphonated B10 sample.

In addition, it can be seen that the water uptake ability and the surface area (Table 15) for sulphonated and unsulphonated samples are equivalent for all mixing times.

These results for water uptake tests indicate that homogeneity and initial drying is an issue but a small one. The most important factor is with mixing time the pores get smaller and the pore surface area increases so there are more sites to trap water.

Table 16: Water uptake for various sulphonated and unsulphonated B-PHP samples for different mixing times.

B-PHP sample	Mixing time, min	% water uptake of unsulphonated sample	% average water uptake of unsulphonated sample	% water uptake of sulphonated sample	% average water uptake of sulphonated sample	Water uptake fold
B10	10	36-43	39	149-198	168	4.3
B20	20	45-51	49	162-216	189	3.9
B30	30	49-59	54	174-225	198	3.7
B40	40	58-68	63	227-269	241	3.8
B50	50	63-72	68	238-287	262	3.9

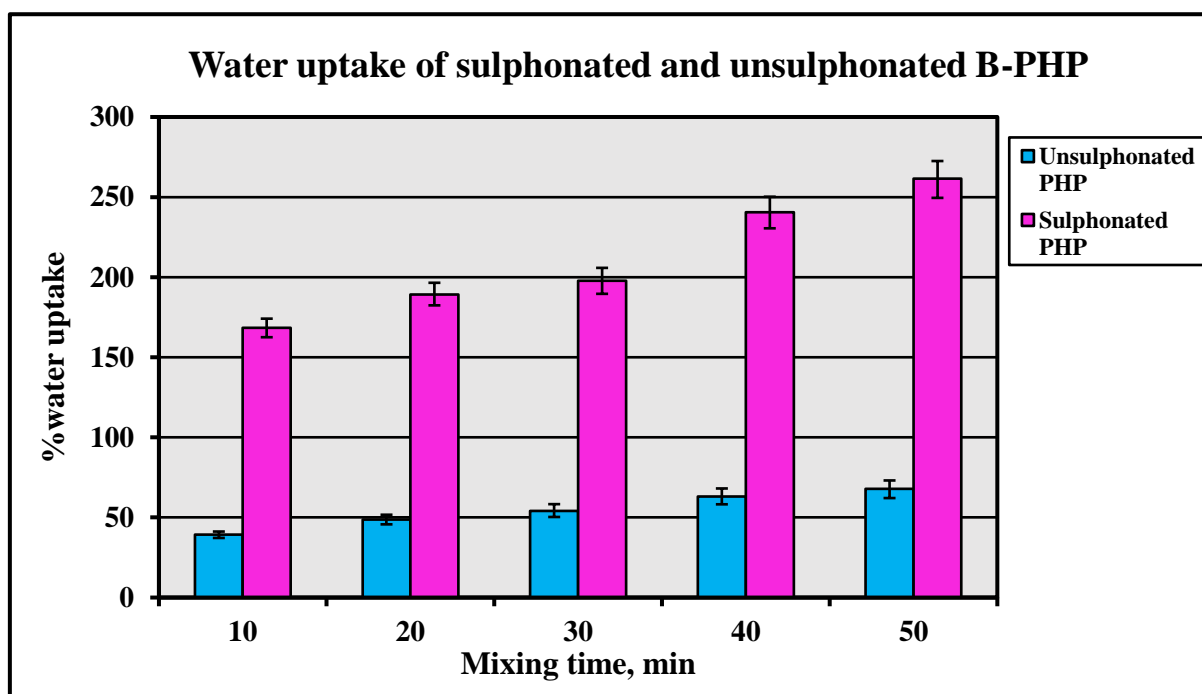


Figure 55: Plot of water uptake of sulphonated and unsulphonated B-PHP for different mixing times.

### 5.2.5 FTIR Analysis of B-PHP

The unsulphonated B-PHP samples spectra for different mixing times look similar and are exhibited in Figure 56. The absorption peaks are named as illustrated in Figure 57 and Table 17 are in agreement with the peaks noticed in silane PHP as are discussed in section 5.5.5. The absorption peaks and the peaks positions of the sulphonated B-PHP samples are shown in Figure 58 through Figure 62 and Table 18. The comparison of sulphonated and unsulphonated B-PHP is given in Figure 63. The absorption intensity of the band range of 800-1400  $\text{cm}^{-1}$  (which attributed to C-H in an aromatic ring) and the band range of 1690–1740 (which is attributed to C=O stretch in a carbonyl group) for sulphonated B-PHP were stronger than that are existent in the unsulphonated B-PHP for the same wavenumber range. For the sulphonated B-PHP, there are clear absorption peaks of –C=S stretch (sulphide group) at 1125, 1126, and 1127  $\text{cm}^{-1}$ . This is due to the sulphonation process using sulphuric acid. Moreover, there are apparent absorption peaks at 3403 and 3417  $\text{cm}^{-1}$  for the sulphonated B-PHP. These absorption peaks are ascribed to –OH group (Sergienko *et al.*, 2002). This is because of using sodium

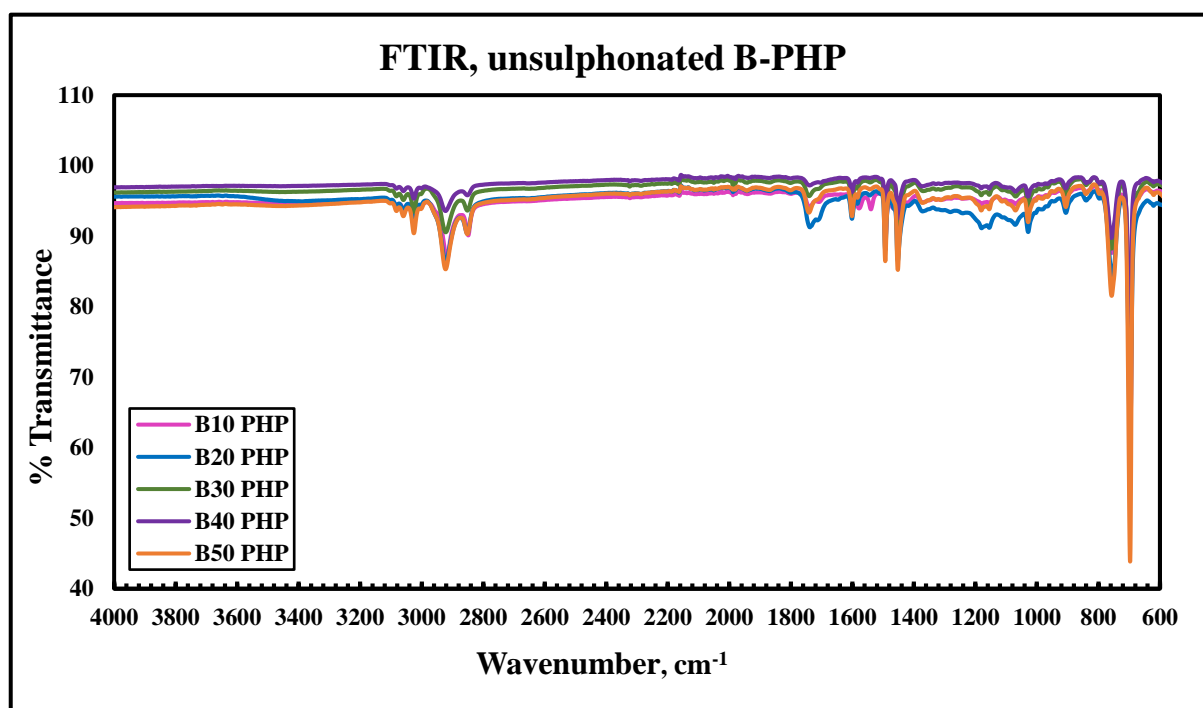


Figure 56: FTIR spectra for all unsulphonated B-PHP samples.

hydroxide in neutralization process during the sulphonation process leaves some hydroxyl groups in the structure.

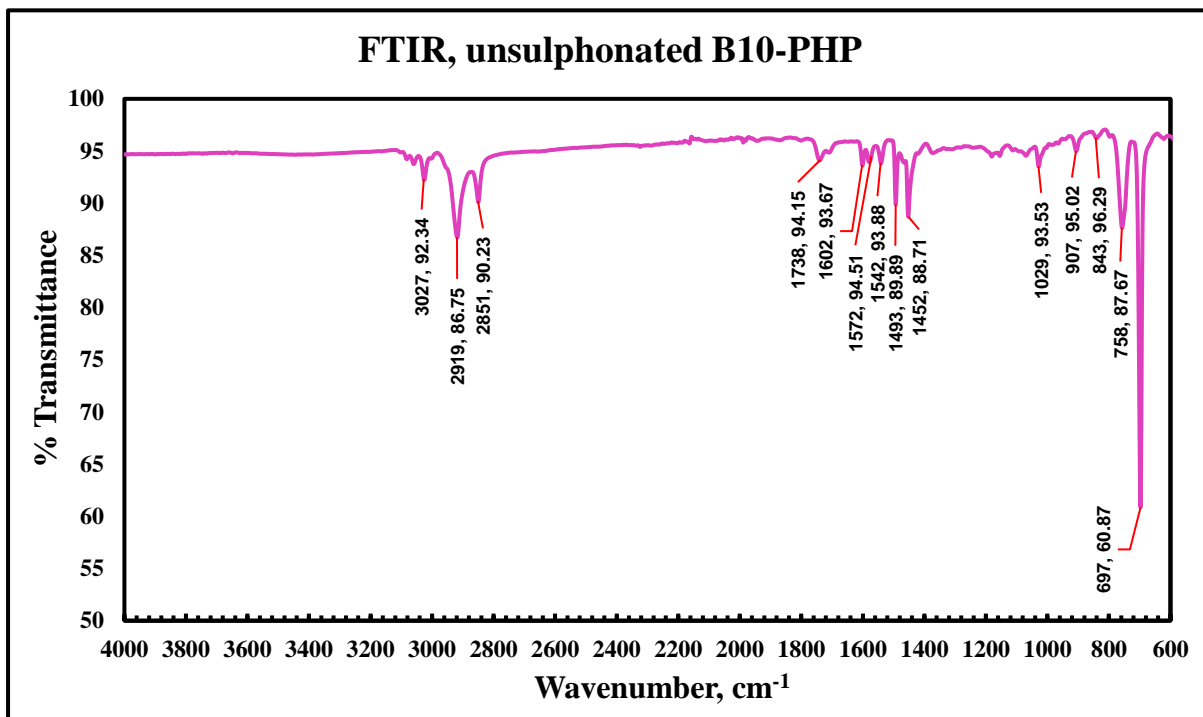


Figure 57: FTIR spectrum for unsulphonated B10 PHP.

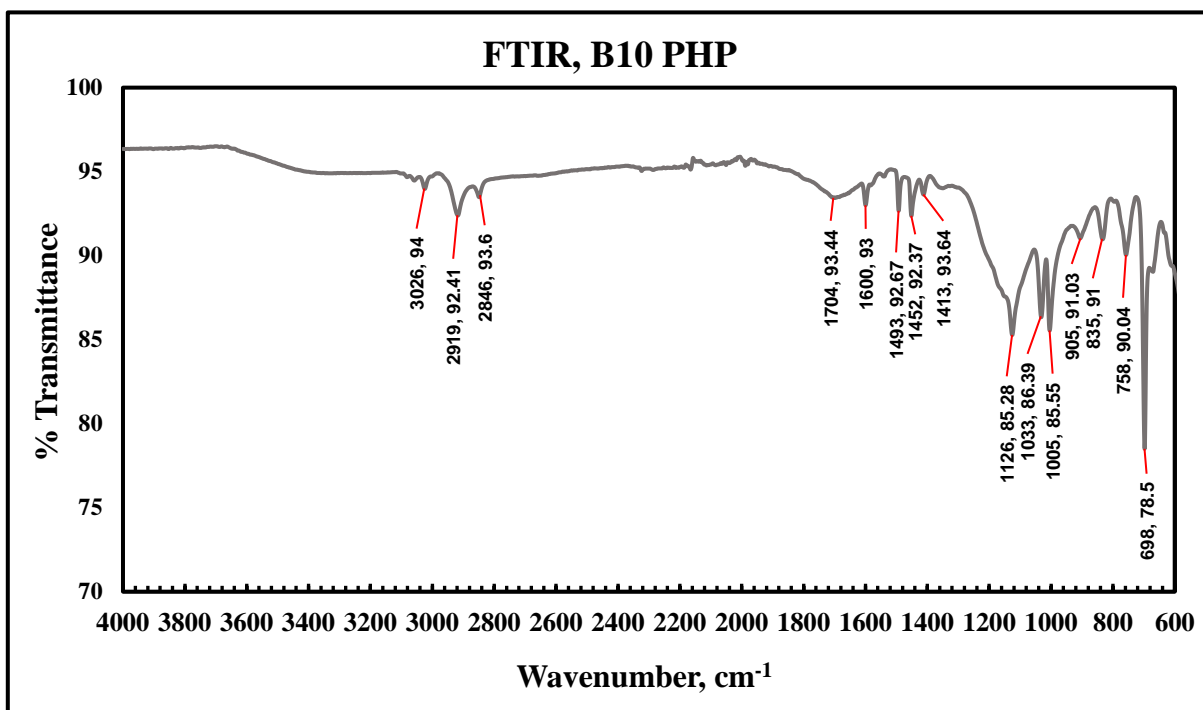


Figure 58: FTIR spectrum for sulphonated B10 PHP.

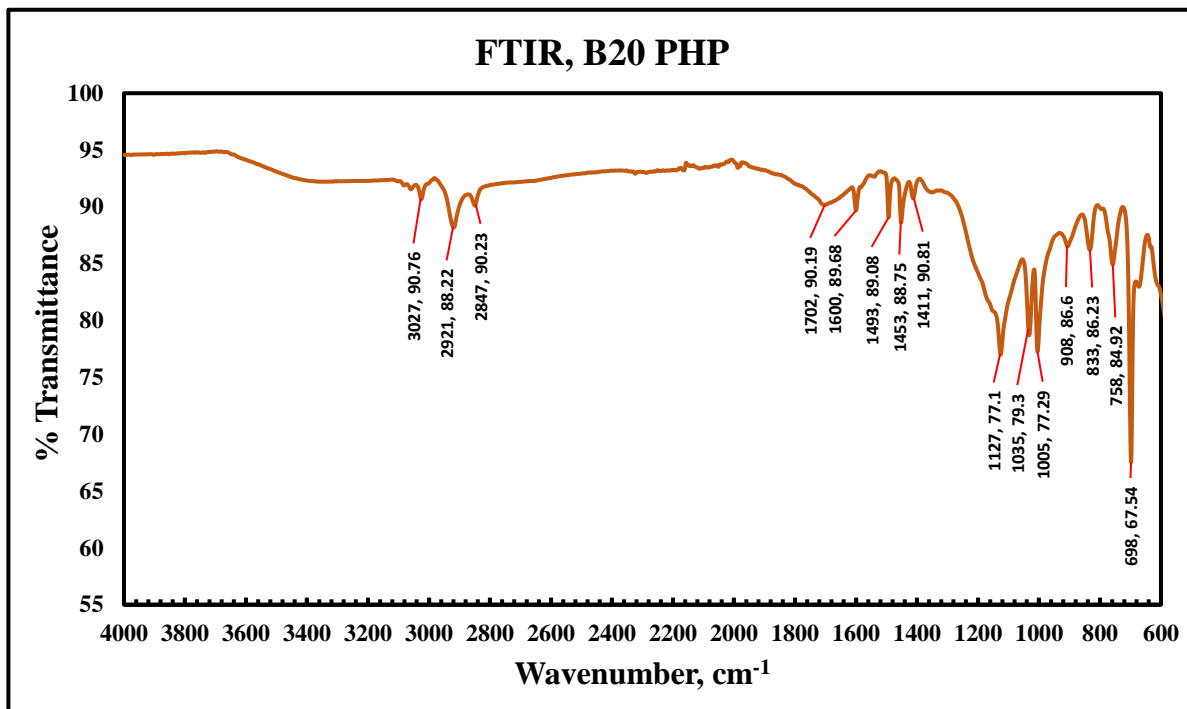


Figure 59: FTIR spectrum for sulphonated B20 PHP.

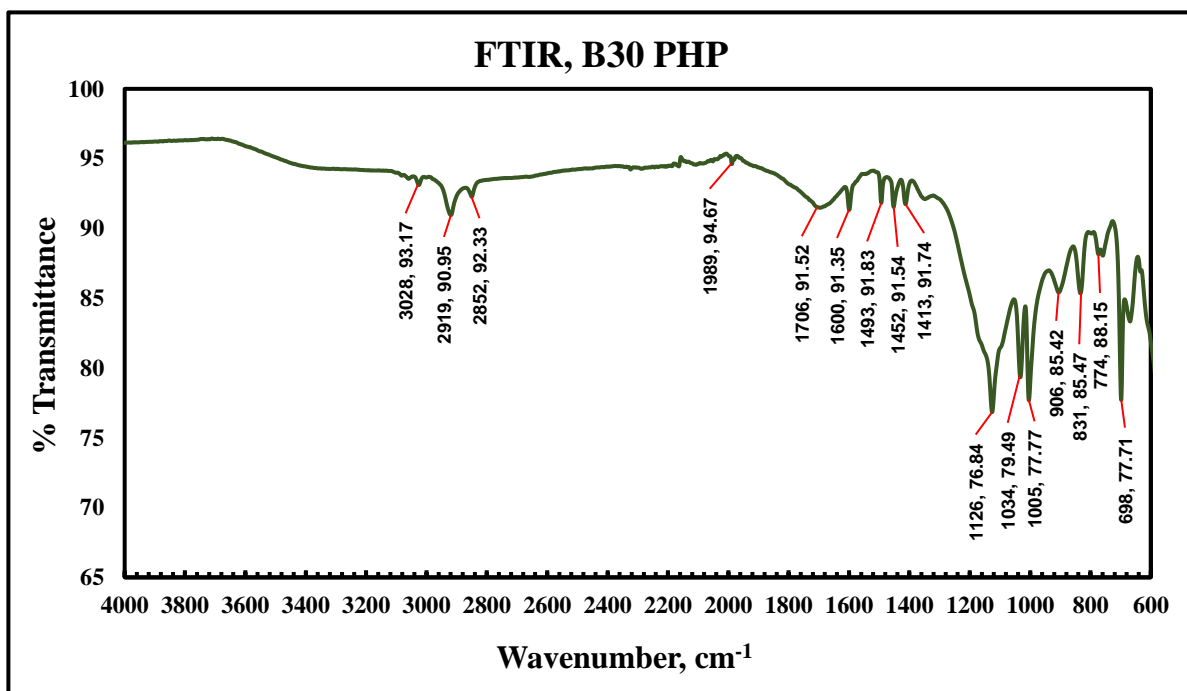


Figure 60: FTIR spectrum for sulphonated B30 PHP.

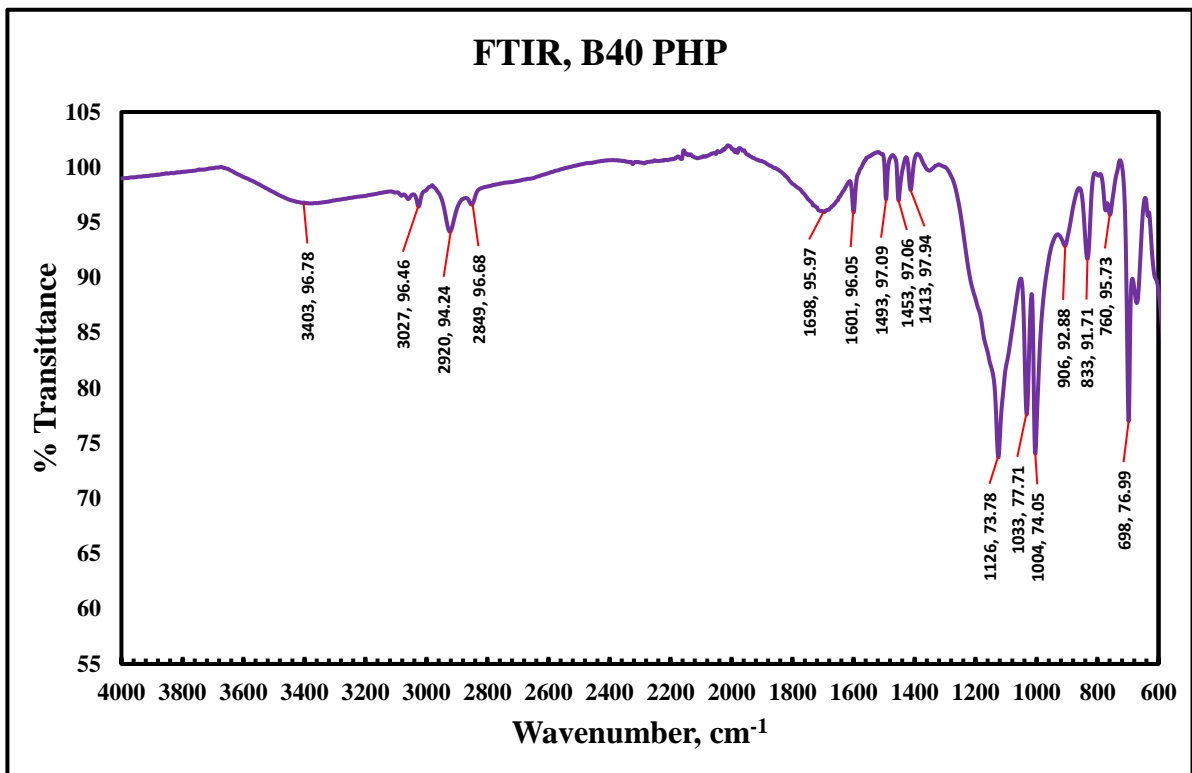


Figure 61: FTIR spectrum for sulphonated B40 PHP.

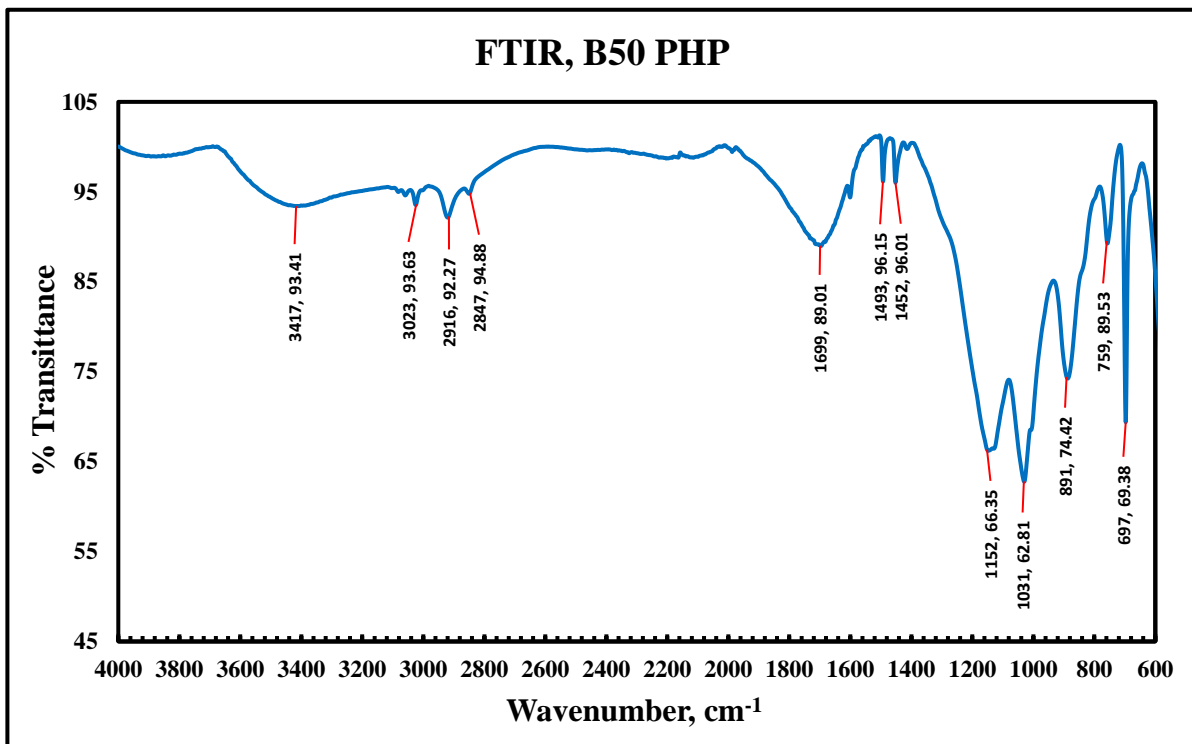


Figure 62: FTIR spectrum for sulphonated B50 PHP

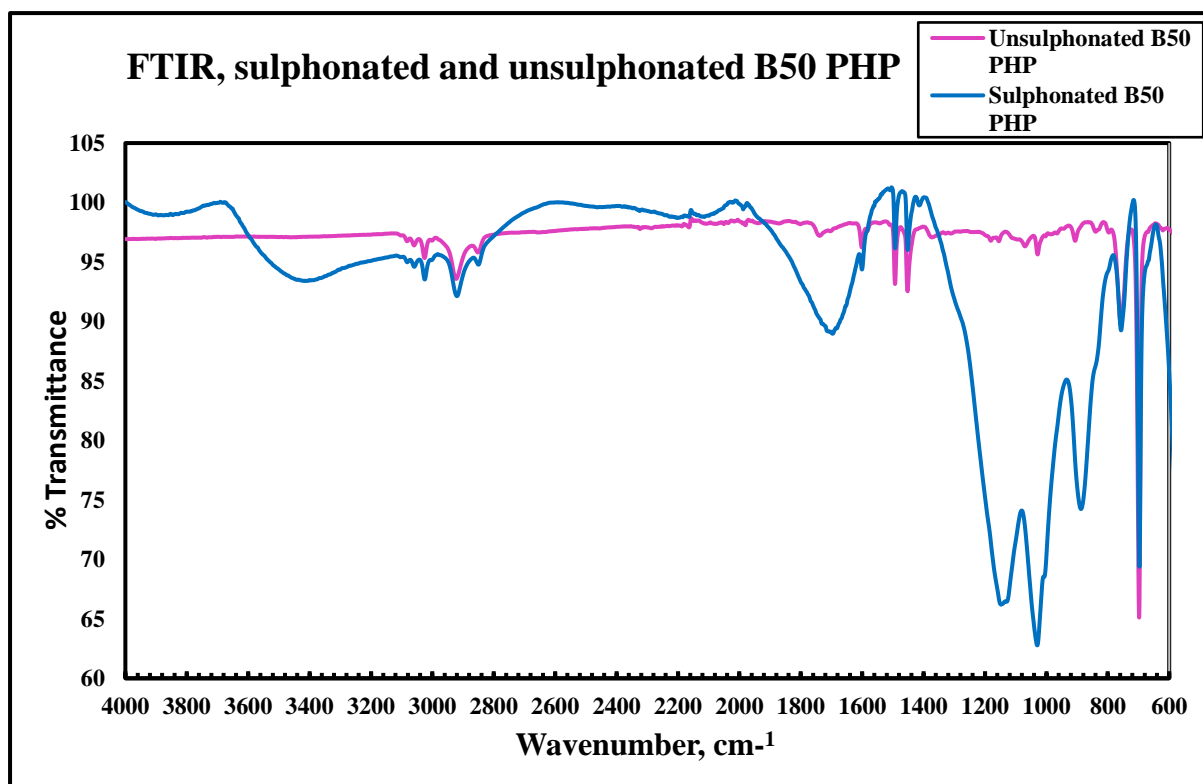


Figure 63: FTIR spectra for sulphonated and unsulphonated B50 PHP.

Table 17: Absorption peaks and peak assignments of unsulphonated B-PHP samples for different mixing times.

Sample peak (cm-1)					Peak origin	References
Mixing time=10 min	Mixing time=20 min	Mixing time=30 min	Mixing time=40 min	Mixing time=50 min		
697	698	697	698	696	Out of plane (C-H) bends of the aromatic ring	(Bhagiyalakshmi <i>et al.</i> , 2010)
758	756	756	757	755	Out of plane (C-H) bends of the aromatic group	(Jiang and Zeng, 2010)
843	833	830	831	832	Distributed phenyl ring and vinyl ring	(Mercier <i>et al.</i> , 2001)
907	905	906	904	906	C=C in phenyl ring	(Hubbard <i>et al.</i> , 1998)
1029	1028	1027	1028	1026	Monosubstituted phenyl ring	(Mercier <i>et al.</i> , 2001)
1452	1452	1453	1451	1453	Aromatic ring backbone – CH-bending vibration	(Vinodh <i>et al.</i> , 2010)
1493	1494	1495	1493	1492	Aromatic ring backbone – CH-bending vibration	(Vinodh <i>et al.</i> , 2010)
1542	–	–	–	–	(C=C) in aromatic ring	(Vinodh <i>et al.</i> , 2010)
1572	–	–	–	172	(C=C) in aromatic ring	(Vinodh <i>et al.</i> , 2010)
1602	1601	1603	1601	1603	(C=C) in aromatic ring	(Vinodh <i>et al.</i> , 2010)
1738	1737	1739	1736	1739	C=O stretch carbonyl group	(Leber <i>et al.</i> , 2007)
2851	2851	2850	2852	2851	C-H stretching vibration of methylene and methyl groups	(Rubino <i>et al.</i> , 2010)
2919	2921	2922	2925	2922	C-H stretching vibration of methylene and methyl groups	(Rubino <i>et al.</i> , 2010)
3027	3025	3026	3025	3024	(C=C-H) stretch in aromatic group	(Ungureanu <i>et al.</i> , 2007)

Table 18: Absorption peaks and peak assignments of sulphonated B-PHP samples for different mixing times.

Sample peak cm <sup>-1</sup>					Peak origin	References
Mixing time=10 min	Mixing time=20 min	Mixing time=30 min	Mixing time=40 min	Mixing time=50 min		
698	698	698	698	697	Out of plane (C–H) bends of the aromatic ring	(Bhagiyalakshmi <i>et al.</i> , 2010)
758	758	774	760	759	Out of plane (C–H) bends of the aromatic group	(Jiang and Zeng, 2010)
835	833	831	833	–	Distributed phenyl ring and vinyl ring	(Mercier <i>et al.</i> , 2001)
905	908	906	906	889	C=C in phenyl ring	(Hubbard <i>et al.</i> , 1998)
1005	1005	1005	1004	–	Monosubstituted phenyl ring	(Mercier <i>et al.</i> , 2001)
1033	1035	1034	1033	1031	Monosubstituted phenyl ring	(Mercier <i>et al.</i> , 2001)
1126	1127	1126	1126	1125	(–C=S) stretch sulphate group	(Fleming and Williams, 1966)
1413	1411	1413	1413	–	(C=C) in aromatic ring	(Vinodh <i>et al.</i> , 2010)
1452	1453	1452	1453	1452	Aromatic ring backbone – CH–bending vibration	(Vinodh <i>et al.</i> , 2010)
1493	1493	1493	1493	1493	Aromatic ring backbone – CH–bending vibration	(Vinodh <i>et al.</i> , 2010)
1600	1600	1600	1601	–	(C=C) in aromatic ring	(Vinodh <i>et al.</i> , 2010)
1704	1702	1706	1698	1699	C=O stretch carbonyl group	(Leber <i>et al.</i> , 2007)
–	–	1989	–	–	C=O stretch carbonyl group	(Leber <i>et al.</i> , 2007)
2848	2847	2852	2849	2847	C–H stretching vibration of methylene and methyl groups	(Rubino <i>et al.</i> , 2010)
2919	2921	2919	2920	2916	C–H stretching vibration of methylene and methyl groups	(Rubino <i>et al.</i> , 2010)
3026\	3027	3028	3027	3023	(C=C–H) stretch in aromatic group	(Ungureanu <i>et al.</i> , 2007)
–	–	–	3403	3417	(–OH) group	(Sergienko <i>et al.</i> , 2002)

### **5.2.6 Summary**

The basic polyHIPE can be produced with smaller pores as the mixing time is increased. The sulphonation process is necessary to introduce surface functionality that makes the polyHIPE hydrophilic and promotes water-uptake. The cell walls are quite smooth which means that the total surface area is limited which also limits water uptake.

## **5.3 In-Situ Sulphonated PolyHIPE (IS-PHP)**

### **5.3.1 Morphology**

SEM images of the IS10, IS20, IS30, IS40 and IS50 PHP structures are demonstrated in Figure 64, which are synthesized by using sulphuric acid in the aqueous phase (the ratios of components are mentioned in Table 8) with various mixing times 10, 20, 30, 40 and 50 minutes. In the SEM images, almost identical structures with coral-like pores can be observed. Moreover, a uniform pore structure and many coalescence pores can be noticed in all images. In addition, the open pores and interconnects between the porous walls are apparent. These structures show the high porosity of B-PHP but the images show their smooth wall surfaces, which might lead to decrease in ability of absorption.

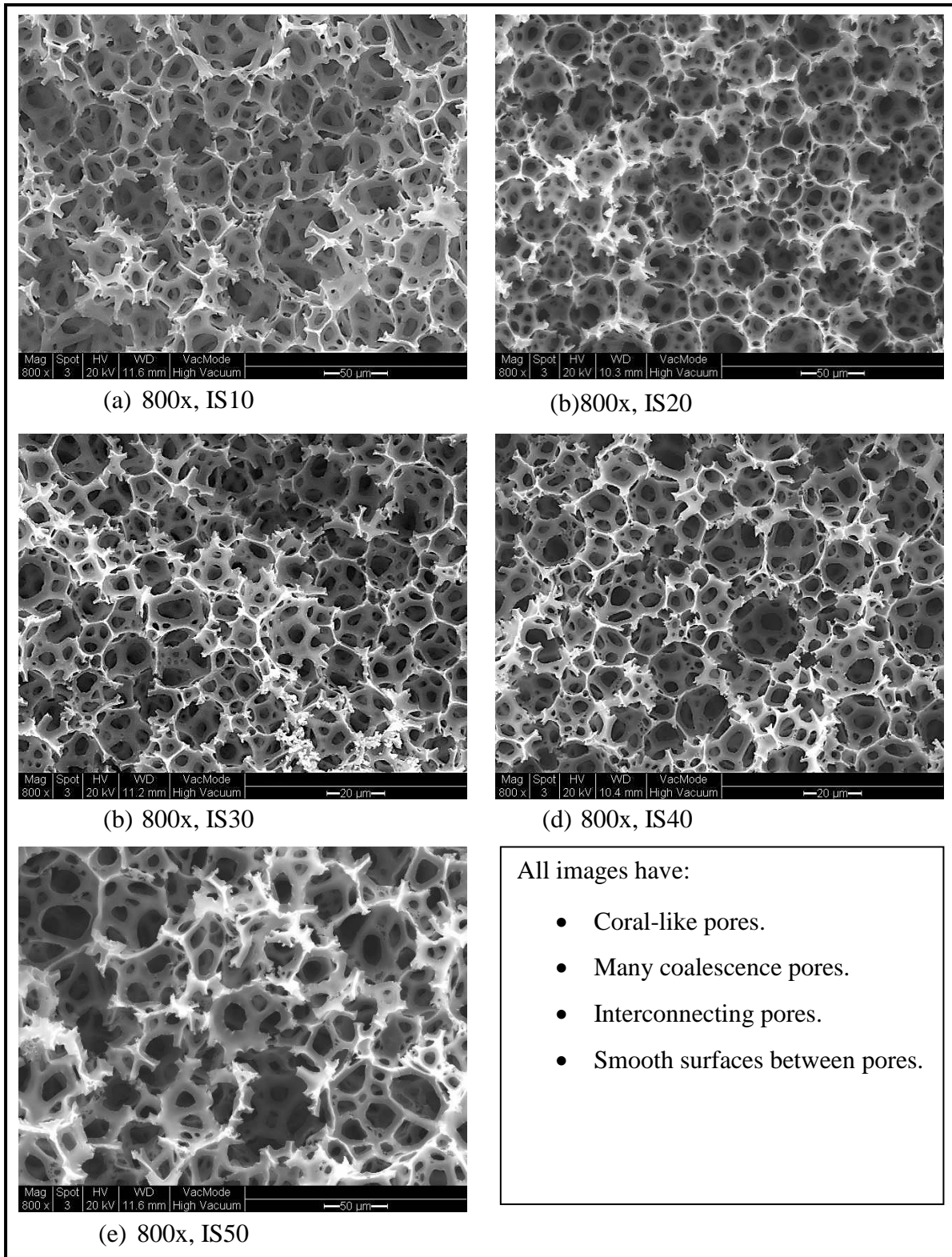


Figure 64: In-situ sulphonated PHP (IS-PHP). (a)  $t_{\text{mix}}=10$  min (b)  $t_{\text{mix}}=20$  min (c)  $t_{\text{mix}}=30$  min (d)  $t_{\text{mix}}=40$  min (e)  $t_{\text{mix}}=50$  min. Oil phase: 74% styrene, 12% DVB and 14% span 80. Aqueous phase: 94% distilled water, 1% potassium persulphate and 5% sulphuric acid. Phase volume = 90%, Dosing time = 10 minutes. Polymerisation temperature = 60 °C, Polymerisation time = 24 hours.

With the aim of verifying the elements present in the IS-PHP structure, Energy Dispersive X-rays (EDX) spectroscopy was undertaken on IS40. The spectra for two locations are shown in Figure 66 and Figure 67 as defined in Figure 65. The results are given in Table 19 for the area of two points at the centre of a pore and at the edge of a pore. The two points show the presence of Carbon, Oxygen and Sulphur, with approximately the similar weight percentage and atomic percentage of these elements in each location. The existence of sulphur in the sample proves the integration of sulphuric acid in the B-PHP, which prove the success of the functionalization process of sulphuric acid of 5% concentration inside the HIPE, while using more than 5% was not successful due to the separation of the HIPE emulsion into the two layers of oil phase and aqueous phase during the polymerisation process perhaps because of effect of sulphuric acid on preventing the formation of free radicals responsible for polyHIPE polymerisation. However, the amount of sulphur incorporated is less than for the post-sulphonated B-PHP.

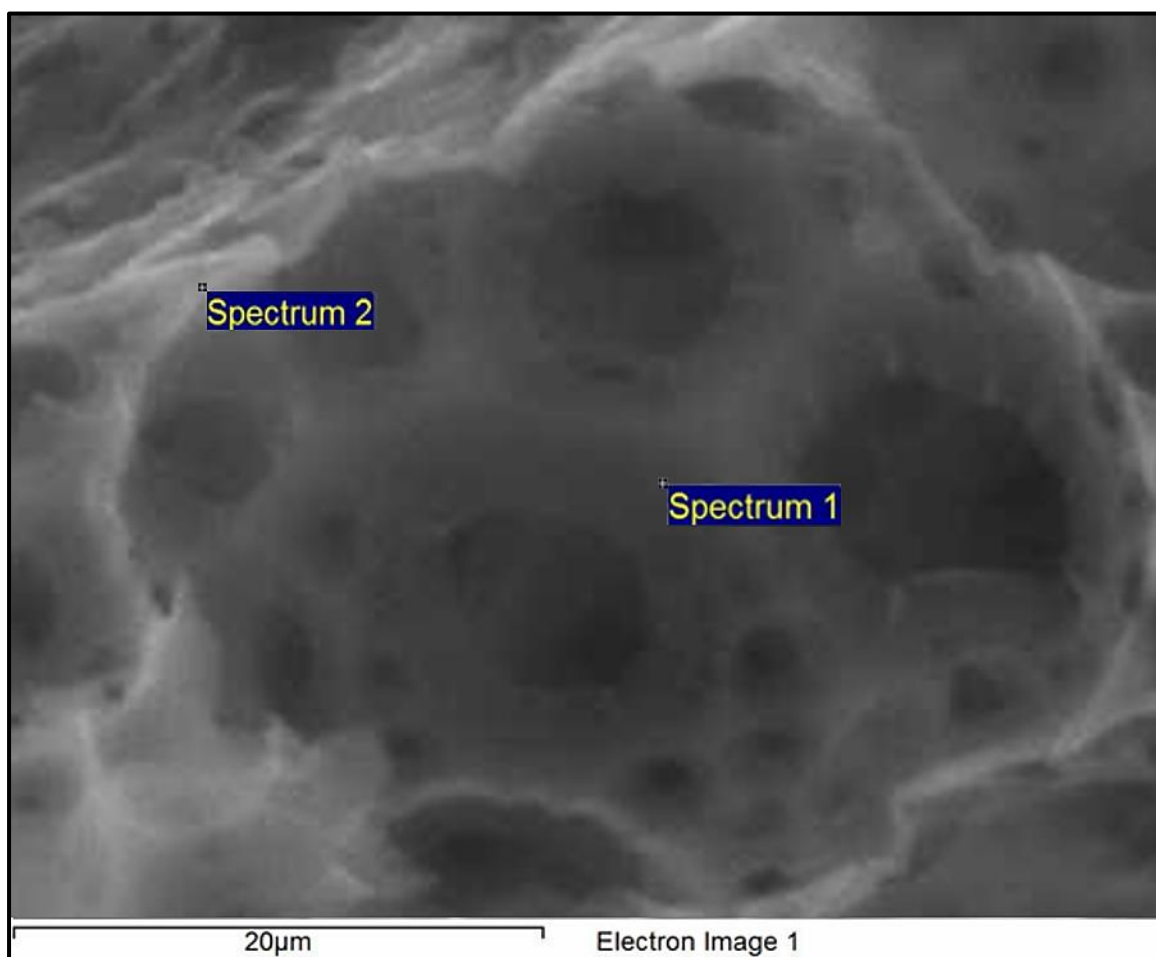


Figure 65: Two points, 1 and 2 for EDX analysis for IS40.

The sulphur content of in situ sulphonated PHP is about 70% of that achieved by post sulphonation in the standard polyHIPE (see section 5.6).

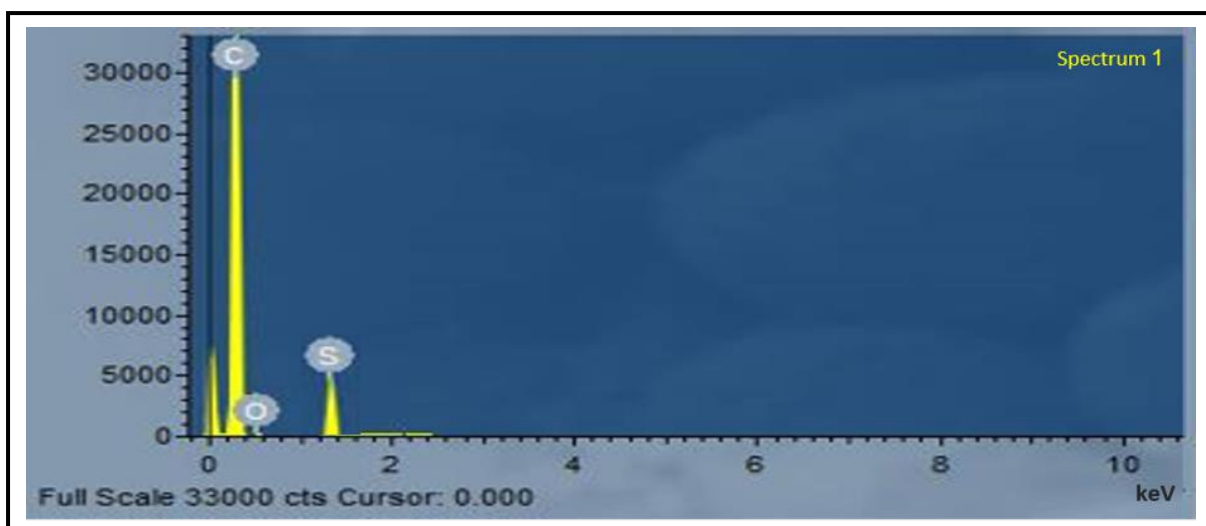


Figure 66: IS40 point 1 EDX spectrum.

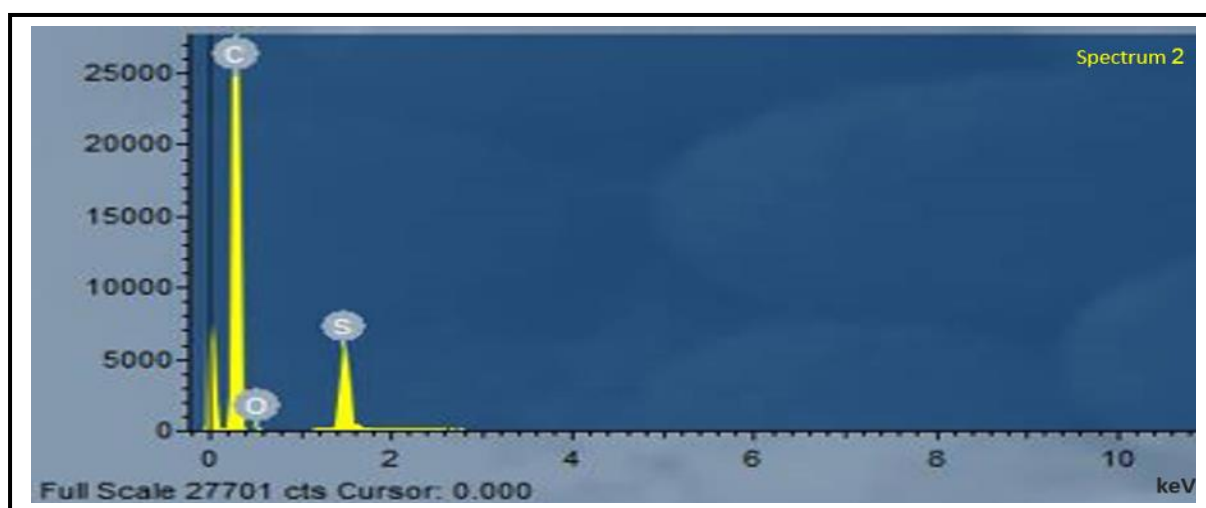


Figure 67: IS40 point 2 EDX spectrum.

Table 19: Summary of the EDX results for the points, 1 and 2 for IS40.

Element	Point 1		Point 2	
	Weight %	Atomic %	Weight %	Atomic %
Carbon	94.46	96.46	94.08	96.22
Oxygen	3.19	2.42	3.30	2.50
Sulphur	2.35	1.12	2.62	1.28
Total	100.00	100.00	100.00	100.00

### 5.3.2 Pore Size Distribution of IS-PHP

The pore and interconnect pore sizes have been determined for all the IS-PHP samples with different mixing times of 10, 20, 30, 40 and 50 minutes, namely IS10, IS20, IS30, IS40 and IS50 by using ImageJ software on SEM images, as illustrated in Figure 52. An average pore size was measured from the coalescence pores and interconnect pores i.e. the maximum in the distribution of pore size at higher pore diameter is due to coalescence pores and the maximum in the pore distribution at lower pore size is due to interconnect pores; the results are displayed in Table 20 and Figure 68. The results show that the pore and interconnect sizes of IS-PHP samples decrease with mixing time up to 40 minutes, after which they increase. Thirty pores from each sample were measured to take the average, where the average value of pore and interconnect pore size was ranging between 10 $\mu$  m and 286 $\mu$  m. This confirming the success of producing a macro porous material with hierarchical structure of IS-PHP as shown in Figure 64.

Table 20: The results of ImageJ analysis of average pore and interconnect sizes, which were determined from the IS-PHP where 30 pores from each sample were measured.

IS-PHP sample	Mixing time (min)	Average pore size ( $\mu$ m)	Average interconnect pore size ( $\mu$ m)
IS10	10	286 $\pm$ 15	19 $\pm$ 5
IS20	20	226 $\pm$ 13	16 $\pm$ 4
IS30	30	186 $\pm$ 10	14 $\pm$ 4
IS40	40	134 $\pm$ 10	10 $\pm$ 3
IS50	50	230 $\pm$ 12	12 $\pm$ 4

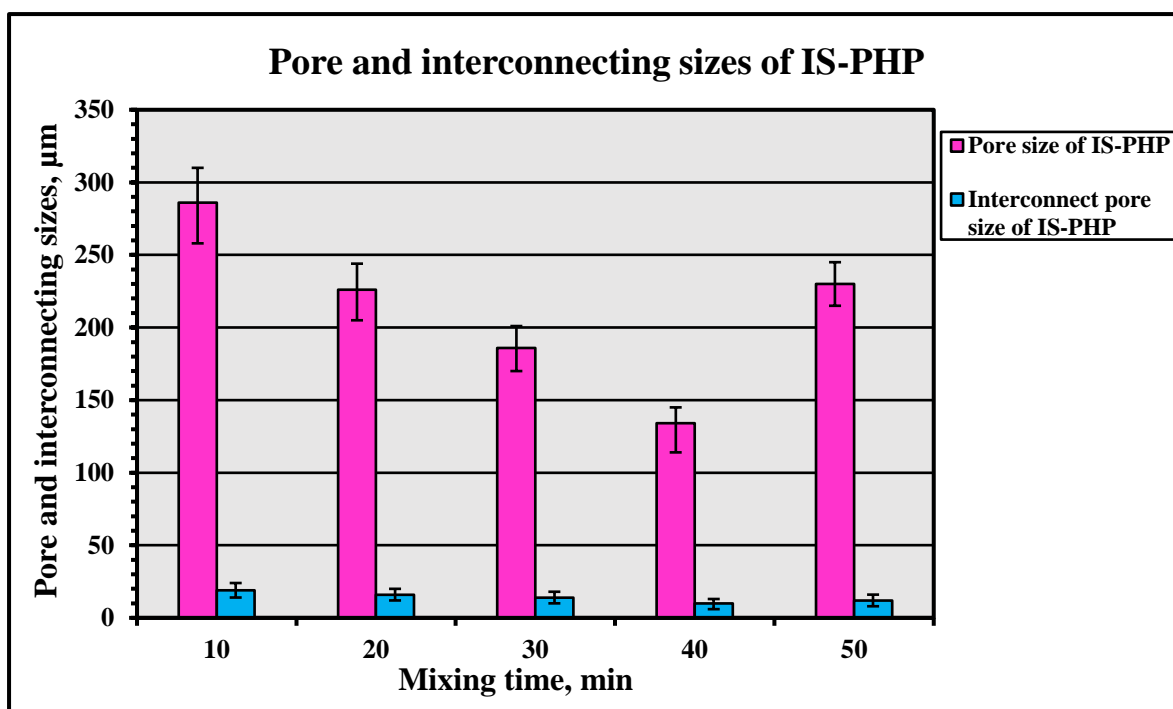


Figure 68: Plot of pore and interconnect sizes of IS-PHP for different mixing times.

### 5.3.3 Surface Area Measurement of IS-PHP

The surface areas of IS-PHP for various mixing times of 10, 20, 30, 40 and 50 minutes were determined by using the BET technique. The outcomes of surface area for various IS-PHP polymers are demonstrated in Table 21 and Figure 69. Overall, it is noticed that the surface area of the IS-PHP increases clearly with the increasing of the mixing time up to 40 minutes followed by a sharp decline at a mixing time of 50 minutes. This shows the effective role of the increasing mixing time (up to 40 minutes) in reducing the size of aqueous phase droplets and spreading them inside the oil phase, leading to decrease of the pore and interconnect pore size and thus increasing the surface area. This is followed by a sharp decrease at mixing time, 50 minutes, which is attributed to pore coalescence and the increased collapse of the walls between pores. In addition, it can be seen that the highest surface area of IS-PHP was achieved at mixing time of 40 minutes, while the lowest surface area of IS-PHP got at mixing time of 10 minutes. Smooth cell walls are produced for a mixing time of 50 minutes leading to a reduction in surface area.

Table 21: Surface area of IS-PHP for different mixing times.

IS-PHP sample	Mixing time (min)	Surface area (m <sup>2</sup> /g)
IS10	10	2±0.5
IS20	20	5±1
IS30	30	9±1
IS40	40	15±2
IS50	50	6±1

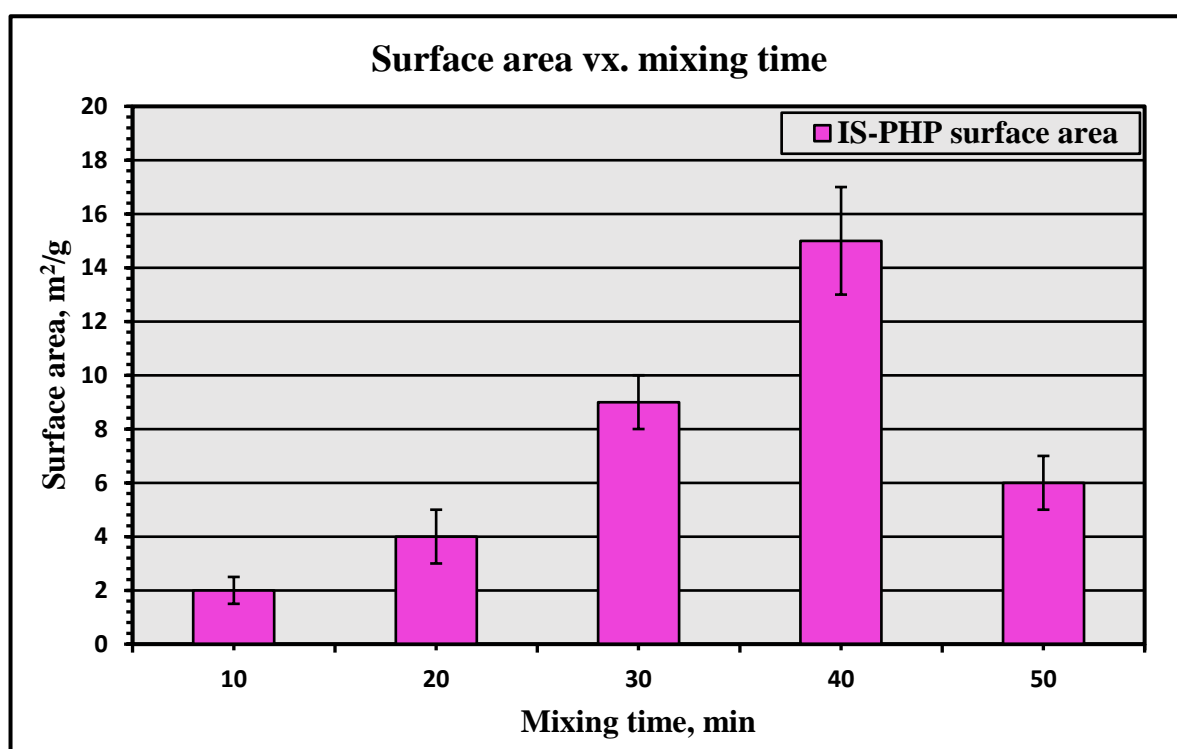


Figure 69: Plot of surface area for various mixing times of IS-PHP.

#### 5.3.4 Water Uptake of IS-PHP

The water uptake of the IS-PHP for various mixing times of 10, 20, 30, 40 and 50 minutes was studied, where three discs for each sample were tested. The results are illustrated in Table 22 and Figure 70. In general, it is noticed that the water uptake capacity of IS-PHP increases slightly with the increasing of mixing time up to 40 minutes followed by a clear decline at a mixing time of 50 minutes. The water uptake of the sample IS40 at mixing time of 40 minutes was significantly higher, 1.6 times compared to IS10 PHP sample. In addition, it can be observed that the water uptake ability and the surface area of IS-PHP are correlated for all mixing times.

The basic post sulphonated PHP had a maximum water uptake of 260% at the maximum mixing time of 50 minutes. This is comparable to what was observed previously (Hasan, 2013; Greco, 2014). However in-situ sulphonated PHP had a maximum water uptake of 220% after 40 minutes of mixing and the water uptake (surface area) declined at longer mixing time. The pore size also increased due to the formation of coalescence pores. Water uptake is maximum when pore size is minimum. The in-situ and post sulphonation processes lead to very similar water uptake if comparable structures are produced.

Table 22: Water uptake of IS-PHP samples for different mixing times.

IS-PHP sample	Mixing time, min	% water uptake of SI-sample	% average water uptake of SI-sample
IS10	10	124-152	134
IS20	20	146-178	160
IS30	30	158-192	173
IS40	40	199-237	220
IS50	50	131-164	143

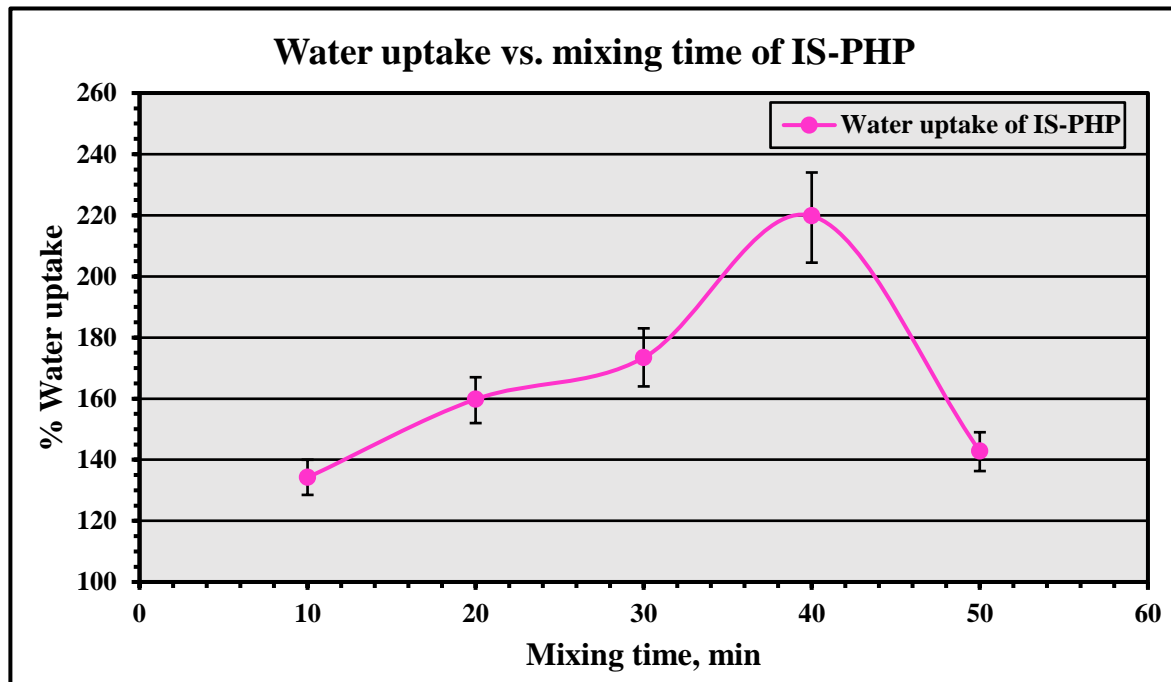


Figure 70: Plot of water uptake of IS-PHP for different mixing times.

### 5.3.5 FTIR Analysis of IS-PHP

The IS-PHP samples IR spectra for different mixing times, look almost identical to one another as exhibited in Figure 72. In general, the results of absorption peaks of the IS-PHP samples as illustrated in Figure 71 and Table 23 are the same as the peaks noticed in sulphonated B-PHP as introduced in section 5.2.5. The peaks look alike except the disappearance of some peaks at 1411 and 1413  $\text{cm}^{-1}$  (which are attributed to C=C in an aromatic ring) as well as the absorption peaks of 3403 and 3417  $\text{cm}^{-1}$  (which are ascribed to –OH groups). While, there are some extra peaks appearing at 1370, 1371 and 1372  $\text{cm}^{-1}$ , attributed to Saturated –CH<sub>3</sub> (Fleming and Williams, 1966) as well as the a wide absorption band of 1530 to 1590  $\text{cm}^{-1}$ , attributed to (C=C) in an aromatic ring (Vinodh *et al.*, 2010).

Thus, the surface structures of the PHP do not significantly depend on the sulphonation process, merely the amount of sulphur incorporation is increased by post sulphonation.

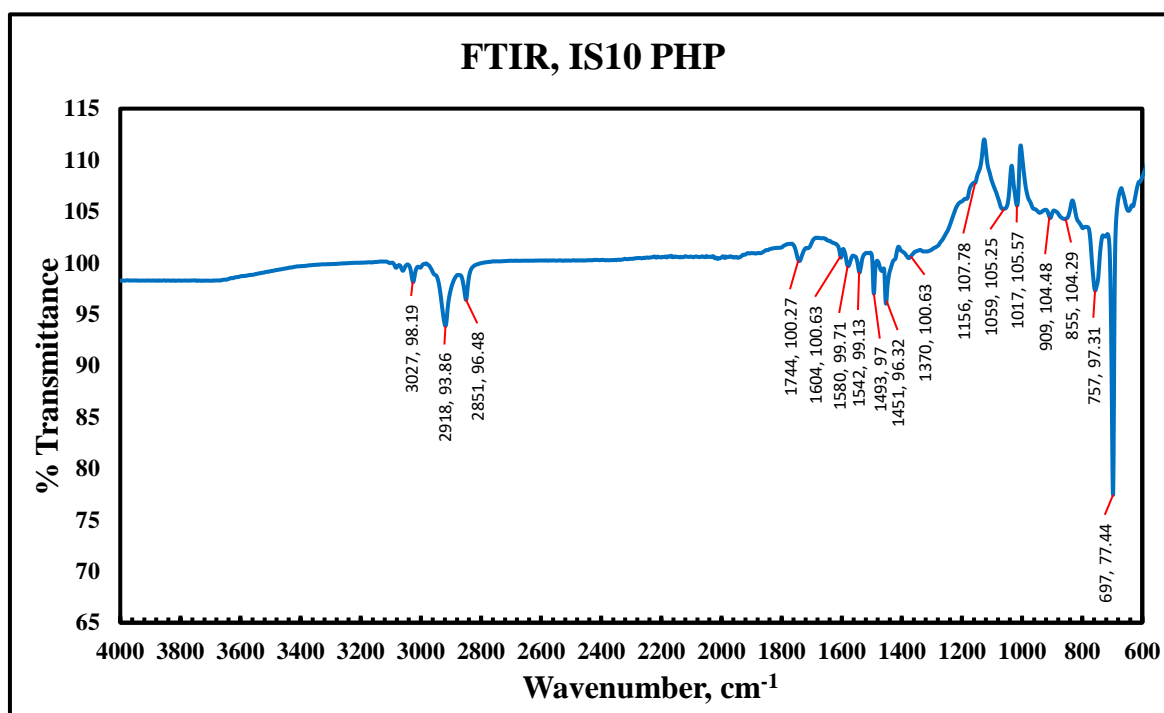


Figure 71: FTIR spectrum for IS10 PHP.

Table 23: Absorption peaks and peaks names of IS-PHP samples for different mixing times.

Sample peak cm <sup>-1</sup>					Peak origin	References
Mixing time=10 min	Mixing time=20 min	Mixing time=30 min	Mixing time=40 min	Mixing time=50 min		
697	698	696	695	697	Out of plane (C–H) bends of the aromatic ring	(Bhagiyalakshmi <i>et al.</i> , 2010)
757	759	758	760	759	Out of plane (C–H) bends of the aromatic group	(Jiang and Zeng, 2010)
855	854	851	852	854	Distributed phenyl ring and vinyl ring	(Mercier <i>et al.</i> , 2001)
909	907	908	901	905	C=C in phenyl ring	(Hubbard <i>et al.</i> , 1998)
1017	1016	1015	1013	1014	Monosubstituted phenyl ring	(Mercier <i>et al.</i> , 2001)
1059	1057	1054	1051	1053	Monosubstituted phenyl ring	(Mercier <i>et al.</i> , 2001)
1156	1157	1156	1155	1156	(–C=S) stretch sulphate group	(Fleming and Williams, 1966)
1370	1371	1370	1372	1370	Saturated –CH <sub>3</sub>	(Fleming and Williams, 1966)
1451	1453	1450	1452	1451	Aromatic ring backbone – CH–bending vibration	(Vinodh <i>et al.</i> , 2010)
1493	1492	1491	1492	1491	Aromatic ring backbone – CH–bending vibration	(Vinodh <i>et al.</i> , 2010)
1542	1541	1540	1543	1541	(C=C) in aromatic ring	(Vinodh <i>et al.</i> , 2010)
1580	1582	1581	1579	1581	(C=C) in aromatic ring	(Vinodh <i>et al.</i> , 2010)
1604	1602	1603	1602	1600	(C=C) in aromatic ring	(Vinodh <i>et al.</i> , 2010)
1744	1742	1741	1699	1698	C=O stretch carbonyl group	(Leber <i>et al.</i> , 2007)
2851	2849	2851	2848	2850	C–H stretching vibration of methylene and methyl groups	(Rubino <i>et al.</i> , 2010)
2918	2920	2921	2918	2921	C–H stretching vibration of methylene and methyl groups	(Rubino <i>et al.</i> , 2010)
3027	3026	3028	3025	3028	(C=C–H) stretch in aromatic group	(Ungureanu <i>et al.</i> , 2007)

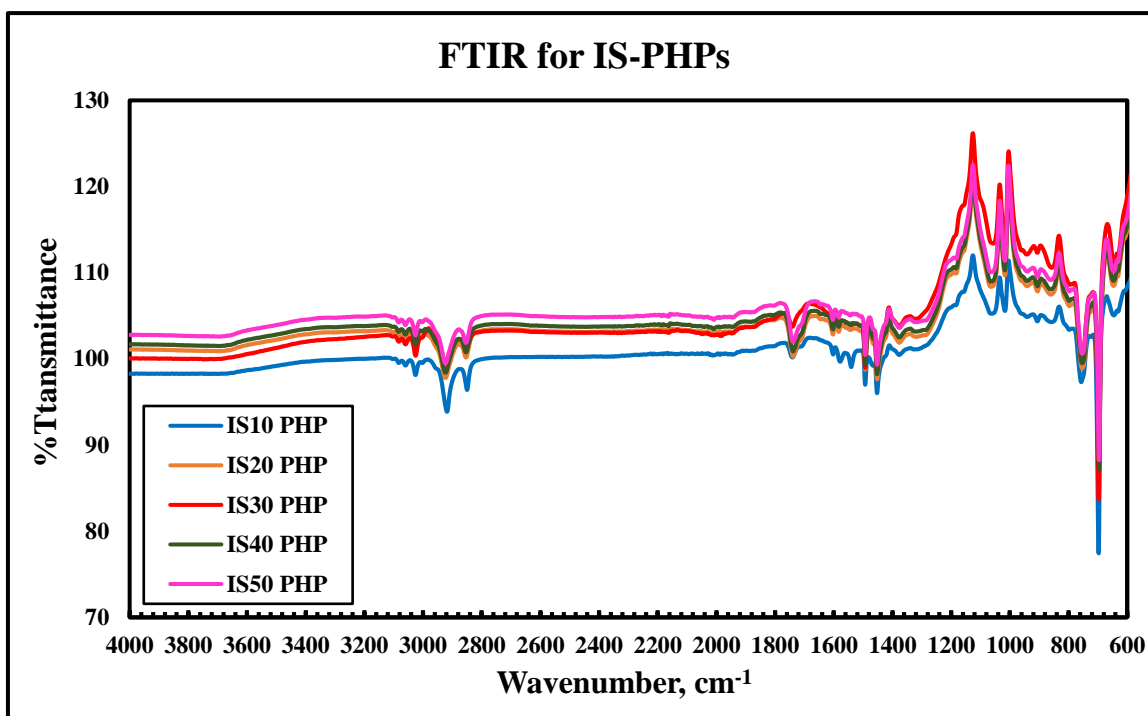


Figure 72: FTIR spectra for all IS-PHP samples.

### 5.3.6 Summary

In situ sulphonation produced a PHP morphology which is almost identical to the basic polyHIPE with post sulphonation except at the highest mixing times when some coalescence occurs. The surface becomes sulphonated in a similar manner to the post-sulphonation of basic polyHIPE but the total surface sulphur content is reduced. This reduces the water uptake ability of the material.

## 5.4 Bindzil PolyHIPE (BZ-PHP)

### 5.4.1 Morphology

Bindzil was put in the solution of the aqueous phase in different percentages of 5%, 10%, 15%, 20%, and 25% to synthesize BZ-PHP (the ratios of components are mentioned in Table 9). Figure 73 shows SEM images of the BZ5, BZ10, BZ15, BZ20 and BZ25 PHP structures. It can be observed in the SEM images that all BZ-PHP samples have uniform structures and the uniformity increases from BZ5 PHP towards BZ25 PHP. This may be due to an increase in the percentage of bindzil (BZ). Moreover, the images show a hierarchical pore structure and

obvious coalescence pores in all BZ-PHP samples. The interconnection of pores can also be observed inside each coalescence pore and in its neighbours. Figure 74, shows at the magnification of 5000, 10000 and 15000x many small pores, pores network between coalescence pores and the interconnected of pores as well as the surface roughness between the holes. These structures illustrate the high value of BZ-PHP surface area.

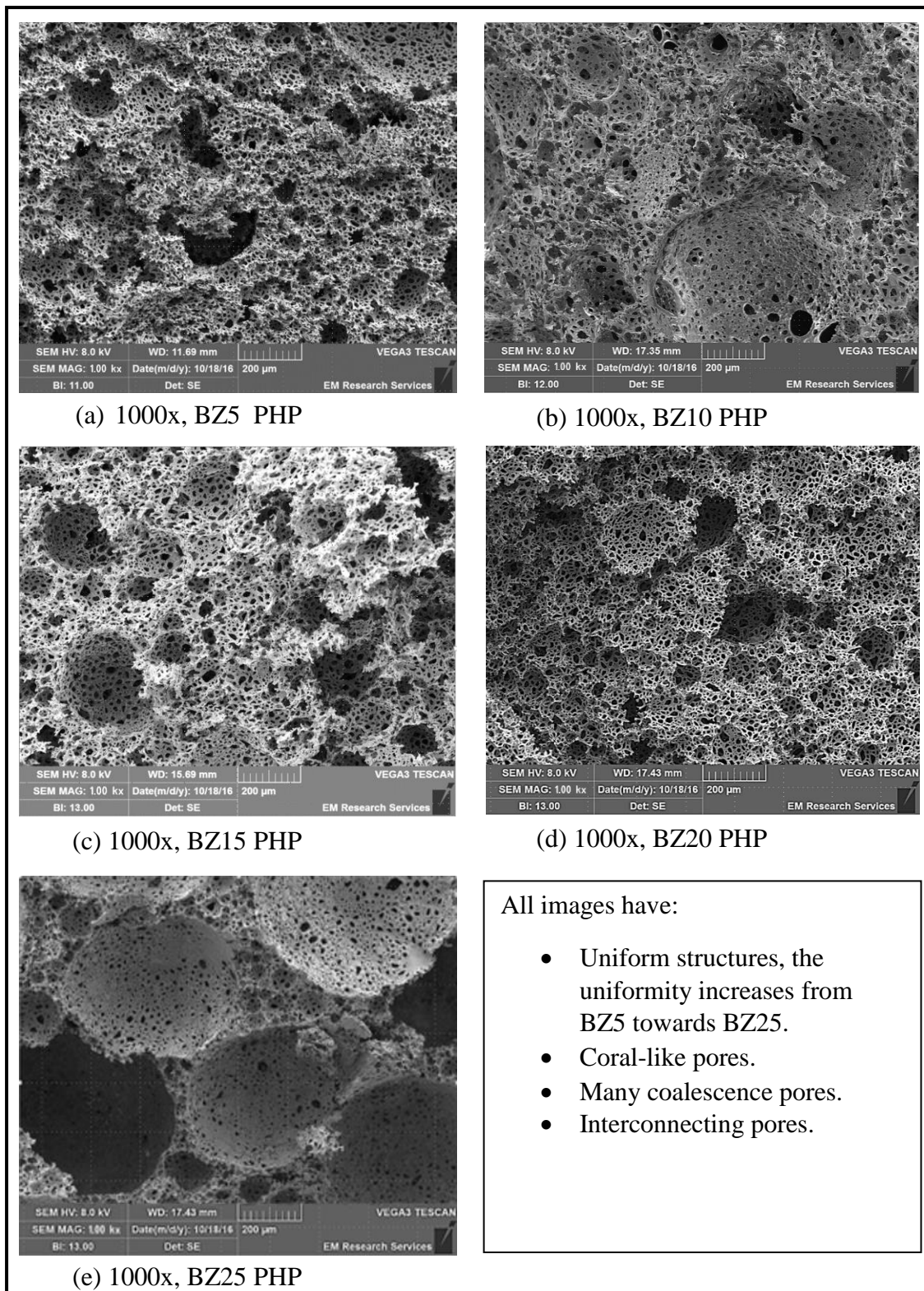


Figure 73: Bindzil PHP (BZ-PHP). (a) 5% bindzil (b) 10% bindzil (c) 15% bindzil (d) 20% bindzil (e) 25% bindzil. Oil phase: 75% styrene, 10% DVB, 14% span 80 and 1% potassium persulphate. Aqueous phase: X% bindzil, (100-X)% distilled water, (e.g. for 15% bindzil. Distilled water was decreased to 85%). Phase volume = 90%, Dosing time = 10 minutes, Mixing time = 50 minutes. Polymerisation temperature = 60 °C, Polymerisation time = 24 hours.

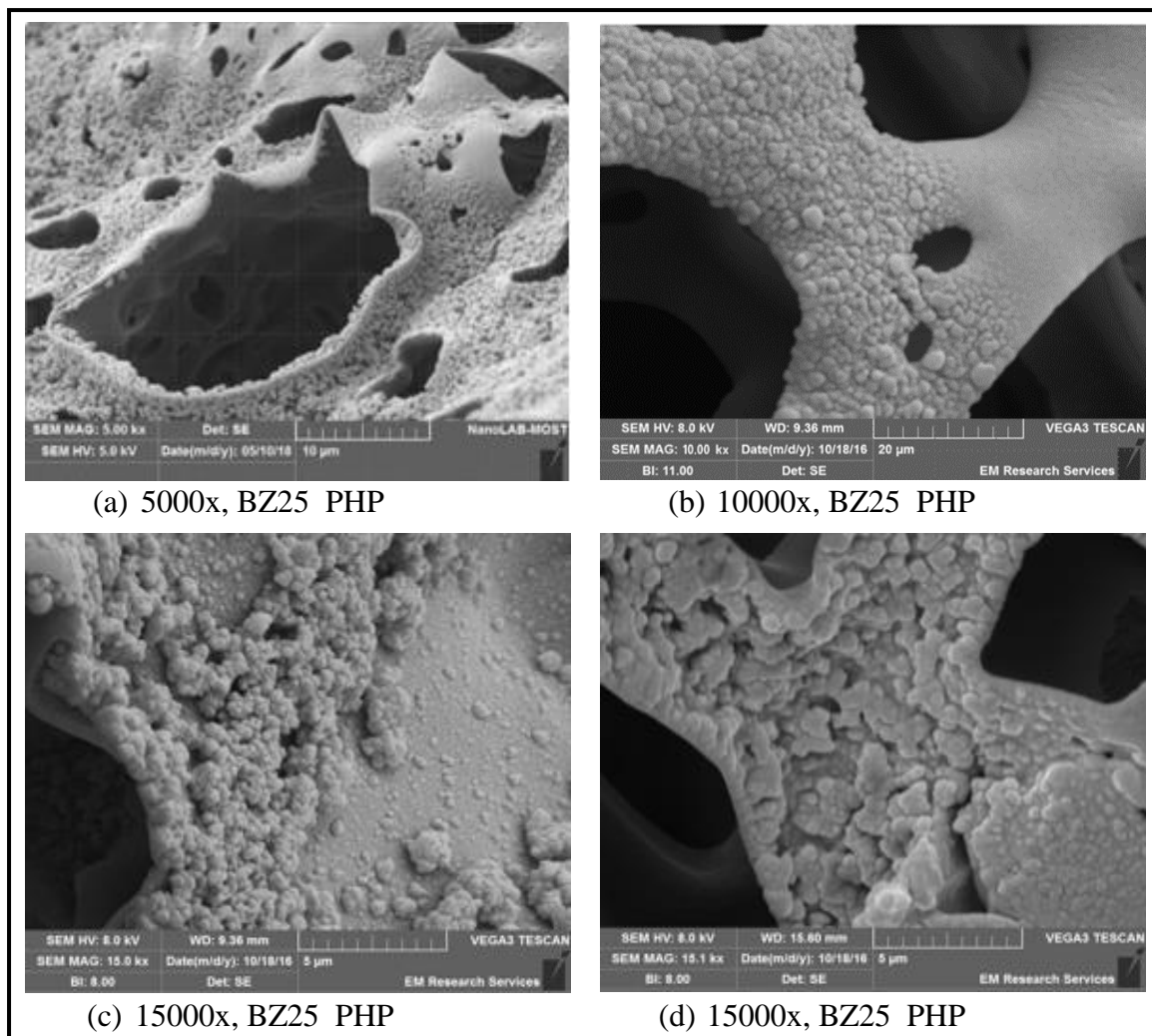


Figure 74: Different magnification images of 5000, 10000 and 15000x of BZ25 PHP for mixing time of 50 minutes.

With the aim of verifying the elements in the BZ-PHP structure, Energy Dispersive X-rays (EDX) spectroscopy was carried out on BZ25. The spectra for the complete area and the three different locations are illustrated in Figure 76, Figure 77, Figure 78 and Figure 79 based on the image in Figure 75. The results are given in Table 24 and Table 25 for the whole area and three points (1, 2 and 3), respectively. The three points and whole area clarify the existence of carbon, silicon, oxygen and sulphur as well as potassium which appears only in whole area (due to the small quantity of Potassium in the initiator used), with approximately similar weight percentage and atomic percentage of these elements at the different analysis locations. The presence of silicon in the sample proves the integration of CC40 bindzil in the BZ-PHP. The silicon content is similar to that achieved in the SL-PHP samples (see next section).

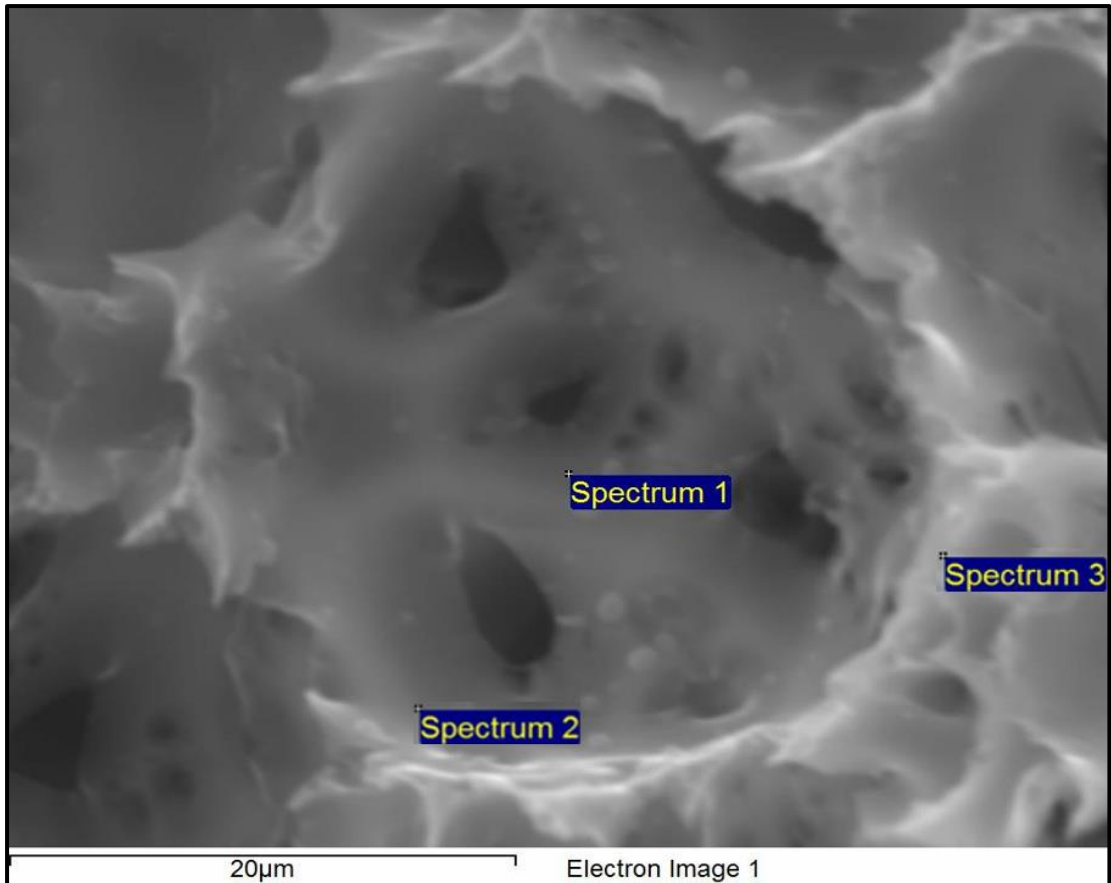


Figure 75: Three points, 1, 2 and 3 for EDX analysis of BZ25.

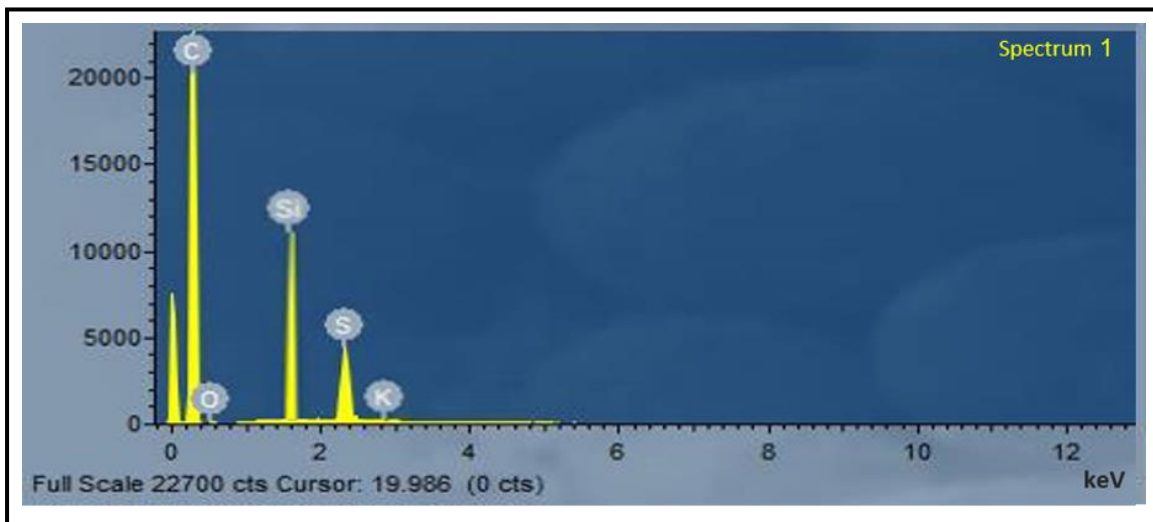


Figure 76: The complete area EDX analysis of image in Figure 89.

Table 24: EDX composition for the all area of the image for BZ25.

Element	Weight %	Atomic%
Carbon	86.87	90.63
Silicon	1.83	0.76
Sulphur	1.97	0.80
Oxygen	9.25	7.78
Potassium	0.08	0.03
Total	100.00	100.00

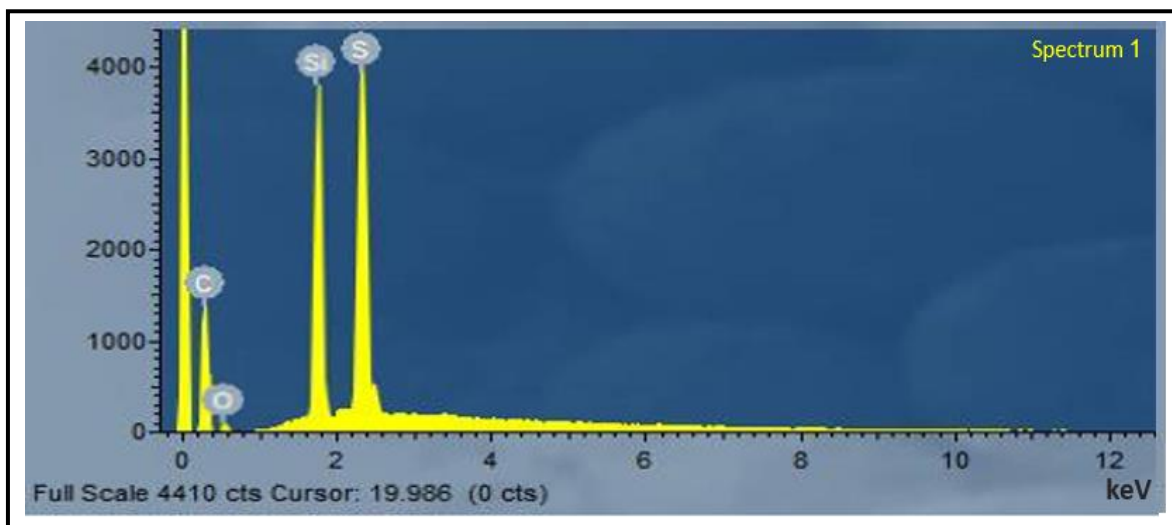


Figure 77: BZ25 point 1 EDX spectrum.

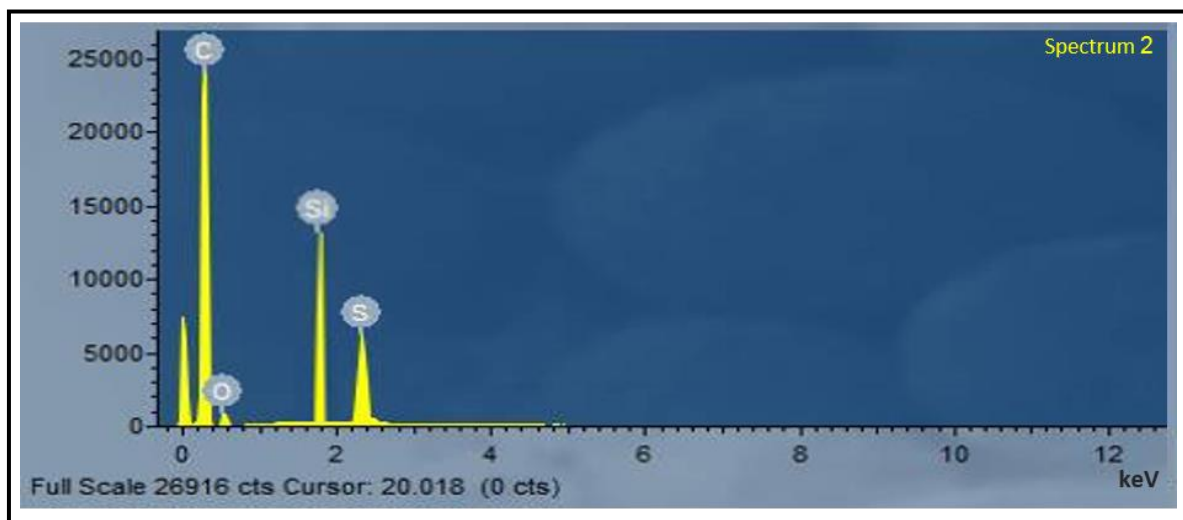


Figure 78: BZ25 point 2 EDX spectrum.

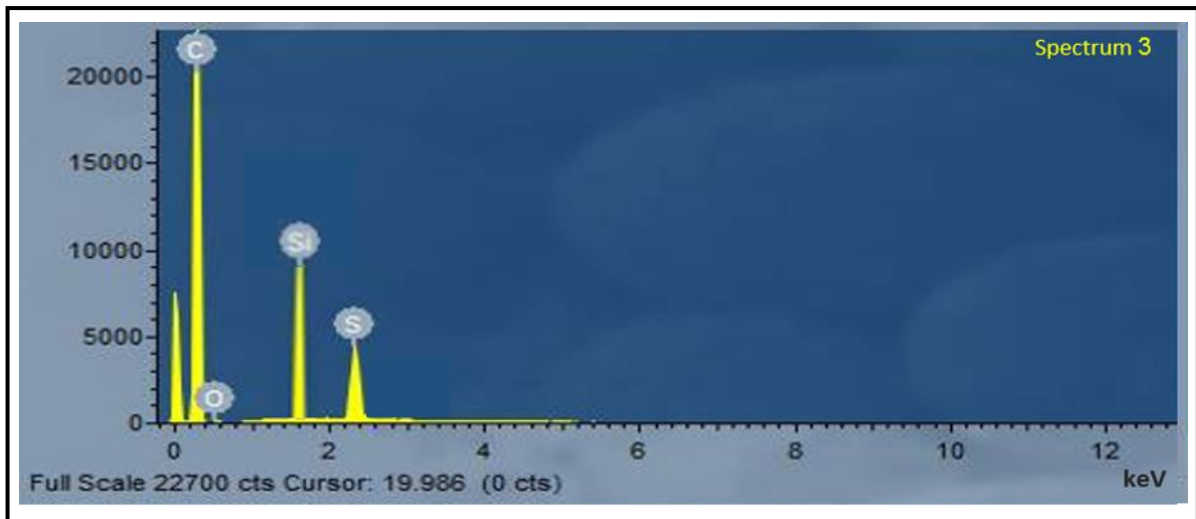


Figure 79: BZ25 point 3 EDX spectrum.

Table 25: Summary of the EDX results for the points, 1, 2 and 3 for BZ25.

Element	Point 1		Point 2		Point 3	
	Weight %	Atomic %	Weight %	Atomic %	Weight %	Atomic %
Carbon	76.38	80.48	79.98	84.62	78.28	81.79
Silicon	6.91	5.16	5.85	4.39	6.22	4.72
Sulphur	5.92	4.24	4.86	3.91	5.53	4.28
Oxygen	10.79	10.12	9.31	7.08	9.97	9.21
Total	100.00	100.00	100.00	100.00	100.00	100.00

#### 5.4.2 Pore Size Distribution of BZ-PHP

The pore and interconnect pore sizes have been measured for all the BZ-PHP samples with different mixing times of 10, 20, 30, 40 and 50 minutes, namely BZ5, BZ10, BZ15, BZ20 and BZ25 by using ImageJ software on SEM images. The results are displayed in Table 26 and Figure 80. The results show that the pore and interconnect sizes of BZ-PHP samples are reduced with mixing time up to 50 minutes. The increase in mixing time makes the size of dispersed phase droplets smaller, due to the effect of continuous mixing. This result corresponds with Greco (2014), who stated that the pore size gets smaller with mixing time since mixing increases homogenisation. Thirty pores from each sample were measured to take the average, where the average value of the pore and interconnect pore sizes was ranging between 7 $\mu$  m and 260 $\mu$  m. It confirms the success of producing a macro porous material with

hierarchical structure of BZ-PHP as shown in Figure 73. Figure 81 shows the pore and interconnecting pore sizes for the BZ25 sample, are the lowest among all the samples produced in study.

Table 26: The results of ImageJ analysis of average pore and interconnect sizes, which were determined from the BZ-PHP where 30 pores from each sample were measured.

BZ-PHP sample	Mixing time (min)	Average pore size ( $\mu$ m)	Average interconnect pore size ( $\mu$ m)
BZ5	10	260 $\pm$ 15	21 $\pm$ 5
	20	241 $\pm$ 14	20 $\pm$ 5
	30	186 $\pm$ 13	18 $\pm$ 4
	40	159 $\pm$ 11	13 $\pm$ 3
	50	144 $\pm$ 10	12 $\pm$ 4
BZ10	10	255 $\pm$ 16	20 $\pm$ 5
	20	210 $\pm$ 14	18 $\pm$ 5
	30	181 $\pm$ 12	15 $\pm$ 4
	40	146 $\pm$ 11	14 $\pm$ 4
	50	132 $\pm$ 10	11 $\pm$ 3
BZ15	10	206 $\pm$ 15	18 $\pm$ 5
	20	196 $\pm$ 14	16 $\pm$ 4
	30	165 $\pm$ 13	15 $\pm$ 4
	40	137 $\pm$ 11	12 $\pm$ 3
	50	129 $\pm$ 10	11 $\pm$ 3
BZ20	10	195 $\pm$ 16	18 $\pm$ 5
	20	173 $\pm$ 14	16 $\pm$ 4
	30	153 $\pm$ 13	15 $\pm$ 4
	40	138 $\pm$ 12	12 $\pm$ 3
	50	121 $\pm$ 10	10 $\pm$ 3
BZ25	10	173 $\pm$ 12	16 $\pm$ 5
	20	164 $\pm$ 11	15 $\pm$ 5
	30	149 $\pm$ 10	14 $\pm$ 4
	40	112 $\pm$ 10	12 $\pm$ 3
	50	99 $\pm$ 9	7 $\pm$ 3

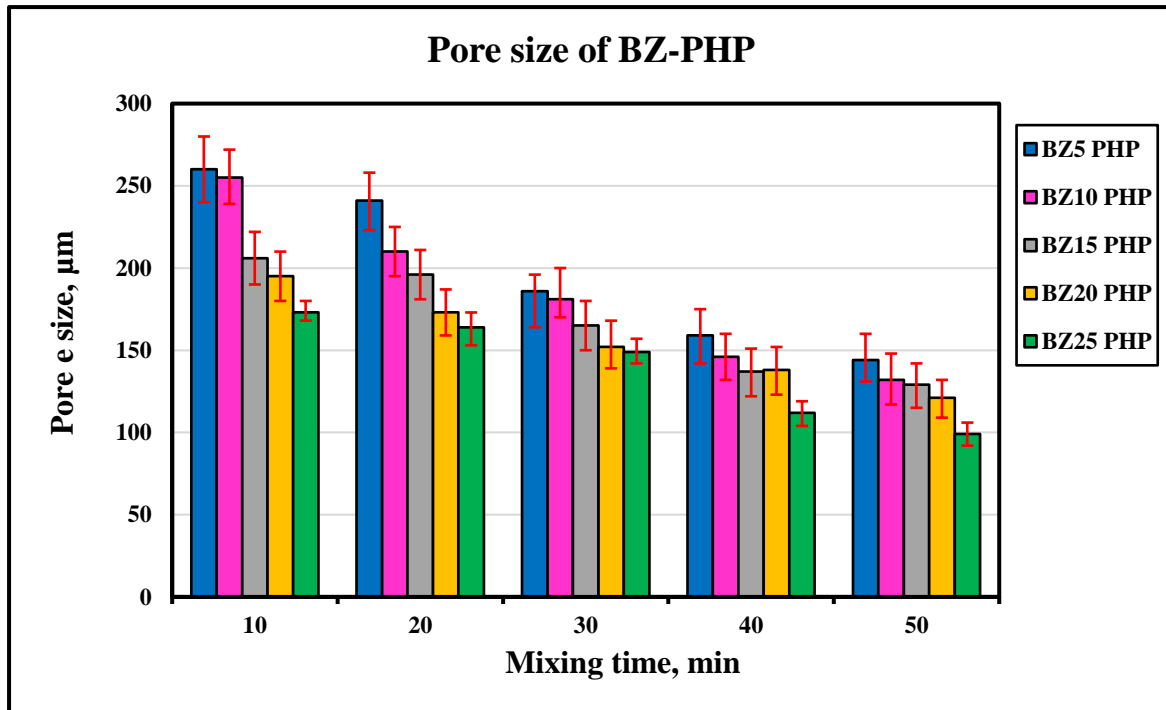


Figure 80: Plot of pore and interconnect sizes of BZ-PHP samples for different mixing times.

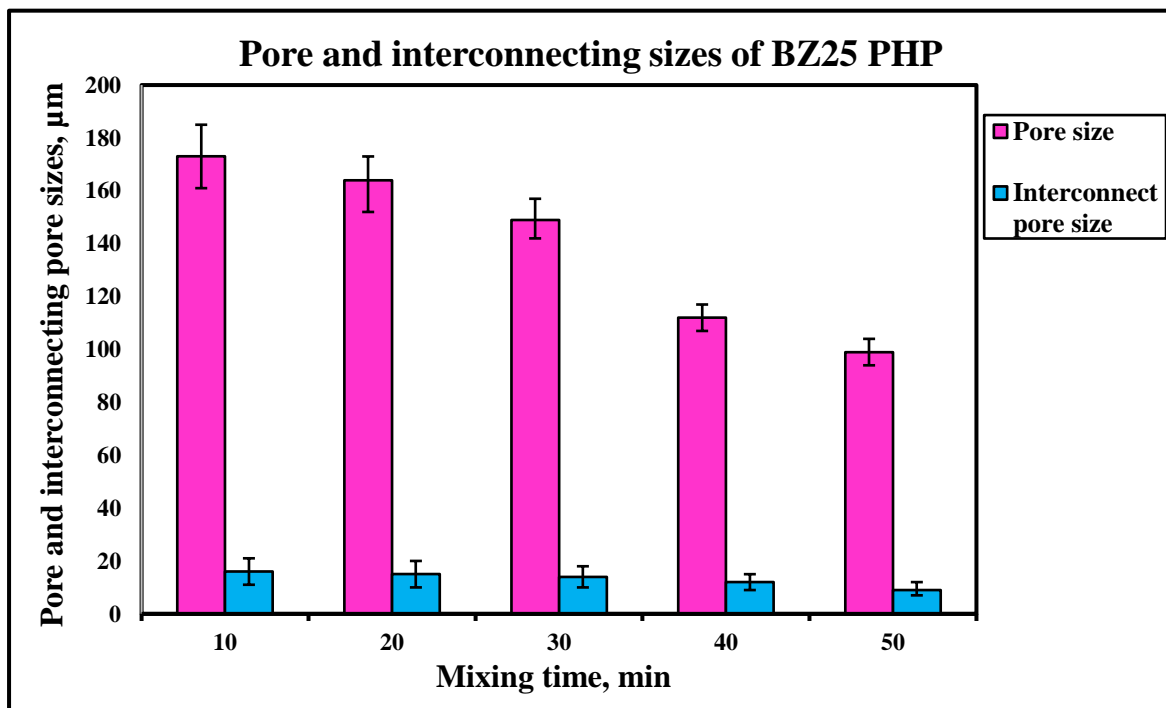


Figure 81: Plot of pore and interconnect sizes of BZ25 PHP samples for different mixing times.

### 5.4.3 Surface Area measuring of BZ-PHP

The surface areas of unsulphonated and sulphonated BZ-PHP samples for different percentages of Bindzil with different mixing times of 10, 20, 30, 40 and 50 minutes were determined by using the BET (Brunauer, Emmet and Teller) Surfer technique. The outcomes of surface area for different Bindzil polyHIPE polymers are presented in Table 27 and Figure 82. In general, it is noticed that the unsulphonated BZ-PHP samples surface area increases slightly with the increase in percentage of bindzil for different mixing times. While, a sulphonated BZ-PHP samples surface area increases significantly compared to unsulphonated BZ-PHP samples with the increase in percentage of Bindzil for different mixing times. In addition, it can be seen that the highest surface area of BZ-PHP was obtained at mixing time of 50 minutes for sulphonated BZ25 PHP 3.3 times more than unsulphonated BZ25 PHP, while the lowest surface area of sulphonated BZ-PHP was obtained at mixing time of 10 minutes for BZ5 PHP was 1.71 times more than unsulphonated BZ5 PHP. This outcome is compatible with the image (structure of BZ25 PHP) shown in Figure 73 due to stability and roughness of surfaces amongst all BZ-PHPs samples. It was found that two components to surface area. The amount of walls and the porosity/roughness of the walls. Sulphonation only changes the latter.

The results of the previous study conducted by Hasan (2013), indicated that the sulphonation of BZ-PHP increases the surface area with an increase in the percentage of BZ-PHP and mixing time. This corresponds to the results of this study as shown in Table 27.

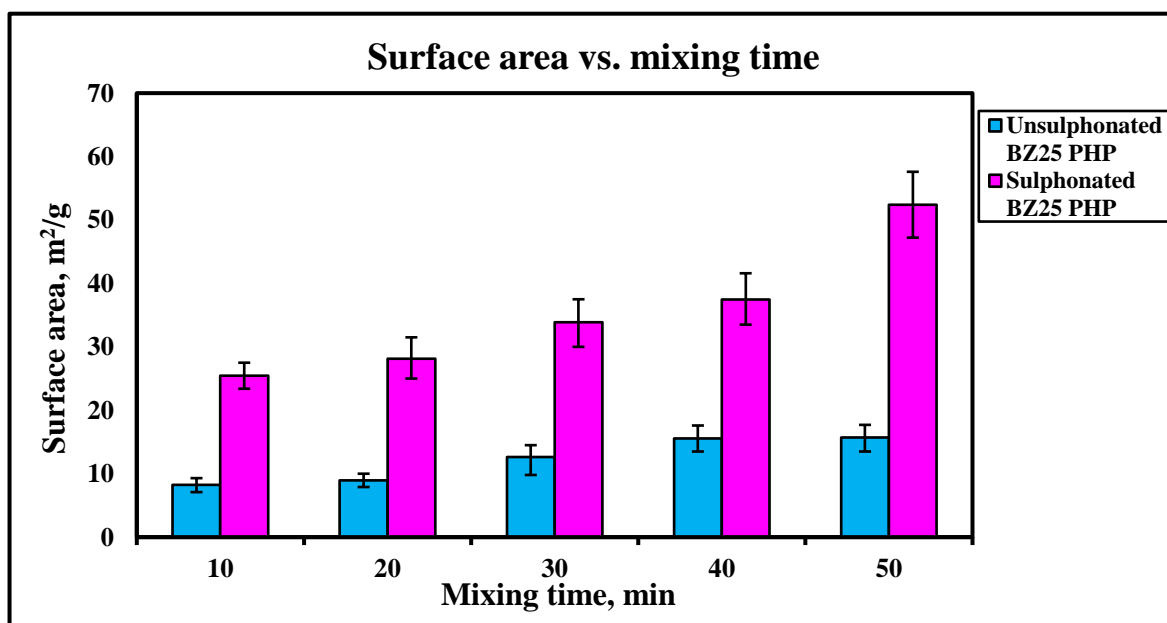


Figure 82: Plot of the surface area of unsulphonated and sulphonated BZ50 PHP for various mixing times.

Table 27: Surface area of unsulphonated and sulphonated BZ-PHP for different mixing times.

BZ-PHP sample	Percentage of bindzil	Mixing time (min)	Surface area of unsulphonated sample (m <sup>2</sup> /g)	Surface area of sulphonated sample (m <sup>2</sup> /g)	Surface area fold
BZ5	5	10	8±1	14±2	1.71
		20	9±1	21±2	2.30
		30	11±1	23±2	2.06
		40	12±1	29±3	2.40
		50	13±2	30±3	2.40
BZ10	10	10	9±1	20±2	2.13
		20	12±1	22±2	1.76
		30	11±1	30±2	2.65
		40	13±1	33±3	2.26
		50	14±2	35±3	2.58
BZ15	15	10	11±1	20±2	1.91
		20	12±1	22±2	1.98
		30	13±1	29±2	2.16
		40	13±1	34±3	2.77
		50	14±2	35±3	2.89
BZ20	20	10	8±1	21±2	2.48
		20	10±1	26±2	2.70
		30	11±1	31±3	2.74
		40	13±2	40±4	3.03
		50	15±2	44±4	2.98
BZ25	25	10	8±1	25±2	3.08
		20	9±1	28±2	3.15
		30	13±2	34±3	2.68
		40	16±2	37±4	2.41
		50	16±2	52±5	3.33

By comparing the surface area of BZ-PHP with the mixing time of 50 minutes and bindzil concentrated of 25% for this study to previous study (Hasan, 2013). The surface area of this study was increased from 16 m<sup>2</sup>/g before sulphonation to 52 m<sup>2</sup>/g after sulphonation (using microwave sulphonation), while for the previous study was increased from 13 m<sup>2</sup>/g before sulphonation to 37 m<sup>2</sup>/g after sulphonation (using thermal sulphonation). This means this study achieved surface area after sulphonation about 15 m<sup>2</sup>/g more than the previous study.

#### 5.4.4 Water Uptake of BZ-PHP

The water uptake of the BZ-PHP with different percentages of Bindzil with different mixing times of 10, 20, 30, 40 and 50 minute was examined, where three discs for each sample were tested, and the results are displayed in Table 28. The outcomes illustrate that the unsulphonated samples have a low ability of water uptake for all mixing times. While, the results illustrate that the sulphonated BZ-PHP samples have a high water uptake capacity that is directly proportional to the increase in bindzil percentage from 5% to 25% as shown in Figure 83. The water uptake of sulphonated BZ25 at a mixing time of 50 minutes was significantly higher, 3.8 times greater than unsulphonated BZ25. While, the sulphonated BZ5 at a mixing time of 10 minutes gave the lowest water uptake at only 1.8 times more than unsulphonated BZ5

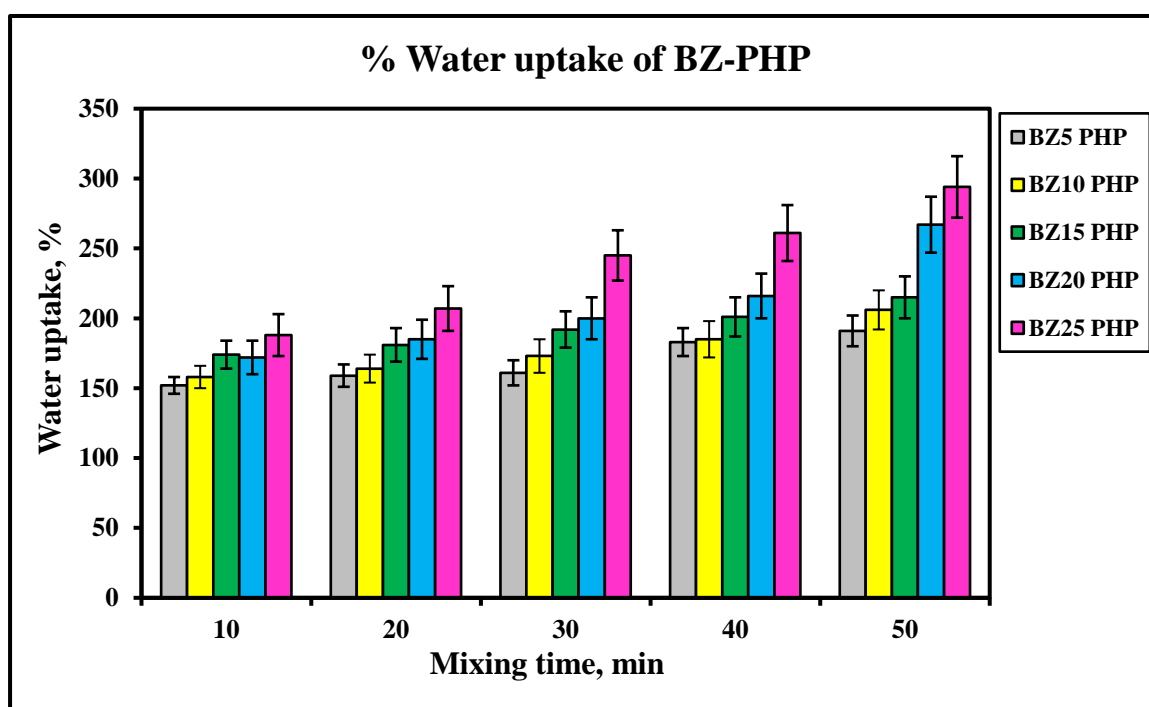


Figure 83: Plot of water uptake of sulphonated BZ-PHP for different percentage of bindzil with various mixing times.

Table 28: Water uptake for various BZ-PHP samples (before and after sulphonation) for different mixing times.

BZ-PHP sample	Mixing time (min)	% water uptake of unsulphonated sample	% average water uptake of unsulphonated sample	% water uptake of sulphonated sample	% average water uptake of sulphonated sample	water uptake fold
BZ5	10	81-90	84	125-178	152	1.8
	20	80-94	88	135-182	159	1.8
	30	77-89	81	133-197	161	2.0
	40	81-92	87	145-210	183	2.1
	50	86-96	91	155-212	191	2.1
BZ10	10	83-97	88	131-184	158	1.8
	20	82-100	91	138-180	164	1.8
	30	85-102	91	142-194	173	1.9
	40	79-91	84	159-215	185	2.2
	50	90-112	103	173-222	206	2.2
BZ15	10	80-96	83	140-202	174	2.0
	20	71-78	79	147-228	181	2.3
	30	70-88	80	155-237	192	2.4
	40	72-90	80	168-251	201	2.5
	50	74-88	82	178-262	215	2.6
BZ20	10	74-91	82	148-213	172	2.1
	20	68-84	74	156-248	185	2.5
	30	67-81	74	172-266	200	2.7
	40	69-87	77	187-284	216	2.8
	50	80-100	89	197-300	267	3.0
BZ25	10	74-87	81	158-231	188	2.3
	20	70-84	76	179-268	207	2.7
	30	71-89	79	195-312	245	3.1
	40	66-83	74	261-348	261	3.5
	50	69-85	77	239-374	294	3.8

### 5.4.5 FTIR Analysis of BZ-PHP

The sulphonated BZ-PHP samples IR spectra for different mixing times, look similar to one another as exhibited in Table 29 and Figures 84 and 85. In general, comparison of the results of absorption peaks of the sulphonated BZ-PHP samples (Table 29) to the peaks of sulphonated B-PHP (Table 18) shows the same results. Table 29, some strong absorption peaks appeared at 1009, 1010 and 1011  $\text{cm}^{-1}$  which are attributed to siloxane ( $-\text{Si}-\text{O}-\text{Si}$ ) stretching vibration (Gamys *et al.*, 2010). These peaks proved that the functionalization of Bindzil inside the HIPE was successful. While, the remaining absorption peaks were similar to the absorption peaks in Table 18, which have been discussed in section 5.2.5.

Table 29: Absorption peaks and peak assignments of sulphonated BZ-PHP samples for different percentages of bindzil with mixing time, 50 minutes.

Sample peak $\text{cm}^{-1}$					Peak origin	References
Bindzil, 5%	Bindzil, 10%	Bindzil, 15%	Bindzil, 20%	Bindzil, 25%		
698	697	697	696	697	Out of plane (C-H) bends of the aromatic ring	(Bhagiyalakshmi <i>et al.</i> , 2010)
759	757	756	758	756	Out of plane (C-H) bends of the aromatic group	(Jiang and Zeng, 2010)
830	831	834	832	830	Distributed phenyl ring and vinyl ring	(Mercier <i>et al.</i> , 2001)
1010	1011	1009	1010	1009	$-\text{Si}-\text{O}-\text{Si}$ stretching vibration	(Gamys <i>et al.</i> , 2010)
1364	1362	1360	1361	1365	Saturated $-\text{CH}_3$	(Fleming and Williams, 1966)
1452	1453	1452	1452	1452	Aromatic ring backbone – CH–bending vibration	(Vinodh <i>et al.</i> , 2010)
1493	1493	1493	1493	1493	Aromatic ring backbone – CH–bending vibration	(Vinodh <i>et al.</i> , 2010)
1600	1600	1600	–	1601	(C=C) in aromatic ring	(Vinodh <i>et al.</i> , 2010)
2846	2847	2852	2847	2848	C–H stretching vibration of methylene and methyl groups	(Rubino <i>et al.</i> , 2010)
2919	2921	2919	2916	2920	C–H stretching vibration of methylene and methyl groups	(Rubino <i>et al.</i> , 2010)
3026	3027	3028	3023	3024	(C=C–H) stretch in aromatic group	(Ungureanu <i>et al.</i> , 2007)

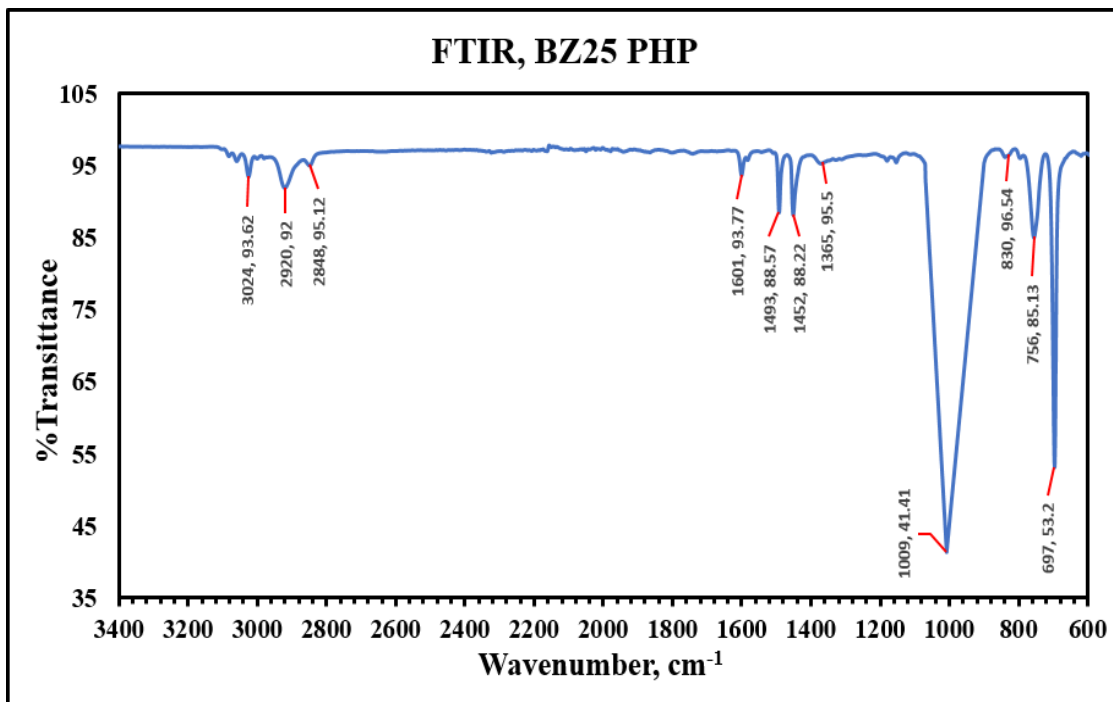


Figure 84: FTIR spectrum for all sulphonated BZ-PHP.

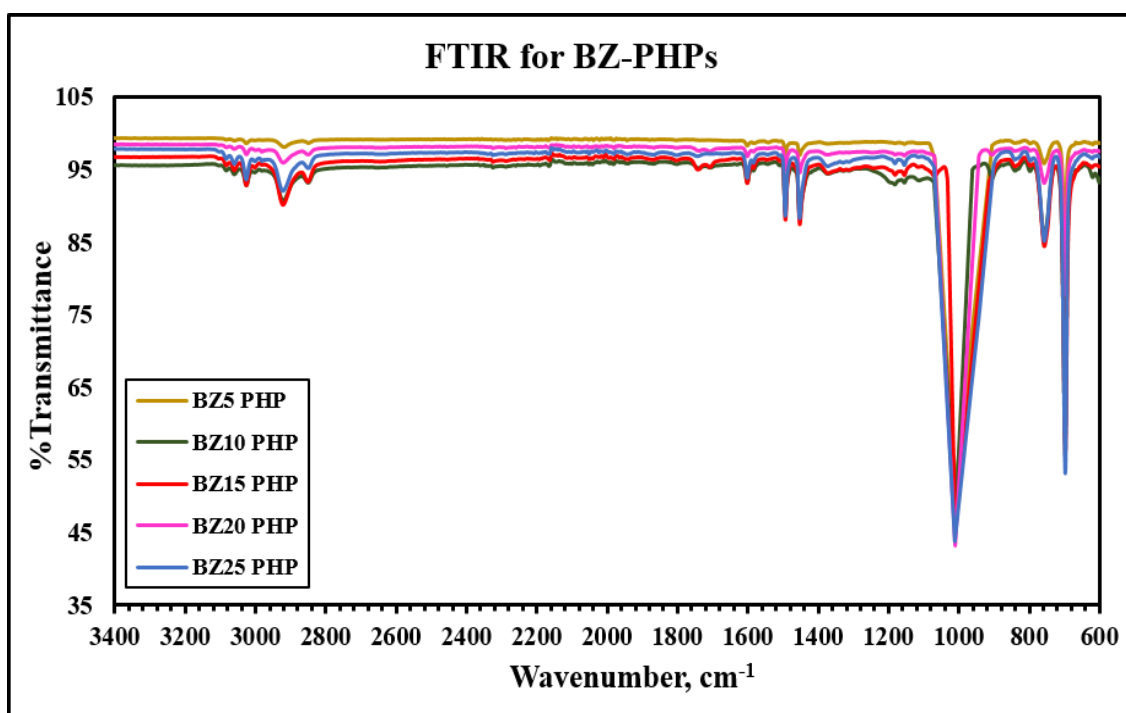


Figure 85: FTIR spectra for sulphonated BZ25 PHP

#### **5.4.6 Summary**

A silica containing polyHIPE with high surface area and good water uptake has been produced. The silicon is present as a surface coating on the polymer walls which is discontinuous and contains small particles which increase surface area. There are regions of uncoated polymer which can be made hydrophilic by sulphonation but there is significant water uptake in the absence of sulphonation due to the hydrophilic silica coating.

## 5.5 Silane (vinyl trimethoxy silane) PolyHIPE (SL-PHP)

Silane (SL) was added in the solution of oil phase in different percentages to synthesize SL-PolyHIPE. Figure 86 shows the resulting SL-PHP.

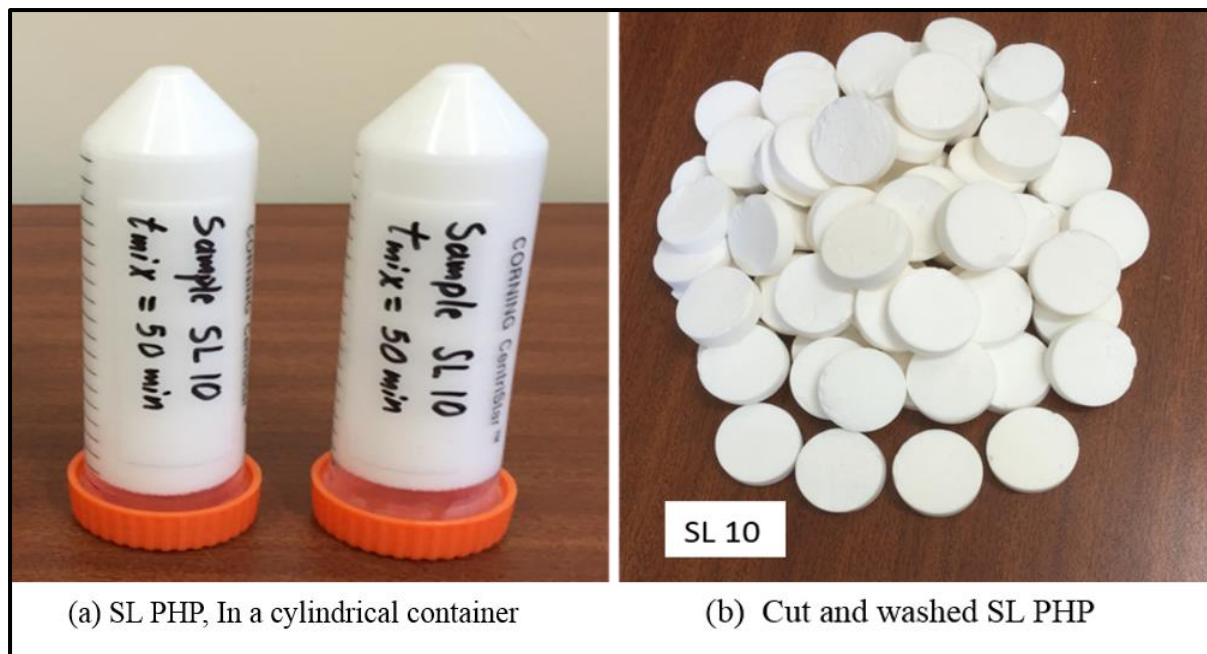


Figure 86: SL-PHP, SL10 with 10% vinyl trimethoxy silane.

### 5.5.1 Morphology

Figure 87 shows SEM images of the SL5, SL10, SL15, SL20 and SL25 PHP structures, which are synthesized with 5%, 10%, 15%, 20%, and 25% of SL (vinyl trimethoxy silane) respectively in the oil phase (the ratios of components are mentioned in Table 10). It can be observed in the SEM images that SL5 PHP has a somewhat open cell structure. However, the rest have a uniform structures and the uniformity increases from SL10 PHP towards SL20 PHP except for SL25 PHP, that is characterised by presence of a big coalescence pores. This may be due to an increase in the percentage of silane (SL). Moreover, as shown in Figure 88, at higher magnification SL10, SL15, SL20 and SL25 PHP show a hierarchical pore structure as well as coalescence pores. The interconnection of pores can also be observed inside each coalescence pore and in its adjacent pores. In addition, at magnification of 2000x Figure 88 (f) shows many small pores, a pore network between coalescence pores and interconnection of pores as well as the surface roughness between the holes. These structures illustrate the high value of silane PHP surface area.

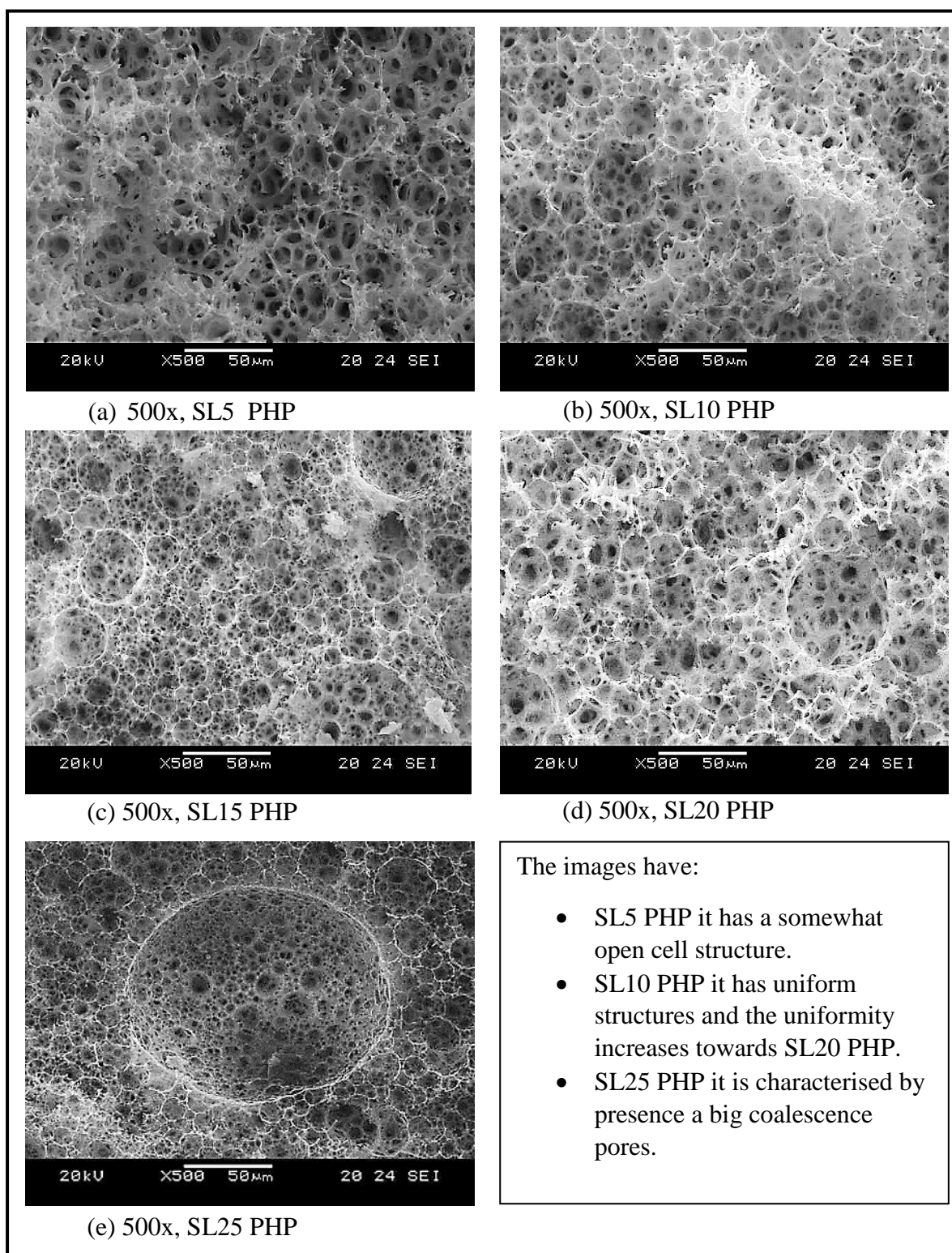


Figure 87: Vinyl trimethoxy silane PHP (SL-PHP). (a) 5% silane (b) 10% silane (c) 15% silane (d) 20% silane (e) 25% silane. Oil phase: X% silane, (76-X)% styrene, 10% DVB, 14% span 80, (e.g. for 10% silane. Styrene was decreased to 66%). Aqueous phase: 99% distilled water, 1% potassium persulphate. Phase volume = 90%, Dosing time = 10 minutes, Mixing time = 50 minutes. Polymerisation temperature = 60 °C, Polymerisation time = 24 hours.

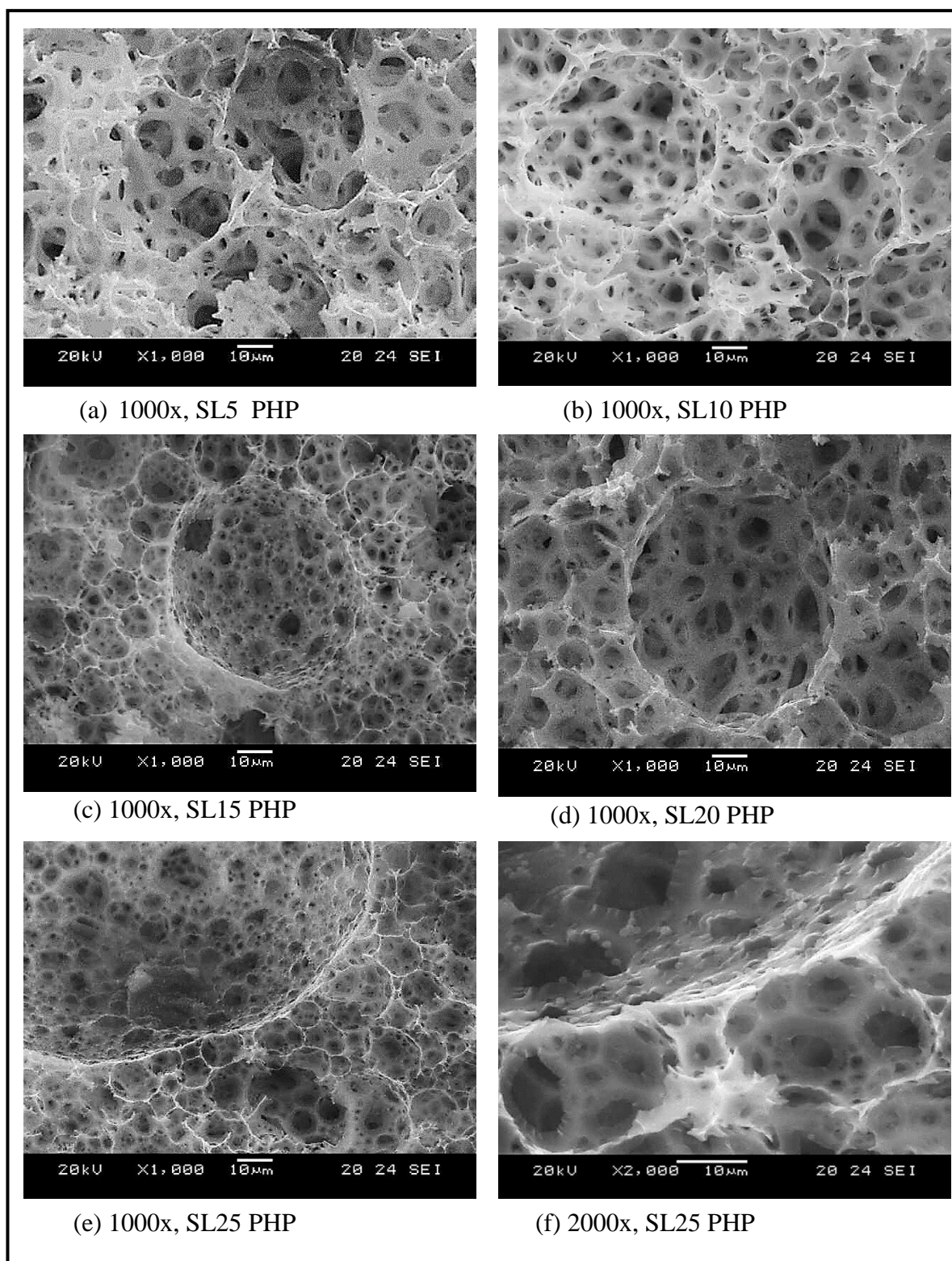


Figure 88: Vinyl trimethoxy silane PHP (SL-PHP). (a) 10% silane (b) 15% silane (c) 20% silane (d, e and f) 25% silane. Oil phase: X% silane, (76-X) styrene, 10% DVB, 14% span 80, (e.g. for 15% silane. Styrene was decreased to 61%). Aqueous phase: 99% distilled water, 1% potassium persulphate. Phase volume = 90%, Dosing time = 10 minutes, Mixing time = 50 minutes. Polymerisation temperature = 60 °C, Polymerisation time = 24 hours.

With the aim of verifying the elements present in the SL-PHP structure, Energy Dispersive X-rays (EDX) spectroscopy was conducted on SL20. The composition for the whole area and three different spectra (points) illustrated in Figure 90, Figure 91, Figure 92 and Figure 93 depending on the image in Figure 89. The results are given in Table 30 and Table 31 for the whole area and the three points (1, 2 and 3), respectively. These clarify the presence of Carbon, Silicon, Oxygen and Sulphur in the SL-PHP but Potassium appears just in whole area (due to the small quantity of Potassium in the initiator used). An approximately similar weight percentage and atomic percentage of these elements is observed at all positions. The existence of silicon in the sample proves the integration of vinyl trimethoxy silane in the SL-PHP.

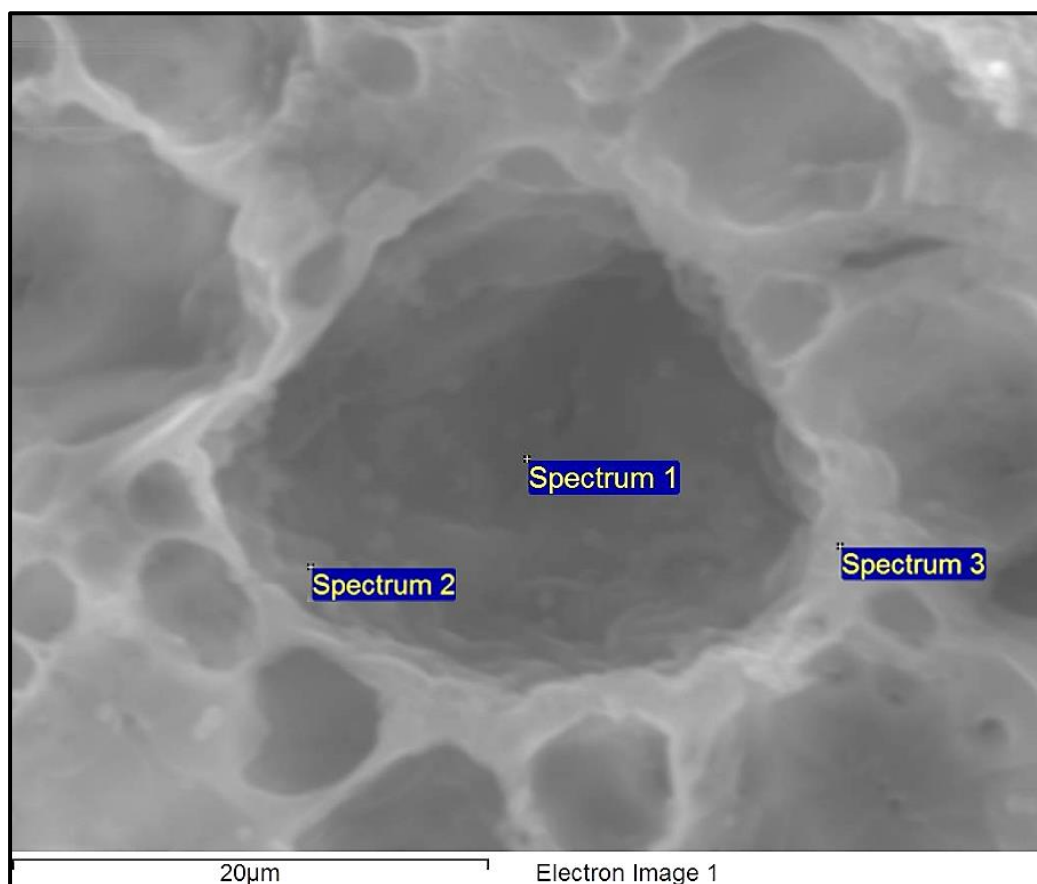


Figure 89: Three points, 1, 2 and 3 for EDX analysis of SL20.

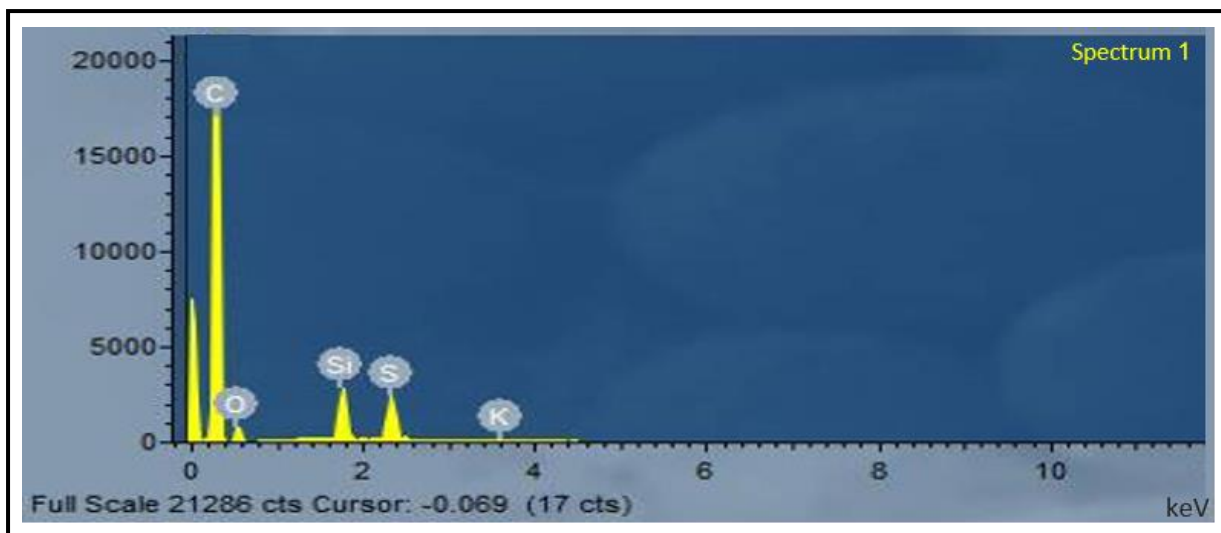


Figure 90: EDX spectrum from the complete area of image in Figure 48.

Table 30: EDX elemental composition for the all area of the image for SL20.

Element	Weight %	Atomic%
Carbon	87.90	91.91
Silicon	1.80	0.80
Sulphur	1.94	0.76
Oxygen	8.29	6.51
Potassium	0.07	0.02
Total	100.00	100.00

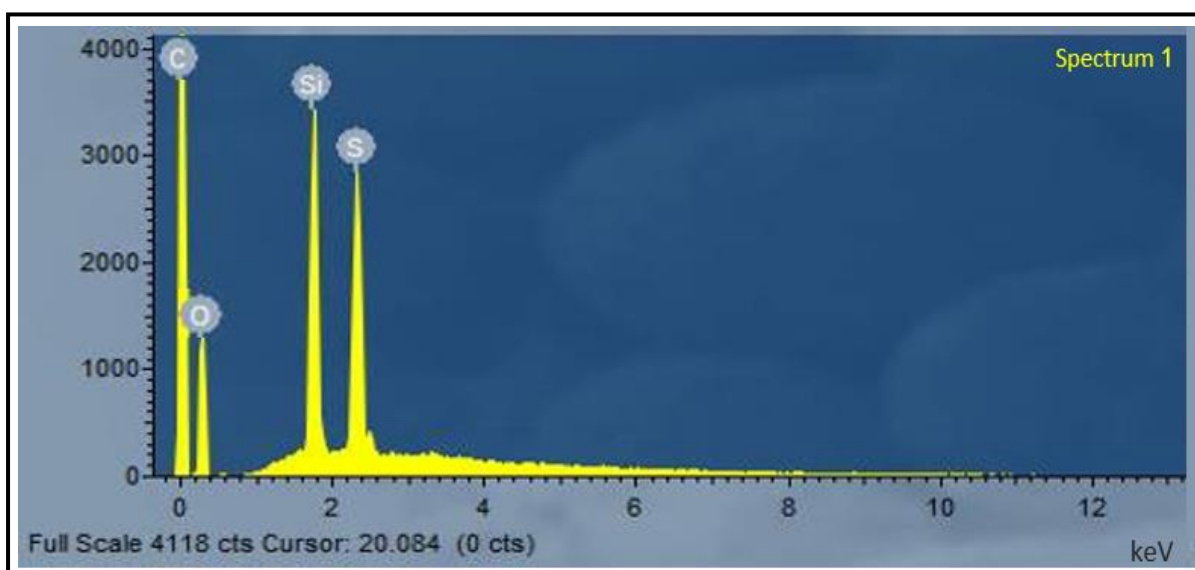


Figure 91: SL20 point 1 EDX spectrum.

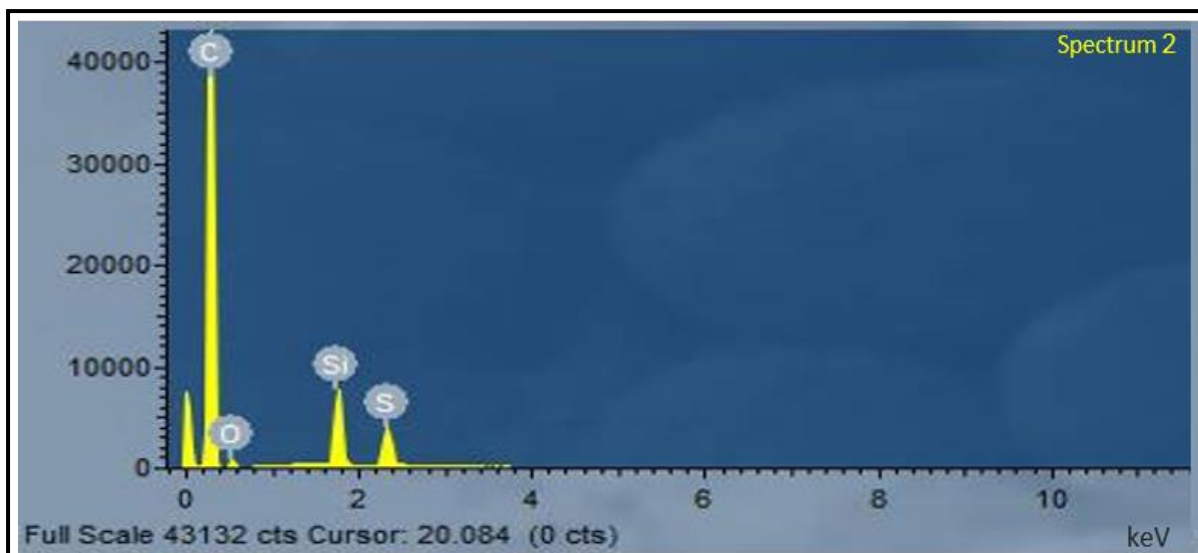


Figure 92: SL20 point 2 EDX spectrum.

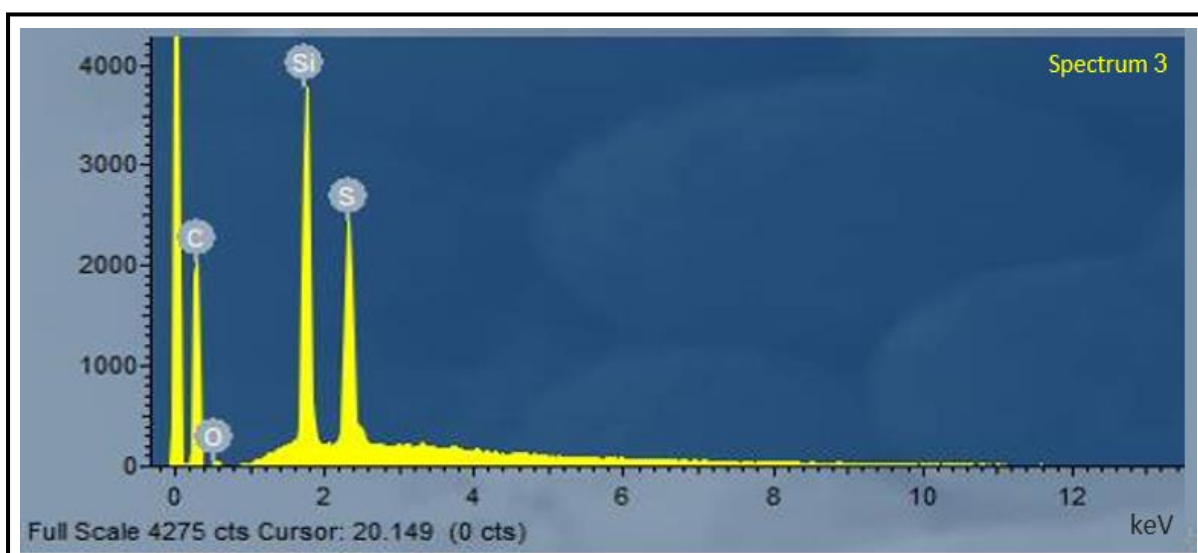


Figure 93: SL20 point 3 EDX spectrum.

Table 31: Summary of the EDX compositions for the points, 1, 2 and 3 for SL20.

Element	Point 1		Point 2		Point 3	
	Weight %	Atomic %	Weight %	Atomic %	Weight %	Atomic %
Carbon	75.39	79.58	79.09	83.47	77.17	80.74
Silicon	7.27	5.63	6.12	4.98	6.63	5.01
Sulphur	6.13	4.66	5.11	4.13	5.95	4.47
Oxygen	11.21	10.13	9.68	7.42	10.25	9.78
Total	100.00	100.00	100.00	100.00	100.00	100.00

### 5.5.2 Pore Size Distribution of SL-PHP

ImageJ software (which depends on SEM micrograph analysis) was utilised to estimate distribution of pore size. The diameters of the pores measured by the ImageJ were an underestimation of the real values because few large pores are clearly visible at the equatorial place (Menner *et al.*, 2008). The pore and interconnect pore sizes have been determined for all the SL-PHP samples, namely SL5, SL10, SL15, SL20 and SL25, with different mixing speeds of 10, 20, 30, 40 and 50 minute, as shown in Figure 52. An average of pore size was measured from the coalescence pores and interconnect pores i.e. the maximum in the pore size distribution at higher pore diameter is due to coalescence pores and the maximum in the pore distribution at lower pore size is due to interconnect pores; where the average value of pore and interconnects pore sizes ranged from 7-243  $\mu$  m. Thirty pores from each sample were measured to take the average and the results are displayed in Table 32.

The average pore size decreases with an increase of silane content from 0 to 20% and increases at higher concentration as shown in Figure 94 and Figure 95. The interconnect pore size is independent of silane concentration. The pore sizes both decrease with mixing time up to the highest time when an increase is observed. Very high concentrations of silane and largest stirring times lead to an increase in formation of coalescence pores.

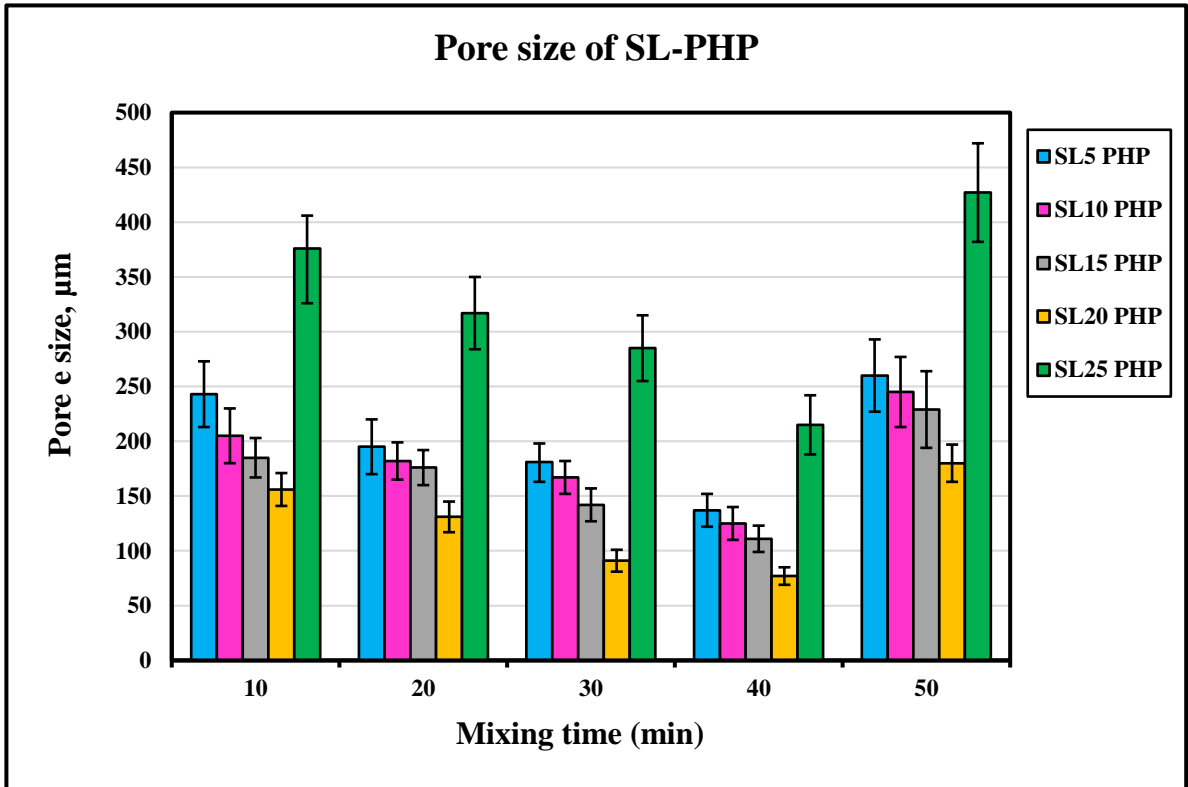


Figure 94: Plot of pore and interconnect sizes of SL-PHP samples for different mixing times.

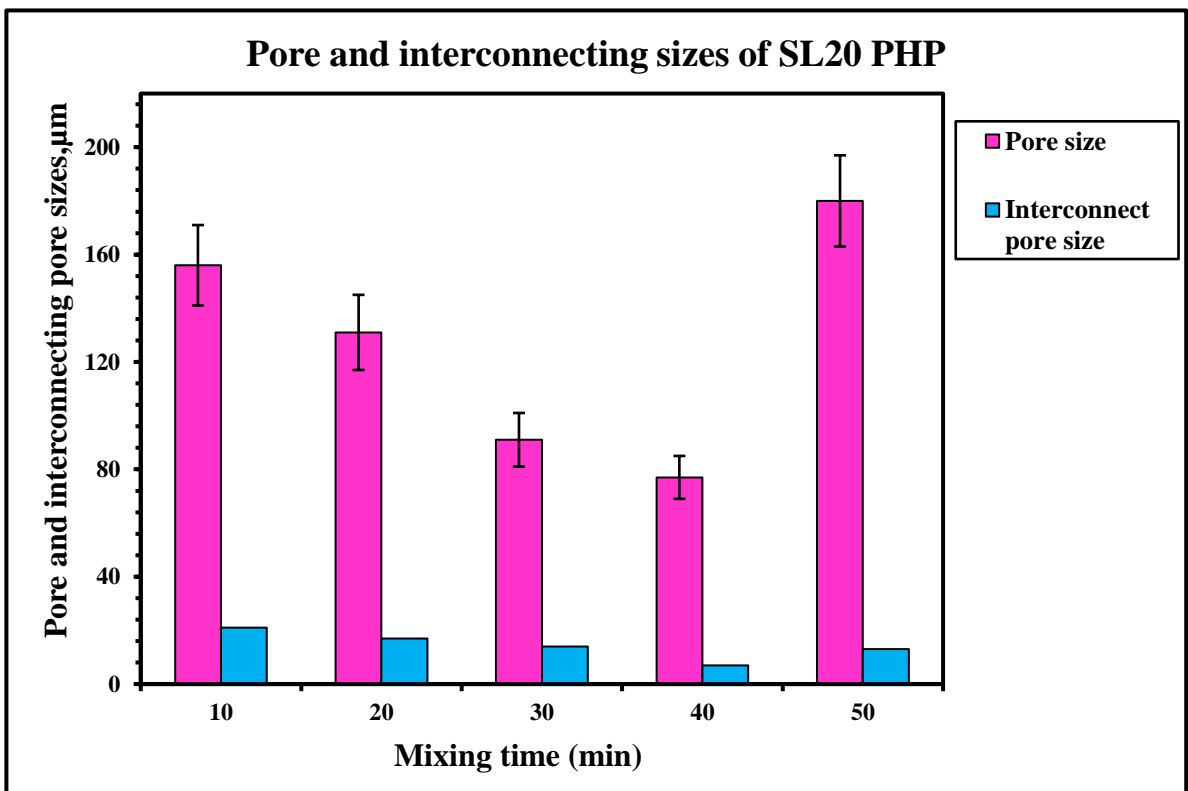


Figure 95: Plot of pore and interconnect sizes of BZ20 PHP samples for different mixing times.

Table 32: The results of ImageJ analysis of average pore and interconnect sizes, which were determined the silane PHP where 30 pores from each sample were measured.

SL-PHP sample	Mixing time (min)	Average pore size ( $\mu$ m)	Average interconnect pore size ( $\mu$ m)
SL5	10	243 $\pm$ 15	22 $\pm$ 5
	20	195 $\pm$ 11	21 $\pm$ 5
	30	181 $\pm$ 10	21 $\pm$ 4
	40	137 $\pm$ 8	14 $\pm$ 3
	50	260 $\pm$ 18	21 $\pm$ 4
SL10	10	205 $\pm$ 14	21 $\pm$ 5
	20	182 $\pm$ 12	20 $\pm$ 5
	30	167 $\pm$ 10	17 $\pm$ 4
	40	125 $\pm$ 8	16 $\pm$ 4
	50	255 $\pm$ 16	22 $\pm$ 5
SL15	10	185 $\pm$ 11	22 $\pm$ 5
	20	176 $\pm$ 10	19 $\pm$ 4
	30	142 $\pm$ 8	17 $\pm$ 4
	40	111 $\pm$ 7	12 $\pm$ 3
	50	229 $\pm$ 15	13 $\pm$ 4
SL20	10	156 $\pm$ 8	21 $\pm$ 5
	20	131 $\pm$ 8	17 $\pm$ 4
	30	91 $\pm$ 6	14 $\pm$ 4
	40	77 $\pm$ 5	7 $\pm$ 3
	50	180 $\pm$ 10	22 $\pm$ 5
SL25	10	376 $\pm$ 19	22 $\pm$ 5
	20	317 $\pm$ 17	20 $\pm$ 5
	30	285 $\pm$ 17	19 $\pm$ 4
	40	215 $\pm$ 15	18 $\pm$ 4
	50	427 $\pm$ 19	24 $\pm$ 5

### 5.5.3 Measurement of Surface Area of SL-PHP

The surface areas of SL-PHP for different percentages of Vinyl trimethoxy silane with different mixing times of 10, 20, 30, 40 and 50 minute were determined by using BET (Brunauer, Emmet and Teller) Surfer technique as described in section 4.3.1.1. The outcomes of surface area for different silane polyHIPE polymers are presented in Table 33 and Figure 96. In general, it is noticed that the SL-PHP surface area increases slightly with an increase in the percentage of silane, and then increases significantly at 20% followed by a sharp decline at 25% silane. In addition, it can be seen that the highest surface area of SL-PHP was obtained at mixing time of 40 minutes, while the lowest surface area of SL-PHP was obtained at mixing time of 5 minutes. This outcome is compatible with the SEM image (structure of SL20 PHP) shown in Figure 88.

Table 33: Surface area of silane polyHIPE.

SL-PHP sample	Percentage of silane (%)	Mixing time (min)	Surface area (m <sup>2</sup> /g)
SL5	5	10	7±1
		20	10±2
		30	12±2
		40	26±3
		50	14±2
SL10	10	10	9±1
		20	14±1
		30	23±3
		40	38±3
		50	26±3
SL15	15	10	14±2
		20	17±2
		30	31±3
		40	43±3
		50	31±3
SL20	20	10	15±2
		20	21±2
		30	43±3
		40	98±5
		50	55±4
SL25	25	10	12±1
		20	18±2
		30	20±2
		40	34±3
		50	26±2

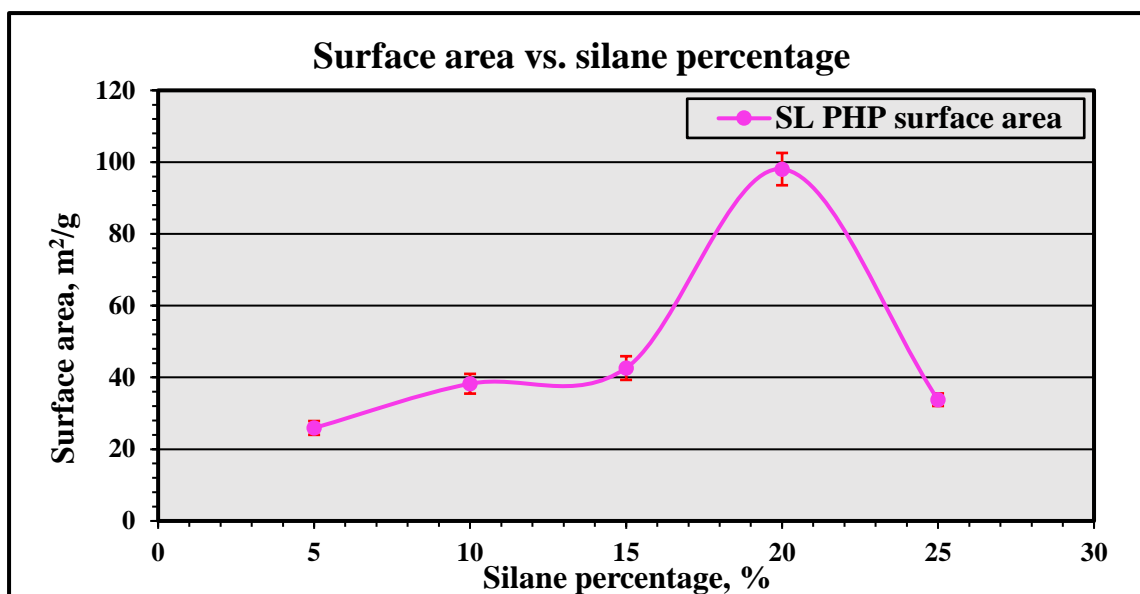


Figure 96: Plot of surface area for various percentages of silane PHP with standard errors for mixing time of 40 minutes.

With the aim to study the impact of leaching through process of washing, the analysis of surface area has been conducted by utilising the unwashed SL20 PHP. Table 34 shows the consequence for bottom and top discs from a single tube. The surface area of the bottom disc is 2 m<sup>2</sup>/g higher than the top disc but this is within the experimental errors. It shows that the difference of the various discs surface areas is not due to the leaching through the process of washing. Consequently, for more trials of silane, the washing by the soxhlet apparatus was carried under the same conditions prior to measurement to minimize scatter.

By comparison between the surface area of SL20 before and after washing, it was found that it was about 30 m<sup>2</sup> more than after washing, may be due to the presence of unreacted chemical.

Table 34: Surface area for different discs of SL20 PHP (unwashed) from a single container.

SL20 sample	Surface area, m <sup>2</sup> /g
Top disc	127±5
Bottom disc	129±5

#### 5.5.4 Water Uptake of SL-PHP

The water uptake of the produced SL-PHP for different percentages of vinyl trimethoxy silane with different mixing times of 10, 20, 30, 40 and 50 minute was examined, where three discs for each sample were tested, the results are displayed in Table 35 and Figure 97. The outcomes

illustrate that the process of sulphonation increases the ability of water uptake of all samples of SL-PHP. Moreover, the results illustrate that the sulphonated SL-PHP samples have a high water uptake capacity that is directly proportional to the increase in silane percentage up to 20%, after which it declined. The water uptake of sulphonated SL20 at mixing time of 40 minutes was significantly higher, 5.8 fold compared to unsulphonated SL20. While, sulphonated SL5 PHP at mixing time of 10 minutes obtained the lowest water uptake of 2.2 times more than unsulphonated SL5 PHP.

Table 35: Water uptake for various SL-PHP samples (before and after sulphonation) for different mixing times.

SL-PHP sample	Mixing time (min)	% water uptake of unsulphonated sample	% average water uptake of unsulphonated sample	% water uptake of sulphonated sample	% average water uptake of sulphonated sample	water uptake fold
SL5	10	77-101	89	164-222	196	2.2
	20	75-99	88	178-234	204	2.3
	30	81-100	90	236-278	254	2.8
	40	80-97	88	243-295	265	3.0
	50	79-98	87	210-266	235	2.7
SL10	10	92-114	103	175-226	206	2.0
	20	80-102	91	224-256	238	2.6
	30	82-95	87	256-342	297	3.4
	40	75-91	83	282-397	335	4.0
	50	81-99	88	233-284	257	2.9
SL15	10	88-103	90	186-227	207	2.3
	20	83-100	90	201-263	234	2.6
	30	85-101	93	267-287	271	2.9
	40	78-97	87	335-472	411	4.7
	50	83-102	92	247-290	268	2.9
SL20	10	76-94	83	208-304	249	3.0
	20	72-90	81	211-309	252	3.1
	30	77-98	86	243-352	303	3.5
	40	75-96	84	394-580	488	5.8
	50	72-90	82	255-373	312	3.8
SL25	10	79-98	89	162-209	188	2.1
	20	78-95	86	174-220	191	2.2
	30	85-103	92	210-245	230	2.5
	40	86-107	96	261-292	279	2.9
	50	82-104	93	192-230	214	2.3

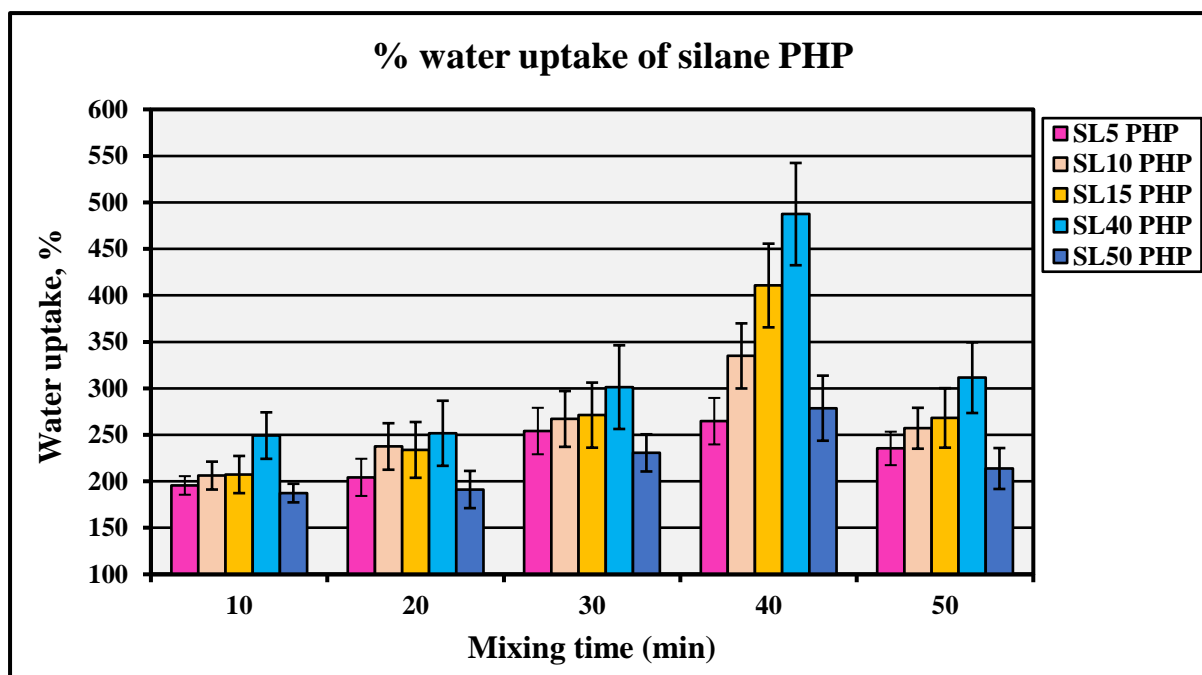


Figure 97: Plot of water uptake of silane PHP for different percentage of silane with various mixing times.

### 5.5.5 FTIR Analysis of Silane PHP

The silane PHP spectra exhibited in Figure 98 through Figure 102 demonstrate the success of the silane integration into the PHP. The band at 1050 to 1230  $\text{cm}^{-1}$  shows remarkable variance in the peak shape (generated with increased silane) that is attributed to unsymmetrical vibration of (-Si-OCH<sub>3</sub>) (Barzin *et al.*, 2006). The peak at this band includes two peaks, as illustrated in Table 36. For rest of the peaks, at the band less than 1050  $\text{cm}^{-1}$  there are some absorption peaks, such as very strong peak at 698  $\text{cm}^{-1}$  and moderate intensity peak at 758  $\text{cm}^{-1}$ , followed by weak intensity peaks at 798, 799, 830, 833, 836, 837, 903, 905, 906, 908, 954, 963, 967, 968 and 1031  $\text{cm}^{-1}$ . The peaks (very strong) at 698 and 758  $\text{cm}^{-1}$  are attributed to C-H bending of the aromatic ring (out-of-plane) (Jiang and Zeng, 2010; Vinodh *et al.*, 2010). According to Mercier *et al.* (2000), the bands of 798, 799, 833, 836 and 837  $\text{cm}^{-1}$  are attributed to a ring of phenyl whilst 903, 905, 906, 908, 954, 963, 967 and 968  $\text{cm}^{-1}$  are attributed to a mixed band of a strong group of vinyl, weak to medium disubstituted phenyl ring and weak monosubstituted phenyl ring. Absorption peaks of 1254, 1370, 1381, 1382, 1386, 1452, 1453, 1493 and 1494  $\text{cm}^{-1}$  are attributed to bending vibration of aromatic ring backbones (-CH-) while 1599, 1601 and 1602  $\text{cm}^{-1}$  are attributed to bands of (C=C) in aromatic rings (Vinodh *et al.*, 2010). The bands of 1734, 1736, 1744, 1979 and 2035  $\text{cm}^{-1}$  are attributed to (C=C) in vinyl rings (Herrera *et al.*,

2005). According to Rubino *et al.* (2010), absorption peaks of 2846, 2850, 2851, 2852, 2913, 2915, 2922, 2923, 2929 and 2981  $\text{cm}^{-1}$  are attributed to (C–H) stretching vibrations of methylene and methyl groups. Absorption peaks of 3026, 3027, 3060, 3063, 3655, 3657 and 3667  $\text{cm}^{-1}$  are attributed to (=C–H) in aromatic rings (Herrera *et al.*, 2005). In the bands of less 1050  $\text{cm}^{-1}$ , it was noticed that the transmittance intensity is inversely proportional to the percentage of silane, which means that increased percentage of silane reduces transmittance intensity. Consequently, the variations in the intensity of peaks proved that the functionalization of silane inside the HIPE was successful.

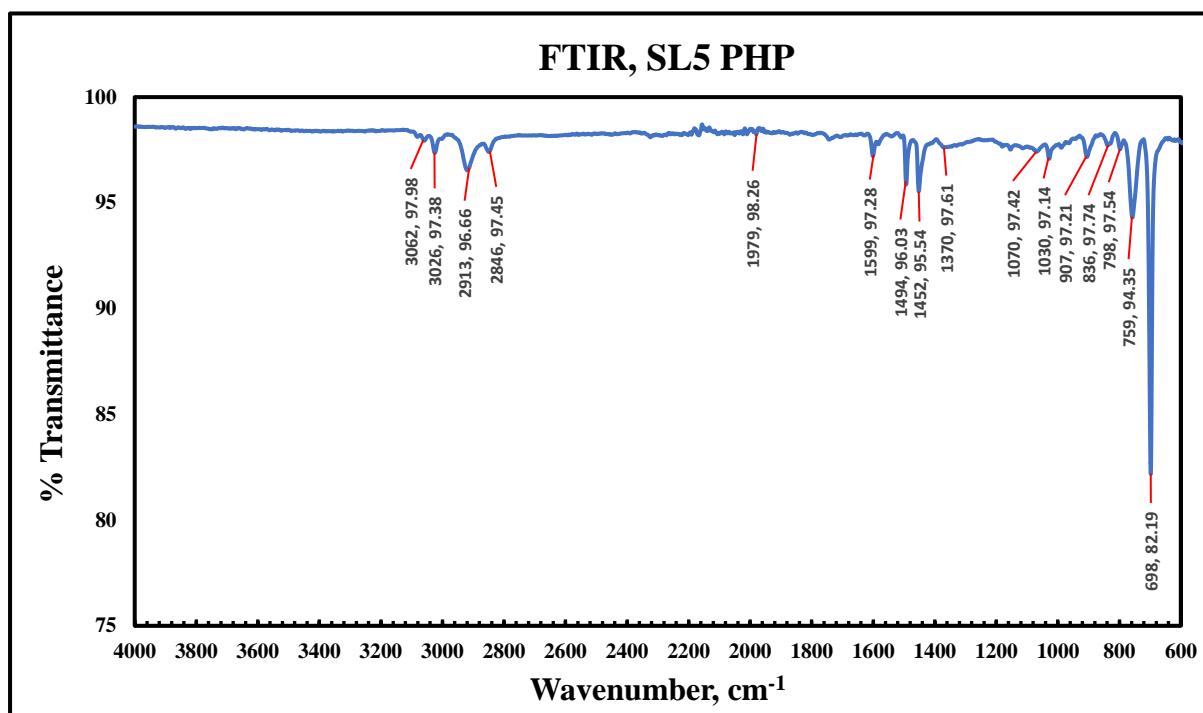


Figure 98: FTIR spectrum for SL5 PHP

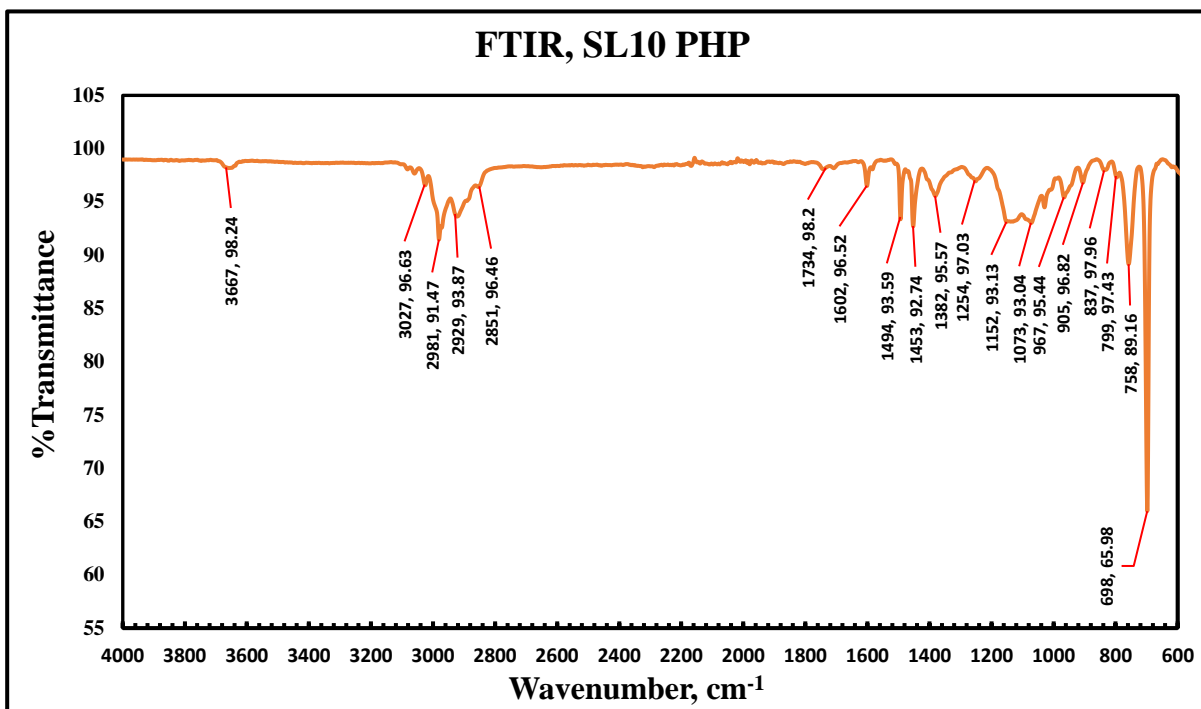


Figure 99: FTIR spectrum for SL10 PHP.

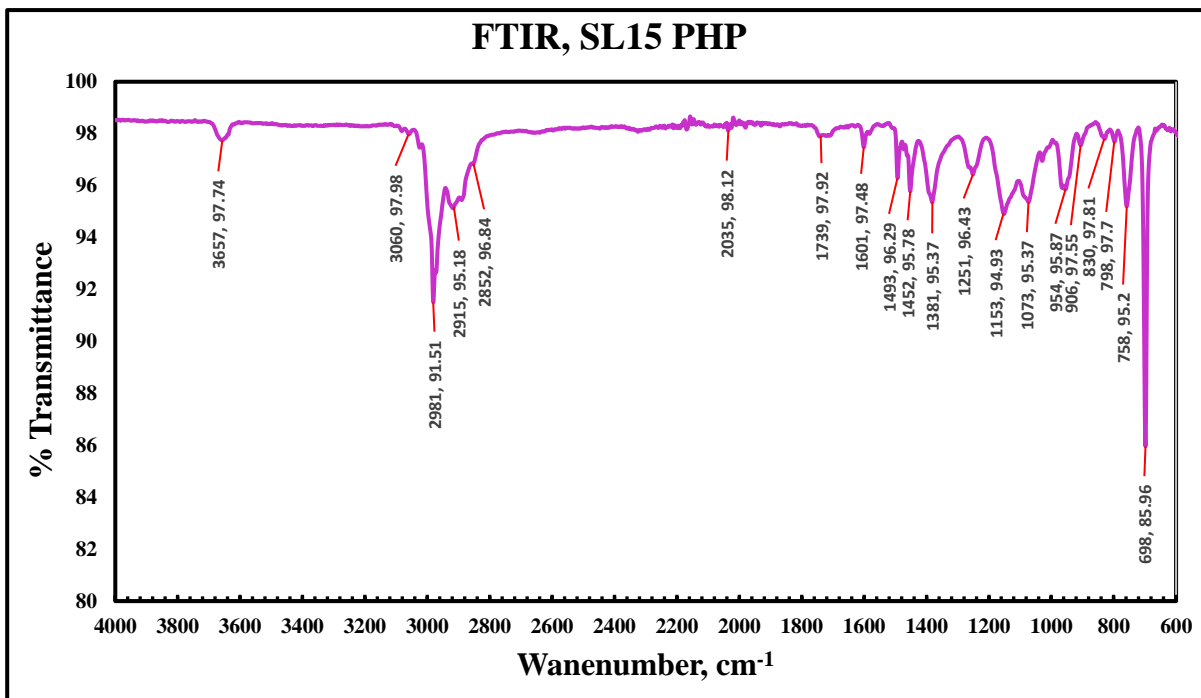


Figure 100: FTIR spectrum for SL15 PHP.

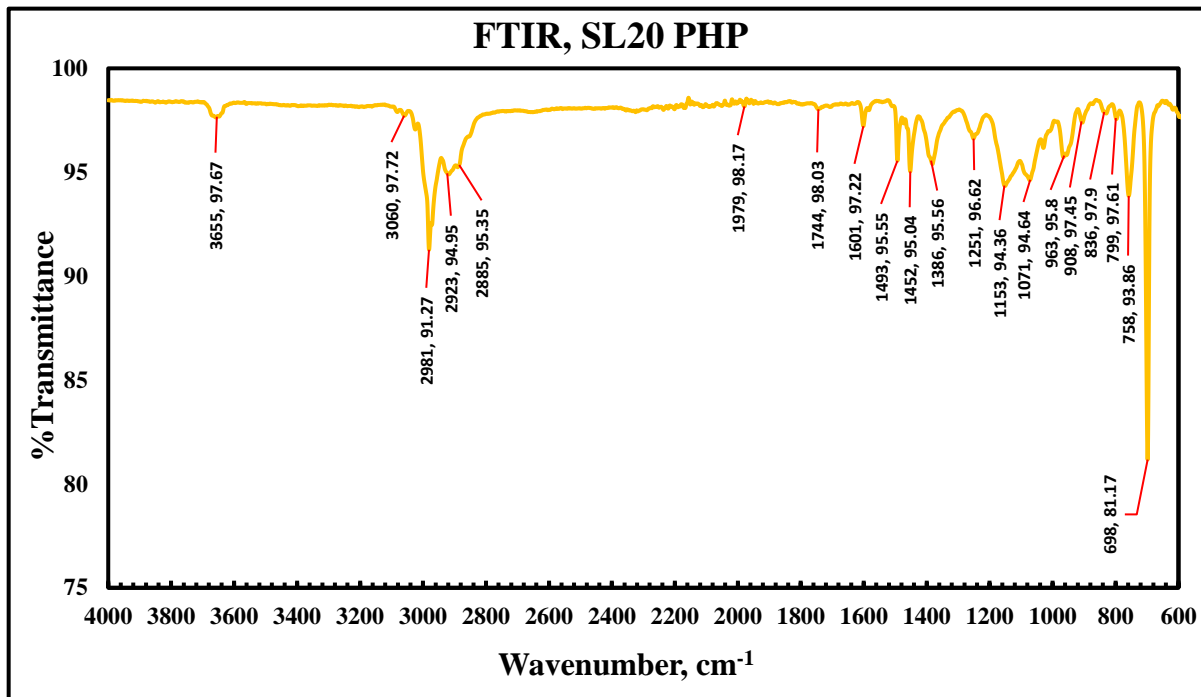


Figure 101: FTIR spectrum for SL20 PHP

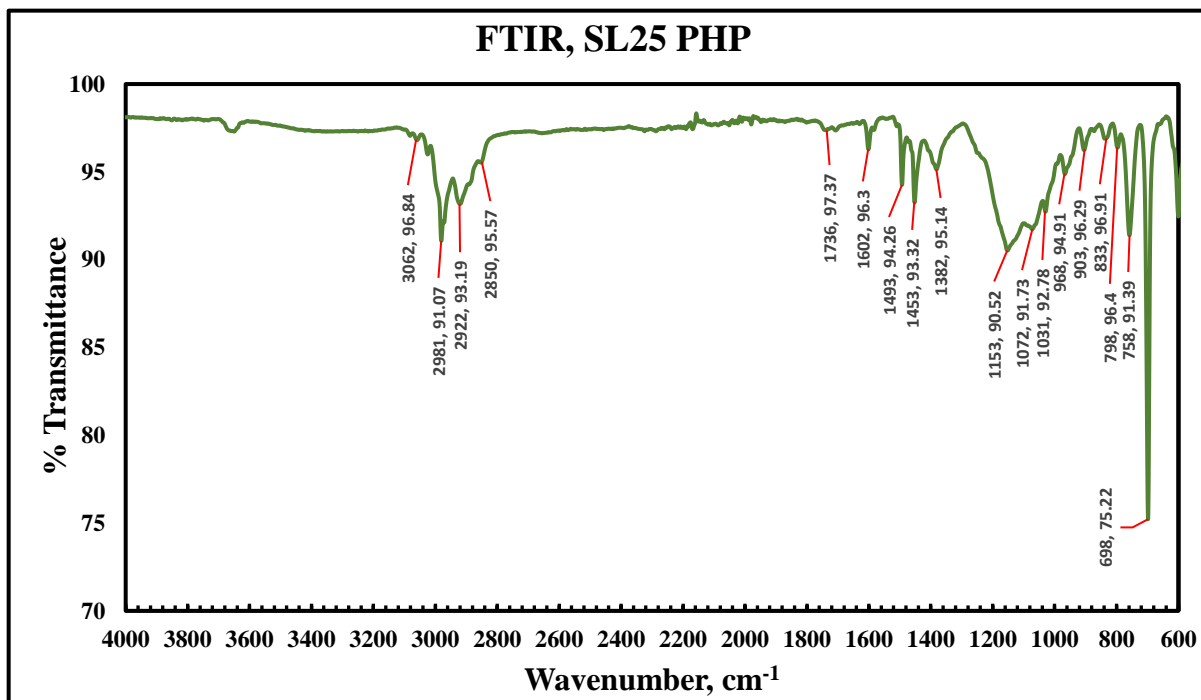


Figure 102: FTIR spectrum for SL25 PHP

Table 36: Position of two peaks of the SL-PHP samples in the stretching band between 1050 and 1230  $\text{cm}^{-1}$ .

SL-PHP sample	Peak wavenumber, $\text{cm}^{-1}$	
SL5	1070	1030
SL10	1152	1073
SL15	1153	1073
SL20	1153	1071
SL25	1153	1072

There is a clear variance in the ( $-\text{Si}-\text{OCH}_3$ ) peaks generated in the extent of the band from 1050 to 1230  $\text{cm}^{-1}$ . The weakest absorption intensity is for SL5 and the strongest absorption intensity is for SL25. The attributed the silane percentage, the greater the strength of adsorption as illustrated in Figure 103. The SL25 spectrum has distinctly different shape in this region. This suggests that for this sample the amount of silane is greater than can be accommodated at the water-oil interface in PHP production.

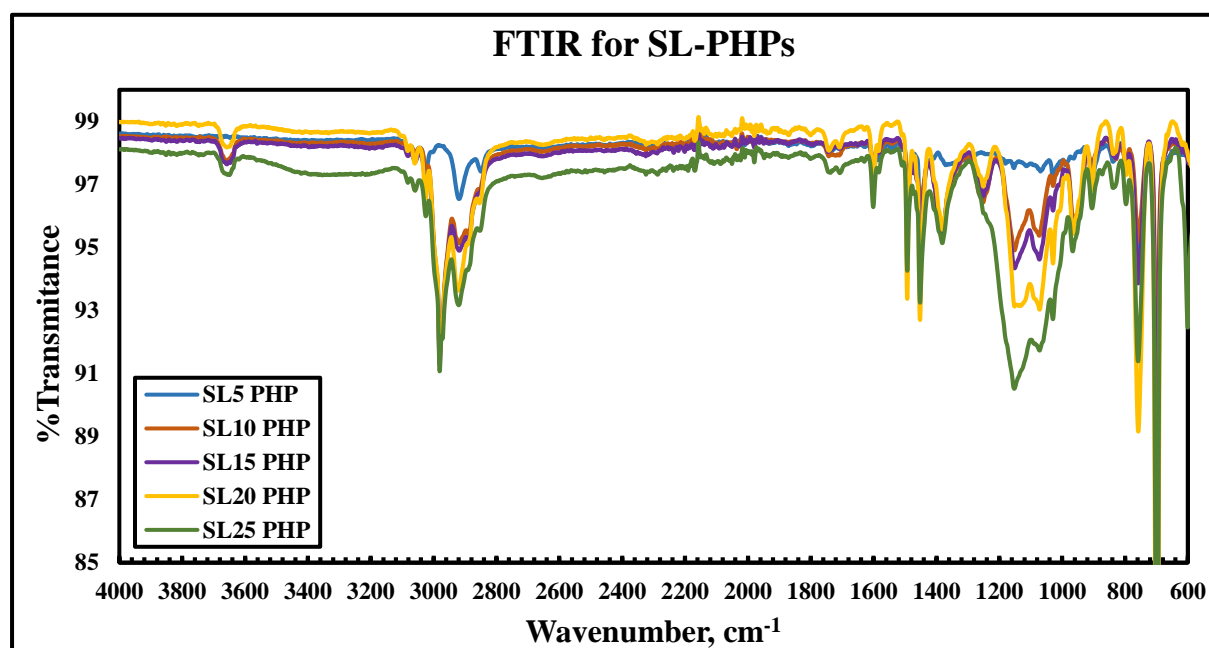


Figure 103: FTIR spectrum for all SL-PHPs for comparison.

### **5.5.6 Summary**

The addition of silane to the oil phase has successfully increased the hydrophilicity and reduced the pore size up to 20% addition. However, sulphonation is still necessary to generate the greatest water uptake. This suggest that the silicon containing groups in the polymerised cell walls do not occupy the aromatic ring positions where sulphonation can occur. The combined effect of Silicon and Sulphur groups can then be achieved.

### **5.6 Optimum Samples**

After analysis the results of producing the four kinds of polyHIPEs, it was found that the best samples that are characterized by a large surface area and a high ability of water uptake are SL20 PHP, B50 PHP, IS40 PHP and BZ25 PHP for SL-PHP, B-PHP, IS-PHP and BZ-PHP, respectively. They will be tested in a separating water experiments from water-in-crude oil emulsions by using the electrostatic technique. The results will then be evaluated to know their ability of water separation.

---

## CHAPTER SIX

---

### 6. PROCEDURES OF FORMING WATER-IN-CRUDE OIL EMULSION AND DEMULSIFICATION OF WATER-IN-CRUDE OIL EMULSION USING COMBINED PHP DEMULSIFIER AND ELECTROSTATIC FIELD

#### 6.1 Overview

This chapter of the thesis is presented in four major parts.

- i. The first part describes the apparatus and experimental procedures employed for the formation of water-in-crude oil emulsions.
- ii. The second part presents the design of the separation process of crude oil and water using an electrostatic technique.
- iii. The third part shows the effect of emulsification variables for respect to:
  - Impact of emulsification variables on stability and viscosity of the emulsions.
  - The crude oil emulsion stability.
- iv. The fourth part describes the conductivity measurement of crude oil emulsions.

#### 6.2 Formation of Water-in-Crude Oil Emulsion

Midland Refineries Company (MRC) supplied the crude oil used in the separation experiments. This crude oil is one product of the oil fields in southern Iraq. The characterization of this crude oil is presented in Appendix 1. It has dark brown color approaching to black and a specific gravity of 0.8067. The viscosity was measured by a co-axial cylinder Geometry Haak VT 550 viscotester manufactured by Thermo Fisher Scientific Company at a temperature of 25 °C and shear rate of 1100 s<sup>-1</sup> and was found to be 86 mPa.s. Brine solution was prepared by using NaCl, CaCl<sub>2</sub> and MgCl<sub>2</sub> salts and deionized water.

Equal volumes of crude oil and water phases were utilised to prepare water-in-crude emulsions, where three kinds of salts have been used to prepare the aqueous phase NaCl, CaCl<sub>2</sub> and MgCl<sub>2</sub> to mimic seawater. By the dilution process the aqueous phase was prepared by adding these salts (anhydrous powder forms) to deionized water. The aqueous phase was had no included

artificial surfactants, a density of 1.028 g/l and contained 5.0 g/l  $MgCl_2$ ; 28.1 g/l NaCl; and 0.6 g/l  $CaCl_2$ .

The model emulsion was prepared in a stainless steel mixer (laboratory scale). The dimensions of homogenizer were a diameter of 0.12 m, height 0.14 m and capacity of 1.6L. The stirrer consists of two 10 cm simple paddle fins stacked at 90 degrees to each other and was hung into the vessel through a hole in the middle of the cover while the bottom of the impeller was placed at the closest possible distance to the bottom of the mixing vessel ( $< 1\text{ mm}$ ) to make sure a good mix is achieved. The rotation speed for this stirrer is over a range 100 to 2000 rpm which was achieved by using an electric motor. To achieve both accessibility and stability the whole unit was mounted onto a frame. Fig 104 shows the schematic drawing of the equipment utilized for the emulsion preparation as described in a previous study (Akay and Vickers, 2003).

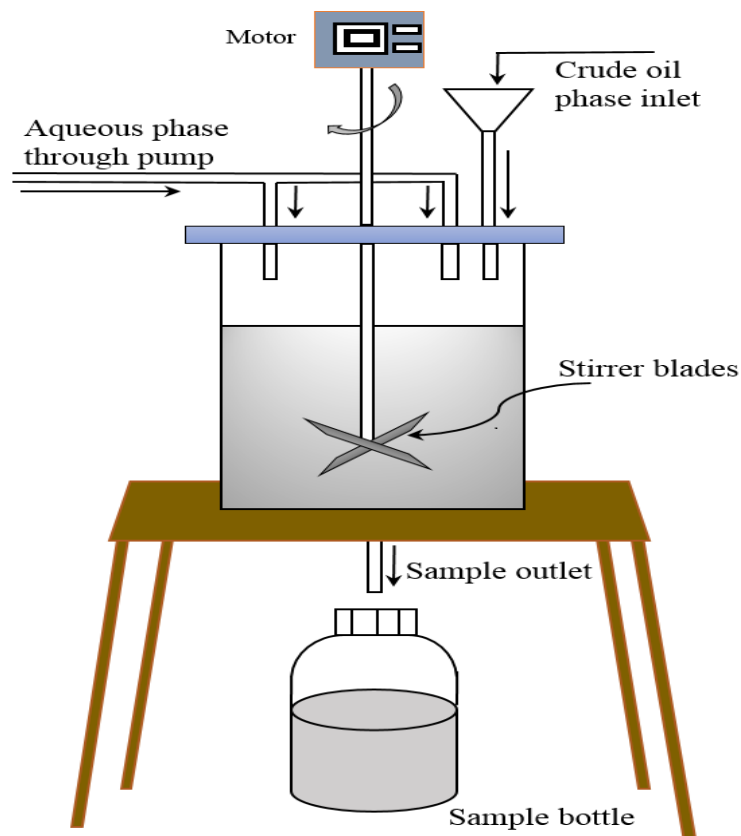


Figure 104: Schematic diagram of the mixer/homogeniser utilised in the emulsion preparation.

With a view to get an emulsion that has a high stability which is easily produced and is similar to that formed with crude oils near the wells and in the offshore oil rigs, a range of trials have been undertaken. Various blending speeds (400, 800 and 2000 rpm) and mixing times (10,20,

25, 30, 40 and 50 minutes) have been utilized in combination and stability tests for the resulting emulsions have been carried out. Blending speed plays the most important role in determining the stability of the produced emulsion rather than mixing time. After three and a half months standing time the most stable emulsion which did not totally and normally demulsify was obtained by using a blending speed of 2000 rpm for forty minutes conducted on the crude oil and formulated aqueous phase. By using a volume of 500 ml for both crude oil and aqueous phase test emulsions were then prepared at a total volume of 1000 ml. Firstly, the crude oil was put manually into the vessel using the tube that penetrates the cover. The aqueous phase was then pumped into the crude oil inside the vessel utilizing a peristaltic pump for a period of ten minutes while mixing continued at speed of 2000 rpm. Figure 105 illustrates the process of preparation in a simplified way. When the preparation process was completed, through an outlet located at the bottom of the vessel, the prepared emulsion was emptied into another container ready to be utilized immediately in the next step of the experiment. This emulsion was prepared just prior to undertaking a separation experiment (on the same day on which the experiment was done) in order to avoid any impact of the ageing that may appear in the emulsion. The viscosity of the 50:50 water-in-crude oil emulsion at shear rate of  $1100 \text{ s}^{-1}$  was 1040 mPa.s and its electrical conductivity at  $25^\circ\text{C}$  was  $0.82 \text{ }\mu\text{s/cm}$

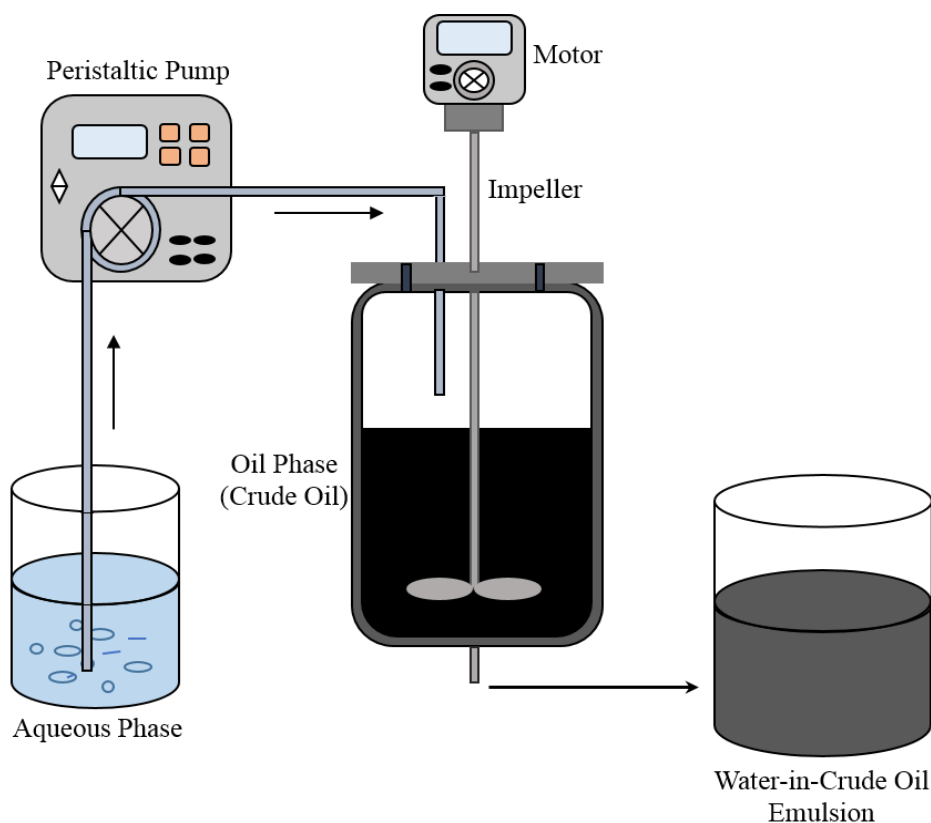


Figure 105: Schematic representation of water in crude oil emulsion preparation

## 6.3 Separation of Crude Oil and Water

The experiments of demulsification that were conducted consist of the two following steps.

- 1- Formulation of a high stability water-in-crude oil emulsion: A water-in-crude oil emulsion was prepared from crude oil supplied by Midland Refineries Company and a freshly prepared brine solution. Numerous batches were prepared of water-in-crude oil emulsions by using various mixing times and blending speeds. The stability of these emulsions was assessed and the viscosity was measured over a specific duration of time. The water-in-crude oil emulsion that had highest shelf life more than 3 months was selected to be used in the following step of the experiment.
- 2- The experiment of demulsification utilizing combined application of PHP demulsifiers and an electric field. The prepared water-in-crude oil emulsion was totally blended with grains of PHP of a specific size range, then pumped through the high-voltage electrostatic separator at specific voltages and flow rates. Both of the separated aqueous and oil phases were collected and the efficiency of the experiment of demulsification evaluated according to the amount of collected phases.

### 6.3.1 Separator Design

A perspex (electrostatic) electric field separation cell was used to carried out water-in-crude oil separation experiment. The electrostatic apparatus was constructed using a Perspex vessel of 12 cm height, 13 cm length and 5 cm width, the parts of the vessel were held together using plastic screws and glue. The vessel was equipped with a copper electrodes (upper and lower electrodes) were used instead of steel electrodes which was used by Akay and Vickers (2003), due to a higher electrical conductivity of the former compared to that latter. Moreover, the distance between the two electrodes has been reduced from 9.1 cm used by Akay and Vickers (2003) to 7.2 cm to ensure a strong electric field, since the strength of the electric field is inversely proportional to the distance between the electrodes and this in turn helps the water droplets to coalesce and separate from crude oil (Bresciani *et al.*, 2010). The electrode were used in the form of plates of copper (the upper plate was non-perforated and connected to the ground to block short-circuiting, while the bottom plate was perforated and fixed to the bottom of the apparatus) and with a thickness of 2 mm to achieved an electric field that includes most of the size of separator compared to the cylindrical electrodes that provide an electric field that does not include most of the size of the separation apparatus (Kim *et al.*, 2002). In addition,

three circular center tubes (cavity) of 8 mm diameter were installed on both sides of the apparatus, which were used for the w/o emulsion inlet, water outlet and w/o the demulsified emulsion outlet respectively, with three valves used to control the flow rate of the emulsion and water as shown in Figures 106. The separation cell consists of an AC high voltage generator (up to 5 kV) which was used to generate the electric fields that created the coalescence of the dispersed water droplets and their expansion to bigger drops, which finally fall freely because of electrostatic force or gravity and collected at the bottom of the system.

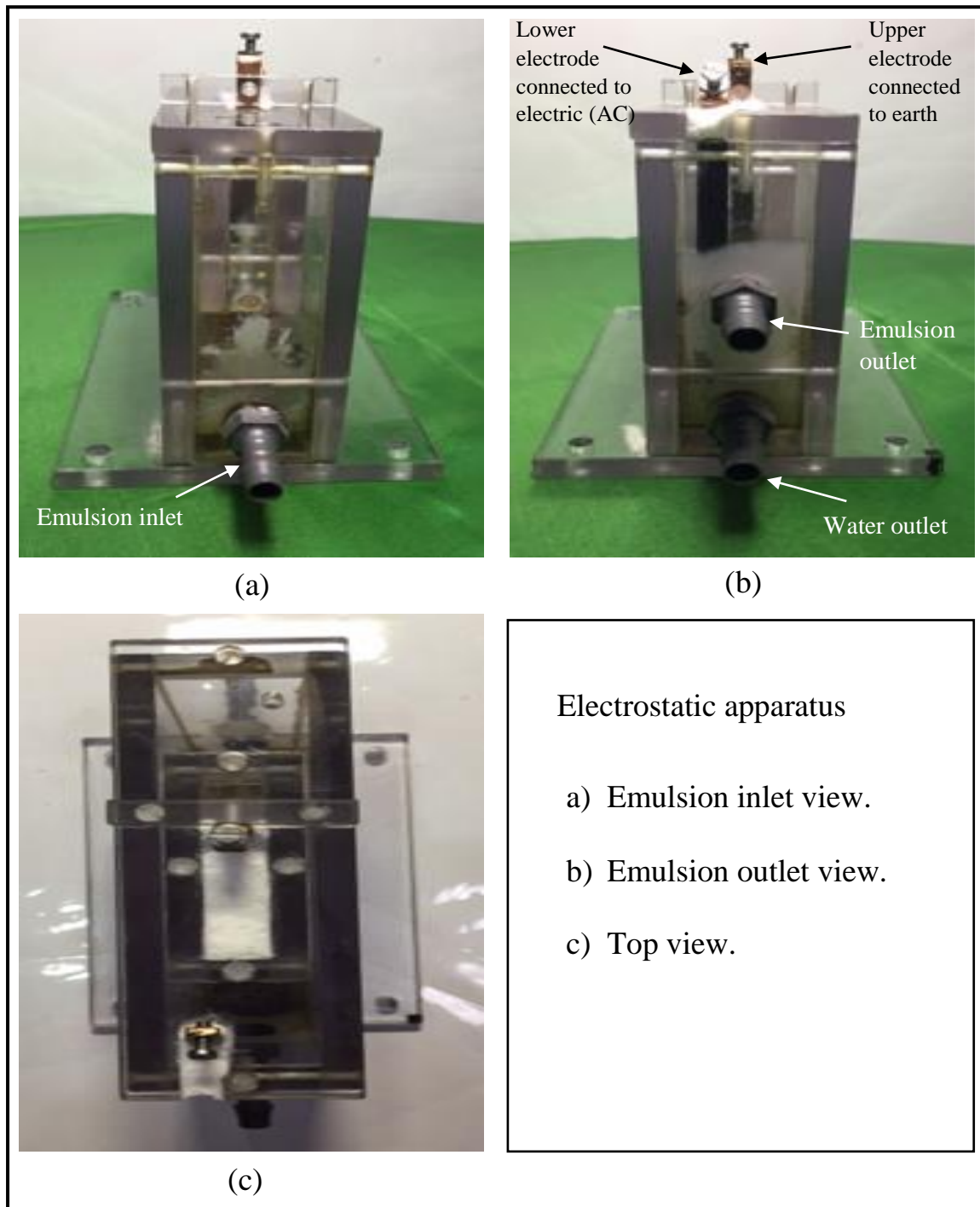


Figure 106: Photographic image of the Perspex (electrostatic) electric field separation cell after use.

0.5 gm of demulsifier was added into 1000 gm emulsion before sending the emulsion through the separation cell and exposure to high electric field, followed by continuous stirring of the mixture utilizing magnetic stirrer during the separation process. The stirred mixture was pumped from the feeding pump through the separator until it was exhausted. For the continuity of the demulsification process, water-in-crude oil emulsion is mixed with the polyHIPE grains in a 5-liter vessel using a magnetic stirrer. This tank uses to compensate for the lack of feeding tank that feeds the separator apparatus as shown in the Figure 107 (a). Both the transformer which is used to transfer the electric voltage of 240 V to 5 KV to the electrode and the electrostatic separator apparatus were placed inside the PVC box to avoid electric shock, the top electrode was earthed while the bottom electrode was linked to the transformer (high voltage source) as shown in Fig 107 (b).

A high voltage electric field of up 69 kV/m AC was available by applying a voltage to the bottom electrode gradually from zero. The power supply equipment was equipped with an ammeter scaled to 13 mA, which is used for a safety reasons; when the current reaches 13 mA the power supply cut off automatically. Thus, 5000 V was applied as the highest level of potential to avoid the current leakage that may occur due to breakdown at high voltage levels. As this system may be dangerous due to the presence of both high electrical voltage and a flammable oil, so, after the unit is turned off, it was left idle for a period of more than ten minutes before any further processing to insure there was no residual electric charge left. The samples were collected from the top and bottom electrodes using glass-measuring cylinders and the emulsion was allowed to duly separate into water and oil phases for ten minutes followed by evaluating the degree for overall separation after 1 hour and 24 hours.

The process of separation of the emulsion was carried out using multiple applied voltages (1, 2, 3, 4 and 5 kV) and different flow rates of the emulsion (100, 250, 500, 750, 1000, 1250 and 1500 ml/min), where the applied voltage was kept constant and the flow rate at the emulsion inlet was varied as mentioned above. The electric field strength is described as the voltage drop per unit distance, which depends on the space between the two copper electrodes. The length between two copper electrodes was 72 mm in this study. The external electric field used in this specific experiment was  $13.89 \text{ kV.m}^{-1}$  or ca.  $14 \text{ kV.m}^{-1}$  at an applied voltage of 1kV. While, for rest of the applied voltages mentioned above the external electric field was 28, 42, 56 and  $69 \text{ kV.m}^{-1}$ , respectively. However, the actual field inside the electrocoalescer cannot be determined accurately because various factors like the unknown behavior of the crude oil/water interface and the effect of insulation loss on its magnitude.

After the end of separation process, collection, drying and SEM/EDX analysis were carried out for the spent demulsifier/adsorber. In separation experiments various types of PHP were used as a demulsifier/ adsorber in order to evaluate the relevance between their chemical and physical structure and how they correlate with performance. The efficiency of the separation for the electro-demulsification process was evaluated by determining the volume of water collected immediately after separation in both outlets (Figure 107 (b)).

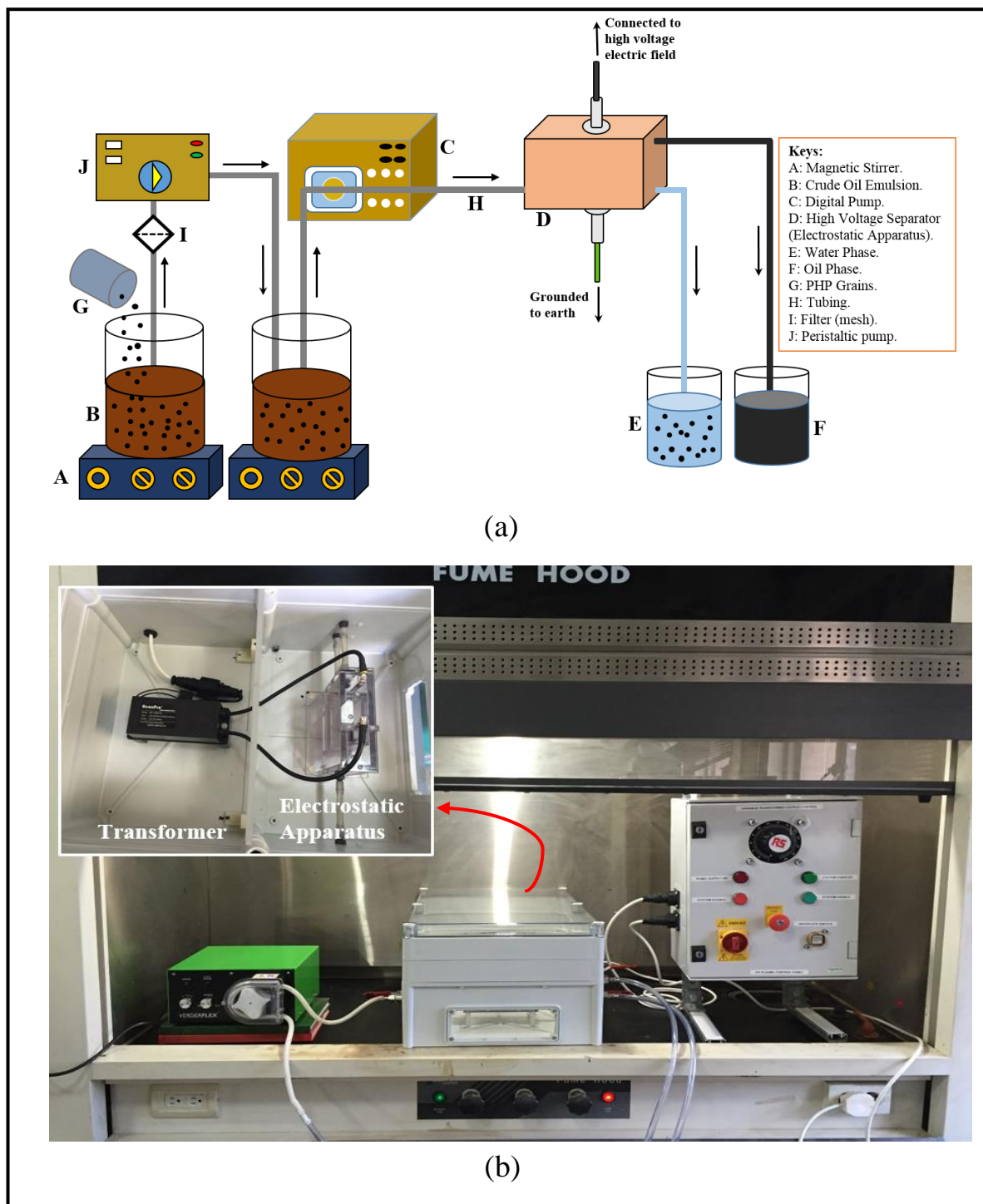


Figure 107: (a) Schematic diagram of the demulsification setup. (b) Photographic image of the demulsification setup.

## 6.4 Effect Emulsification Variables

### 6.4.1 Impact of Emulsification Variables on Stability and Viscosity of the Emulsions

Table 37 lists the several batches of water-in-crude oil emulsions that were prepared in order to obtain the high stability emulsion by using various processing parameters, namely mixing time and agitation speed that would be utilized in the separation experiments of the water/oil emulsions. An equal ratio of the aqueous and oil phases (50%) was used (to mimic the water content in southern Iraqi crude oil after the extraction process namely of 47-53%) without adding any artificial surfactants to stabilize the emulsions because of the natural surfactants and impurities that were already present in crude oil (i.e. asphaltenes, wax, resins, nitrogen, oxygen, sulphur and some other elements mostly metals like iron, copper, vanadium, nickel, etc.). The prepared emulsions stability was based on the reduction of particle size during the blending and energy input of the agitating process.

Table 37: Specifics of the prepared water-in-crude oil emulsions.

Water-in-crude oil emulsion	Volume of oil phase (ml)	Volume of aqueous phase (ml)	Mixing speed (rpm)	Duration of agitation time (min)	Stability* (day)
I	500	500	400	10	12
II	500	500	400	20	17
III	500	500	400	30	23
IV	500	500	400	40	29
V	500	500	400	50	29
VI	500	500	800	50	61
VII	500	500	2000	25	114

Stability\*: period of time, which a water-in-crude oil emulsion takes to totally demulsified naturally.

By using the co-axial cylinder Geometry Haak VT 550 viscotester measurement, the viscosities of the original crude oil and these emulsions were measured, these measurements have been undertaken to monitor the impact of agitating speed and the agitating time on the stability of the water-in-crude oil emulsions (i.e. droplet size).

In theory, the viscosity of an emulsion is inversely proportional to the droplet size. Thus, with the decrease in the droplet size and the distribution of particle size getting narrower with raising

agitating speed and agitating time, the viscosity of the prepared emulsions was expected to be high. Figure 108 depicts the experimental results that were found to be in agreement with this explanation to a certain extent. The figure obviously demonstrates that the origin crude oil has remarkably lower viscosity in contrast to the crude oil emulsions and displays Newtonian behaviour as the viscosity of the crude oil stayed constant as a function of shear rate. On the other hand, the prepared emulsions show small non-Newtonian flow features in terms of pseudo-plastic behaviour though the decline in viscosity was small as a function of shear rate.

The emulsion viscosity also displays a growing trend with the agitating time and agitation speed with the most stable emulsion (emulsion VII) found to have the highest viscosity. Furthermore, a clear jump in viscosity is remarkable when the agitation speed was raised by a factor of two (e.g. from 400 to 800 to 2000 rpm) in contrast to the limited effect of extending the agitating time only. At the later stage of mixing, the changes in viscosity were minimal; raising the mixing time more than an ideal time achieves only a small improvement in the emulsion properties since, apparently, after the optimum period of time, there is no significant decrease in the particle size.

Increasing the mixing time is more significant for the stability of the emulsions produced (Table 37). However, although several of the emulsions have been agitated for fifty minutes (the lengthened agitating time) at low (400 rpm) or moderate (800 rpm) speed of agitation, the produced emulsions were stable for up to two months only. Nevertheless, when the speed of agitation was increased to 2000 rpm, the prepared emulsions were more stable in spite of the fact that they had been emulsified in the agitator for twenty-five minutes only.

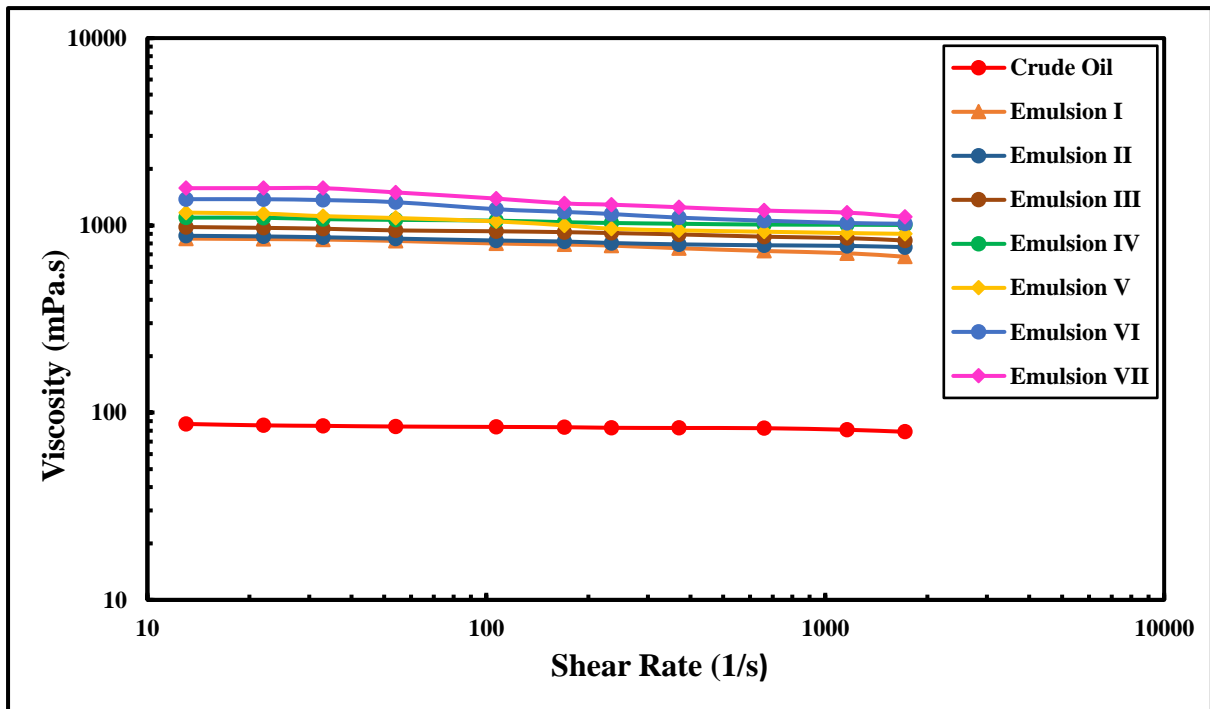


Figure 108: Crude oil viscosity of seven samples (Emulsion I-VII) of various levels of stability versus shear rate drawn on a logarithmic scale.

#### 6.4.2 The Crude Oil Emulsion Stability

Practically, there is no certain measure for the stability of an emulsion. A “bottle test” is usually used (Wang and Alvarado, 2009) to estimate the stability of complex emulsions as it is a quick and simple observation for the range of phase separation with time and gives important information with respect to both emulsion stability and separated water clarity. A bottle test has been conducted on all of the emulsions which were initially prepared as mentioned in the previous section. However, further study with respect to stability has been undertaken on the most stable emulsion only. Thus, rest of the section will only concentrate on this specific emulsion.

The slow progress of the natural demulsification process which was obtained by the “bottle test” experiments was visually monitored as illustrated in Figure 109. The outcome of that test was represented graphically as shown in Fig 110, the emulsion of water-in-crude oil which was prepared at 2000 rpm and blending time of twenty five minutes (after fifteen minutes dosing time of the aqueous phase), fully demulsified (separated to similar quantity of oil and water phases) a hundred and fourteen days after the preparation process.

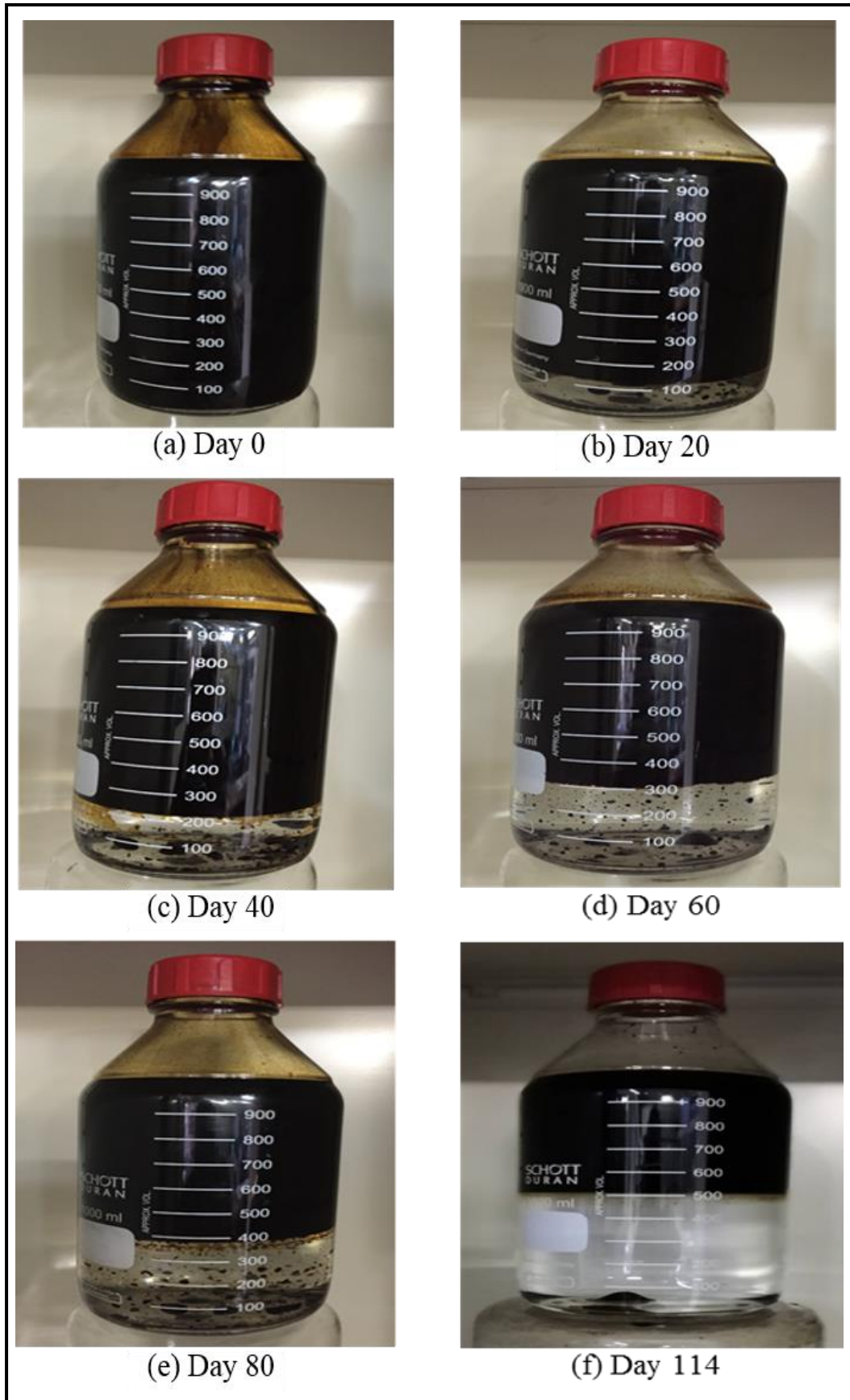


Figure 109: Photographic representation of the bottle test performed on crude oil emulsions.

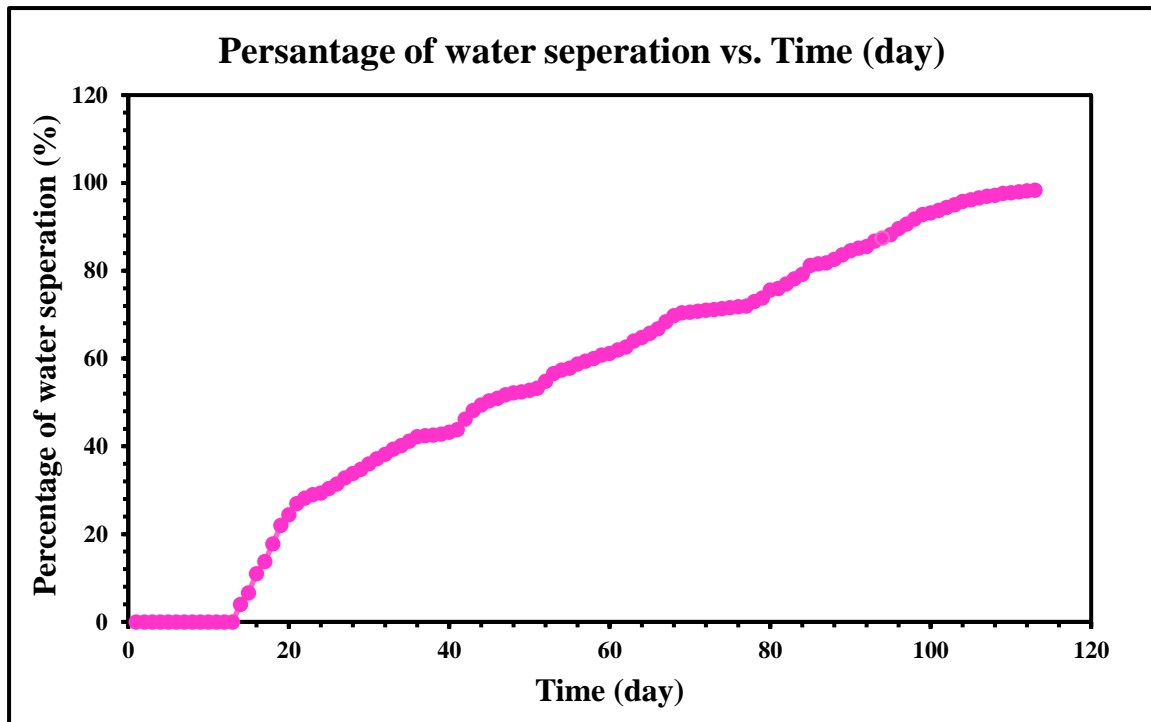


Figure 110: The progress of natural phase separation (demulsification) of the crude oil emulsion prepared at 2000 rpm mixing and 25 minutes agitation time.

### 6.5 Conductivity Measurement of Crude Oil Emulsions

The conductivities of feed (the inlet crude oil emulsion) samples and outlet crude oil emulsion have been recorded once collected. The measured conductivities with respect to feed stream utilising an electrostatic field at various conditions of separations are showed in Table 38. It can be seen that the samples of fresh (inlet) emulsion (the volume water content of 50%) have conductivities higher than samples of the outlet emulsions. This variance in value of conductivity attributed to the equivalent water volume in every emulsion, where the conductivity is directly proportional to the water content in emulsions (Sjoblom, 2005). This means the outlet emulsion samples have water content of volume lower than fresh samples, this is a proof of the success of the electrostatic separator in the separation of water from water-in-crude oil emulsions. The effect of emulsion flow rate is relatively small but the electric field strength has a much greater effect a demulsification.

Table 38: Conductivity of inlet (fresh) and outlet emulsions samples for various flow rates with applied voltage of 1.0 and 5.0 kV.

Emulsion flow rate, ml/min	Voltage Applied (kV)	Sample	Conductivity, $\mu\text{s/cm}$
100	1	fresh emulsion	$0.82\pm 0.03$
		outlet emulsion	$0.58\pm 0.02$
	5	fresh emulsion	$0.82\pm 0.03$
		outlet emulsion	$0.48\pm 0.02$
250	1	fresh emulsion	$0.82\pm 0.03$
		outlet emulsion	$0.55\pm 0.02$
	5	fresh emulsion	$0.82\pm 0.03$
		outlet emulsion	$0.51\pm 0.02$
500	1	fresh emulsion	$0.82\pm 0.03$
		outlet emulsion	$0.53\pm 0.02$
	5	fresh emulsion	$0.82\pm 0.03$
		outlet emulsion	$0.49\pm 0.02$
750	1	fresh emulsion	$0.82\pm 0.03$
		outlet emulsion	$0.52\pm 0.02$
	5	fresh emulsion	$0.82\pm 0.03$
		outlet emulsion	$0.46\pm 0.02$
1000	1	fresh emulsion	$0.82\pm 0.03$
		outlet emulsion	$0.51\pm 0.02$
	5	fresh emulsion	$0.82\pm 0.03$
		outlet emulsion	$0.45\pm 0.02$
1250	1	fresh emulsion	$0.82\pm 0.03$
		outlet emulsion	$0.49\pm 0.02$
	5	fresh emulsion	$0.82\pm 0.03$
		outlet emulsion	$0.43\pm 0.02$
1500	1	fresh emulsion	$0.82\pm 0.03$
		outlet emulsion	$0.47\pm 0.02$
	5	fresh emulsion	$0.82\pm 0.03$
		outlet emulsion	$0.42\pm 0.02$

---

## CHAPTER SEVEN

---

### 7. RESULTS AND DISCUSSIONS OF DEMULSIFICATION EXPERIMENTS OF WATER-IN-CRUDE OIL EMULSION USING COMBINED PHP DEMULSIFIER AND ELECTROSTATIC FIELD AND REUSE OF SPENT PHP IN THE DEMULSIFICATION PROCESS

#### 7.1 Outlet

This chapter of the thesis is presented in four major categories.

- i. The first part shows the results of the effect of the inlet flow rate on demulsification of water-in-crude oil emulsions.
- ii. The second part demonstrates effect of the electric field strength on demulsification of water-in-crude oil emulsions.
- iii. The third part shows the SEM analysis, EDX analysis and water uptake measurement of PHP-I, and discusses the results.
- iv. The fourth part explains the reuse of PHP in separation of water from water-in-crude oil emulsions using an electrostatic field.

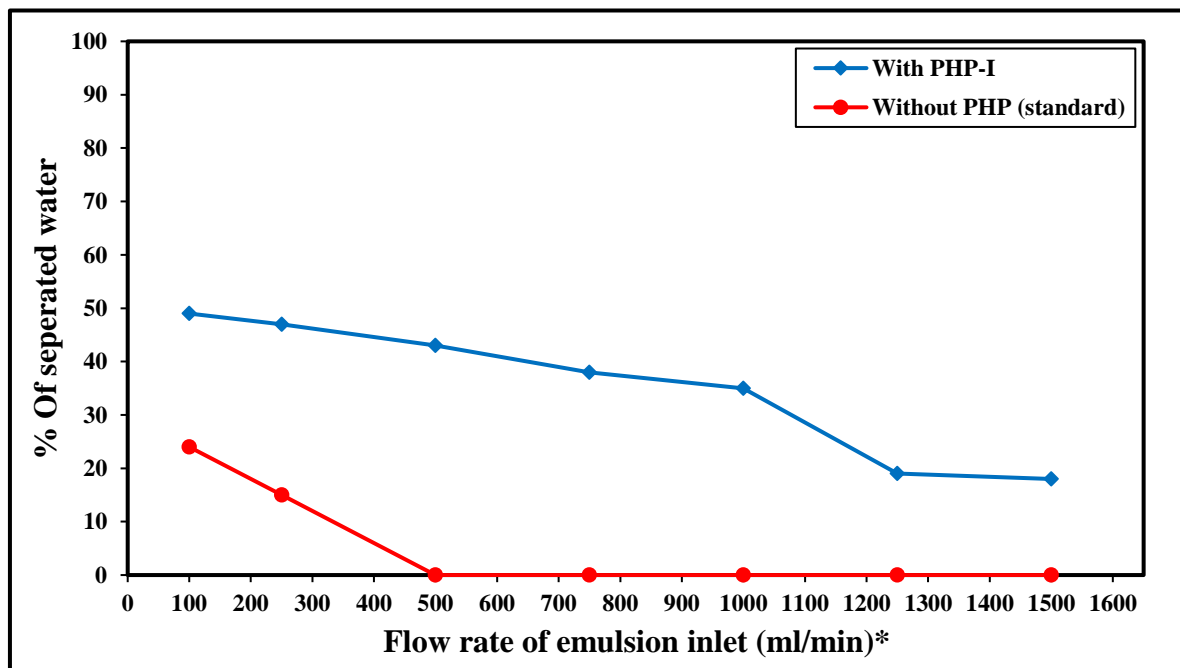
#### 7.2 Separation Studies

The polyHIPE particles are added to the crude oil emulsion which is transferred to the separator after mixing via a peristaltic pump. Whilst in the crude oil emulsion the polyHIPE can absorb water. The polyHIPE is partly filtered from the remaining emulsion just before the separator by a steel mesh. Smaller pieces of polyHIPE pass through the separator and are collected with the water phase. This is done to prevent clogging of the oil inlet.

##### 7.2.1 Effect of Inlet Flow Rate Variation

The impact of the flow rate of emulsions on the separation efficiency was assessed using the optimum samples of polyHIPEs produced namely SL20, BZ25, B50 and IS40 corresponding

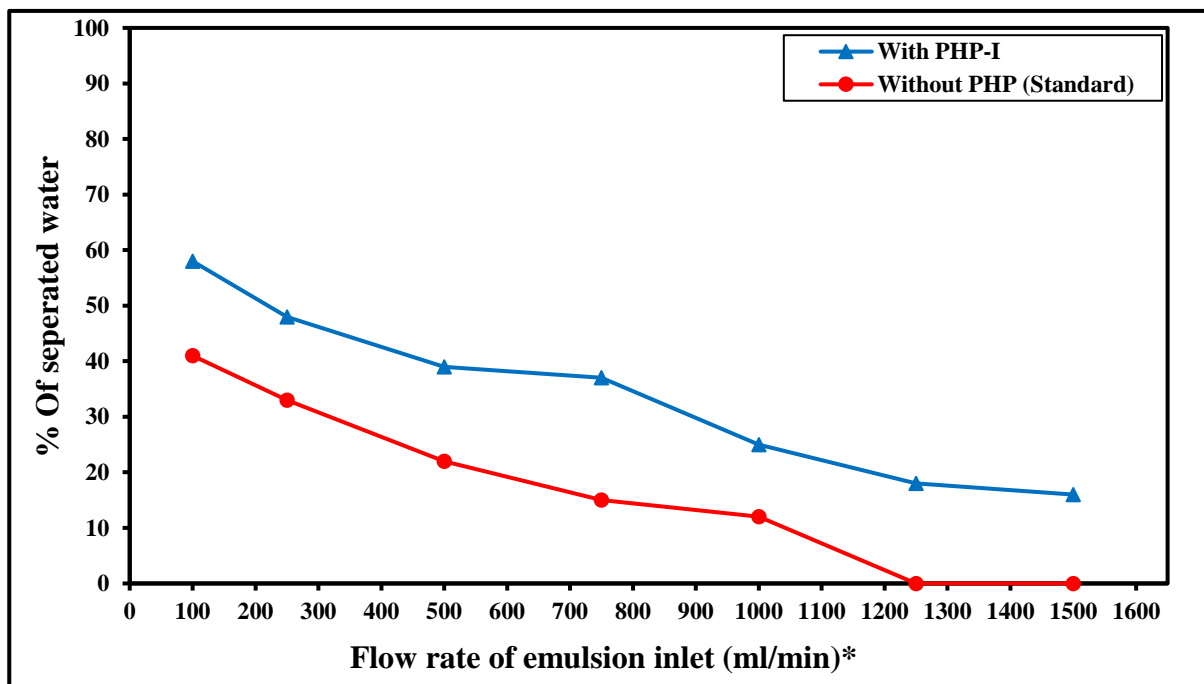
to PHP-I, PHP-II, PHP-III and PHP-IV, respectively. These were prepared from scratch and further functionalized and modified chemically (as discussed in section 4.2), then processed and sieved to convert them into granules with sizes ranging from 540-750  $\mu\text{m}$  with a view to use them as demulsifiers in the experiments of separation. Separation experiments were carried out at a high electric field strength ranging from 14-69  $\text{kV/m}$  (1-5  $\text{kV}$  applied over the distance of 0.072 m between the two separation electrodes). The emulsion inlet flow rate was changed from 100  $\text{ml/min}$  to 1500  $\text{ml/min}$ . According to the performance of the continuous demulsification process, the outcomes of the experiment predicted that the oil/water separation efficiency was considerably increased when the PHP demulsifier was added to the model emulsion prior to the high-voltage electric field separation. In Figure 111, the difference of separation degree is shown as a function of emulsion inlet flow rate promptly after the passage of the emulsion over the electric separator with presence and absence of PHP-I as demulsifier by using a fixed voltage of 5  $\text{kV}$  (equivalent 69  $\text{kV/m}$ ) and various inlet flow rate of the emulsion. In the absence of PHP I, when the flow rate is over approximately 500  $\text{ml/min}$  there is no immediate separation. While, the performance of separation with the presence of PHP-I was moderate at a low emulsion inlet flow rate and low with a high inlet flow rate.



\*1  $\text{ml}\cdot\text{min}^{-1} = 1 \times 10^{-6} \text{ m}^3 \cdot \text{min}^{-1}$

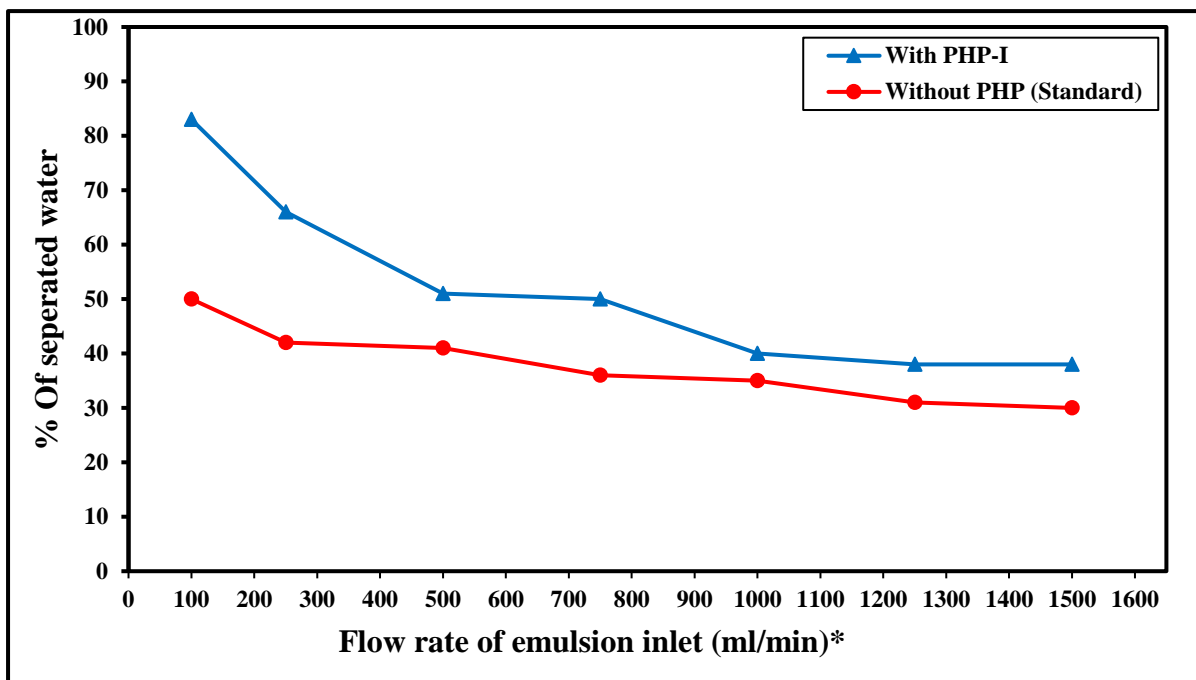
Figure 111: Difference of percent water separated with emulsion flow rate through the electrostatic separator at 5.0  $\text{kV}$  ( $69 \text{ kV}\cdot\text{m}^{-1}$ ) applied voltage immediately after emerging from separator in the presence and absence of PHP-I.

Figure 112 and 113 show the efficiency of separation after a standing time of 1 and 24 hours respectively in the presence of PHP-I demulsifier. The impact of PHP-I becomes insignificant with increasing standing time from 1 to 24 hours while the impact is noticeable at comparatively minimal flow rate as illustrate in these Figures. However, the outcomes depicted show that the existence of PHP-I demulsifier and steady-strength electric field have enhanced the demulsification process, particularly at a low flow rate of emulsion. It is expected that the surfactant breaks down easily and loose its surface activity in the presence of high electric field (Odirile, 2000).



\*1 ml.min<sup>-1</sup> = 1 x10<sup>-6</sup> m<sup>3</sup>/min

Figure 112: Difference of percent water separated with emulsion flow rate through the electrostatic separator at 5.0 kV (69 kV.m<sup>-1</sup>) applied voltage, 1-hour after emerging from separator in the presence and absence of PHP-I.



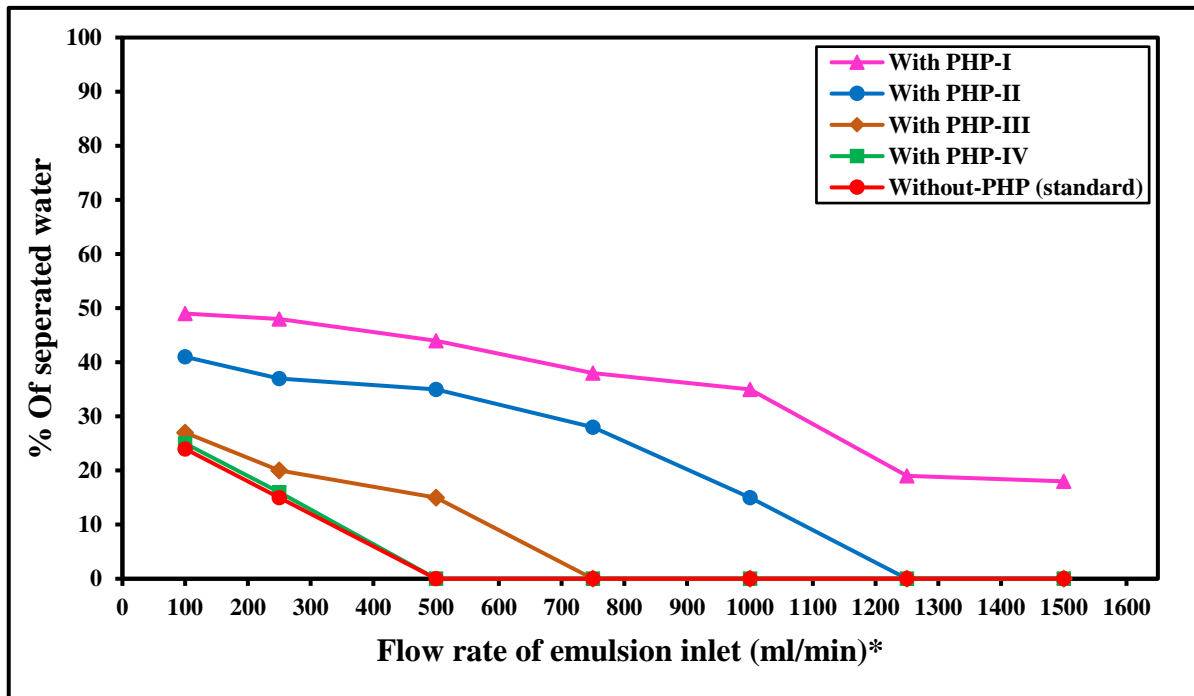
\*1 ml.min<sup>-1</sup> = 1 x10<sup>-6</sup> m<sup>3</sup>/min

Figure 113: Difference of percent water separated with emulsion flow rate through the electrostatic separator at 5.0 kV (69 kV.m<sup>-1</sup>) applied voltage, 24-hour after emerging from separator in the presence and absence of PHP-I.

As for the PHP-II, PHP-III and PHP-IV, the experiments of demulsification were carried out under the similar conditions as former cases (with electric field strength and emulsion inlet flow rate as the major variables). Figures 114 to 116 illustrate the variation in the degree of separation using PHP-II, PHP-III and PHP-IV at fixed applied voltage of 5 kV and changing flow rate (from 100 ml/min to 1500 ml/min) instantly, after 1 hour and 24 hours after the start of the water/oil separation process. The performance of the demulsifiers are compared with PHP-I and a standard (with the absence of any PHP) as a reference on the same graph. The outcome illustrated on Figure 114 indicated that the addition of PHP-III and PHP-IV as demulsifier with moderate to high flow rate did not generate any instant separation, but PHP-II achieved a clear instant separation of 43% at medium flow rate. Nevertheless, after 1 hour, the separation efficiency of the demulsification using PHP-II and PHP-III as demulsifier at all flow rates produced a dramatic enhancement with nearly constant performance of 50% and 41%, respectively as shown in Figure 115. While, in the same situation PHP-IV was still unable to achieve a significant separation.

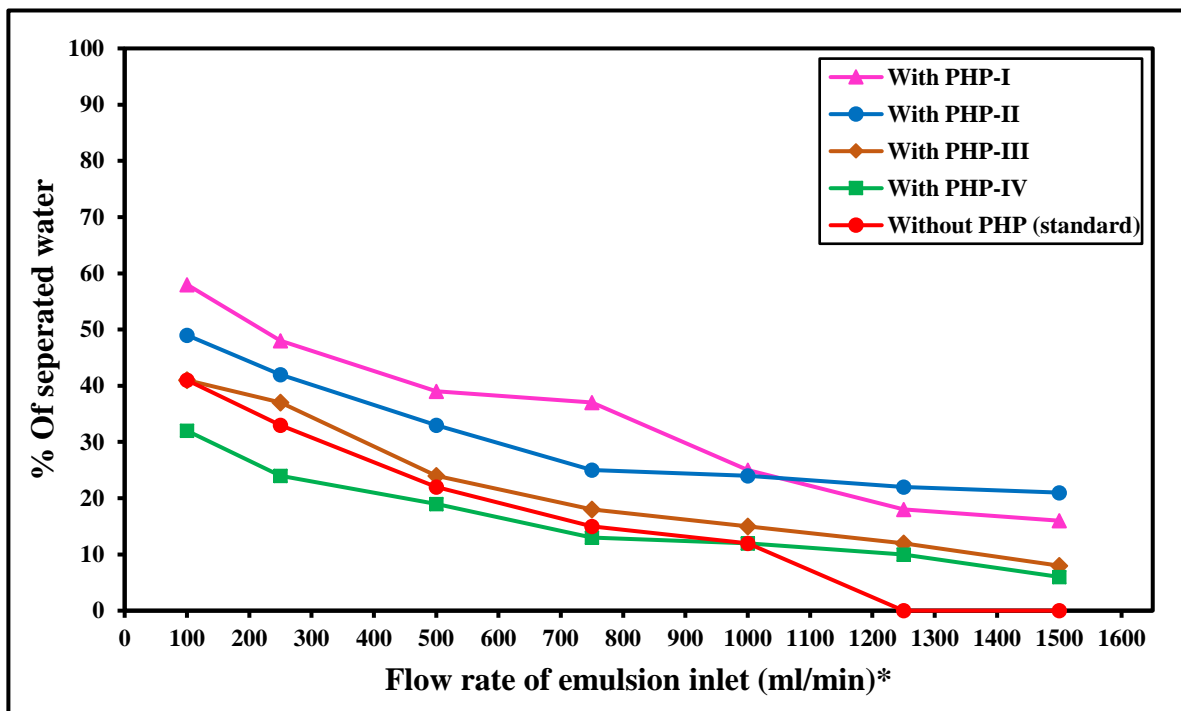
Figure 116 shows that after 24 hours, the performance of the PHP-III and PHP-IV was considerably enhanced with better separation. However, their effectiveness as a demulsifier

still lagged behind the PHP-I particularly at low flow rate. On other hand, PHP-II, at all flow rates still produced constant separation and there was slight but significant improvement in separation efficiency from 1 to 24 hours. Moreover, the constancy in the efficiency of separation of the emulsion using PHP-II as demulsifier at all flow rates is interesting as other experiments (including the standard) show a descending trend in efficiency of separation with increasing flow rate of emulsion.



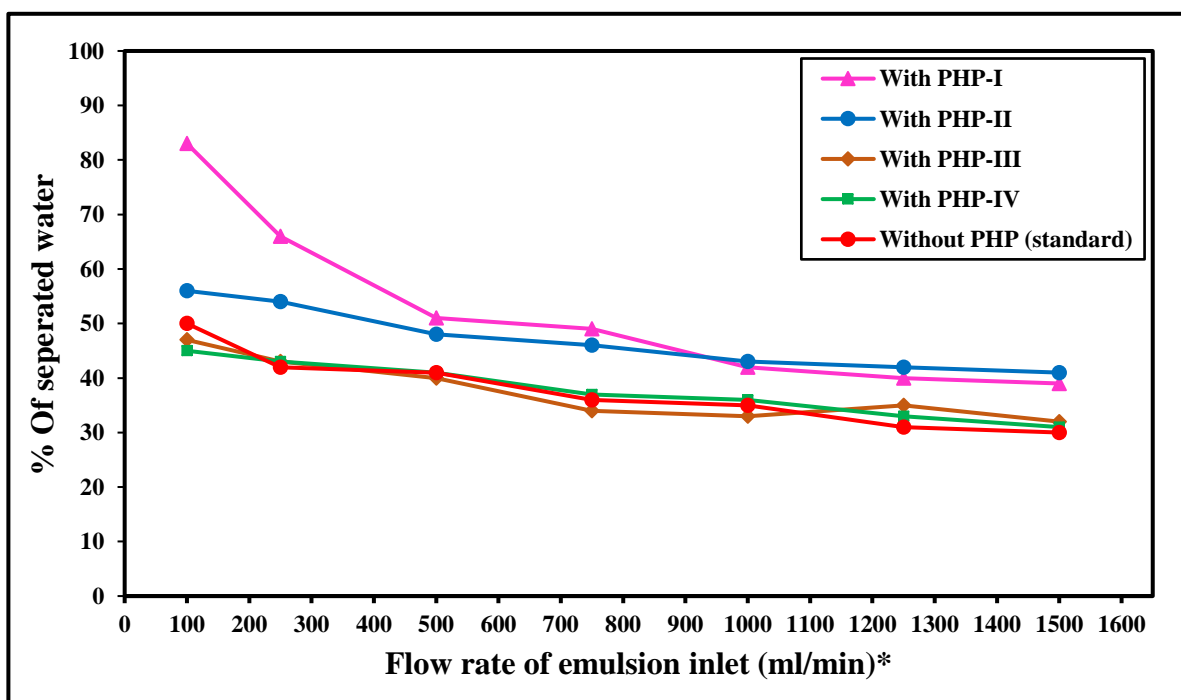
\*1 ml.min<sup>-1</sup> = 1x10<sup>6</sup> m<sup>3</sup>/min

Figure 114: Difference of percent water separated with emulsion flow rate through the electrostatic separator at 5.0 kV (69 kV.m<sup>-1</sup>) applied voltage immediately after emerging from separator in the presence of PHP-I, PHP-II, PHP-III, PHP-IV and absence of PHP (standard).



\*1 ml.min<sup>-1</sup> = 1x10<sup>6</sup> m<sup>3</sup>/min

Figure 115: Difference of percent water separated with emulsion flow rate through the electrostatic separator at 5.0 kV (69 kV.m<sup>-1</sup>) applied voltage, 1 hour after emerging from separator in the presence of PHP-I, PHP-II, PHP-III, PHP-IV and absence of PHP (standard).



\*1 ml.min<sup>-1</sup> = 1x10<sup>6</sup> m<sup>3</sup>/min

Figure 116: Difference of percent water separated with emulsion flow rate through the electrostatic separator at 5.0 kV (69 kV.m<sup>-1</sup>) applied voltage, 24 hours after emerging from separator in the presence of PHP-I, PHP-II, PHP-III, PHP-IV and absence of PHP (standard).

### 7.2.2 Effect of Electric Field Strength Variation

Under constant inlet flow rate of emulsion of  $100 \text{ ml}\cdot\text{min}^{-1}$  and increasing electric field strength the performance of PHP-I as a demulsifier in oil/water experiments of separation was also examined. Comparable to the former results, a remarkable separation (over 20%) occurred instantly after the passage of emulsion out of the separator with the presence of PHP-I as demulsifier as shown in Figure 117, although the electric field was at the minimum value. In constant in the absence of PHP-I and at the same electric field strength separation was not observed. Indeed, in the absence of PHP-I demulsifier, the demulsification take places instantly as the emulsion passage through the separator only when the electric field strength is greater than  $35 \text{ kV/m}$  (equivalent to  $2.5 \text{ kV}$ ). Interestingly, at the same strength of electric field along with PHP-I demulsifier a slight increase in efficiency of separation was observed. This indicates that the optimal strength of the electric field is range in between  $35$  to  $45 \text{ kV/m}$ . After an hour of standing, a slight increase in the separation efficiency was also observed in the absence of PHP-I demulsifier as illustrated in Figure 118. However, no significant enhancement in the separation efficiency was observed with regard to both cases even after 24 hours of standing as shown in Figure 119. Moreover, overall PHP-I has done a reasonable job in improving the performance of the demulsification process.

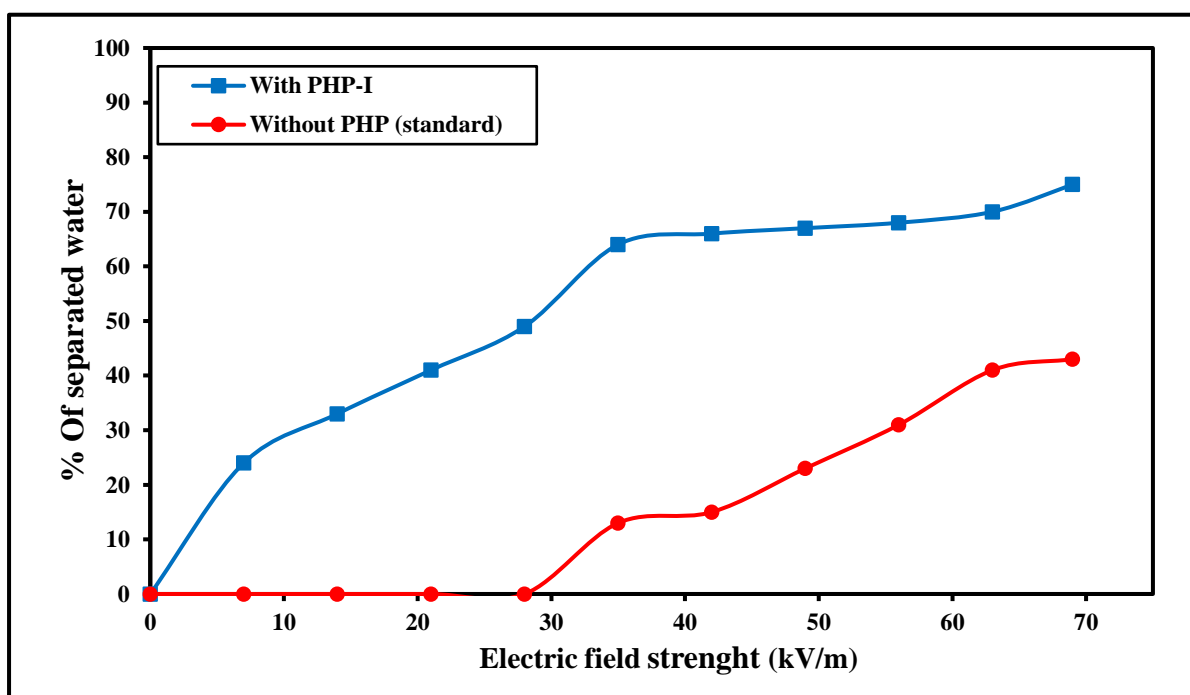


Figure 117: Difference of percent water separated with electric field strength at constant flow rate of  $100 \text{ ml/min}$ , immediately after passing through the separator in the presence and absence of PHP-I.

Chemical separation methods often achieve separation efficiency of 70-80% which is comparable to what has achieved with the electric field/PHP combination.

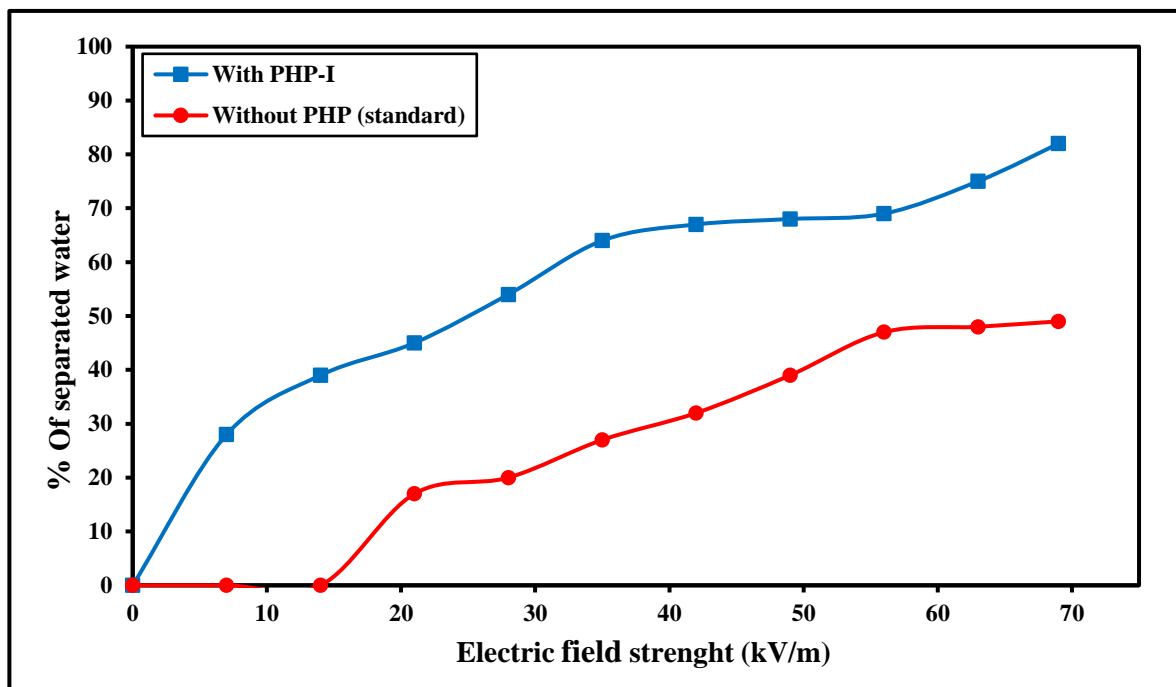


Figure 118: Difference of percent water separated with electric field strength at constant flow rate of 100 ml/min, 1-hours after passing through the separator in the presence and absence of PHP-I.

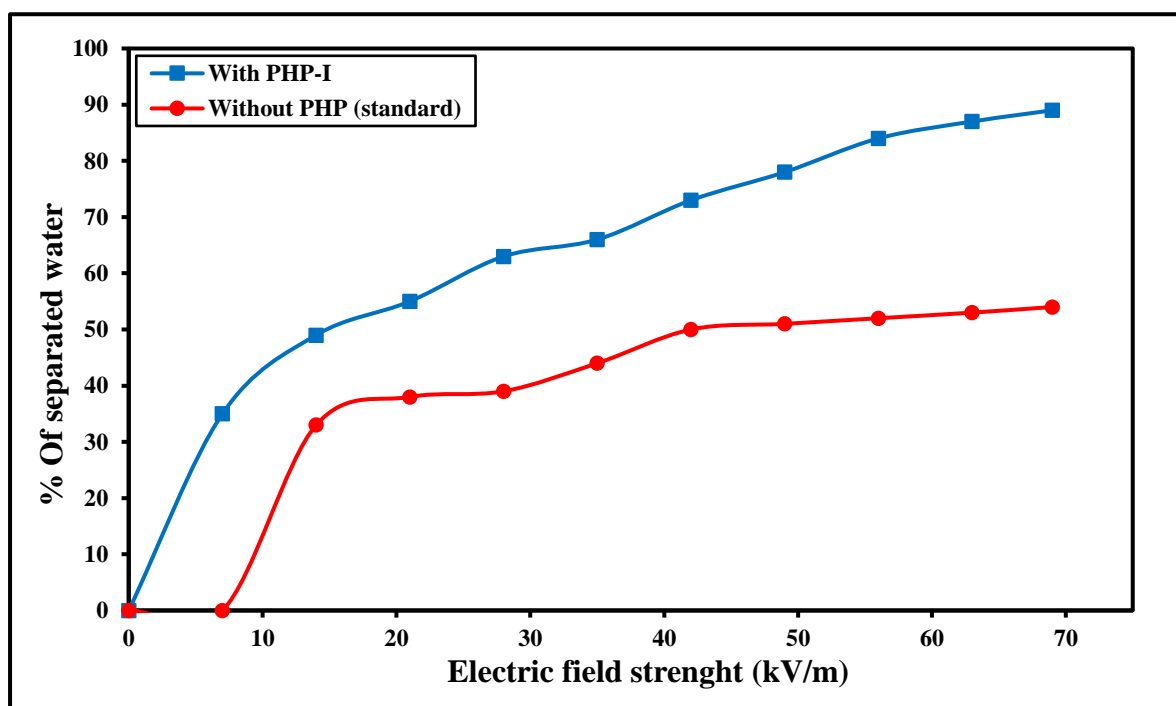


Figure 119: Difference of percent water separated with electric field strength at constant flow rate of 100 ml/min, 24-hour after passing through the separator in the presence and absence of PHP-I.

The impact of electric field strength on the efficiency of the separation of PHP-II, PHP-III and PHP-IV as contrasted to PHP-I and without demulsifier (standard) instantly after separation is illustrated in Figure 120. While, the effect of electric field strength on performance of the demulsification after 1 and 24 hours is shown in Figure 121 and Figure 122 respectively. Figure 120 indicated that the PHP-II, PHP-III and PHP-IV did not produce any separation at comparatively low electric field strength. In addition, the water/oil separation experiment carried out in the absence of demulsifiers (standard) appears to have comparable performance of separation only at very high electric field strength in contrast to the experiments undertaken in the presence of PHPs as demulsifiers. Nonetheless, these polymers showed some development in terms of separation efficiency leaving the emulsion for 1 hour (Figure 121). After 24 hours, the performance of PHP-II, PHP-III and PHP-IV as shown in Figure 122 keep enhancing while demulsification can be observed over the complete electric field range. From these experiments the PHP-I was found to be better than PHP-II, PHP-III and PHP-IV. Thus, the performance of the demulsifiers must be correlated with their physical and chemical properties in order to further explore of separation process mechanisms.

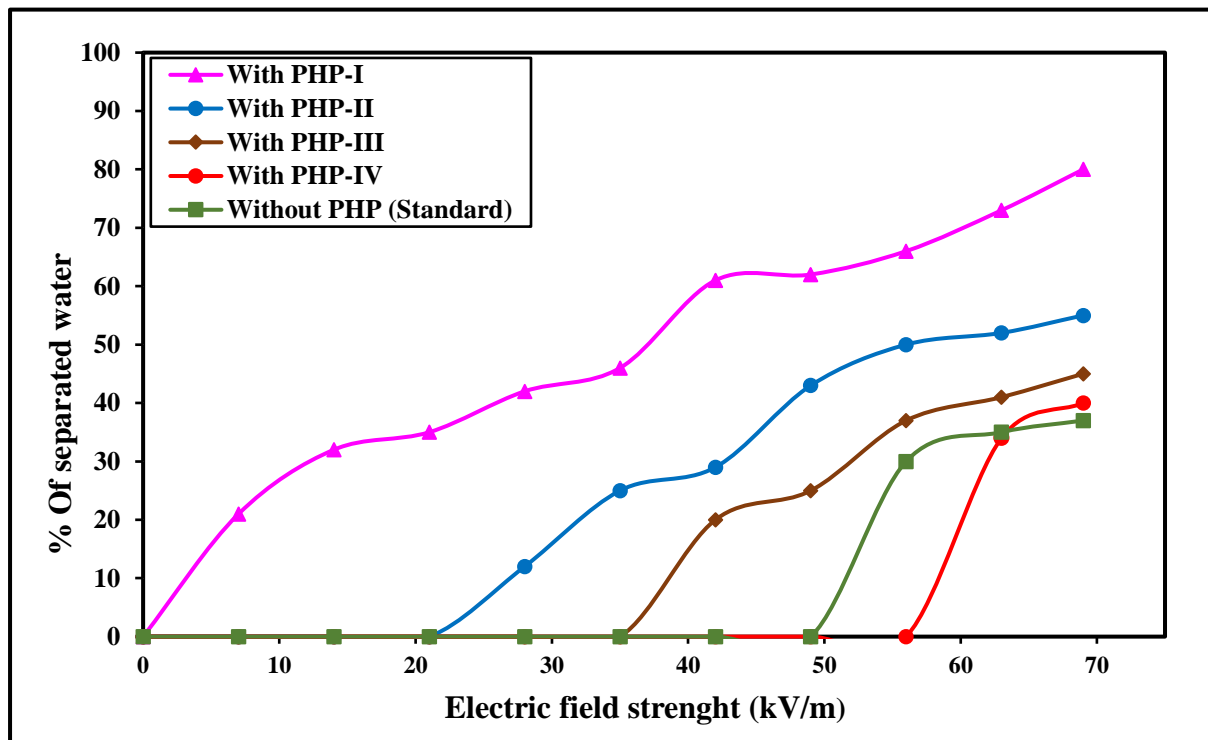


Figure 120: Difference of percent water separated with electric field strength at constant flow rate of 100 ml/min immediately after passing through the separator in the presence of PHP-I, PHP-II, PHP-III, PHP-IV and absence of PHP (Standard).

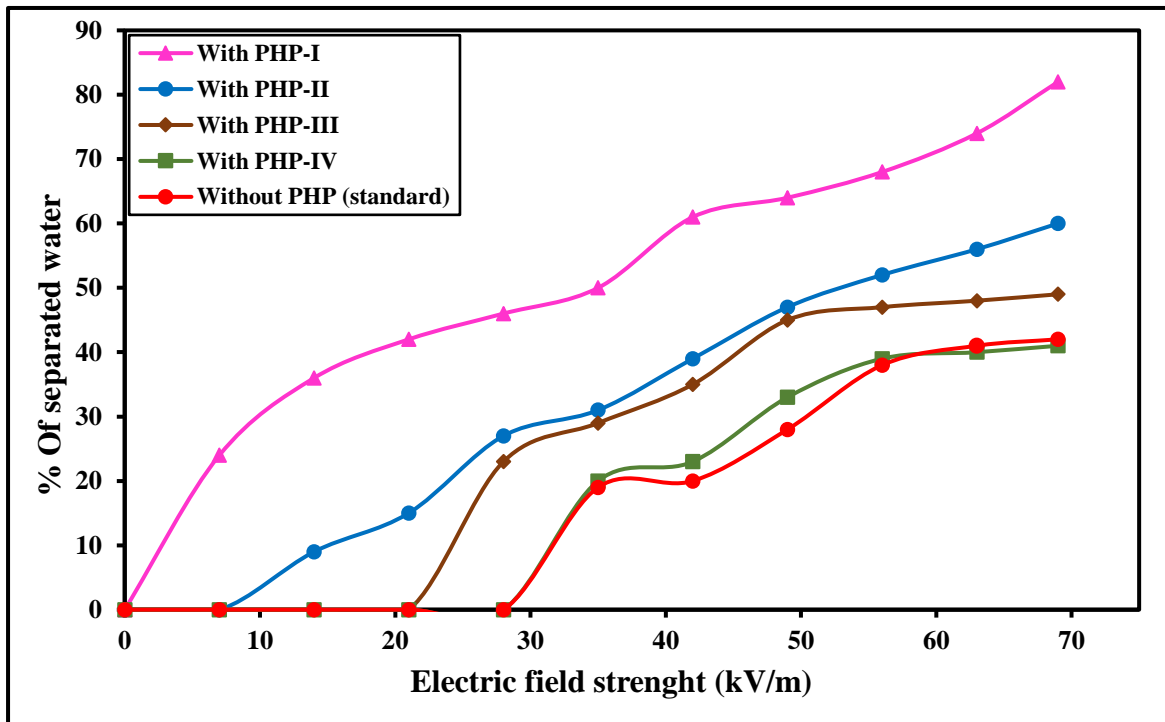


Figure 121: Deference of percent water separated with electric field strength at constant flow rate of 100 mi/min, 1-hour after passing through the separator in the presence of PHP-I, PHP-II, PHP-III and PHP-IV and absence of PHP (standard).

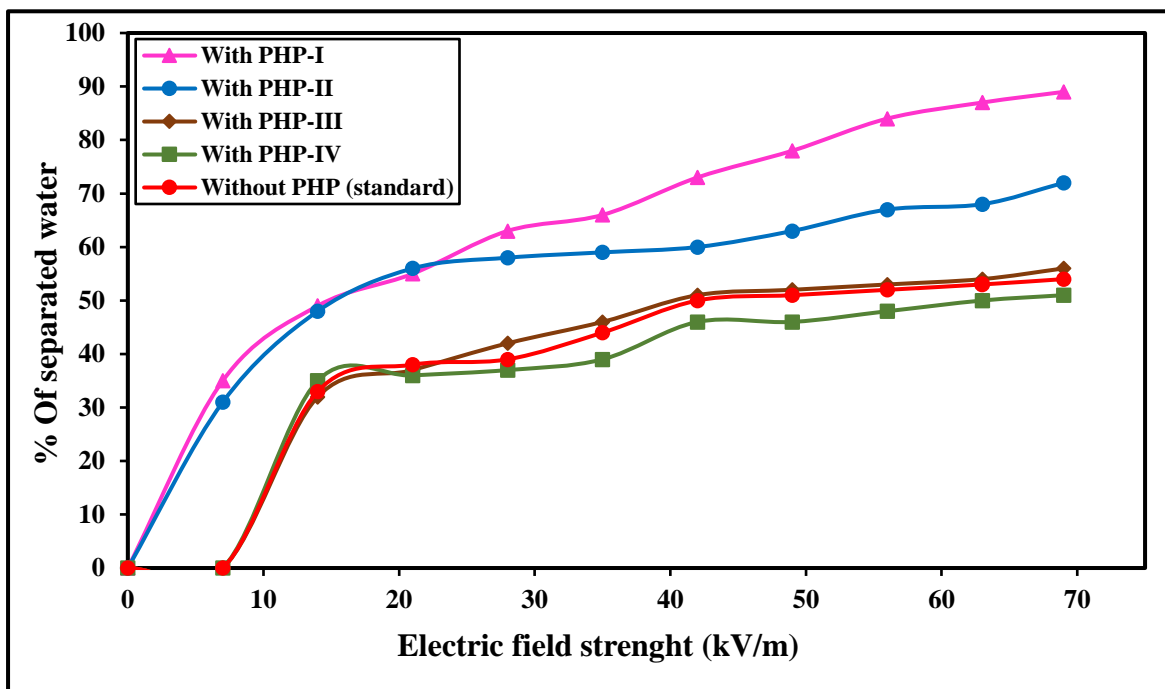


Figure 122: Deference of percent water separated with electric field strength at constant flow rate of 100 mi/min, 24-hour after passing through the separator in the presence of PHP-I, PHP-II, PHP-III and PHP-IV and absence of PHP (standard).

### 7.3 SEM analysis, EDX analysis and water uptake of PHP-I

PHP-I has been selected to be analysed by SEM among other PHP samples as it was the best adsorber/demulsifier (based on separation efficiency) compared with PHP-II, PHP-III and PHP-IV. Figure 123 (a) shows the SEM micrograph of PHP-I before using it in the experiment of separation. Whilst Figure 123 (b), the SEM image illustrates the appearance of spent PHP-I adsorber/demulsifier which was utilised in the separation experiment. After completing the demulsification process, PHP-I was collected, dried and sent to the SEM for analysis (no other test were conducted) to estimate its ability to remove surface-active materials which cause crude oil emulsification. It can be seen that the porous structure partially collapses as a result of a mechanical stresses produced from emulsion pumping along with the drying process and shows some closed pores, which resulted perhaps due to the use of PHP-I more than once and the accumulation of surface-active material that has been absorbed by the PHP-I in the pores. Nonetheless, these dried samples recovered their original properties when they were put in water and started swelling again.

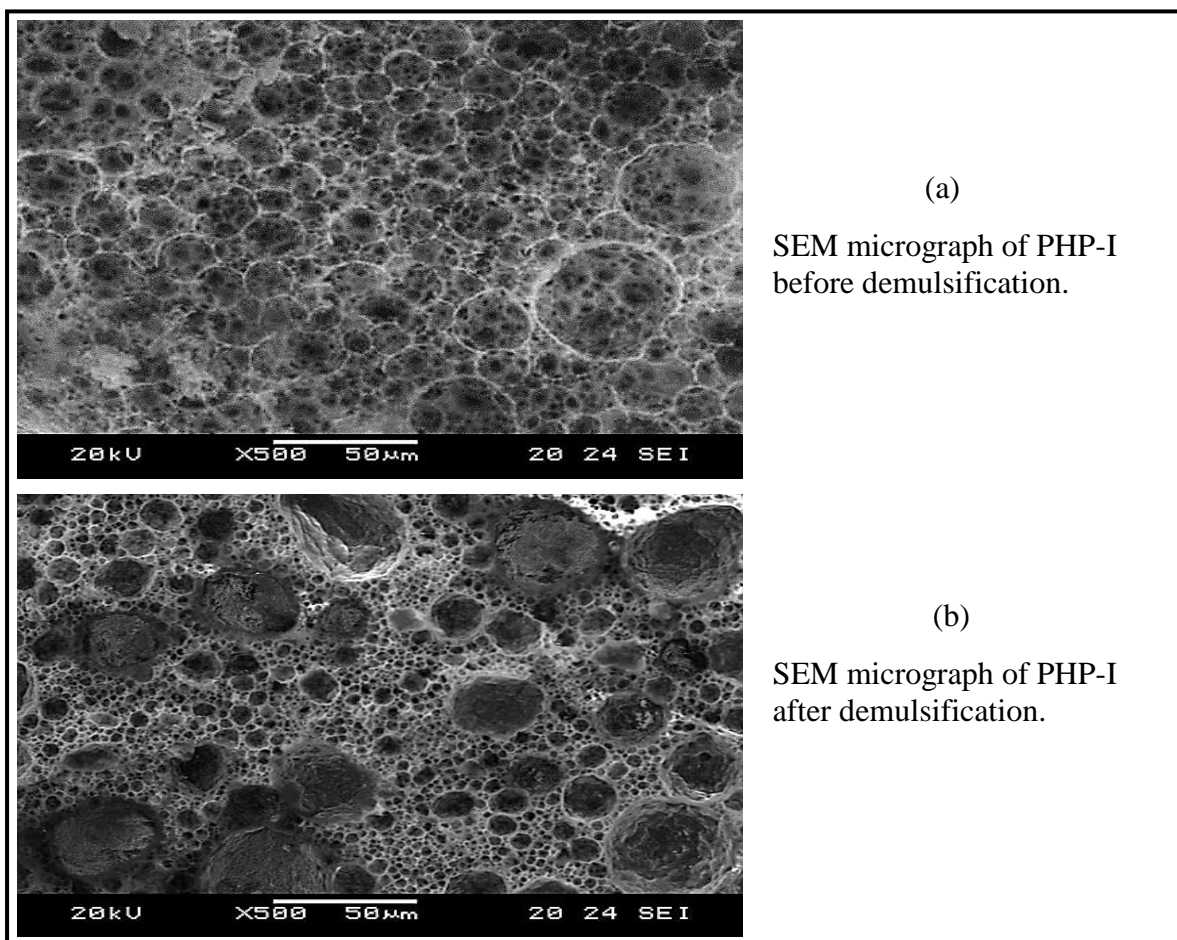


Figure 123: SEM micrograph of the PHP-I (a) before the separation experiment (at 500x magnification) and (b) after the separation experiment (at 500x magnification).

With the aim of verifying the elements of PHP-I structure after demulsification process. PHP-I was subjected to Energy Dispersive X-rays (EDX) spectroscopy. The result is demonstrated in Figure 124 and Table 39. The EDX of PHP-I polymer indicated the presence of some more elements, such as Mg, Na, Cl and Ca, which were not present initially in the PHP-I but were attached onto PHP-I from the crude oil. This verifies that PHP-I has ability to adsorb some other elements from the crude oil in addition to its capacity to improve the separation efficiency during the demulsification process using electrostatic field. Thus, PHP-I demulsifier has the further feature attributed to the ability to decrease the metals existing in the crude oil.

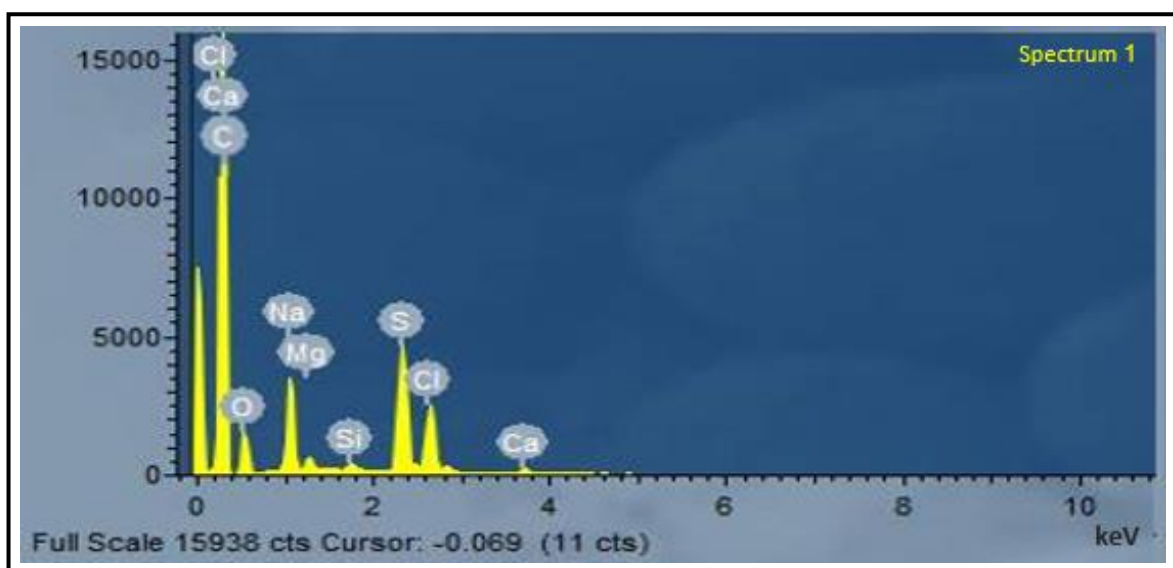


Figure 124: EDX spectrum of spent PHP-I adsorber/demulsifier.

Table 39: EDX analysis result of PHP-I after demulsification, including the main elements adsorbed by PHP-I namely: Mg, Na, Cl and Ca.

Element	Weight %	Atomic %
C	83.56	89.57
O	8.69	6.99
Na	1.93	1.08
Mg	0.22	0.12
Si	0.63	0.29
S	3.91	1.57
Cl	0.89	0.32
Ca	0.17	0.06
Total	100.00	100.00

Standard PHP has been found to be an effective material for removal of metal ions from wastewater previously by an ion exchange mechanism (Kahdim, 2017), as it succeeded in removing 40% of the existing nickel ion, which are toxic material and affects life and a similar process is expected to be occurring here. In this study a similar process has been achieved by using original PHP-I, where Mg, Ca and Na ions have been removed from crude oil that are cause crude oil emulsification by an ion exchange mechanism.

With the aim to verify the capacity of spent PHP-I to adsorb water, the water uptake test of spent PHP-I was repeated three times. It was observed that the water uptake ability of spent PHP-I was still good, but it was slightly lower than the water uptake ability of original PHP-I (about 73% of the original PHP-I capacity) as shown in Figure 125. Therefore, it was tested in separation experiments again to assess its separation ability as shown in section (6.3.6).

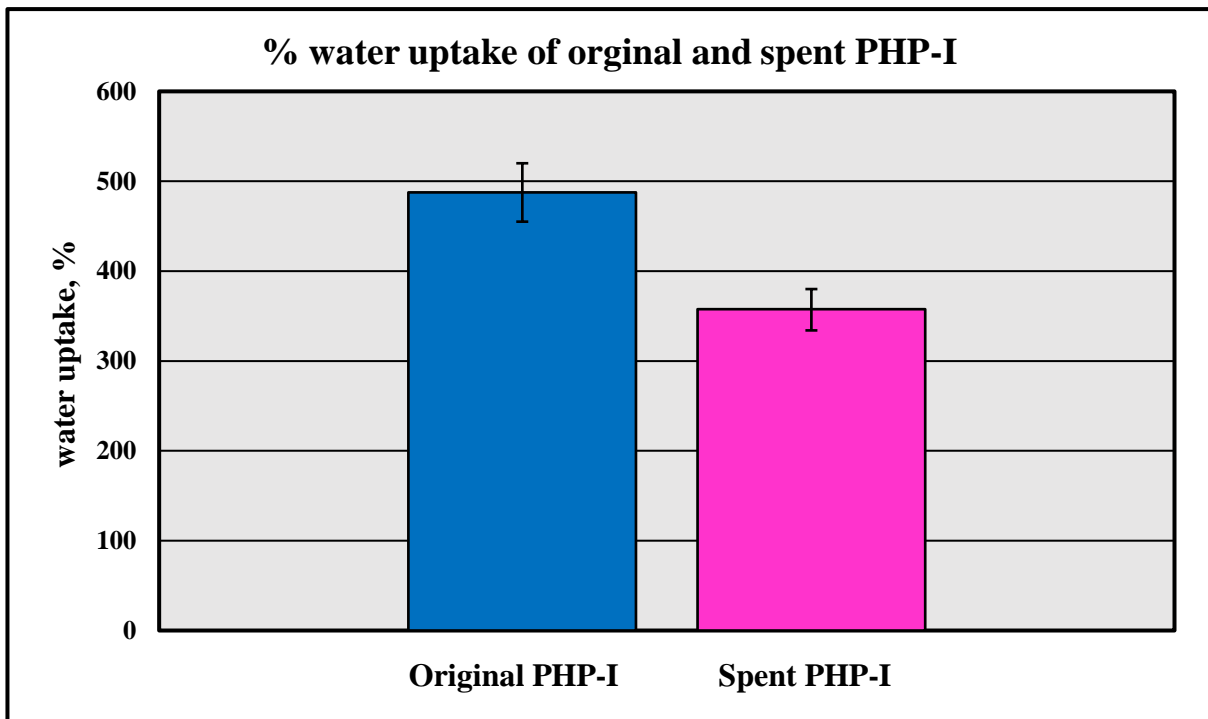


Figure 125: Plot of water uptake of the original and spent PHP-I

## 7.4 Reuse of Spent PHP-I in Separation Experiments Using Electrostatic Field

In order to find out how efficient the spent PHP-I is in promoting the separation of water and the active-surfaces from the water-in-crude oil emulsion, the separation experiment was conducted using the spent PHP-I sample, along with the electrostatic separator. The separation process has been carried out using water-in-crude oil emulsion at inlet flow rate of emulsion of  $100 \text{ ml}\cdot\text{min}^{-1}$  and variable electric field strength (from 1 to 5 kV applied voltage). It was observed that the separation efficiency of original PHP-I, spent PHP-I and without PHP standard are 89, 71 and 54% of separated water, respectively at the highest electric field as shown in Figure 126. The spent PHP-I has achieved a higher separation efficiency than the separation efficiency in the absence of PHP, but does not reach to the separation efficiency of the original PHP-I.

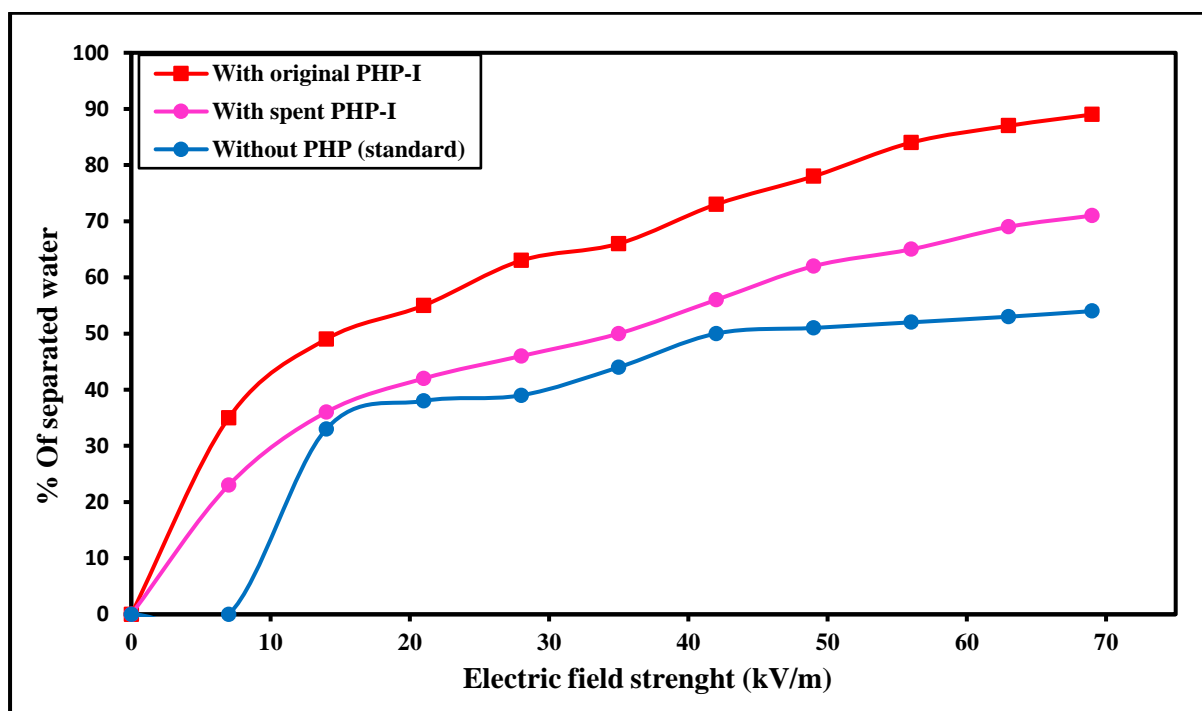


Figure 126: Difference of percent water separated with electric field strength at constant flow rate of  $100 \text{ ml}/\text{min}$ , 24 hours after passing through the separator in the presence of original PHP-I, spent PHP-I and absence of PHP (standard).

With the purpose of verifying the elements in the spent PHP-I structure after demulsification process, the spent PHP-I was subjected to Energy Dispersive X-rays (EDX) spectroscopy. The result is shown in Figure 127 and Table 40. It can be realized that the spent PHP-I polymer included same elements which were presence in the original PHP-I, namely Mg, Na and Ca, that were adsorbed from the crude oil. This shows that spent PHP-I also has sufficient capacity

to remove more elements from the crude oil in addition to its separation efficiency and has not reached saturation behavior. Thus, spent PHP-I demulsifier also has the ability to decrease the metals existing in the crude oil but with less efficiency than in the original PHP-I.

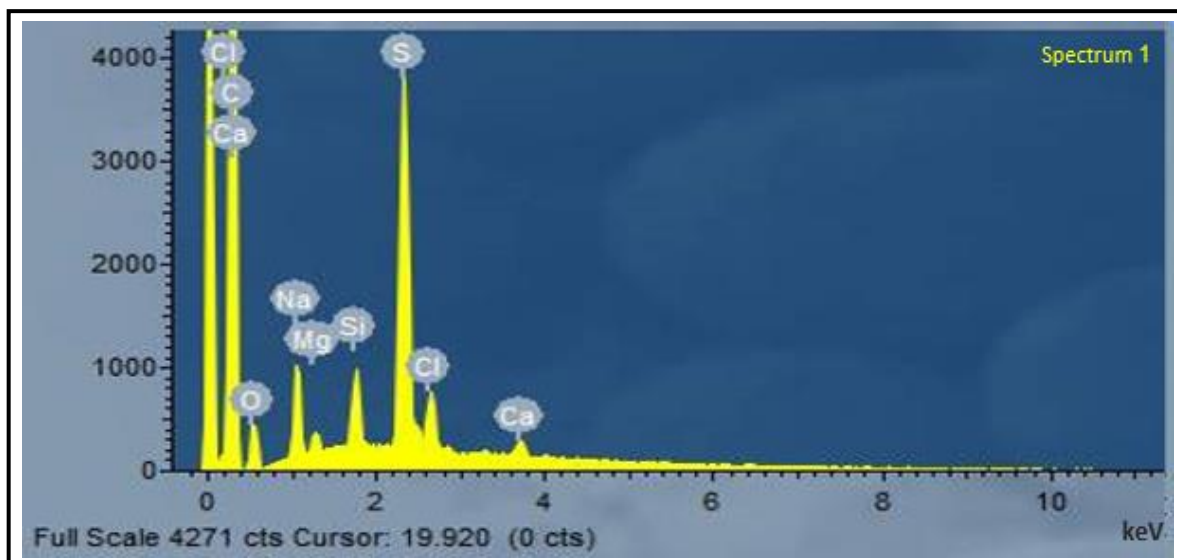


Figure 127: EDX spectrum of reused spent PHP-I adsorber/demulsifier.

Table 40: EDX analysis result of reused spent PHP-I after demulsification, including the main elements adsorbed by PHP-I namely: Mg, Na, Cl and Ca.

Element	Weight %	Atomic %
C	84.03	89.77
O	8.54	6.87
Na	1.72	1.04
Mg	0.20	0.11
Si	0.60	0.26
S	3.98	1.61
Cl	0.78	0.29
Ca	0.15	0.05
Total	100.00	100.00

## 7.5 Mechanism of Demulsification

From the experiments conducted here it is clear that in the demulsification process water droplets in the emulsion must contact the PHP particles and be absorbed by them. In the absence of an electric field there is little or no demulsification by the PHP particles in the emulsion, but even a low field results in better demulsification than is achieved without PHP at high field. Thus the following mechanism might be proposed:

- 1) The PHP particles in the emulsion contact a small number of water drops. This increases with time due to sedimentation and Brownian motion of the water drops.
- 2) The hydrophilic surfaces of the polyHIPE allow the droplets to spread on the surface due to a low contact angle (Figure 13) which breaks up the droplet and absorbs the water in the PHP.
- 3) The water is absorbed within the particle and not released back into the emulsion. The high water uptake ability and high surface area is critical to remove as much water as possible.
- 4) The presence of the electrostatic field allows the charged water droplets to move in the emulsion and makes them more likely to encounter a PHP particle where they can be absorbed. The larger PHP particles may also charge but their inertia means that they are likely to be relatively immobile. Even at low fields the water droplets can move far enough to encounter the PHP and be removed.
- 5) At high fields water-water droplet coalescence occurs as usually seen in an electrocoalescer.
- 6) The properties of the PHP can be optimized to attract the water (hydrophilic) and store a large amount of water in the microporous structure.
- 7) If the polymer is dried before reuse it can work in the similar way. Ion exchange processes can remove metal ions from the water phase in the emulsion but these processes are not reversible by simple drying. Thus the number of absorption sites in the PHP will be reduced and the demulsification efficiency will be reduced after each use.

Thus, the combination of functionalised PHP with high water uptake ability and high surface area with an electrostatic field is a good candidate for demulsification. The ability to operate at lower field and shorter residence times makes the technique potentially alternative for industrial applications.

---

## CHAPTER EIGHT

---

### 8. CONCLUSIONS AND FUTURE WORKS RECOMMENDATIONS

#### 8.1 Outline

This chapter introduces the study overview and an assessment of the results obtained from the preparation of hydrophilic micro-porous PHPs as well as the water separation of water-in-crude oil emulsions, justifying the methodology used in the work. Furthermore, the direction and limitations for the future work are also discussed.

#### 8.2 Introduction

In this project, in order to perform a philosophy of a process intensification (PI) in demulsification water-in-crude oil emulsions, the work has been conducted using a combination of electric fields and hydrophilic PHPs. Several macro-porous PHPs have been produced and then sulphonated to make them hydrophilic. In order to choose the optimized samples in demulsification process, the PHPs samples were assessed in terms of morphology, surface area, pore size distribution, water uptake, FTIR and EDX analyses. Moreover, equal volumes of crude oil and water phases (aqueous phase) were utilised to prepare water-in-crude emulsions, where three kinds of salts have been used to prepare the aqueous phase NaCl, CaCl<sub>2</sub> and MgCl<sub>2</sub> to mimic seawater. In demulsification experiments, different flow rates of water-in-crude oil emulsions and various electric field strengths (applied voltages) have been utilised to evaluate their effect on the separation efficiency, as well as the ability to remove surface-active species. In addition, the separation of water and the active-surface elements from the water-in-crude oil emulsion using the electrostatic separator with spent PHP have been carried out and examined. There were three main aims of this study; 1) comprehensive study of the demulsification mechanism by utilising various types of demulsifiers, 2) the synthesizing of macro-porous demulsifiers, 3) to eliminate the need for larger demulsification equipment by developing a novel approach for the separation of emulsions through the combined impacts of demulsifier and electric field.

### 8.3 Findings Summary

The previously developed technique of intensified demulsification of water-in-crude oil with high stability (Akay and Vickers, 2003) was enhanced by the combination of electrostatic separation technique and the macro-porous demulsifier/adsorber which is based on sulphonated microporous polymers with a high internal volume, normally 90% voids.

The electrostatic separator was developed as follows: copper electrodes (energized and earth electrodes) were used instead of steel electrodes, due to a higher electrical conductivity of the former compared to that of later. In addition, the distance between the two electrodes has been reduced from 9.1 cm that was used by Akay and Vickers (2003) to 7.2 cm to ensure a strong electric field kept, since the strength of the electric field is inversely proportional to the distance between the electrodes and this in turn helps the water droplets to coalesce and separate from crude oil (Bresciani *et al.*, 2010).

This study demonstrates that this combination can fulfill water separation from highly stable water-in-crude oil emulsions. With the aim to enhance the efficiency of separation this study also advanced hydrophilic macroporous polymers with a high surface area, commonly called as polyHIPE polymer (PHP). This was achieved by producing silane and bindzil polyHIPEs via polymerisation of high internal phase emulsion and then sulphonated compared to one type (sulphonated standard PHP with a low surface area) that was used by Akay and Vickers (2003). The following are the conclusions drawn from this study.

#### 8.3.1 PolyHIPE Polymers

Four different PolyHIPE-based demulsifiers namely, silane polyHIPE and bindzil polyHIPE with different percentages of silane and bindzil, respectively, and standard sulphonated polyHIPE and in-situ sulphonated polyHIPE with different mixing times have been prepared. After production a number of tests were undertaken to determine the best materials to be used for demulsification tests including morphology (SEM), surface area and pore size distribution, water uptake and EDX and FTIR analyses. It was observed that the silane PHP had a high surface area of 98 m<sup>2</sup>/g and a high water absorption capacity compared to other PHPs, that is, bindzil, standard and insitu PHP, which have 52, 35 and 15 m<sup>2</sup>/g, respectively. Moreover, the silane PHP has the best pore and interconnecting pore sizes of 77-7 μm among other PHPs, which are the bindzil PHP of 99-8 μm, standard PHP of 108-8 μm and insitu PHP of 134-10

$\mu\text{m}$ . It was found that the best samples among all these polyHIPEs that are characterized by a large surface area, a high ability of water uptake and the best pore and interconnecting pore sizes are SL20, BZ25, B50 and IS40 for SL-PHP, BZ-PHP, B-PHP and IS-PHP, respectively. These optimum samples were used in a separating water experiments from water-in-crude oil emulsions by using an electrostatic coalescence technique. The water uptake results show the higher hydrophilicity of the silicon containing PHPs

### ***8.3.2 PolyHIPEs Sulphonation***

Through integration of the low concentration of sulphuric acid (sulphonation agent) with the aqueous phase of emulsion at the stage of emulsification of the production IS-PHP, the result was a sulphonated microporous polymer material without the formation of wastes. Unfortunately, the IS-PHP surface area was small, and its water absorption ability was low as well. Thus, the other methods of sulphonation that have been used are microwave irradiation and thermal methods in the sulphonation of the other PHPs. The sulphonation of both Bindzil-PHP and silane-PHP by the microwave irradiation method and the sulphonation of B-PHP by the thermal method were successful, where the result was not only increasing the microscale connectivity between the pores but also increasing the nanoscale connectivity and the surface area for each, (especially the sulphonated silane-PHP where there has been a clear development of surface area). By comparing the two-sulphonation methods, it appears that the microwave irradiation method is the best because it is easy and needs a little time (commonly 5 minutes) to conduct and its results are better (higher degree of sulphonation).

### ***8.3.3 Water-in-crude oil emulsions***

Several batches of water-in-crude oil emulsions were prepared in order to obtain a high stability emulsion by using an equal ratio of the aqueous and oil phases (50%), where three kinds of salts have been used to prepare the aqueous phase NaCl, CaCl<sub>2</sub> and MgCl<sub>2</sub> to mimic seawater. These batches of water-in-crude oil emulsions were produced with various processing parameters, namely agitation time and agitation speed. At a agitating speed of 400 rpm and different agitating times are 10, 20, 30, 40 and 50 minutes, the stability (i.e. the period of time, which a water-in-crude oil emulsion takes to totally demulsify naturally) was 12, 17, 23, 29 and 29 days, respectively. Moreover, at agitating speed of 800 rpm with agitating time of 50

minutes achieved stability of 61 days, while at agitating speed of 2000 rpm with agitating time of 25 minutes stability of 114 days was achieved.

As mentioned above, it can be concluded that the stability of water-in-crude oil emulsions is significantly influenced by the mixing speed while it is slightly improved by mixing time. In other words, a highest stability of 114 days was achieved at the highest mixing speed of 2000 rpm, although the mixing time was a little of 25 minutes. While, at a lowest mixing time of 400 rpm, the stability increased slightly from 12 to 29 days although the mixing time was significantly increased from 10 to 50 minutes.

The optimum water-in-crude oil emulsion, which was selected and used in demulsification experiments, which eventually resulted in a high stability of 114 days. This emulsion can be prepared and used in demulsification experiments without undergoing a significant change so that emulsion stability does not affect demulsification results.

#### ***8.3.4 Demulsification of water-in-crude oil emulsions***

In this study, the influence of different factors on the efficiency of demulsification and removal of the surface-active species have been evaluated. One of these factors is the type of PHP demulsifiers which were used; four optimum demulsifiers of produced polyHIPEs demulsifiers, namely SL20, BZ25, B50 and IS40 corresponding to PHP-I, PHP-II, PHP-III and PHP-IV, respectively. Another factor was the inlet flow rate of the water-in-crude oil emulsion, which was used in various inlet flow rates from 100 ml/min to 1500 ml/min. The final factor is the electric field strength, which depends on different applied voltages from 1-5 kV (equivalent to 14-69 kV/m).

After conducting many demulsification experiments under the factors mentioned above, it was found that the optimum demulsifiers mentioned above have achieved best separation efficiencies at the inlet flow rate of the water-in-crude oil emulsion of 100 mL/minute and applied voltage of 5 kV. PHP-I, the silane-PHP, achieved a significant separation efficiency of 89% compared to the separation efficiency with absence of PHP of 51%. PHP-II (the Bindzil PHP) attained a satisfactory separation efficiency of 72%, while PHP-III (standard PHP) and PHP-IV (in situ PHP) obtained unsatisfactory separation efficiencies of 56% and 54%, respectively. Moreover, the optimum demulsifiers (PHP-I and PHP-II) achieved a high ability

to remove surface-active species from crude oil that cause emulsification of crude oil such as Mg, Na, and Ca salts.

According to above results, it can be concluded that the best separation efficiency was 89% by using the silane demulsifier PHP at a flow rate of 100 ml/min and an applied voltage of 5 kV. Moreover, it could be said that the standard and in situ sulphonation of the demulsifier PHP is not sufficient to enhance the separation efficiency of demulsifier PHP that is proved by the results of PHP-III and PHP-IV, where they achieved only a slight increase in separation efficiency of 5% and 3%, more than separation efficiency without the presence of demulsifier PHP. On the other hand, it can be concluded that the addition of other materials such as silane and silica at certain percentages during the production of demulsifier PHP followed by sulphonation, will increase the ability of demulsifier PHP to enhance the separation efficiency. That is proved by the results of PHP-I and PHP-II, where they achieved a significant increase in separation efficiency of 38% and 21%, respectively more than separation efficiency when demulsifier PHP was not used. Moreover, due to the nature of ion-exchange for the demulsifier PHP, the optimum demulsifiers, especially PHP-I and PHP-II do not just enhance the separation efficiency, but they show a high ability to reduce the causes of the emulsification crude oil by their capacity to remove surface-active species from crude oil such as Mg, Na, and Ca chlorides.

### ***8.3.5 Reuse Spent PHP-I Demulsifier in Demulsification Experiments***

With the aim to find out how efficient the spent PHP-I is used in promoting the separation of water and the active-surfaces from the water-in-crude oil emulsion, the demulsification was conducted using the spent PHP-I sample (dried), along with electrostatic separator, using inlet flow rate of water-in-crude oil emulsion of 100 ml.min<sup>-1</sup> and variable electric field strength (from 1 - 5 kV applied voltage). This experiment achieved a separation efficiency of 71%. This meant that the spent PHP-I enhanced the separation efficiency by 20% more than separation efficiency when demulsifier PHP was not used. However, with the presence the original demulsifier PHP-I more than 18% separation efficiency was achieved. Moreover, its ability to remove surface-active species from crude oil such as Mg, Na, Cl and Ca cause emulsification of crude oil was maintained.

Generally, it can be concluded that the PHP-I demulsifier achieved reasonable results in terms of the percentage of separation and removal of surface-active species, but still needs some chemical modification to achieve reliable results to reuse it more than once.

#### **8.4 Final Remarks**

Demulsification of the emulsions of water-in-crude oil is a complicated field that is of significant importance in petroleum processing such that impractical approaches to resolve such emulsions may cause massive economical and environmental effects. Some of the existing demulsification methods used are more appropriate for treatment of the emulsion of oil-in water as compared to the emulsion of water-in-crude oil. Moreover, many of these methods of separation are feasible only with massive equipment. As a result, they are unsuitable for oil production offshore. The oilrigs demand small size equipment with high performance as well as reducing the nominal moving parts because of inadequate space. This study has attempted to intensify the demulsification with the aim of these requirements. Other areas of process intensification will benefit from the development of PHP. Such applications include bioprocess intensification, tissue engineering, and catalysis. Therefore, efforts geared towards producing such materials via a scaled-up, sustainable and robust technology would promote the PHP applications in these areas.

## 8.5 Future Work Recommendations.

- 1- The mechanism of demulsification process has not been completely understood. In order to achieve this goal, a feasible mathematical model that takes into account all variables of water-in-crude oil emulsion flow rates, applied voltage, type of demulsifier and viscosity and stability of the water-in-crude oil emulsion should be developed.
- 2- A bench-scale electrocoalescer was used to conduct the separation experiments of crude oil/water. However, the direct upscaling of the process data might not lead to the same outcomes. Therefore, it is necessary to conduct these experiments on a larger scale with a larger volume of emulsion to be separated and using equipment of greater capacity i.e. large-scale electrocoalescer. In particular the effect of residence time on demulsification efficiency needs to be determined in different unit designs. The mechanism robustness and degradation of the PHP grains also needs to be assessed in scale-up application.
- 3- Moreover, the effectiveness of high surface area polymer-based demulsifier could be enhanced by further functionalisation research for instance, silane systems with high hydrophilicity could be developed with improved water retention. Thus, for future applications it is relevant measure and understand the surface chemistry and water retention of this high surface area polymer in oil/water separation.

---

## REFERENCES

---

1. Abdurahman, H.N., Yunus, R.M. and Jemaat, Z. (2007) 'Chemical demulsification of water-in-crude oil emulsions', *Journal of Applied Sciences*, 7(2), pp. 196-201.
2. Abdurahman, N.H., Rosli, Y.M., Azhari, N.H. and Hayder, B.A. (2012) 'Pipeline transportation of viscous crudes as concentrated oil-in-water emulsions', *Journal of Petroleum Science and Engineering*, 90, pp. 139-144.
3. Acevedo, S., Escobar, G., Gutiérrez, L.B., Rivas, H. and Gutiérrez, X. (1993) 'Interfacial rheological studies of extra-heavy crude oils and asphaltenes: role of the dispersion effect of resins in the adsorption of asphaltenes at the interface of water-in-crude oil emulsions', *Colloids and Surfaces A: Physicochemical and Engineering Aspects*, 71(1), pp. 65-71.
4. Ahmed, N.S., Nassar, A.M., Zaki, N.N. and Gharieb, H.K. (1999) 'Formation of fluid heavy oil-in-water emulsions for pipeline transportation', *Fuel*, 78(5), pp. 593-600.
5. Akay, G. (1995) 'Flow induced phase inversion in powder structuring by polymers', *Polymer Powder Technology*, pp. 542-587.
6. Akay, G. (1998) 'Flow-induced phase inversion in the intensive processing of concentrated emulsions', *Chemical Engineering Science*, 53(2), pp. 203-223.
7. Akay, G. (2006) 'Bioprocess and chemical process intensification', *Encyclopaedia of Chemicals Processing*, 1, pp. 183-199.
8. Akay, G. (2014) *Process Intensification and Miniaturisation: Principles and Applications in Biological, Chemical and Environmental Technologies*. Newnes.
9. Akay, G., Bhumgara, Z. and Wakeman, R. (1995) 'Self-Supported Porous Channel Filtration Modules-Preparation, Properties and Performance', *Chemical engineering research & design*, 73(7), pp. 782-797.
10. Akay, G., Birch, M.A. and Bokhari, M.A. (2004) 'Microcellular polyHIPE polymer supports osteoblast growth and bone formation in vitro', *Biomaterials*, 25(18), pp. 3991-4000.

11. Akay, G., Bokhari, M., Byron, V. and Dogru, M. (2005a) 'Development of nano-structured micro-porous materials and their application in bioprocess–chemical process intensification and tissue engineering', *Chemical engineering: Trends and developments*. John Wiley & Sons, New York, pp. 171-197.
12. Akay, G. and Calkan, B. (2015) 'Preparation of nanostructured microporous metal foams through flow induced electroless deposition', *Journal of Nanomaterials*, 16(1), p. 271.
13. Akay, G., Dogru, M., Calkan, B. and Calkan, O. (2005b) *Symposium on Microreactor Technology and Process Intensification held at the 226th American Chemical Society National Meeting*. Newcastle University.
14. Akay, G., Downes, S. and Price, V. (2000) 'Microcellular polymers as cell growth media and novel polymers', *European Patent EP1183328*.
15. Akay, G., Keskinler, B., Cakici, A. and Danis, U. (1998) 'Phosphate removal from water by red mud using crossflow microfiltration', *Water Research*, 32(3), pp. 717-726.
16. Akay, G., S. Downes and V. J. Price (2002a) ' ', *European Patent*, 1, 183, 328.
17. Akay, G., S. Downes and V. J. Price (2002b) 'European Patent 1,183, 328'.
18. Akay, G. and Tong, L. (2000) 'Intensive structuring: intensive processing of microstructured materials by flow induced phase inversion', *Chemical Engineering & Technology: Industrial Chemistry-Plant Equipment-Process Engineering-Biotechnology*, 23(3), pp. 285-288.
19. Akay, G. and Vickers, J. (2003) 'Method for separating oil in water emulsions', *European Patent*, 1.
20. Akbari, S., Nour, A., Jamari, S. and Rajabi, A. (2016) 'Demulsification of water-in-crude oil emulsion via conventional heating and microwave heating technology in their optimum conditions', *Australian Journal of Basic and Applied Sciences*, 10(4), pp. 66-74.
21. Akmaz, S., Iscan, O., Gurkaynak, M. and Yasar, M. (2011) 'The structural characterization of saturate, aromatic, resin, and asphaltene fractions of Batiraman crude oil', *Petroleum Science and Technology*, 29(2), pp. 160-171.
22. Al-Roomi, Y., George, R., Elgibaly, A. and Elkamel, A. (2004) 'Use of a novel surfactant for improving the transportability/transportation of heavy/viscous crude oils', *Journal of Petroleum Science and Engineering*, 42(2-4), pp. 235-243.

23. Ali, M.F. and Alqam, M.H. (2000) 'The role of asphaltenes, resins and other solids in the stabilization of water in oil emulsions and its effects on oil production in Saudi oil fields', *Fuel*, 79(11), pp. 1309-1316.
24. Ali, M.F., Bukhari, A. and Misbah-ul-Hasan (1989) 'Structural characterization of Arabian heavy crude oil residue', *Fuel science & technology international*, 7(8), pp. 1179-1208.
25. Allan, R. and Mason, S. (1961) 'Effects of electric fields on coalescence in liquid+ liquid systems', *Transactions of the Faraday Society*, 57, pp. 2027-2040.
26. Andersen, S.I. and Speight, J.G. (2001) 'Petroleum resins: separation, character, and role in petroleum', *Petroleum science and technology*, 19(1-2), pp. 1-34.
27. Angle, C.W. (2001) 'Chemical demulsification of stable crude oil and bitumen emulsions in petroleum recovery—a review', in *Encyclopedic handbook of emulsion technology*. CRC Press, pp. 542-595.
28. Aomari, N., Gaudu, R., Cabioch, F. and Omari, A. (1998) 'Rheology of water in crude oil emulsions', *Colloids and Surfaces A: Physicochemical and Engineering Aspects*, 139(1), pp. 13-20.
29. Armit, J.W. and Robinson, R. (1925) 'CCXI.—Polynuclear heterocyclic aromatic types. Part II. Some anhydronium bases', *Journal of the Chemical Society, Transactions*, 127, pp. 1604-1618.
30. Aronson, M.P. and Petko, M.F. (1993) 'Highly concentrated water-in-oil emulsions: Influence of electrolyte on their properties and stability', *Journal of Colloid and Interface Science*, 159(1), pp. 134-149.
31. Aryafar, H. and Kavehpour, H.P. (2009) 'Electrocoalescence: effects of DC electric fields on coalescence of drops at planar interfaces', *Langmuir*, 25(21), pp. 12460-12465.
32. Aske, N. (2002) 'Characterisation of crude oil components, asphaltene aggregation and emulsion stability by means of near infrared spectroscopy and multivariate analysis', *Norwegian University of Science and Technology*, p. 49.
33. Aske, N., Kallevik, H. and Sjöblom, J. (2001) 'Determination of saturate, aromatic, resin, and asphaltenic (SARA) components in crude oils by means of infrared and near-infrared spectroscopy', *Energy & Fuels*, 15(5), pp. 1304-1312.
34. Atta, A., Crawford, D.G., Koch, C.R. and Bhattacharjee, S. (2011) 'Influence of electrostatic and chemical heterogeneity on the electric-field-induced destabilization of thin liquid films', *Langmuir*, 27(20), pp. 12472-12485.

35. Aveyard, R., Binks, B.P., Fletcher, P.D.I. and Lu, J.R. (1990) 'The resolution of water-in-crude oil emulsions by the addition of low molar mass demulsifiers', *Journal of Colloid and Interface Science*, 139(1), pp. 128-138.
36. Azodi, M. and Nazar, A.R.S. (2013) 'An experimental study on factors affecting the heavy crude oil in water emulsions viscosity', *Journal of Petroleum Science and Engineering*, 106, pp. 1-8.
37. Bailes, P. (1981) 'An Experimental Investigation into the Use of High Voltage, DC Field for Liquid Phase Separation', *Trans. Inst. Chem. Eng.*, 59, pp. 229-237.
38. Bailes, P. (1987) 'Column Liquid Contacting with Vigorous an Agitation Balanced by Electrostatic Coalescence', *Chem. Eng. Res. Des.*, 65, pp. 514-523.
39. Bailes, P. and Larkai, S. (1982) 'Liquid phase separation in pulsed d. c. fields', *Transactions of the Institution of Chemical Engineers*, 60(2), pp. 115-121.
40. Bailes, P. and Larkai, S. (1984) 'Influence of phase ratio on electrostatic coalescence of water-in-oil dispersions', *Transactions of the Institution of Chemical Engineers*, 62, pp. 33-8.
41. Bailes, P. and Watson, M. (1992) 'Electrostatic and centrifugal separation of liquid dispersions', *UK Patent A*, 2249741.
42. Barbetta, A. and Cameron, N.R. (2004) 'Morphology and surface area of emulsion-derived (PolyHIPE) solid foams prepared with oil-phase soluble porogenic solvents: Span 80 as surfactant', *Macromolecules*, 37(9), pp. 3188-3201.
43. Barbetta, A., Cameron, N.R. and Cooper, S.J. (2000) 'High internal phase emulsions (HIPEs) containing divinylbenzene and 4-vinylbenzyl chloride and the morphology of the resulting PolyHIPE materials', *Chemical Communications*, (3), pp. 221-222.
44. Barby, D. and Haq, Z. (1982) 'Eur. Pat. 0060138'.
45. Barby, D. and Haq, Z. (1985) 'Low density porous cross-linked polymeric materials and their preparation and use as carriers for included liquids'. Google Patents.
46. Barzin, J., Azizi, H. and Morshedian, J. (2006) 'Preparation of silane-grafted and moisture cross-linked low density polyethylene: Part I: Factors affecting performance of grafting and cross-linking', *Polymer-Plastics Technology and Engineering*, 45(8), pp. 979-983.
47. Becher, P. (1966) 'Emulsions: Theory and Practice, 2nd Edition. Florida, Litton Educational Publishing Company.'

48. Benayoune, M., Khezzer, L. and Al-Rumhy, M. (1998) 'Viscosity of water in oil emulsions', *Petroleum science and technology*, 16(7-8), pp. 767-784.
49. Bezemer, C. and Croes, G. (1955) 'Motion of water droplets of an emulsion in a non-uniform field', *British Journal of Applied Physics*, 6(6), p. 224.
50. Bhagiyalakshmi, M., Anuradha, R., Do Park, S. and Jang, H.T. (2010) 'Octa (aminophenyl) silsesquioxane fabrication on chlorofunctionalized mesoporous SBA-15 for CO<sub>2</sub> adsorption', *Microporous and Mesoporous Materials*, 131(1-3), pp. 265-273.
51. Bhardwaj, A. and Hartland, S. (1994) 'Dynamics of emulsification and demulsification of water in crude oil emulsions', *Industrial & engineering chemistry research*, 33(5), pp. 1271-1279.
52. Bhardwaj, A. and Hartland, S. (1998) 'Studies on build up of interfacial film at the crude oil/water interface', *Journal of dispersion science and technology*, 19(4), pp. 465-473.
53. Bhumgara, Z.G. (1995) *A study of the development of polyhipe foam materials for use in separation processes*. University of Exeter.
54. Binks, B. and Lumsdon, S. (1999) 'Stability of oil-in-water emulsions stabilised by silica particles', *Physical Chemistry Chemical Physics*, 1(12), pp. 3007-3016.
55. Binks, B.P. (2002) 'Particles as surfactants—similarities and differences', *Current opinion in colloid & interface science*, 7(1-2), pp. 21-41.
56. Binks, B.P. and Whitby, C.P. (2004) 'Silica particle-stabilized emulsions of silicone oil and water: aspects of emulsification', *Langmuir*, 20(4), pp. 1130-1137.
57. Bokhari, M. (2003) *Bone tissue engineering using novel microcellular polymers*. University of Newcastle upon Tyne.
58. Bokhari, M., Birch, M. and Akay, G. (2003) 'Polyhipe Polymer: A Novel Scaffold for In Vitro Bone Tissue Engineering', in *Tissue Engineering, Stem Cells, and Gene Therapies*. Springer, pp. 247-254.
59. Boode, K. and Walstra, P. (1993) 'Partial coalescence in oil-in-water emulsions 1. Nature of the aggregation', *Colloids and Surfaces A: Physicochemical and Engineering Aspects*, 81, pp. 121-137.
60. Borwankar, R.P. and Case, S.E. (1997) 'Rheology of emulsions, foams and gels', *Current opinion in colloid & interface science*, 2(6), pp. 584-589.
61. Bresciani, A.E., Mendonça, C.F., Alves, R.M. and Nascimento, C.A. (2010) 'Modeling the kinetics of the coalescence of water droplets in crude oil emulsions

- subject to an electric field, with the cellular automata technique', *Computers & Chemical Engineering*, 34(12), pp. 1962-1968.
62. Brown, A. and Hanson, C. (1965) 'Effect of oscillating electric fields on coalescence in liquid+ liquid systems', *Transactions of the Faraday Society*, 61, pp. 1754-1760.
  63. Buist, I., Guarino, A., DeVitis, D., Nolan, K., Lewis, A., Smith, B. and Lane, J. (2002) 'Extending temporary storage capacity with emulsion breakers'.
  64. Buist, I., Lewis, A., Guarino, A. and Mullin, J. (2005) *International Oil Spill Conference*. American Petroleum Institute.
  65. Burke, D., Akay, G. and Bilsborrow, P. (2006) *CHISA: 17th International Congress of Chemical and Process Engineering*. Newcastle University.
  66. Byron, V.J. (2000) *The development of microcellular polymers as a support for tissue engineering*. University of Newcastle.
  67. Calkan, B. (2007) *Preparation of novel nano-structured macro-and meso-porous metal foams for process intensification and miniaturization*. University of Newcastle Upon Tyne.
  68. Calkan, O.F., M. Dogru and A. Galip (2005) 'Nano-structured micro-porous catalyses for intensified catalyses', *7th World Congress of Chemical Engineering, Glasgow, Scotland, IChemE*.
  69. Cameron, N.R. (2005) 'High internal phase emulsion templating as a route to well-defined porous polymers', *Polymer*, 46(5), pp. 1439-1449.
  70. Cameron, N.R. and Barbetta, A. (2000) 'The influence of porogen type on the porosity, surface area and morphology of poly (divinylbenzene) PolyHIPE foams', *Journal of Materials Chemistry*, 10(11), pp. 2466-2471.
  71. Cameron, N.R. and Sherrington, D.C. (1997) 'Synthesis and Characterization of Poly (aryl ether sulfone) PolyHIPE Materials', *Macromolecules*, 30(19), pp. 5860-5869.
  72. Cameron, N.R., Sherrington, D.C., Ando, I. and Kurosu, H. (1996) 'Chemical modification of monolithic poly (styrene-divinylbenzene) polyHIPE® materials', *Journal of Materials Chemistry*, 6(5), pp. 719-726.
  73. Charles, G.E. and Mason, S.G. (1960) 'The mechanism of partial coalescence of liquid drops at liquid/liquid interfaces', *Journal of Colloid Science*, 15(2), pp. 105-122.

74. Charles, G.E.a.S.G.M. (1960a) 'the coalescence of liquid drops at liquid with fat liquid/liquid interfaces ', *Colloid Science*, 13, pp. 112-117.
75. Charles, G.E.a.S.G.M. (1960b) 'The mechanism of partial coalescence of liquid drops at liquid/liquid interface ', *Colloid Science* 15, pp. 105-112.
76. Charles, G.E.a.S.G.M. (1961) 'The coalescence of liquids drops with fat liquid/liquid interfaces', *Colloid Science*, 15, pp. 236-267.
77. Chen, C.-T., Maa, J.-R., Yang, Y.-M. and Chang, C.-H. (1998) 'Effects of electrolytes and polarity of organic liquids on the coalescence of droplets at aqueous-organic interfaces', *Surface science*, 406(1-3), pp. 167-177.
78. Chen, C., Guo, J., An, N., Pan, Y., Li, Y. and Jiang, Q. (2012) 'Study of asphaltene dispersion and removal for high-asphaltene oil wells', *Petroleum Science*, 9(4), pp. 551-557.
79. Chen, Q., Liang, W. and Song, C. (2014) 'Effect of electric field strength on crude oil emulsion's demulsification and dehydration', *High Voltage Engineering*, 40, pp. 173-180.
80. Chen, T., Mohammed, R., Bailey, A., Luckham, P. and Taylor, S. (1994) 'Dewatering of crude oil emulsions 4. Emulsion resolution by the application of an electric field', *Colloids and Surfaces A: Physicochemical and Engineering Aspects*, 83(3), pp. 273-284.
81. Chen, X., Yuan, W., Jiang, M. and Xie, X. (2018) 'Surface glycopolymer-modified functional macroporous polyHIPE obtained by ATRP for the removal of boron in water', *New Journal of Chemistry*, 42(3), pp. 2104-2112.
82. Chiesa, M., Ingebrigtsen, S., Melheim, J.A., Hemmingsen, P.V., Hansen, E.B. and Hestad, Ø. (2006) 'Investigation of the role of viscosity on electrocoalescence of water droplets in oil', *Separation and purification technology*, 50(2), pp. 267-277.
83. Chiesa, M., Melheim, J., Pedersen, A., Ingebrigtsen, S. and Berg, G. (2005) 'Forces acting on water droplets falling in oil under the influence of an electric field: numerical predictions versus experimental observations', *European Journal of Mechanics-B/Fluids*, 24(6), pp. 717-732.
84. Clark, P.E. and Pilehvari, A. (1993) 'Characterization of crude oil-in-water emulsions', *Journal of Petroleum Science and Engineering*, 9(3), pp. 165-181.
85. Clarkson, M. and Smedley, S. (1988) 'Electrical conductivity and permittivity measurements near the percolation transition in a microemulsion: I. Experiment', *Physical Review A*, 37(6), p. 2070.

86. Clause, D., Gomez, F., Dalmazzone, C. and Noik, C. (2005) 'A method for the characterization of emulsions, thermogravimetry: Application to water-in-crude oil emulsion', *Journal of colloid and interface science*, 287(2), pp. 694-703.
87. Clause, M. (1983) 'Encyclopedia of emulsion technology', *Basic theory. Dielectric Properties Of Emulsions And Related Systems New York: Marcel Dekker Inc*, pp. 481-715.
88. Cottrell, F.G. and Speed, J.B. (1911) 'Separating and collecting particles of one liquid suspended in another liquid'. Google Patents.
89. Dale, J., Bennett, B., Aplin, A. and Larter, S. (1997) 'The partition behaviour of alkylphenols and aromatic hydrocarbons in North Sea crude oil and coexisting water', *Geofluids II*, 7, pp. 10-14.
90. Davis, H.T. (1994) 'Factors determining emulsion type: Hydrophile—lipophile balance and beyond', *Colloids and Surfaces A: Physicochemical and Engineering Aspects*, 91, pp. 9-24.
91. Demirbas, A. (2015) 'Recovery of gasoline and diesel range hydrocarbons from waste vegetable oils', *Petroleum Science and Technology*, 33(19), pp. 1703-1711.
92. Demirbas, A. (2016) 'Deposition and flocculation of asphaltenes from crude oils', *Petroleum Science and Technology*, 34(1), pp. 6-11.
93. Demirbaş, A. (2002) 'Asphaltene yields from five types of fuels via different methods', *Energy conversion and management*, 43(8), pp. 1091-1097.
94. Demirbas, A. and Taylan, O. (2016) 'Removing of resins from crude oils', *Petroleum Science and Technology*, 34(8), pp. 771-777.
95. Dezhi, S., Chung, J.S., Xiaodong, D. and Ding, Z. (1999) 'Demulsification of water-in-oil emulsion by wetting coalescence materials in stirred-and packed-columns', *Colloids and Surfaces A: Physicochemical and Engineering Aspects*, 150(1-3), pp. 69-75.
96. Dicharry, C., Arla, D., Siquin, A., Graciaa, A. and Bouriat, P. (2006) 'Stability of water/crude oil emulsions based on interfacial dilatational rheology', *Journal of colloid and interface science*, 297(2), pp. 785-791.
97. Djuve, J., Yang, X., Fjellanger, I., Sjöblom, J. and Pelizzetti, E. (2001) 'Chemical destabilization of crude oil based emulsions and asphaltene stabilized emulsions', *Colloid and Polymer Science*, 279(3), pp. 232-239.

98. Dogru, M., Beltran, M.R., Mitra, S., Erdem, A. and Park, E.S. (2019) 'Updraft Gasification of Waste and Produced Syngas Treatment', in *Waste Management and Resource Efficiency*. Springer, pp. 741-752.
99. Draxler, J. and Marr, R. (1993) 'Design criteria for electrostatic deemulsifiers', *International Chemical Engineering (A Quarterly Journal of Translations from Russia, Eastern Europe and Asia);(United States)*, 33(1).
100. Drelich, A., Gomez, F., Clause, D. and Pezron, I. (2010) 'Evolution of water-in-oil emulsions stabilized with solid particles: Influence of added emulsifier', *Colloids and Surfaces A: Physicochemical and Engineering Aspects*, 365(1-3), pp. 171-177.
101. Dudášová, D., Flåten, G.R., Sjöblom, J. and Øye, G. (2009) 'Study of asphaltene adsorption onto different minerals and clays: Part 2. Particle characterization and suspension stability', *Colloids and Surfaces A: Physicochemical and Engineering Aspects*, 335(1-3), pp. 62-72.
102. Dudášová, D., Simon, S., Hemmingsen, P.V. and Sjöblom, J. (2008) 'Study of asphaltene adsorption onto different minerals and clays: Part 1. Experimental adsorption with UV depletion detection', *Colloids and Surfaces A: Physicochemical and Engineering Aspects*, 317(1-3), pp. 1-9.
103. Eddy, H.C. (1932) 'Method and apparatus for treating oil under vacuum', *US patent 1 796 750*.
104. Eddy, H.C. (1936) 'Method and apparatus for breaking emulsions', *US patent 2 083 285*.
105. Eddy, H.C. (1937) 'Method and apparatus for dehydrating petroleum', *USA Patent 2 083 801*.
106. Edmondson, J. (1998) 'Method and apparatus of oil/water de-emulsification', *US Patent O ce*, 5.
107. Ekott, E.J. and Akpabio, E.J. (2010) 'A review of water-in-crude oil emulsion stability, destabilization and interfacial rheology', *Journal of Engineering and Applied Sciences*, 5(6), pp. 447-452.
108. El Gamal, M., Mohamed, A.-M.O. and Zekri, A.Y. (2005) 'Effect of asphaltene, carbonate, and clay mineral contents on water cut determination in water-oil emulsions', *Journal of Petroleum science and Engineering*, 46(3), pp. 209-224.
109. Elektorowicz, M., Habibi, S. and Chifrina, R. (2006) 'Effect of electrical potential on the electro-demulsification of oily sludge', *Journal of colloid and interface science*, 295(2), pp. 535-541.

110. Eley, D., Hey, M. and Symonds, J. (1988) 'Emulsions of water in asphaltene-containing oils 2. Rheology', *Colloids and surfaces*, 32, pp. 103-112.
111. Elsharkawy, A.M., Al-Sahhaf, T.A. and Fahim, M.A. (2008) 'Characterization of asphaltenes and resins separated from water-in-oil emulsions', *Petroleum Science and Technology*, 26(2), pp. 153-169.
112. Elsharkawy, A.M., Oakley, F. and Mann, D.A. (2005) 'The role and regulation of hepatic stellate cell apoptosis in reversal of liver fibrosis', *Apoptosis*, 10(5), pp. 927-939.
113. 'The eniginnering toolBox', (2019), available at [https://www.engineeringtoolbox.com/api-gravity-d\\_1212.html](https://www.engineeringtoolbox.com/api-gravity-d_1212.html).
114. Eow, J.S. and Ghadiri, M. (2002) 'Electrostatic enhancement of coalescence of water droplets in oil: a review of the technology', *Chemical Engineering Journal*, 85(2-3), pp. 357-368.
115. Eow, J.S. and Ghadiri, M. (2003a) 'The behaviour of a liquid–liquid interface and drop-interface coalescence under the influence of an electric field', *Colloids and Surfaces A: Physicochemical and Engineering Aspects*, 215(1-3), pp. 101-123.
116. Eow, J.S. and Ghadiri, M. (2003b) 'Drop–drop coalescence in an electric field: the effects of applied electric field and electrode geometry', *Colloids and Surfaces A: Physicochemical and Engineering Aspects*, 219(1-3), pp. 253-279.
117. Eow, J.S. and Ghadiri, M. (2003c) 'Motion, deformation and break-up of aqueous drops in oils under high electric field strengths', *Chemical Engineering and Processing: Process Intensification*, 42(4), pp. 259-272.
118. Eow, J.S., Ghadiri, M. and Sharif, A.O. (2002) 'Electrostatic and hydrodynamic separation of aqueous drops in a flowing viscous oil', *Chemical Engineering and Processing: Process Intensification*, 41(8), pp. 649-657.
119. Eow, J.S., Ghadiri, M. and Sharif, A.O. (2007) 'Electro-hydrodynamic separation of aqueous drops from flowing viscous oil', *Journal of Petroleum Science and Engineering*, 55(1-2), pp. 146-155.
120. Eow, J.S., Ghadiri, M., Sharif, A.O. and Williams, T.J. (2001) 'Electrostatic enhancement of coalescence of water droplets in oil: a review of the current understanding', *Chemical engineering journal*, 84(3), pp. 173-192.
121. Eow, J.S.a.M.G. (2002) 'Electrocoalesce-separators for the separation of aqueous drops from a flowing dielectric viscous liquid', *Separation and purification technology*, 29, pp. 63-77.

122. Eow, J.S.a.M.G. (2003) 'The behaviour of a liquid-liquid interface and drop-interface coalescence under the influence of an electric field', *Colloids and Surfaces A: Physicochemical and Engineering Aspects*, 215, pp. 101-123.
123. Ese, M.-H., Galet, L., Clause, D. and Sjöblom, J. (1999) 'Properties of Langmuir surface and interfacial films built up by asphaltenes and resins: influence of chemical demulsifiers', *Journal of colloid and interface science*, 220(2), pp. 293-301.
124. Faibish, R.S. and Cohen, Y. (2001) 'Fouling-resistant ceramic-supported polymer membranes for ultrafiltration of oil-in-water microemulsions', *Journal of Membrane Science*, 185(2), pp. 129-143.
125. Fakhru'l-Razi, A., Pendashteh, A., Abdullah, L.C., Biak, D.R.A., Madaeni, S.S. and Abidin, Z.Z. (2009) 'Review of technologies for oil and gas produced water treatment', *Journal of hazardous materials*, 170(2-3), pp. 530-551.
126. Feng, X., Wang, S., Hou, J., Wang, L., Cepuch, C., Masliyah, J. and Xu, Z. (2011) 'Effect of hydroxyl content and molecular weight of biodegradable ethylcellulose on demulsification of water-in-diluted bitumen emulsions', *Industrial & Engineering Chemistry Research*, 50(10), pp. 6347-6354.
127. Ficken, K.J., Wooller, M.J., Swain, D., Street-Perrott, F.A. and Eglinton, G. (2002) 'Reconstruction of a subalpine grass-dominated ecosystem, Lake Rutundu, Mount Kenya: a novel multi-proxy approach', *Palaeogeography, Palaeoclimatology, Palaeoecology*, 177(1-2), pp. 137-149.
128. Figueroa, C.E. and Wagner, J.P. (1997) 'A liquid membrane approach for removal of metallic species from resinous extracts under imposed electrical fields', *Bioresource technology*, 60(2), pp. 153-160.
129. Fingas, M. (1995) 'Water-in-oil emulsion formation: A review of physics and mathematical modelling', *Spill Science & Technology Bulletin*, 2(1), pp. 55-59.
130. Fingas, M. (2014) *Handbook of oil spill science and technology*. John Wiley & Sons.
131. Fingas, M. and Fieldhouse, B. (2003) 'Studies of the formation process of water-in-oil emulsions', *Marine pollution bulletin*, 47(9-12), pp. 369-396.
132. Fingas, M. and Fieldhouse, B. (2004) 'Formation of water-in-oil emulsions and application to oil spill modelling', *Journal of Hazardous Materials*, 107(1-2), pp. 37-50.

133. Fingas, M. and Fieldhouse, B. (2009) 'Studies on crude oil and petroleum product emulsions: Water resolution and rheology', *Colloids and Surfaces A: Physicochemical and Engineering Aspects*, 333(1-3), pp. 67-81.
134. Fingas, M., Fieldhouse, B.G. and Mullin, J.V. (2001) 'Environmental emulsions', in *Encyclopedic Handbook of Emulsion Technology*. Marcel Dekker New York, pp. 409-442.
135. Fisher, H.F. (1931) 'Method of inverting the phase emulsion', *US Patent 1 838 379*.
136. Fleming, I. and Williams, D.H. (1966) 'Spectroscopic methods in organic chemistry', *McGraw-Hill, New York*, 19, p. 56.
137. Førdedal, H., Schildberg, Y., Sjöblom, J. and Volle, J.-L. (1996) 'Crude oil emulsions in high electric fields as studied by dielectric spectroscopy. Influence of interaction between commercial and indigenous surfactants', *Colloids and Surfaces A: Physicochemical and Engineering Aspects*, 106(1), pp. 33-47.
138. Fredrick, E., Walstra, P. and Dewettinck, K. (2010) 'Factors governing partial coalescence in oil-in-water emulsions', *Advances in colloid and interface science*, 153(1-2), pp. 30-42.
139. Friberg, S.E.a.J.Y. (2001) 'Emulsion Stability. Emulsion and Emulsions stability. J. Sjoblom. New York, Marcel Dekker', pp. 1-39.
140. Galarneau, A., Villemot, F., Rodriguez, J., Fajula, F. and Coasne, B. (2014) 'Validity of the t-plot method to assess microporosity in hierarchical micro/mesoporous materials', *Langmuir*, 30(44), pp. 13266-13274.
141. Galvin, C.P. (1986) 'Design principles for electrical coalescers', *ICHEME Symposium Series*, 88, pp. 101-113.
142. Galvin, K., Pratten, S., Shankar, N., Evans, G., Biggs, S. and Tunaley, D. (2001) 'Production of high internal phase emulsions using rising air bubbles', *Chemical engineering science*, 56(21-22), pp. 6285-6293.
143. Galvin, P. (2013) 'Design principles for electrical coalescers', *Proc. Extraction" 84, EFCE*, 43, pp. 101-113.
144. Gamys, C.G., Beyou, E. and Bourgeat-Lami, E. (2010) 'Micellar behavior of well-defined polystyrene-based block copolymers with triethoxysilyl reactive groups and their hydrolysis–condensation', *Journal of Polymer Science Part A: Polymer Chemistry*, 48(4), pp. 784-793.

145. Gang, L., QiongHua, L. and PanSheng, L. (1997) 'Break-down of liquid membrane emulsion under high electric field', *Journal of membrane science*, 128(1), pp. 1-6.
146. Ghadiri, M. and Eow, J. (2003) 'Separating components of liquid/liquid emulsion using electrostatic force', *UK Patent Application, GB2377397*, 15.
147. Ghannam, M.T., Hasan, S.W., Abu-Jdayil, B. and Esmail, N. (2012) 'Rheological properties of heavy & light crude oil mixtures for improving flowability', *Journal of Petroleum Science and Engineering*, 81, pp. 122-128.
148. Gharbi, K., Benyounes, K. and Khodja, M. (2017) 'Removal and prevention of asphaltene deposition during oil production: A literature review', *Journal of Petroleum Science and Engineering*, 158, pp. 351-360.
149. Giraldo, J., Nassar, N.N., Benjumea, P., Pereira-Almao, P. and Cortés, F.B. (2013) 'Modeling and prediction of asphaltene adsorption isotherms using Polanyi's modified theory', *Energy & Fuels*, 27(6), pp. 2908-2914.
150. Goldszal, A. and Bourrel, M. (2000) 'Demulsification of crude oil emulsions: correlation to microemulsion phase behavior', *Industrial & engineering chemistry research*, 39(8), pp. 2746-2751.
151. Goto, M., Irie, J., Kondo, K. and Nakashio, F. (1989) 'Electrical demulsification of W/O emulsion by continuous tubular coalescer', *Journal of Chemical Engineering of Japan*, 22(4), pp. 401-406.
152. Greco, P.P. (2014) *Development of novel polymeric and composite Nano-Structured Micro-Porous Materials for impact resistance applications*. Newcastle University.
153. Gregory, D.P., Sharpies, M. and Tucker, I. M. (1989) *Eur Pat Appl 299762*.
154. Gutiérrez, J.M., González, C., Maestro, A., Solè, I., Pey, C.M. and Nolla, J. (2008) 'Nano-emulsions: New applications and optimization of their preparation', *Current Opinion in Colloid & Interface Science*, 13(4), pp. 245-251.
155. Ha, J.-W. and Yang, S.-M. (1998) 'Effect of nonionic surfactant on the deformation and breakup of a drop in an electric field', *Journal of colloid and interface science*, 206(1), pp. 195-204.
156. Ha, J.-W. and Yang, S.-M. (1999) 'Breakup of a multiple emulsion drop in a uniform electric field', *Journal of Colloid and Interface Science*, 213(1), pp. 92-100.

157. Haibach, K., Menner, A., Powell, R. and Bismarck, A. (2006) 'Tailoring mechanical properties of highly porous polymer foams: Silica particle reinforced polymer foams via emulsion templating', *Polymer*, 47(13), pp. 4513-4519.
158. Hainey, P., Huxham, I., Rowatt, B., Sherrington, D. and Tetley, L. (1991) 'Synthesis and ultrastructural studies of styrene-divinylbenzene polyhipe polymers', *Macromolecules*, 24(1), pp. 117-121.
159. Hajivand, P. and Vaziri, A. (2015) 'Optimization of demulsifier formulation for separation of water from crude oil emulsions', *Brazilian Journal of Chemical Engineering*, 32(1), pp. 107-118.
160. Haq, Z. (1985) 'Porous cross-linked absorbent polymeric materials'. Google Patents.
161. Harbottle, D., Chen, Q., Moorthy, K., Wang, L., Xu, S., Liu, Q., Sjöblom, J. and Xu, Z. (2014) 'Problematic stabilizing films in petroleum emulsions: Shear rheological response of viscoelastic asphaltene films and the effect on drop coalescence', *Langmuir*, 30(23), pp. 6730-6738.
162. Hasan, H. (2013) *Preparation of novel composite polyHIPE polymers and their applications in intensified removal of tars from syngas*. Newcastle University.
163. Hauertmann, H., Degener, W. and Schügerl, K. (1989) 'Electrostatic coalescence: reactor, process control, and important parameters', *Separation Science and Technology*, 24(3-4), pp. 253-273.
164. Hayman, M., Smith, K., Cameron, N. and Przyborski, S. (2004) 'Enhanced neurite outgrowth by human neurons grown on solid three-dimensional scaffolds', *Biochemical and biophysical research communications*, 314(2), pp. 483-488.
165. Hayman, M., Smith, K., Cameron, N. and Przyborski, S. (2005) 'Growth of human stem cell-derived neurons on solid three-dimensional polymers', *Journal of biochemical and biophysical methods*, 62(3), pp. 231-240.
166. Hemmingsen, P.V., Silset, A., Hannisdal, A. and Sjöblom, J. (2005) 'Emulsions of heavy crude oils. I: Influence of viscosity, temperature, and dilution', *Journal of dispersion science and technology*, 26(5), pp. 615-627.
167. Herbsman, A.M. (1933) 'Method of treating petroleum emulsion', *US Patent 1 931 112*.
168. Herrera, N.N., Letoffe, J.-M., Reymond, J.-P. and Bourgeat-Lami, E. (2005) 'Silylation of laponite clay particles with monofunctional and trifunctional vinyl alkoxysilanes', *Journal of Materials Chemistry*, 15(8), pp. 863-871.

169. Hong, I.K., Kim, S.I. and Lee, S.B. (2018) 'Effects of HLB value on oil-in-water emulsions: Droplet size, rheological behavior, zeta-potential, and creaming index', *Journal of Industrial and Engineering Chemistry*, 67, pp. 123-131.
170. Hoshyargar, V. and Ashrafizadeh, S.N. (2013) 'Optimization of flow parameters of heavy crude oil-in-water emulsions through pipelines', *Industrial & Engineering Chemistry Research*, 52(4), pp. 1600-1611.
171. Hou, J., Feng, X., Masliyah, J. and Xu, Z. (2012) 'Understanding interfacial behavior of ethylcellulose at the water–diluted bitumen interface', *Energy & Fuels*, 26(3), pp. 1740-1745.
172. Hubbard, K.L., Finch, J.A. and Darling, G.D. (1998) 'The preparation and characteristics of poly (divinylbenzene-co-ethylvinylbenzene), including Ambeflite XAD-4. Styrenic resins with pendant vinylbenzene groups', *Reactive and Functional Polymers*, 36(1), pp. 17-30.
173. Ilyin, S., Pakhmanova, O., Kostyuk, A. and Antonov, S. (2017) 'Effect of the Asphaltene, Resin, and Wax Contents on the Physicochemical Properties and Quality Parameters of Crude Oils', *Petroleum Chemistry*, 57(12), pp. 1141-1143.
174. Ino, H. (1983) 'Demulsification of W/O Emulsion under Applied AC Potential', *Kagaku Kogaku Ronbunshu*, 9, pp. 263-269.
175. Isaacs, E. and Chow, R. (1992) 'Practical aspects of emulsion stability', *Advances in Chemistry Series*, (231), pp. 51-77.
176. Isaacs, E., Huang, H., Chow, R. and Babchin, A. (1991) 'Coalescence Behavior of Water-in-Oil Emulsions', in *Particle Technology and Surface Phenomena in Minerals and Petroleum*. Springer, pp. 157-171.
177. Isaacs, E.E., Huang, H., Babchin, A.J. and Chow, R.S. (1990) 'Electroacoustic method for monitoring the coalescence of water-in-oil emulsions', *Colloids and surfaces*, 46(2), pp. 177-192.
178. Ivanov, I.B. and Kralchevsky, P.A. (1997) 'Stability of emulsions under equilibrium and dynamic conditions', *Colloids and Surfaces A: Physicochemical and engineering aspects*, 128(1-3), pp. 155-175.
179. Jafari, A., Tynjälä, T., Mousavi, S.M. and Sarkomaa, P. (2008) 'Simulation of heat transfer in a ferrofluid using computational fluid dynamics technique', *International Journal of Heat and Fluid Flow*, 29(4), pp. 1197-1202.
180. Jang, W. and Lee, Y. (2000) 'Dynamics of emulsification and demulsification of water in crude oil emulsions', *J. Ind. Eng. Chem*, 6, pp. 85-92.

181. Jiang, G. and Zeng, J. (2010) 'Preparation of nano-TiO<sub>2</sub>/polystyrene hybride microspheres and their antibacterial properties', *Journal of applied polymer science*, 116(2), pp. 779-784.
182. Johansen, E.J., Skjävö, I.M., Lund, T., Sjöblom, J., Söderlund, H. and Boström, G. (1988) 'Water-in-crude oil emulsions from the norwegian continental shelf part I. Formation, characterization and stability correlations', *Colloids and surfaces*, 34(4), pp. 353-370.
183. Jones, T.J., E. L. Neustadter and K. P. Whittingham (1978) *Journal of Canadian Petroleum Technology*, 17, pp. 100-109.
184. Kahdim, M.S. (2017) 'Characterisatrionof a nonporous polymers for water treatment'.
185. Kang, W., Jing, G., Zhang, H., Li, M. and Wu, Z. (2006) 'Influence of demulsifier on interfacial film between oil and water', *Colloids and Surfaces A: Physicochemical and Engineering Aspects*, 272(1-2), pp. 27-31.
186. Khadim, M.A. and Sarbar, M.A. (1999) 'Role of asphaltene and resin in oil field emulsions', *Journal of Petroleum Science and Engineering*, 23(3-4), pp. 213-221.
187. Khajehesamedini, A., Anzai, T.K., Castor Jr, C.A., Nele, M. and Pinto, J.C. (2018) 'Hybrid Modeling of the Electrocoalescence Process in Water-in-Oil Emulsions', *Energy & Fuels*, 32(4), pp. 5596-5610.
188. Kilpatrick, P.K. (2012) 'Water-in-crude oil emulsion stabilization: Review and unanswered questions', *Energy & Fuels*, 26(7), pp. 4017-4026.
189. Kilpatrick, P.K. and Spiecker, P.M. (2001) 'Asphaltene emulsions', in *Encyclopedic handbook of emulsion technology*. CRC Press, pp. 705-728.
190. Kim, B.-Y., Moon, J.H., Sung, T.-H., Yang, S.-M. and Kim, J.-D. (2002) 'Demulsification of water-in-crude oil emulsions by a continuous electrostatic dehydrator', *Separation science and technology*, 37(6), pp. 1307-1320.
191. Kim, S.-H., Shin, C.-K., Ahn, C.-H. and Kim, G.-J. (2006) 'Syntheses and application of silica monolith with bimodal meso/macroscopic pore structure', *Journal of Porous Materials*, 13(3-4), pp. 201-205.
192. Kim, Y.-H., Wasan, D. and Breen, P. (1995) 'A study of dynamic interfacial mechanisms for demulsification of water-in-oil emulsions', *Colloids and Surfaces A: Physicochemical and Engineering Aspects*, 95(2-3), pp. 235-247.

193. Kimmins, S.D. and Cameron, N.R. (2011) 'Functional porous polymers by emulsion templating: recent advances', *Advanced Functional Materials*, 21(2), pp. 211-225.
194. Kokal, S., Tang, T., Schramm, L. and Sayegh, S. (1995) 'Electrokinetic and adsorption properties of asphaltenes', *Colloids and Surfaces A: Physicochemical and Engineering Aspects*, 94(2-3), pp. 253-265.
195. Kralova, I., Sjöblom, J., Øye, G., Simon, S., Grimes, B.A. and Paso, K. (2011) 'Heavy crude oils/particle stabilized emulsions', *Advances in colloid and interface science*, 169(2), pp. 106-127.
196. Kreutzer, M.T., Kapteijn, F., Moulijn, J.A. and Heiszwolf, J.J. (2005) 'Multiphase monolith reactors: chemical reaction engineering of segmented flow in microchannels', *Chemical Engineering Science*, 60(22), pp. 5895-5916.
197. Krieger, I.M. (1972) 'Rheology of monodisperse latices', *Advances in Colloid and Interface science*, 3(2), pp. 111-136.
198. Kronberg, B. and Lindman, B. (2003) *Surfactants and polymers in aqueous solution*. John Wiley & Sons Ltd., Chichester.
199. Kumar, K., Nikolov, A.D. and Wasan, D.T. (2001) 'Mechanisms of stabilization of water-in-crude oil emulsions', *Industrial & engineering chemistry research*, 40(14), pp. 3009-3014.
200. Lackowski, M. (2015) 'Dielectrophoresis flow control of volatile fluids in microchannels', *Journal of Thermal Science*, 24(5), pp. 427-431.
201. Langevin, D. and Argillier, J.-F. (2016) 'Interfacial behavior of asphaltenes', *Advances in colloid and interface science*, 233, pp. 83-93.
202. Langevin, D., Poteau, S., Hénaut, I. and Argillier, J.F. (2004) 'Crude oil emulsion properties and their application to heavy oil transportation', *Oil & gas science and technology*, 59(5), pp. 511-521.
203. Leber, N., Fay, J.D., Cameron, N.R. and Krajnc, P. (2007) '2, 4, 6-trichlorophenyl acrylate emulsion-templated porous polymers (PolyHIPes). Morphology and reactivity studies', *Journal of Polymer Science Part A: Polymer Chemistry*, 45(17), pp. 4043-4053.
204. Lee, C.-M., Sams, G.W. and Wagner, J. (2001) 'Power consumption measurements for ac and pulsed dc for electrostatic coalescence of water-in-oil emulsions', *Journal of electrostatics*, 53(1), pp. 1-24.

205. Lee, C. (2003) 'Improved electrically enhanced phase separation methods for difficult to resolve oily continuous emulsions'.
206. Lee, R.F. (1999) 'Agents which promote and stabilize water-in-oil emulsions', *Spill Science & Technology Bulletin*, 5(2), pp. 117-126.
207. Lesaint, C., Glomm, W.R., Lundgaard, L.E. and Sjöblom, J. (2009) 'Dehydration efficiency of AC electrical fields on water-in-model-oil emulsions', *Colloids and Surfaces A: Physicochemical and Engineering Aspects*, 352(1-3), pp. 63-69.
208. Less, S., Hannisdal, A., Bjørklund, E. and Sjöblom, J. (2008a) 'Electrostatic destabilization of water-in-crude oil emulsions: Application to a real case and evaluation of the Aibel VIEC technology', *Fuel*, 87(12), pp. 2572-2581.
209. Less, S., Hannisdal, A. and Sjöblom, J. (2008b) 'An Electrorheological Study on the Behavior of Water-in-Crude Oil Emulsions Under Influence of a DC Electric Field and Different Flow Conditions', *Journal of Dispersion Science and Technology*, 29(1), pp. 106-114.
210. Levine, S. and Bowen, B. (1992) 'Capillary interaction of spherical particles adsorbed on the surface of an oil/water droplet stabilized by the particles. Part II', *Colloids and Surfaces*, 65(4), pp. 273-286.
211. Lewis, A. (2004) 'Determination of the limiting oil viscosity for chemical dispersion at sea', *MCA Project MSA*, 10(9), p. 180.
212. Li, B., Sun, Z., Wang, Z., Jin, Y. and Fan, Y. (2016a) 'Effects of high-frequency and high-voltage pulsed electric field parameters on water chain formation', *Journal of Electrostatics*, 80, pp. 22-29.
213. Li, C., Wang, J. and Zhang, W. (2016b) 'Silicone-polyether Copolymers as New Steam Turbine Oil Demulsifiers', *Journal of Petroleum Science and Technology*, 6(2), pp. 84-89.
214. Li, H.M., Liu, J.C., Zhu, F.M. and Lin, S.A. (2001) 'Synthesis and physical properties of sulfonated syndiotactic polystyrene ionomers', *Polymer international*, 50(4), pp. 421-428.
215. Li, Y., Fan, D., Shi, W. and JIN, Q.-h. (2010) 'Performance evaluation and field application of a dispersing and plug-removing agent for colloidal bitumen in heavy oil reservoirs', *Journal of Xi'an Shiyou University (Natural Science Edition)*, 2, p. 014.
216. Lipp, P., Lee, C., Fane, A. and Fell, C. (1988) 'A fundamental study of the ultrafiltration of oil-water emulsions', *Journal of Membrane Science*, 36, pp. 161-177.

217. Lissant, K.J. (1974) 'Emulsions and Emulsions Technology Part 1.', *New York: Marcel Dekker Inc.*
218. Lissant, K.J. (1976) 'Emulsions and Emulsion Technology. New York, Marcel Dekker, Inc.'
219. Lobo, A., Cambiella, Á., Benito, J.M., Pazos, C. and Coca, J. (2006) 'Ultrafiltration of oil-in-water emulsions with ceramic membranes: Influence of pH and crossflow velocity', *Journal of Membrane Science*, 278(1-2), pp. 328-334.
220. Maa, Y.-F. and Hsu, C. (1996) 'Liquid-liquid emulsification by rotor/stator homogenization', *Journal of Controlled Release*, 38(2-3), pp. 219-228.
221. Mahadik, D., Lee, K.-Y., Ghorpade, R. and Park, H.-H. (2018) 'Superhydrophobic and Compressible Silica-polyHIPE Covalently Bonded Porous Networks via Emulsion Templating for Oil Spill Cleanup and Recovery', *Scientific reports*, 8(1), p. 16783.
222. Maia Filho, D.C., Ramalho, J.B.V.S., Spinelli, L.S. and Lucas, E.F. (2012) 'Aging of water-in-crude oil emulsions: Effect on water content, droplet size distribution, dynamic viscosity and stability', *Colloids and Surfaces A: Physicochemical and Engineering Aspects*, 396, pp. 208-212.
223. Mansurov, I., Il'yasova, E. and Vygovskoi, V. (1987) 'Shear strength of interfacial films of asphaltenes', *Chemistry and Technology of Fuels and Oils*, 23(2), pp. 96-98.
224. Marlow, B., Sresty, G., Hughes, R. and Mahajan, O. (1987) 'Colloidal stabilization of clays by asphaltenes in hydrocarbon media', *Colloids and Surfaces*, 24(4), pp. 283-297.
225. Márquez, M.L., Rogel, E. and Reif, I. (1996) 'Molecular dynamics simulation of isopropyl naphthalene sulfonate at the water/heptane interface', *Colloids and Surfaces A: Physicochemical and Engineering Aspects*, 106(2-3), pp. 135-148.
226. Martínez-Palou, R., de Lourdes Mosqueira, M., Zapata-Rendón, B., Mar-Juárez, E., Bernal-Huicochea, C., de la Cruz Clavel-López, J. and Aburto, J. (2011) 'Transportation of heavy and extra-heavy crude oil by pipeline: A review', *Journal of petroleum science and engineering*, 75(3-4), pp. 274-282.
227. Mason, S., May, K. and Hartland, S. (1995) 'Drop size and concentration profile determination in petroleum emulsion separation', *Colloids and Surfaces A: Physicochemical and engineering aspects*, 96(1-2), pp. 85-92.

228. Mason, T. (1999) 'New fundamental concepts in emulsion rheology', *Current Opinion in Colloid & Interface Science*, 4(3), pp. 231-238.
229. May, K., Jeelani, S. and Hartland, S. (1998) 'Influence of ionic surfactants on separation of liquid–liquid dispersions', *Colloids and Surfaces A: Physicochemical and Engineering Aspects*, 139(1), pp. 41-47.
230. McLean, J.D. and Kilpatrick, P.K. (1997) 'Effects of asphaltene solvency on stability of water-in-crude-oil emulsions', *Journal of Colloid and Interface Science*, 189(2), pp. 242-253.
231. McLean, J.D., Spiecker, P.M., Sullivan, A.P. and Kilpatrick, P.K. (1998) 'The role of petroleum asphaltenes in the stabilization of water-in-oil emulsions', in *Structures and Dynamics of Asphaltenes*. Springer, pp. 377-422.
232. Menner, A., Haibach, K., Powell, R. and Bismarck, A. (2006) 'Tough reinforced open porous polymer foams via concentrated emulsion templating', *Polymer*, 47(22), pp. 7628-7635.
233. Menner, A., Salgueiro, M., Shaffer, M.S. and Bismarck, A. (2008) 'Nanocomposite foams obtained by polymerization of high internal phase emulsions', *Journal of Polymer Science Part A: Polymer Chemistry*, 46(16), pp. 5708-5714.
234. Menon, V. and Wasan, D. (1984) 'Coalescence of water-in-shale oil emulsions', *Separation Science and Technology*, 19(8-9), pp. 555-574.
235. Mercier, A., Deleuze, H. and Mondain-Monval, O. (2000) 'Preparation and functionalization of (vinyl) polystyrene polyHIPE®.: Short routes to binding functional groups through a dimethylene spacer', *Reactive and Functional Polymers*, 46(1), pp. 67-79.
236. Mercier, A., Deleuze, H. and Mondain-Monval, O. (2001) 'Thiol Addition to the Pendant Vinylbenzene Groups of (Vinyl) polystyrene PolyHIPE Via a Batch and a Cross-Flow Method', *Macromolecular Chemistry and Physics*, 202(13), pp. 2672-2680.
237. Meredith, W. (1923) 'Dehydrator', *USA Patent 1 452 207*.
238. Mezzenga, R., Ruokolainen, J., Fredrickson, G.H. and Kramer, E.J. (2003) 'High internal phase polymeric emulsions by self-assembly of colloidal systems', *Macromolecules*, 36(12), pp. 4466-4471.
239. Mhatre, S., Simon, S., Sjöblom, J. and Xu, Z. (2018) 'Demulsifier assisted film thinning and coalescence in crude oil emulsions under DC electric fields', *Chemical Engineering Research and Design*, 134, pp. 117-129.

240. Mhatre, S., Vivacqua, V., Ghadiri, M., Abdullah, A., Al-Marri, M., Hassanpour, A., Hewakandamby, B., Azzopardi, B. and Kermani, B. (2015) 'Electrostatic phase separation: A review', *Chemical Engineering Research and Design*, 96, pp. 177-195.
241. Midtgård, O.-M. (2009) 'Electrostatic field theory and circuit analysis in the design of coalescers with pulsed dc voltage', *Chemical Engineering Journal*, 151(1-3), pp. 168-175.
242. Mills, P.L., Quiram, D.J. and Ryley, J.F. (2007) 'Microreactor technology and process miniaturization for catalytic reactions—A perspective on recent developments and emerging technologies', *Chemical Engineering Science*, 62(24), pp. 6992-7010.
243. Mohamed, R. (2011) 'Preparation of nano-structured macro-porous materials'.
244. Mohamed, R., Noor, Z., Calkan, O., Calkan, B., Ndlovu, T., Burke, D. and Akay, G. (2006) *CHISA: 17th International Congress of Chemical and Process Engineering*. Newcastle University.
245. Mohammadi, M., Shahhosseini, S. and Bayat, M. (2014) 'Electrocoalescence of binary water droplets falling in oil: Experimental study', *Chemical Engineering Research and Design*, 92(11), pp. 2694-2704.
246. Mohammed, R., Bailey, A., Luckham, P. and Taylor, S. (1993) 'Dewatering of crude oil emulsions 2. Interfacial properties of the asphaltic constituents of crude oil', *Colloids and Surfaces A: Physicochemical and Engineering Aspects*, 80(2-3), pp. 237-242.
247. Mohammed, R., Bailey, A., Luckham, P. and Taylor, S. (1994) 'Dewatering of crude oil emulsions 3. Emulsion resolution by chemical means', *Colloids and Surfaces A: Physicochemical and Engineering Aspects*, 83(3), pp. 261-271.
248. Mohebali, G., Kaytash, A. and Etemadi, N. (2012) 'Efficient breaking of water/oil emulsions by a newly isolated de-emulsifying bacterium, *Ochrobactrum anthropi* strain RIPI5-1', *Colloids and Surfaces B: Biointerfaces*, 98, pp. 120-128.
249. Mooney, M. (1964) 'The viscosity of concentrated suspension of spherical particles', *Journal of Colloid Science*, 1, pp. 195-201.
250. Moran, K. and Czarnecki, J. (2007) 'Competitive adsorption of sodium naphthenates and naturally occurring species at water-in-crude oil emulsion droplet surfaces', *Colloids and Surfaces A: Physicochemical and Engineering Aspects*, 292(2-3), pp. 87-98.

251. Mousavi, S., Ghadiri, M. and Buckley, M. (2014) 'Electro-coalescence of water drops in oils under pulsatile electric fields', *Chemical Engineering Science*, 120, pp. 130-142.
252. Nalawade, A.C., Ghorpade, R.V., Shadbar, S., Qureshi, M.S., Chavan, N., Khan, A.A. and Ponrathnam, S. (2016) 'Inverse high internal phase emulsion polymerization (i-HIPE) of GMMA, HEMA and GDMA for the preparation of superporous hydrogels as a tissue engineering scaffold', *Journal of Materials Chemistry B*, 4(3), pp. 450-460.
253. Naranda, J., Sušec, M., Maver, U., Gradišnik, L., Gorenjak, M., Vukasović, A., Ivković, A., Rupnik, M.S., Vogrin, M. and Krajnc, P. (2016) 'Polyester type polyHIPE scaffolds with an interconnected porous structure for cartilage regeneration', *Scientific reports*, 6, p. 28695.
254. Noor, Z.Z. (2006) *Intensification of separation processes using functionalised polyhipe polymers*. University of Newcastle upon Tyne.
255. Nour, A.H., Anisa, A.I. and Nour, A.H. (2012) 'Demulsification of water-in-oil (W/O) emulsion via microwave irradiation: An optimization', *Scientific Research and Essays*, 7(2), pp. 231-243.
256. Nour, A.H., Yunus, R.M. and Anwaruddin, H. (2007) 'Water-in-crude oil emulsions: Its stabilization and demulsification', *Journal of Applied Sciences*, 7(22), pp. 3512-3517.
257. Odirile, P.T. (2000) *Electric field intensification of surfactant mediated separations*. University of Newcastle.
258. Olijve, J., Mori, F. and Toda, Y. (2001) 'Influence of the molecular-weight distribution of gelatin on emulsion stability', *Journal of colloid and interface science*, 243(2), pp. 476-482.
259. Oliveira, P.F., Santos, I.C., Vieira, H.V., Fraga, A.K. and Mansur, C.R. (2017) 'Interfacial rheology of asphaltene emulsions in the presence of nanoemulsions based on a polyoxide surfactant and asphaltene dispersant', *Fuel*, 193, pp. 220-229.
260. Opawale, F.O. and Burgess, D.J. (1998) 'Influence of interfacial properties of lipophilic surfactants on water-in-oil emulsion stability', *Journal of colloid and interface science*, 197(1), pp. 142-150.
261. Pal, R. (1996) 'Effect of droplet size on the rheology of emulsions', *AICHE Journal*, 42(11), pp. 3181-3190.

262. Pal, R. (1998) 'A novel method to correlate emulsion viscosity data', *Colloids and Surfaces A: Physicochemical and Engineering Aspects*, 137(1-3), pp. 275-286.
263. Pal, R. and Rhodes, E. (1989) 'Viscosity/concentration relationships for emulsions', *Journal of Rheology*, 33(7), pp. 1021-1045.
264. Panchenkov, G. and Vinogradov, V. (1970) 'Water-in-oil emulsion in a constant homogeneous electric field', *Chemistry and Technology of Fuels and Oils*, 6(6), pp. 438-441.
265. Paterson, T. (2017) *PolyHIPE Microspheres for Injectable Bone Tissue Engineering Applications*. University of Sheffield.
266. Pearce, C. (1954) 'The mechanism of the resolution of water-in-oil emulsions by electrical treatment', *British Journal of Applied Physics*, 5(4), p. 136.
267. Pekdemir, T., Akay, G., Dogru, M., Merrells, R. and Schleicher, B. (2003a) 'Demulsification of highly stable water-in-oil emulsions', *Separation science and technology*, 38(5), pp. 1161-1183.
268. Pekdemir, T., Akay, G., Dogru, M., Merrells, R.E. and Schleicher, B. (2003b) 'Demulsification of highly stable water-in-oil emulsions', *Separation science and technology*, 38(5), pp. 1161-1183.
269. Pethig, R., Huang, Y., Wang, X.-B. and Burt, J.P. (1992) 'Positive and negative dielectrophoretic collection of colloidal particles using interdigitated castellated microelectrodes', *Journal of Physics D: Applied Physics*, 25(5), p. 881.
270. Pohar, A. and Plazl, I. (2009) 'Process intensification through microreactor application', *Chemical and biochemical engineering quarterly*, 23(4), pp. 537-544.
271. Pohl, H.A. (1951) 'The motion and precipitation of suspensoids in divergent electric field', *Applied Physics*, 29, pp. 1182-1188.
272. Pohl, H.A. (1958) 'Some effects of nonuniform fields on dielectrics', *Journal of Applied Physics*, 29(8), pp. 1182-1188.
273. Pohl, H.A. (1978) *Dielectrophoresis: The behavior of neutral matter in nonuniform electric fields (Cambridge Monographs on physics)*. Cambridge/New York: Cambridge University Press.
274. Pradilla, D., Simon, S. and Sjöblom, J. (2015) 'Mixed interfaces of asphaltenes and model demulsifiers part I: Adsorption and desorption of single components', *Colloids and Surfaces A: Physicochemical and Engineering Aspects*, 466, pp. 45-56.

275. Ptasinski, K. and Kerkhof, P. (1992) 'Electric field driven separations: Phenomena and applications', *Separation science and technology*, 27(8-9), pp. 995-1021.
276. Pulko, I. and Krajnc, P. (2012) 'High internal phase emulsion templating—a path to hierarchically porous functional polymers', *Macromolecular rapid communications*, 33(20), pp. 1731-1746.
277. Pulko, I., Smrekar, V., Podgornik, A. and Krajnc, P. (2011) 'Emulsion templated open porous membranes for protein purification', *Journal of Chromatography A*, 1218(17), pp. 2396-2401.
278. Qiu, Y.-R., Zhong, H. and Zhang, Q.-X. (2009) 'Treatment of stable oil/water emulsion by novel felt-metal supported PVA composite hydrophilic membrane using cross flow ultrafiltration', *Transactions of Nonferrous Metals Society of China*, 19(3), pp. 773-777.
279. Quintero, C., Noik, C., Dalmazzone, C. and Grossiord, J. (2009) 'Formation kinetics and viscoelastic properties of water/crude oil interfacial films', *Oil & Gas Science and Technology-Revue de l'IFP*, 64(5), pp. 607-616.
280. Ramos, A., Morgan, H., Green, N.G. and Castellanos, A. (1999) 'The role of electrohydrodynamic forces in the dielectrophoretic manipulation and separation of particles', *Journal of Electrostatics*, 47, pp. 71-81.
281. Rane, J.P., Pauchard, V., Couzis, A. and Banerjee, S. (2013) 'Interfacial rheology of asphaltenes at oil–water interfaces and interpretation of the equation of state', *Langmuir*, 29(15), pp. 4750-4759.
282. Reinking, L. (2007) 'Examples of image analysis using ImageJ', *Image J documentation*.
283. Richardson, E.G. (1953) 'The flow emulsions', *Journal of Colloid Science*, 8, pp. 367-373.
284. Robins, M.M., Watson, A.D. and Wilde, P.J. (2002) 'Emulsions—creaming and rheology', *Current Opinion in Colloid & Interface Science*, 7(5-6), pp. 419-425.
285. Rommel, W., Meon, W. and Blass, E. (1992) 'Hydrodynamic modeling of droplet coalescence at liquid-liquid interfaces', *Separation science and technology*, 27(2), pp. 129-159.
286. Rondón, M., Pereira, J.C., Bouriati, P., Graciaa, A., Lachaise, J. and Salager, J.-L. (2007) 'Breaking of water-in-crude-oil emulsions. 2. Influence of asphaltene

- concentration and diluent nature on demulsifier action', *Energy & fuels*, 22(2), pp. 702-707.
287. Roodbari, N.H., Badiei, A., Soleimani, E. and Khaniani, Y. (2016) 'Tweens demulsification effects on heavy crude oil/water emulsion', *Arabian Journal of Chemistry*, 9, pp. S806-S811.
288. Rubino, M., Netramai, S., Auras, R. and Annous, B.A. (2010) 'Effect of chlorine dioxide gas on physical, thermal, mechanical, and barrier properties of polymeric packaging materials', *Journal of applied polymer science*, 115(3), pp. 1742-1750.
289. Rudzinski, W.E., Aminabhavi, T.M., Sassman, S. and Watkins, L.M. (2000) 'Isolation and characterization of the saturate and aromatic fractions of a Maya crude oil', *Energy & fuels*, 14(4), pp. 839-844.
290. Saether, O., Sjoblom, J. and Dukhin, S.S. (2004) 'Droplet flocculation and coalescence in dilute oil-in-water emulsions', *Food emulsions*, pp. 175-220.
291. Sams, G.W. and Zaouk, M. (2000) 'Emulsion resolution in electrostatic processes', *Energy & fuels*, 14(1), pp. 31-37.
292. Schoeggl, P., Koegeler, H.-M., Gschweidl, K., Kokal, H., Williams, P. and Hulak, K. (2002) *Automated EMS calibration using objective driveability assessment and computer aided optimization methods* (0148-7191). SAE Technical Paper.
293. Schorling, P.-C., Kessel, D. and Rahimian, I. (1999) 'Influence of the crude oil resin/asphaltene ratio on the stability of oil/water emulsions', *Colloids and Surfaces A: Physicochemical and Engineering Aspects*, 152(1-2), pp. 95-102.
294. Schulman, J.H.a.J.L. (1954) 'Trans. Faraday Soc.', 50, pp. 598-612.
295. Schuster, D. (1985) *Encyclopedia of Emulsion Technology: Applications*. CRC Press.
296. Scott, T.C., DePaoli, D.W. and Sisson, W.G. (1994) 'Further development of the electrically driven emulsion-phase contactor', *Industrial & engineering chemistry research*, 33(5), pp. 1237-1244.
297. Sergienko, A.Y., Tai, H., Narkis, M. and Silverstein, M.S. (2002) 'Polymerized high internal-phase emulsions: Properties and interaction with water', *Journal of applied polymer science*, 84(11), pp. 2018-2027.
298. Shakorflow, A.M. (2012) *Process intensification in the demulsification of water-in-crude oil emulsions via crossflow microfiltration through a hydrophilic polyHIPE polymer (PHP)*. Newcastle University.
299. Sherman, P. (1968) 'Emulsion Science. London, Academic Press.'

300. Sherrington, D.C. (1998) 'Preparation, structure and morphology of polymer supports', *Chemical Communications*, (21), pp. 2275-2286.
301. Simões, E.A.F., Carbonell-Estrany, X., Rieger, C.H.L., Mitchell, I., Fredrick, L., Groothuis, J.R. and Palivizumab Long-Term Respiratory Outcomes Study, G. (2010) 'The effect of respiratory syncytial virus on subsequent recurrent wheezing in atopic and nonatopic children', *Journal of Allergy and Clinical Immunology*, 126(2), pp. 256-262.
302. Sjöblom, J. (2005) 'NMR Characterization of Emulsions', in *Emulsions and Emulsion Stability*. CRC Press, pp. 303-330.
303. Sjöblom, J. (2006) 'Emulsions and emulsion stability. CRC'. Taylor&Francis, Boca Raton.
304. Sjöblom, J., Aske, N., Auflem, I.H., Brandal, Ø., Havre, T.E., Sæther, Ø., Westvik, A., Johnsen, E.E. and Kallevik, H. (2003) 'Our current understanding of water-in-crude oil emulsions.: Recent characterization techniques and high pressure performance', *Advances in Colloid and Interface Science*, 100, pp. 399-473.
305. Sjöblom, J., Hemmingsen, P.V. and Kallevik, H. (2007) 'The role of asphaltenes in stabilizing water-in-crude oil emulsions', in *Asphaltenes, heavy oils, and petroleomics*. Springer, pp. 549-587.
306. Sjöblom, J., Mingyuan, L., Christy, A.A. and Gu, T. (1992) 'Water-in-crude-oil emulsions from the Norwegian continental shelf 7. Interfacial pressure and emulsion stability', *Colloids and surfaces*, 66(1), pp. 55-62.
307. Skodvin, T. and Sjöblom, J. (1996) 'Dielectric spectroscopy on W/O emulsions under influence of shear forces', *Colloid and Polymer Science*, 274(8), pp. 754-762.
308. Speight, J. (2004a) 'Petroleum asphaltenes-Part 2: The effect of asphaltene and resin constituents on recovery and refining processes', *Oil & gas science and technology*, 59(5), pp. 479-488.
309. Speight, J.G. (1999) 'The chemical and physical structure of petroleum: effects on recovery operations', *Journal of Petroleum Science and Engineering*, 22(1-3), pp. 3-15.
310. Speight, J.G. (2004b) 'New approaches to hydroprocessing', *Catalysis Today*, 98(1-2), pp. 55-60.
311. Spiecker, P.M. and Kilpatrick, P.K. (2004) 'Interfacial rheology of petroleum asphaltenes at the oil– water interface', *Langmuir*, 20(10), pp. 4022-4032.

312. Stankiewicz, A. and Moulijn, J.A. (2002) 'Process intensification', *Industrial & Engineering Chemistry Research*, 41(8), pp. 1920-1924.
313. Stevens, G., Pratt, H. and Tai, D. (1990) 'Droplet coalescence in aqueous electrolyte solutions', *Journal of colloid and interface science*, 136(2), pp. 470-479.
314. Subramanian, D., May, N. and Firoozabadi, A. (2017) 'Functional molecules and the stability of water-in-crude oil emulsions', *Energy & Fuels*, 31(9), pp. 8967-8977.
315. Subramaniyan, A., Kumaraguruparan, G., Venkatesan, R. and Vignesh, A. (2014) 'Selection of nanofluid for heat transfer applications from existing models of thermal conductivity', *International Journal of Nano Dimension*, 5, pp. 213-222.
316. Sullivan, A.P. and Kilpatrick, P.K. (2002) 'The effects of inorganic solid particles on water and crude oil emulsion stability', *Industrial & Engineering Chemistry Research*, 41(14), pp. 3389-3404.
317. Sullivan, A.P., Zaki, N.N., Sjöblom, J. and Kilpatrick, P.K. (2007) 'The Stability of Water-in-Crude and Model Oil Emulsions', *The Canadian Journal of Chemical Engineering*, 85(6), pp. 793-807.
318. Sun, D., Duan, X., Li, W. and Zhou, D. (1998) 'Demulsification of water-in-oil emulsion by using porous glass membrane', *Journal of membrane science*, 146(1), pp. 65-72.
319. Suslick, K.S. (1998) 'Kirk-Othmer encyclopedia of chemical technology', *John Wiley&Sons: New York, NY, USA*, 26, pp. 517-541.
320. Suzuki, T., Itoh, M., Takegami, Y. and Watanabe, Y. (1982) 'Chemical structure of tar-sand bitumens by <sup>13</sup>C and <sup>1</sup>H nmr spectroscopic methods', *Fuel*, 61(5), pp. 402-410.
321. Sztukowski, D.M. and Yarranton, H.W. (2005) 'Oilfield solids and water-in-oil emulsion stability', *Journal of colloid and interface science*, 285(2), pp. 821-833.
322. Tai, H., Sergienko, A. and Silverstein, M. (2001) 'Organic-inorganic networks in foams from high internal phase emulsion polymerizations', *Polymer*, 42(10), pp. 4473-4482.
323. Tambe, D., Paulis, J. and Sharma, M.M. (1995) 'Factors controlling the stability of colloid-stabilized emulsions: IV. Evaluating the effectiveness of demulsifiers', *Journal of colloid and interface science*, 171(2), pp. 463-469.

324. Tarantsev, K., Krasnaya, E., Chirkov, V. and Ashikhmin, I. (2013) 'Breakdown of water-oil emulsions in an electric field', *Chemical and Petroleum Engineering*, 49(7-8), pp. 435-439.
325. Taylor, S. (1996) 'Theory and Practice of Electrically-Enhanced Phase Separation of Water-in-Oil Emulsions', *Chemical engineering research & design*, 74(5), pp. 526-540.
326. Taylor, S.E. (1988) 'Investigations into the electrical and coalescence behaviour of water-in-crude oil emulsions in high voltage gradients', *Colloids and Surfaces*, 29(1), pp. 29-51.
327. Taylor, S.E. (1995 ) 'Approaches and Limitations to the Intensification of Electrically-Enhanced Phase Separation of Water-in-Oil Emulsions', *Proceedings of the First International Confernce on Science, Engineering and Technology of Intensive Processing*.
328. Teigen, K.E. and Munkejord, S.T. (2010) 'Influence of surfactant on drop deformation in an electric field', *Physics of Fluids*, 22(11), p. 112104.
329. Thaler, W.A. (1983) 'Hydrocarbon-soluble sulfonating reagents. Sulfonation of aromatic polymers in hydrocarbon solution using soluble acyl sulfates', *Macromolecules*, 16(4), pp. 623-628.
330. Theron, A., Zussman, E. and Yarin, A.L. (2001) 'Electrostatic field-assisted alignment of electrospun nanofibres', *Nanotechnology*, 12(3), p. 384.
331. Thommes, M., Kaneko, K., Neimark, A.V., Olivier, J.P., Rodriguez-Reinoso, F., Rouquerol, J. and Sing, K.S. (2015) 'Physisorption of gases, with special reference to the evaluation of surface area and pore size distribution (IUPAC Technical Report)', *Pure and Applied Chemistry*, 87(9-10), pp. 1051-1069.
332. Thompson, D.G., Taylor, A.S. and Graham, D.E. (1985) 'Emulsification and demulsification related to crude oil production', *Colloids and Surfaces*, 15, pp. 175-189.
333. Thumbarathy, D. (2018) *a Preparation of functional polyHIPE polymers for agro-process and bio-process applications*. Newcastle; e University.
334. Tshilumbu, N.N., Kharatyan, E. and Masalova, I. (2014) 'Effect of nanoparticle hydrophobicity on stability of highly concentrated emulsions', *Journal of Dispersion Science and Technology*, 35(2), pp. 283-292.
335. Umar, A., Saaid, I. and Sulaimon, A. (2017) 'The Roles of Polar Compounds in the Stability and Flow Behavior of Water-in-Oil Emulsions', in *ICIPEG 2016*. Springer, pp. 643-653.

336. Ungureanu, S., Birot, M., Laurent, G., Deleuze, H., Babot, O., Julian-Lopez, B., Achard, M.-F., Popa, M.I., Sanchez, C. and Backov, R. (2007) 'One-Pot Syntheses of the First Series of Emulsion Based Hierarchical Hybrid Organic– Inorganic Open-Cell Monoliths Possessing Tunable Functionality (Organo– Si (HIPE) Series)', *Chemistry of Materials*, 19(23), pp. 5786-5796.
337. Urdahl, O., Williams, T., Bailey, A. and Thew, M. (1996) 'Electrostatic destabilization of water-in-oil emulsions under conditions of turbulent-flow', *Chemical engineering research & design*, 74(2), pp. 158-165.
338. Van Gerven, T. and Stankiewicz, A. (2009) 'Structure, energy, synergy, time □ The fundamentals of process intensification', *Industrial & engineering chemistry research*, 48(5), pp. 2465-2474.
339. Vander Kloet, J., Schramm, L.L. and Shelfantook, B. (2002) 'Application of the hydrophile–lipophile balance concept to the classification of demulsifiers and bituminous froth and its components', *Fuel processing technology*, 75(1), pp. 9-26.
340. Verruto, V.J., Le, R.K. and Kilpatrick, P.K. (2009) 'Adsorption and molecular rearrangement of amphoteric species at oil– water interfaces', *The Journal of Physical Chemistry B*, 113(42), pp. 13788-13799.
341. Vickers, J. (2001) *Organic effluent treatment in nuclear fuel reprocessing: Interfacial crud*. University of Newcastle upon Tyne.
342. Vinodh, R., Ilakkiya, A., Elamathi, S. and Sangeetha, D. (2010) 'A novel anion exchange membrane from polystyrene (ethylene butylene) polystyrene: synthesis and characterization', *Materials Science and Engineering: B*, 167(1), pp. 43-50.
343. Wagner, J. and Nelson, J. (2016) 'A New Approach Toward Improving our Understanding of Electrically Enhanced Coalescence', *Journal of Sustainable Energy Engineering*, 4(1), pp. 37-58.
344. Wagner, J.P. and Hsu, E.C. (1983) 'Methods and apparatus for electrostatically resolving emulsions'. Google Patents.
345. Walsh, D., Stenhouse, J., Kingsbury, L. and Webster, E. (1996) 'PolyHIPE foams: Production, characterisation, and performance as aerosol filtration materials', *Journal of Aerosol Science*, 27, pp. S629-S630.
346. Walsh, D.C., Stenhouse, J. I. T., Kingsbury, L. P., Webster, E. J. (1996) 'PolyHIPE Foams: Production, Characterisation and performance as Aerosol Filtration Materials', *Journal of Aerosol Science*, 27, pp. S629-S630.

347. Wang, S.S., Lee, C.J. and Chan, C.C. (1994) 'Demulsification of water-in-oil emulsions by use of a high voltage ac field', *Separation science and technology*, 29(2), pp. 159-170.
348. Wang, X. and Alvarado, V. (2009) 'Direct current electrorheological stability determination of water-in-crude oil emulsions', *The Journal of Physical Chemistry B*, 113(42), pp. 13811-13816.
349. Wasan, D.T. and Nikolov, A.D. (2001) 'Structure and stability of emulsions', *Encyclopedic handbook of emulsion technology*. CRC Press, Boca Raton, pp. 59-70.
350. Waterman (1965) 'Electrical coalescers. Chemical engineering progress: ' 61, pp. 51-72.
351. Werner, A., Behar, F., De Hemptinne, J. and Behar, E. (1998) 'Viscosity and phase behaviour of petroleum fluids with high asphaltene contents', *Fluid phase equilibria*, 147(1-2), pp. 343-356.
352. Wiącek, A.E. and Chibowski, E. (2002) 'Zeta potential and droplet size of n-tetradecane/ethanol (protein) emulsions', *Colloids and Surfaces B: Biointerfaces*, 25(1), pp. 55-67.
353. Williams, J.M., Gray, A.J. and Wilkerson, M.H. (1990) 'Emulsion stability and rigid foams from styrene or divinylbenzene water-in-oil emulsions', *Langmuir*, 6(2), pp. 437-444.
354. Williams, J.M. and Wroblewski, D.A. (1988) 'Spatial distribution of the phases in water-in-oil emulsions. Open and closed microcellular foams from cross-linked polystyrene', *Langmuir*, 4(3), pp. 656-662.
355. Williams, J.M. and Wroblewski, D.A. (1989) 'Microstructures and properties of some microcellular foams', *Journal of materials science*, 24(11), pp. 4062-4067.
356. Williams, T., Bailey, A. and Thew, M. (1995) 'The electrostatic destabilisation of water-in-oil emulsions in turbulent flow', *ELECTROSTATICS 1995*, 143, pp. 13-16.
357. Williams, T.J. and Bailey, A.G. (1986) 'Changes in the size distribution of a water-in-oil emulsion due to electric field induced coalescence', *IEEE Transactions on Industry Applications*, (3), pp. 536-541.
358. Winslow Jr, J.D. (1977) 'Electrical treater with ac-dc electrical fields'. Google Patents.
359. Woelflin, W. (1937) 'Process and apparatus for treating emulsions', *US Patent 2 083 802*.

360. Wong, S., Lim, J. and Dol, S. (2015) 'Crude oil emulsion: A review on formation, classification and stability of water-in-oil emulsions', *Journal of Petroleum Science and Engineering*, 135, pp. 498-504.
361. Wu, J., Xu, Y., Dabros, T. and Hamza, H. (2003) 'Effect of demulsifier properties on destabilization of water-in-oil emulsion', *Energy & fuels*, 17(6), pp. 1554-1559.
362. Xie, Q. and Yan, Z. (1993) 'Study on condition of breakdown emulsion by pulse electric field', *Membr. Sci. Technol.*, 13, pp. 51-55.
363. Yahaya Khan, M., Abdul Karim, Z., Hagos, F.Y., Aziz, A.R.A. and Tan, I.M. (2014) 'Current trends in water-in-diesel emulsion as a fuel', *The Scientific world journal*, 2014.
364. Yan, Z., Elliott, J.A. and Masliyah, J.H. (1999) 'Roles of various bitumen components in the stability of water-in-diluted-bitumen emulsions', *Journal of colloid and interface science*, 220(2), pp. 329-337.
365. Yang, F., Tchoukov, P., Dettman, H., Teklebrhan, R.B., Liu, L., Dabros, T., Czarnecki, J., Masliyah, J. and Xu, Z. (2015) 'Asphaltene subfractions responsible for stabilizing water-in-crude oil emulsions. Part 2: Molecular representations and molecular dynamics simulations', *Energy & Fuels*, 29(8), pp. 4783-4794.
366. Yang, F., Tchoukov, P., Pensini, E., Dabros, T., Czarnecki, J., Masliyah, J. and Xu, Z. (2014) 'Asphaltene subfractions responsible for stabilizing water-in-crude oil emulsions. Part 1: interfacial behaviors', *Energy & Fuels*, 28(11), pp. 6897-6904.
367. Yarranton, H.W., Hussein, H. and Masliyah, J.H. (2000) 'Water-in-hydrocarbon emulsions stabilized by asphaltenes at low concentrations', *Journal of colloid and interface science*, 228(1), pp. 52-63.
368. Yasar, M., Akmaz, S. and Gurkaynak, M. (2009) 'Investigation of the molecular structure of Turkish asphaltenes', *Petroleum Science and Technology*, 27(10), pp. 1044-1061.
369. Yen, T. (1974) 'Structure of petroleum asphaltene and its significance', *Energy Sources, Part A recovery, Utilization, And Environmental Effects*, 1(4), pp. 447-463.
370. Zadymova, N.M., Skvortsova, Z.N., Traskine, V.Y., Kulikov-Kostyushko, F.A., Kulichikhin, V.G. and Malkin, A.Y. (2017) 'Rheological properties of heavy oil emulsions with different morphologies', *Journal of Petroleum Science and Engineering*, 149, pp. 522-530.

371. Zaki, N.N. (1997) 'Surfactant stabilized crude oil-in-water emulsions for pipeline transportation of viscous crude oils', *Colloids and surfaces A: Physicochemical and engineering aspects*, 125(1), pp. 19-25.
372. Zaki, N.N., Maysour, N.E. and Abdel-Azim, A.-A.A. (2000) 'Polyoxyalkylenated amines for breaking of water-in-oil emulsions stabilized by asphaltenes and clay', *Petroleum science and technology*, 18(9-10), pp. 1009-1025.
373. Zapryanov, Z., Malhotra, A., Aderangi, N. and Wasan, D. (1983) 'Emulsion stability: an analysis of the effects of bulk and interfacial properties on film mobility and drainage rate', *International Journal of Multiphase Flow*, 9(2), pp. 105-129.
374. Zehetner, J., Schöggel, P., Dank, M. and Meitz, K. (2009) *Simulation of Driveability in Real-time* (0148-7191). SAE Technical Paper.
375. Zhang, H. and Cooper, A.I. (2005) 'Synthesis and applications of emulsion-templated porous materials', *Soft Matter*, 1(2), pp. 107-113.
376. Zhang, J., Xu, J.-y., Gao, M.-c. and Wu, Y.-x. (2013) 'Apparent viscosity of oil-water (coarse) emulsion and its rheological characterization during the phase inversion region', *Journal of Dispersion Science and Technology*, 34(8), pp. 1148-1160.
377. Zhang, L., Shi, C., Lu, Q., Liu, Q. and Zeng, H. (2016) 'Probing Molecular Interactions of Asphaltenes in Heptol Using a Surface Forces Apparatus: Implications on Stability of Water-in-Oil Emulsions', *Langmuir*, 32(19), pp. 4886-4895.
378. Zhang, S. (2017) *Interfacial Properties of Asphaltenes at Oil/Water Interface*. University of Alberta.
379. Zhang, S., Wang, D., Fan, P.-P. and Sun, L.-P. (2015) 'Enhancement of gas-to-liquid oxygen transfer in the presence of fine solid particles for air-exposed multiphase system', *Chemical Engineering Research and Design*, 100, pp. 434-443.
380. Zhang, T. and Guo, Q. (2017) 'Continuous preparation of polyHIPE monoliths from ionomer-stabilized high internal phase emulsions (HIPEs) for efficient recovery of spilled oils', *Chemical Engineering Journal*, 307, pp. 812-819.
381. Zhang, X., Basaran, O.A. and Wham, R.M. (1995) 'Theoretical prediction of electric field-enhanced coalescence of spherical drops', *AIChE Journal*, 41(7), pp. 1629-1639.
382. Zhang, Y., Liu, Y. and Ji, R. (2011) 'Dehydration efficiency of high-frequency pulsed DC electrical fields on water-in-oil emulsion', *Colloids and Surfaces A: Physicochemical and Engineering Aspects*, 373(1-3), pp. 130-137.

## APPENDIX

Appendix 1: Crude oil characterization of Southern Iraq supplying Midland Refineries Company (MRC) used in the demulsification experiments.

Test	Result	Method
API gravity @ 15.6 ° C	30.6	ASTM-D 1298
SP. gravity @ 15.6 ° C/ 15.5 ° C	0.8729	ASTM-D (table 3) (petroleum measurement table)
Density at 15 ° C	0.8725	
Sulfur content wt. %	3.11	ASTM-4294
Kin. viscosity Cst.		ASTM-D 445
@ 10 ° C	28.00	—
@ 21.1 ° C	16.9	—
@ 37.8 ° C	9.7	—
@ 50.0 ° C	6.5	—
Pour point ° C	Below-30	ASTM-D97
R.V.P kg/cm <sup>2</sup>	0.56	ASTM-D323
Water and sediment vol. %	0.2	IP-75
Salt content wt. %	0.0072	IP-77 and ASTM-D3230
Ram. carbon residue wt. %	5.4	ASTM-D524
Asphaltenes content wt. %	2.03	JPI-5S-45-95
Ash content wt. %	0.0140	ASTM-D482
Vanadium PPM	62.19	ASTM-D6728
Nickel PPM	19.69	ASTM-D6728
KUOP characterization factor	11.9	UOP method 375
Water content vol. %	0.15	IP-74
Distillation		IP-24
IBP ° C	46	—
Rec. @ 50.0 ° C	0.5	—
@ 75.0 ° C	3.5	—
@ 100.0 ° C	7.0	—
@ 125.0 ° C	11.0	—
@ 150.0 ° C	16.00	—
@ 175.0 ° C	20.0	—
@ 200.0 ° C	25.0	—
@ 225.0 ° C	30.0	—
@ 250.0 ° C	34.0	—
@ 275.0 ° C	39.0	—
@ 300.0 ° C	44.0	—
Total distil. Vol. %	45.0	—